REGULATION OF NMDA RECEPTOR CHANNEL BLOCK AND DESENSITIZATION BY INTRACELLULAR CALCIUM

by

Matthew B. Phillips

Bachelor of Science, Furman University, 2015

Submitted to the Graduate Faculty of the

Dietrich School of Arts and Sciences in partial fulfillment

of the requirements for the degree of

Doctor of Philosophy

University of Pittsburgh

2021

UNIVERSITY OF PITTSBURGH

DIETRICH SCHOOL OF ARTS AND SCIENCES

This dissertation was presented

by

Matthew B. Phillips

It was defended on

July 6, 2021

and approved by

Dr. Elias Aizenman, Professor, Department of Neurobiology

Dr. Stephen D. Meriney, Professor, Department of Neuroscience

Dr. Tija C. Jacob, Associate Professor, Department of Pharmacology and Chemical Biology

Dr. Zachary P. Wills, Assistant Professor, Department of Neurobiology

Dr. Kevin S. Jones, Assistant Professor, Department of Pharmacology, University of Michigan

Dissertation Advisor: Dr. Jon W. Johnson, Professor, Department of Neuroscience

REGULATION OF NMDA RECEPTOR CHANNEL BLOCK AND DESENSITIZATION BY INTRACELLULAR CALCIUM

Matthew B. Phillips, PhD

University of Pittsburgh, 2021

N-methyl-**D**-aspartate receptors (NMDARs) are ligand-gated ion channels found at nearly all vertebrate excitatory synapses that contribute to a multitude of nervous system functions. Unique biophysical properties, including high Ca^{2+} permeability, voltage-dependent Mg^{2+} block, and slow gating kinetics, allow NMDARs to control the magnitude and timing of Ca^{2+} influx following synaptic events. Ca^{2+} influx through NMDARs drives an array of signaling pathways that regulate critical neuronal functions such as synaptic plasticity and cell survival. Abnormal NMDAR activity is involved in a remarkable range of nervous system disorders including schizophrenia, major depressive disorder, stroke, neuropathic pain, and neurodegenerative diseases. Specifically, NMDAR overactivation can lead to accumulation of toxic levels of Ca^{2+} that initate cell death signaling pathways. Because of the core involvement of NMDARs in normal brain physiology as well as brain pathologies, NMDARs are attractive targets for neurotherapeutic drugs. The NMDAR channel blocker memantine, a clinically approved treatment for Alzheimer's disease, displays a combination of clinical utility and tolerability unique amongst NMDAR antagonists. We recently discovered that memantine enhances NMDAR desensitization by stabilizing a Ca^{2+}-dependent desensitized receptor state. Stabilization of a Ca^{2+}-dependent state by memantine offers a rational mechanism by which memantine can target specific NMDAR subpopulations involved in disease: preferential inhibition of NMDARs in neurons experiencing long durations of high Ca^{2+} influx. Therefore, we systematically investigated the relation between channel blocker potency, intracellular Ca^{2+} concentration ($[Ca^{2+}]_i$, and NMDAR desensitization. We found that while potency of memantine depended on $[Ca^{2+}]_i$, the potency of another clinically

useful channel blocker, ketamine, was $[Ca^{2+}]_i$-independent. Utilizing this discrepancy, we compared the memantine and ketamine binding sites and identified a residue in the NMDAR transmembrane domain that strongly contributes to NMDAR desensitization and memantine potency. Lastly, we characterized novel NMDAR channel blockers and discovered that potency of a memantine derivative was also dependent on $[Ca^{2+}]_i$. The data presented in this dissertation provide key insight into how $[Ca^{2+}]_i$ affects channel blocker activity and NMDAR desensitization, and ultimately improve our understanding of the structural and functional mechanisms underlying the effects of channel blocking drugs on NMDAR function.

TABLE OF CONTENTS

<div align="center">

LIST OF TABLES

</div>

<div align="center">

x

</div>

LIST OF FIGURES

PREFACE

The process of writing and defending this dissertation was a transformative, cathartic, and immensely validating experience. The accomplishments and work that this dissertation represents, however, belong to far more than me alone. The Center for Neuroscience at the University of Pittsburgh has been an immensely supportive environment that stimulated my growth both inside and outside of the lab. The past and current members of the Johnson lab I thank for sharing with me their depth of experience and enduring my quirks as I developed from a young graduate student, worried by his lack of knowledge, into a scientist that embraces it. Dr. Nathan Glasgow deserves specific thanks – we are all shades of Nate. His natural mentorship ability and intelligence provided me with an inspiring model to emulate, and his influence can be seen throughout this dissertation. I thank my committee, Drs. Steve Meriney, Tija Jacob, Zak Wills, my outside examiner Dr. Kevin Jones, and my committee chair Dr. Elias Aizenman for providing invaluable guidance and fostering my ability to both defend and accurately evaluate my own ideas. The CNUP also provided a wealth of external mentors who greatly contributed to my scientific and professional growth, including Dr. Peter Strick, who I thank for sharing with me his wealth of wisdom and experience. I owe an immeasurable debt to my mentor, Dr. Jon Johnson. Jon is a wellspring of brilliance, patience, and compassion. His unwavering integrity, attention to detail, dedication to training, and boundless curiosity makes Jon a phenomenal mentor and a constant source of inspiration. I am exceedingly fortunate to have been able to observe, train under, and work alongside Jon. If I become even half the scientist and person Jon is, I will consider myself a resounding success.

All of my past and future successes also belong to my friends and family. My new family, the Stans, I thank for the constant support, guidance, example, and love that they provide. My

1.0 GENERAL INTRODUCTION

Armed with only a limited vocabulary, neurons can generate an effectively infinite number of specific, meaningful messages to elicit an astoundingly diverse array of thoughts, behaviors, and experiences. While we possess a superficial grasp of neuronal vernacular, enough to recognize and even translate certain phrases, our understanding of basic construction of these remarkably complex messages is still limited. Understanding how to combine symbols to form words and phrases, and how these words and phrases can be combined to express complex statements, is critical to achieving literacy in a new language. Like letters to written English, ion channel signals are the constitutive units of the neuronal language – meaningless in isolation, but immensely powerful when organized.

Ion channels are proteins that allow ions to flow across cell membranes and are necessary for the transmission of information between nervous system cells. Neurons, the cells responsible for the majority of signaling in the nervous system, transmit information to and receive information from other neurons through specialized structures called synapses. Synaptic transmission involves the release of molecules known as neurotransmitters from a presynaptic neuron onto the cell membrane of a postsynaptic neuron, where receptor proteins bind the neurotransmitter. These neurotransmitter receptors then convert the chemical signal from the presynaptic neuron into a physiological response in the postsynaptic neuron. The transduction of chemical signals into electrical responses is performed by ligand-gated ion channels, neurotransmitter receptors that activate in response to agonist binding and permit ion flux across cellular membranes. The cumulative opening of many ligand-gated ion channels alters the concentrations of intracellular ions and the membrane voltage of the postsynaptic neuron, which both have profound consequences on neuronal function. The specific combination of ion channels opened by

concomitant synaptic inputs either electrically excites or inhibits the cell, determining whether the signal will be propagated to other downstream neurons. Ligand-gated ion channel activity can also alter the concentrations of intracellular ions in the postsynaptic neuron, which can lead to the strengthening or weakening of specific synaptic inputs and regulate gene expression. Through these mechanisms, ion channels govern the activity of individual neurons and, in turn, shape the neuronal ensembles that drive higher-level nervous system function.

Ionotropic glutamate receptors (iGluRs), a family of ligand-gated ion channels activated by the amino acid glutamate, are the primary mediators of fast excitatory transmission in the central nervous system. Among iGluRs, *N*-methyl-D-aspartate receptors (NMDARs) are particularly important for both the electrical and chemical components of signal transduction. NMDARs are expressed in nearly all nervous system cells and normal NMDAR activity is vital both to basic neuronal physiology and higher-level brain function. Likewise, NMDAR dysfunction is a central feature of many nervous system disorders, making NMDARs attractive pharmacological targets for treatment of various neurological and psychiatric disorders. Unfortunately, modulating NMDAR activity with therapeutic drugs has proven to be excruciatingly complicated due to the near-ubiquitous involvement of NMDARs in normal brain function. Compounds that inhibit NMDARs by binding in and blocking ion flux through the NMDAR channel, known as channel blockers, are currently the most clinically efficacious NMDAR-targeting neurotherapeutic drugs. While the mechanism of inhibition employed by channel blockers seems quite simple, channel blockers exert additional, more nuanced effects on ion channel function that may contribute to their clinical profiles. The work presented in this dissertation details the ability of NMDAR channel blockers, with a primary focus on the clinically useful NMDAR channel blocker memantine, to act as dual-mechanism inhibitors that both block and modulate the gating of the NMDAR channel.

This introduction aims to accomplish four main tasks. First, I will discuss ion channel gating and the relation between channel gating and channel block. Second, I will review the basic characteristics of NMDARs, the receptor at the center of this dissertation research, and the inherent complexity of their pharmacology. Next, I will detail the effects of channel blockers on NMDAR state transitions to illustrate how channel blockers can act as powerful tools for the study of NMDAR channel function. I will then introduce the concept of state-specific antagonism and describe a strategy for targeting of specific NMDAR states with channel blockers.

1.1 ION CHANNEL GATING

(Adapted from **Appendix A** (Phillips *et al.*, 2020))

Neuronal information processing depends on the distribution and properties of the ion channels found in neuronal membranes. Channel gating, perhaps the most basic characteristic of ion channels alongside ion permeation, refers to the ability of ion channels to either open and allow transmembrane ion flux or to close and prevent ion flux. The gating mechanisms employed by ligand-gated ion channels are divided into three general categories: activation, deactivation, and desensitization. Activation refers to the transition of ion channels from closed to open states following application of agonist. Deactivation refers to the transition of channels from open to closed states following removal of agonist. Desensitization is canonically defined as a decrease in the fraction of channels that are in the open state (termed open probability, or P_{open}) in the maintained presence of agonist (Katz & Thesleff, 1957). Desensitization is typically a direct consequence of agonist binding. A fourth gating mechanism that resembles desensitization but is not driven by agonist binding has been referred to both as desensitization and inactivation (Mayer & Westbrook, 1985; Legendre *et al.*, 1993; Hille, 2001; Glasgow *et al.*, 2017), although

3

inactivation is a term typically used to describe a different mechanism employed by voltage-gated channels (Hille, 2001). While driven by different underlying mechanisms, both desensitization and inactivation ultimately describe nonconducting channel states that do not respond to typical activating stimuli (Katz & Thesleff, 1957; Hille, 2001). Gating mechanisms of ion channels are finely tuned and are essential to normal nervous system function, with even minor aberrations of channel gating often resulting in disease. While most known channelopathies involve dysfunction of voltage-gated channels, naturally occurring genetic variants that alter the gating of ligand-gated ion channels are increasingly associated with neurological disorders, including epilepsy, intellectual disability, and autism (Yuan *et al.*, 2015).

Studies of drugs that inhibit channel function provide valuable insight into ion channel gating mechanisms. Channel blockers, antagonists that bind in and prevent ion flux through ion channels, have been successfully used to probe both the structure of ion channel pores and the kinetics of channel gating. Channel gating requires conformational changes in or near the channel pore (i.e., the transmembrane ion conduction pathway), and channel blockers are known to interact differentially with channels in open, closed, inactivated, and desensitized states (Heidmann & Changeux, 1986; Benveniste & Mayer, 1995; Blanpied *et al.*, 2005; Purohit & Grosman, 2006; Glasgow *et al.*, 2017). Thus, channel blockers are exceptionally well-positioned, both figuratively and literally, for use as analytic probes in studies of channel gating.

1.1.1 Reciprocal interactions between channel block and channel gating

Channel gating can profoundly influence channel block, and channel block can profoundly influence channel gating. The initial binding of channel blockers often depends on gating state. Most blockers of ligand-gated ion channels can only enter and bind to the channel while agonist is bound and the channel is in the open state (Figure 1A). Such blockers are descriptively named

4

open channel blockers and are the focus of this dissertation. In some cases, open channel blockers are also termed "use-dependent" (Courtney, 1975). A blocker is termed use-dependent if inhibition by the blocker (1) requires activation of the channel, and (2) increases with duration of channel activation until an equilibrium between blocker binding and unbinding is reached (Figure 1A). The actions of almost all known ligand-gated ion channel blockers have been found to be at least partially dependent on channel opening, binding either exclusively or with much faster kinetics when the channel is open.

Channel blocker unbinding also depends on gating transitions. If closure of the channel gate and agonist unbinding can occur while the blocker is bound, the blocker may become "trapped" in the channel (Figure 1C,D), unable to unbind until agonist is reapplied. Interestingly, some trapping blockers display the ability to escape from a fraction of blocked channels even after removal of agonist, a phenomenon termed "partial trapping" that is not fully understood (Blanpied *et al.*, 1997; Sobolevsky & Yelshansky, 2000; Mealing *et al.*, 2001; Bolshakov *et al.*, 2003; Kotermanski *et al.*, 2009). On the other hand, sequential or "foot-in-door" channel blockers physically occlude closure of the channel gate (Figure 1E).

The depth of the blocking site, size of the channel blocker, location of the channel gate, and gating-associated conformational changes all contribute to whether channels can close while the blocker is bound. These features dictate the structural interactions between channel blockers and the receptor's gating machinery, which in turn determine the influence that the channel blocker can reciprocally exert on gating transitions.

Bound channel blockers can affect gating transitions in three general ways. Blockers can:

1. Alter agonist binding and/or unbinding kinetics;
2. Stabilize channel open states;
3. Stabilize channel closed states.

For example, the binding of large sequential blockers to open channels prevents both transition of channels into closed states (Figure 1E) and agonist unbinding (Armstrong, 1971; Ruff, 1977; Neher & Steinbach, 1978; Benveniste & Mayer, 1995; Sobolevsky *et al.*, 1999). In contrast, smaller trapping blockers can interact with either open or closed channel states and can therefore have many possible effects on channel gating (Figure 1D). For example, trapping blockers can stabilize open or closed channels and/or facilitate entry into or recovery from desensitized states (Blanpied *et al.*, 2005; Glasgow *et al.*, 2017; Song *et al.*, 2018). The inherent intertwining of channel gating and block allows channel blockers to be leveraged as powerful tools for the study of ion channel structure and function.

Figure 1. Interplay between channel gating and open channel block.

A, Schematic depicting inhibition of current (black line) by a prototypical open channel blocker. Three agonist applications (green bars) are shown. The first agonist application in the absence of blocker shows the control response. The second agonist application, which follows the application and removal of a blocker (red bar), shows that the blocker cannot access its binding site when the channel is closed. The third agonist application, which is made in the presence of a blocker, shows that the blocker can access its binding site and inhibit agonist-activated current when the channel is in the open state. Entry of a blocker into open channels accelerates the apparent decay of the response and decreases the steady state response. Because the blocker cannot bind until the channel opens, peak current in response to the first agonist

application in the presence of the blocker may be unaffected, as shown here. However, if blocker binding is fast relative to current activation kinetics, the peak response may be reduced. **B**, Ion channels can transition between open, ion permeable states and closed, impermeable states. k_c is transition rate into closed state and k_o is transition rate into open state. **C**–**E,** The size of channel blocking compounds (red) and depth of the blocking site affects blocker interactions with the channel gate. **C**, Small channel blockers, such as inorganic cations, can block open channels without preventing channel closure or affecting gating transitions. k_{on} is blocker binding rate and k_{off} is blocker unbinding rate. When the channel is blocked by a blocker that does not interact with the gate, channel closing rate is k'_c and channel opening rate is k'_o. **D**, Small-to-intermediate-sized organic channel blockers can block open channels without preventing channel closure, but nevertheless can interact with the channel gate, either accelerating or decelerating gating transitions. When the channel is blocked by a blocker that interacts with the gate, channel closing rate is k''_c and channel opening rate is k''_o. **E**, Large, organic, sequential/foot-in-door blockers can block open channels and prevent channel closure. k'''_c is channel closing rate when the channel is blocked by a sequential/foot-in-the-door blocker.

1.2 IONOTROPIC GLUTAMATE RECEPTORS

iGluRs are members of the pore loop superfamily of ion channels, integral membrane proteins that mediate the majority of ion flux across neuronal membranes (Hille, 2001; Traynelis *et al.*, 2010). Fast excitatory synaptic transmission in the central nervous system is primarily mediated by iGluRs, and proper functioning of iGluRs is vital to synaptogenesis, synaptic plasticity, signal integration, and information transfer between neurons (Traynelis *et al.*, 2010; Paoletti *et al.*, 2013). Due to the integral roles iGluRs play in neuronal function and their ubiquitous expression, aberrant iGluR activity contributes to a wide variety of neuronal dysfunctions that can drive nervous system disorders (Zorumski & Olney, 1993; Javitt, 2004; Lau & Zukin, 2007; Bowie, 2008; Burnashev & Szepetowski, 2015; Lee *et al.*, 2015; Yuan *et al.*, 2015; Salpietro *et al.*, 2019).

iGluRs are divided into three main classes by structure: α-amino-3-hydroxyl-5-methyl-4-isoxazole-propionate receptors (AMPARs), kainate receptors (KARs), and the aforementioned NMDARs. A fourth division of the iGluR family, δ receptors, shares substantial sequence homology with other iGluRs. Surprisingly, despite forming functional ion channels (Ady *et al.*, 2014; Benamer *et al.*, 2018; Gantz *et al.*, 2020), δ receptors show no ligand-gated ion channel function (Yamazaki *et al.*, 1992; Araki *et al.*, 1993; Lomeli *et al.*, 1993; Orth *et al.*, 2013). All iGluRs assemble as complexes of four membrane-spanning subunits that form a central pore. Each iGluR subunit contributes exclusively to one subtype of iGluR: GluA1–4 form AMPARs, GluN1, GluN2A-D, and GluN3A-B form NMDARs, and GluK1–5 form KARs. Despite this wide diversity, all iGluR subunits possess a similar general structure (shown in Figure 2A using an NMDAR as an example) consisting of four discrete, semiautonomous domains, namely, an extracellular amino-terminal domain (ATD), an extracellular ligand-binding domain (LBD), a transmembrane domain (TMD), and an intracellular carboxy-terminal domain (CTD, which was deleted from the structure shown in Figure 2). Each iGluR subunit possesses an agonist-binding site located within

9

the LBD. The four TMDs of iGluRs form the pore, and thus the site of channel blocker binding (Figure 2B). Within the TMD lies the glutamine (Q) – arginine (R) – asparagine (N) (QRN) site, a site found at the tip of the re-entrant loop (M2 loop) in the iGluR pore (Figure 2C) that helps form the selectivity filter and plays a crucial role in the differential cation selectivity and channel block of the three iGluR classes (Hume *et al.*, 1991; Sommer *et al.*, 1991; Burnashev, Monyer, *et al.*, 1992; Burnashev, Schoepfer, *et al.*, 1992; Premkumar & Auerbach, 1996). Recent mid- and high-resolution structures of AMPAR (Twomey *et al.*, 2017, 2018; Twomey & Sobolevsky, 2018; Nakagawa, 2019) and NMDAR (Song *et al.*, 2018; Chou *et al.*, 2020) TMDs provided great insight into iGluR gating transitions and channel block.

1.3 NMDA RECEPTORS

NMDARs display numerous biophysical properties unique amongst the iGluR family, including high Ca^{2+} permeability, slow gating kinetics, dependence on co-agonism for gating, and voltage-dependent block by magnesium (Mg^{2+}) ions (Mayer *et al.*, 1984, 1987; Nowak *et al.*, 1984; Johnson & Ascher, 1987; Vicini *et al.*, 1998; Wyllie *et al.*, 1998; Traynelis *et al.*, 2010). These characteristics allow NMDARs to control Ca^{2+} influx during synaptic activity and therefore play a pivotal role in synaptic development and plasticity (Sheng *et al.*, 1994; Malenka & Bear, 2004; Akgül & McBain, 2016). NMDARs are obligate heterotetramers, typically composed of two GluN1 subunits (eight splice variants), which bind glycine or d-serine, and two GluN2 subunits (GluN2A–GluN2D), which bind glutamate. A third group of subunits, GluN3A-B, also bind glycine/d-serine (although d-serine acts only as a partial agonist (Grand *et al.*, 2018)) and can assemble with GluN1 and GluN2 subunits to form NMDARs activated by glutamate and glycine/d-serine. Interestingly, GluN3 subunits can also assemble just with GluN1 subunits to form unconventional

NMDARs activated solely by glycine/d-serine. However, these GluN1/3 receptors only pass weak currents in physiological conditions, so their role in neuronal function is largely unknown, though recent work has begun to shed light on their contribution to learning mechanisms (Grand *et al.*, 2018; Otsu *et al.*, 2019). Conventional NMDARs consisting of two GluN1 subunits and two GluN2 subunits rely on the binding of both glutamate and glycine/d-serine for activation (Johnson & Ascher, 1987; Mothet *et al.*, 2000) and, unlike AMPARs and KARs, require all four agonist binding domains to be occupied for the channel to transition to the open state (Benveniste & Mayer, 1991; Clements & Westbrook, 1991; Schorge *et al.*, 2005). Additionally, conventional NMDARs possess a conserved asparagine at the QRN site of each subunit (Figure 2C) that confers sensitivity to block by Mg^{2+} and high Ca^{2+} permeability, even relative to Ca^{2+}-permeable AMPAR and KARs (Mori *et al.*, 1992; Burnashev *et al.*, 1995; Premkumar & Auerbach, 1996).
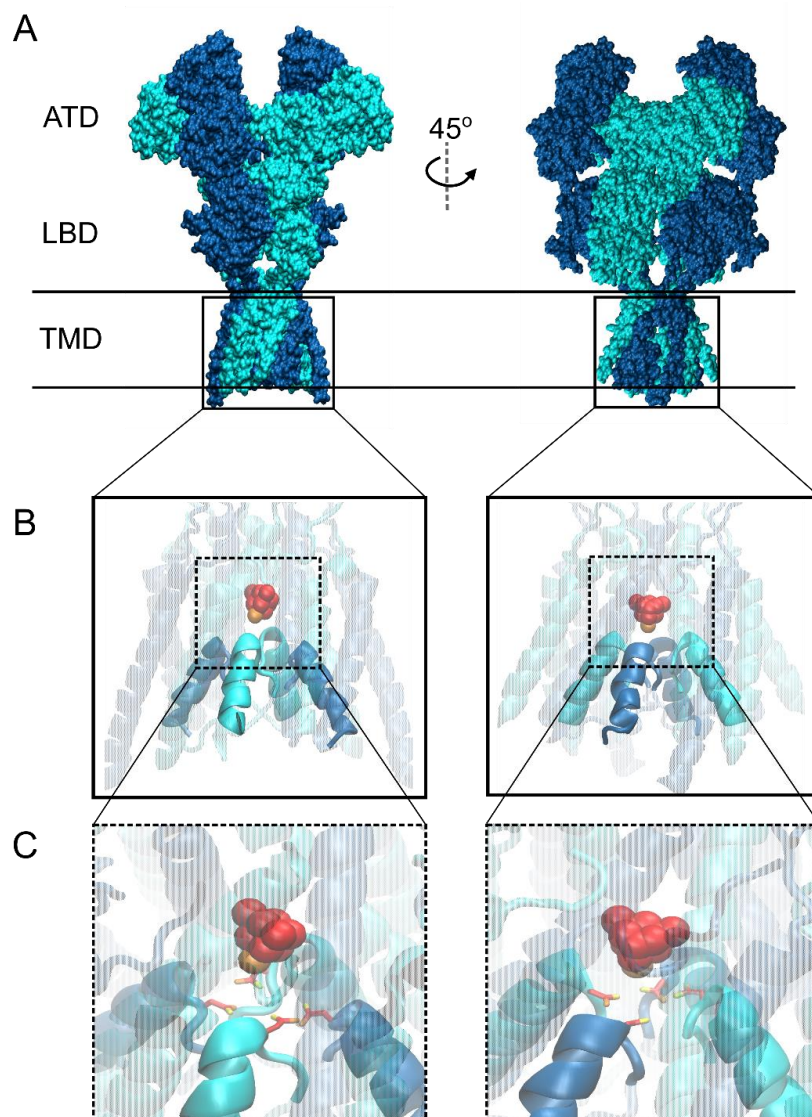
Figure 2. General NMDAR structure and putative blocking site.

A, Recently published structure of an NMDAR in an "active" state showing domain topology shared by all iGluR subtypes (ATD, amino-terminal domain; LBD, ligand-binding domain; TMD, transmembrane domain; Protein Data Bank (PDB) code 6WHT; (Chou *et al.*, 2020)). GluN1 subunit is depicted in dark blue and GluN2B in cyan. Horizontal lines show the approximate locations of the outer and inner surfaces of the membrane. **B**, Blow-up of NMDAR TMD (boxes in A) with docked channel blocker memantine (space-filling; carbons are red, nitrogen is orange) displaying typical site of channel block. Most channel blocking compounds show intimate interaction with the external tip of the iGluR selectivity filter formed by the re-

entrant M2 loops of each subunit (opaque; M1, M3, and M4 transmembrane helices are transparent for visualization of blocking site). **C**, Magnified view of memantine coordination by the QRN site asparagine residues GluN1 N616 and GluN2B N615 (shown in stick format), which are critically involved in NMDAR channel blocker binding (Mori *et al.*, 1992; Ferrer-Montiel *et al.*, 1998; Lemke *et al.*, 2014; Mesbahi-Vasey *et al.*, 2017; Fedele *et al.*, 2018). Autodock Vina was used for molecular docking of memantine to PDB 6WHT, and structural images were prepared using the program Visual Molecular Dynamics (VMD) (Humphrey *et al.*, 1996; Trott & Olson, 2010; Chou *et al.*, 2020).

1.3.1 Diversity of NMDAR subunits

NMDAR subtype is defined by the identity of the subunits that compose a receptor. The subunit composition of NMDARs, primarily the identity of the glutamate-binding GluN2 subunits, dictates their functional characteristics. Many key biophysical properties of NMDARs are governed by the GluN2 subunit. There is a clear dichotomy between the GluN2A-B subunits and the GluN2C-D subunits in terms of gating kinetics, channel conductance, ion permeability, and channel block. GluN1/2A and GluN1/2B diheteromers display far faster activation and desensitization kinetics, higher permeability to Ca^{2+}, greater single channel conductance, and stronger voltage-dependent channel block by Mg^{2+} than GluN1/2C and GluN1/2D diheteromers (Monyer *et al.*, 1992, 1994; Burnashev *et al.*, 1995; Kuner & Schoepfer, 1996; Qian *et al.*, 2005; Gielen *et al.*, 2009; Traynelis *et al.*, 2010; Siegler Retchless *et al.*, 2012; Wyllie *et al.*, 2013; Paoletti *et al.*, 2013; Glasgow *et al.*, 2015). Of particular importance to the work presented in this dissertation, desensitization of NMDARs substantially differs by subtype. While desensitization of GluN1/2C and GluN1/2D receptors is extremely weak, GluN1/2A and GluN1/2B receptors both display multiple forms of desensitization (Monyer *et al.*, 1994; Krupp *et al.*, 1996, 1998). The biophysical differences between NMDAR subtypes contribute to their role neuronal function, primarily by shaping the duration of the synaptic response, and thus have great influence on neuronal function and plasticity (Nevian & Sakmann, 2004, 2006; Urakubo *et al.*, 2008; Carter & Jahr, 2016). GluN2 subunit expression also differs greatly by subcellular localization, brain region, and over the course of development (Monyer *et al.*, 1992, 1994; Watanabe *et al.*, 1992; Ishii *et al.*, 1993; Akazawa *et al.*, 1994; Zhong *et al.*, 1995; Misra *et al.*, 2000; Brickley *et al.*, 2003; Dunah & Standaert, 2003; Martel *et al.*, 2012; Kellermayer *et al.*, 2018), further enhancing the impressive diversity of roles NMDARs can play in neuronal function.

Most characterization of the functional differences found between NMDAR subtypes has been performed on diheteromeric receptors, which are comprised of two GluN1 subunits and two identical GluN2 subunits, expressed in heterologous cells. However, nearly all neurons express multiple different GluN2 subunits, which can co-assemble to form triheteromeric receptors comprised of two GluN1 subunits and two different types of GluN2 subunits. Multiple studies have reported evidence of GluN1/2A/2B, GluN1/2A/2C, and GluN1/2B/2D receptors in neurons (Sheng *et al.*, 1994; Chazot *et al.*, 1994; Luo *et al.*, 1997; Chazot & Stephenson, 1997; Dunah *et al.*, 1998; Tovar & Westbrook, 1999; Misra *et al.*, 2000; Piña-Crespo & Gibb, 2002; Brickley *et al.*, 2003; Dunah & Standaert, 2003; Lu *et al.*, 2006; Brothwell *et al.*, 2008; Rauner & Köhr, 2011; Gray *et al.*, 2011; Tovar *et al.*, 2013; Huang & Gibb, 2014; Bhattacharya *et al.*, 2018; Swanger *et al.*, 2018). Furthermore, GluN1/2A/2B receptors are likely to be the most prevalent form of NMDAR expressed in the neocortex and hippocampus (Sheng *et al.*, 1994; Luo *et al.*, 1997; Gray *et al.*, 2011; Rauner & Köhr, 2011; Paoletti *et al.*, 2013; Tovar *et al.*, 2013; Stroebel *et al.*, 2018). Though triheteromeric receptors are difficult to study in isolation, recent advances have allowed for functional isolation or expression of modified isolated triheteromeric NMDARs in heterologous cells (Hansen *et al.*, 2014; Stroebel *et al.*, 2014; Yi *et al.*, 2017). Triheteromeric NMDARs display distinct biophysical characteristics relative to their diheteromeric counterparts. For example, GluN1/2A/2B receptors exhibit agonist affinity, maximal P_{open}, and gating kinetics intermediate to GluN1/2A and GluN1/2B diheteromers. Interestingly, the intermediate properties of triheteromers are not simply the average of the properties expressed by their related diheteromers but instead may be shifted toward one of the GluN2 subunits (Hansen *et al.*, 2014; Stroebel *et al.*, 2014, 2018; Sun *et al.*, 2017; Bhattacharya *et al.*, 2018), generating a sort of "dominance" by one of the two GluN2 subunits. In all, the 360 possible combinations of GluN1 splice variants and GluN2 subunits give NMDAR receptors the potential to express a staggering array of functional diversity.

15

1.3.2 NMDAR-mediated Ca^{2+} influx – a double-edged sword

NMDARs are involved in nearly all aspects of synaptic function and play a critical role in synaptic plasticity (Malenka & Bear, 2004; Lüscher & Malenka, 2012). The unique combination of slow gating kinetics, voltage-dependent channel block by Mg^{2+}, and high Ca^{2+} permeability possessed by NMDARs allows them to dictate the timing and magnitude of Ca^{2+} influx following synaptic activity. These features also allow NMDARs to act as coincidence detectors. For example, if one weak synaptic input releases glutamate onto a postsynaptic neuron, NMDARs will open, but will not pass substantial current due to Mg^{2+} block. However, if that same weak synaptic input releases glutamate while the postsynaptic cell is depolarized due to other strong synaptic inputs, Mg^{2+} will unblock from the NMDARs at the weak synapse and Ca^{2+} will flow into the postsynaptic compartment. Ca^{2+} acts as a powerful second messenger and initiates an extensive array of signaling cascades that can either weaken or strengthen synaptic connections. Intracellular Ca^{2+} concentration ([Ca^{2+}]$_i$) regulates the expression of synaptic plasticity, with brief bouts of high [Ca^{2+}]$_i$ pushing the synapse toward potentiation while sustained, small increases in [Ca^{2+}]$_i$ push synapses toward depression. Interestingly, recent studies have also reported that glutamate binding to the GluN2 subunit can elicit NMDAR-mediated synaptic depression without the need for Ca^{2+} influx (Nabavi *et al.*, 2013; Babiec *et al.*, 2014; Stein *et al.*, 2015). However, this non-ionotropic mechanism of NMDAR signaling still requires the maintenance of resting levels of [Ca^{2+}]$_i$ (Nabavi *et al.*, 2013), illustrating the importance of tightly regulated [Ca^{2+}]$_i$ to synaptic plasticity.

NMDAR-mediated Ca^{2+} influx is also heavily involved in neuronal survival. Physiological levels of NMDAR signaling promote activity of the cAMP response element binding protein (CREB), which is critical for both neuronal survival and plasticity, and the PI3K-Akt signaling pathway, which counters pro-apoptotic signaling (Brunet *et al.*, 1999; Hardingham, 2006; Dick &

Bading, 2010). However, excessive NMDAR activity leads to buildup of abnormally high $[Ca^{2+}]_i$ and subsequent activation of cell death signaling pathways (Choi, 1987, 1992; Tymianski *et al.*, 1993; Lau & Tymianski, 2010), a process known as excitotoxicity. Excitotoxicity is heavily involved in many neuropathologies and is a key feature of cell death following ischemia, Huntington's disease, Alzheimer's disease, and Alzheimer's disease-related dementias (Zorumski & Olney, 1993; Lipton, 1999, 2004; Hynd *et al.*, 2004; Koutsilieri & Riederer, 2007; Dong *et al.*, 2009; Olivares *et al.*, 2012; Mota *et al.*, 2014; Gardoni & Di Luca, 2015; Wang & Reddy, 2017). Some studies have suggested that subcellular localization or NMDAR subtype plays a role in determining whether NMDAR activity drives a cell toward survival rather than death, with GluN2A-containing synaptic receptors signaling for cell survival and GluN2B-containing extrasynaptic receptors eliciting cell death (Hardingham *et al.*, 2002; Léveillé *et al.*, 2008; Papadia *et al.*, 2008; Okamoto *et al.*, 2009; Kaufman *et al.*, 2012; Martel *et al.*, 2012; Yan *et al.*, 2020). However, other reports argue against such a clear dichotomy and show that synaptic, GluN2A-containing NMDARs are involved, perhaps even necessary and sufficient, for eliciting excitotoxicity (von Engelhardt *et al.*, 2007; Papouin *et al.*, 2012; Wroge *et al.*, 2012; Zhou *et al.*, 2013). Despite this debate, it is clear that NMDAR-mediated Ca^{2+} influx must be tightly regulated for maintenance of proper neuronal function.

1.4 NMDA RECEPTOR CHANNEL BLOCK

Due to their many roles in normal and pathological brain function, NMDARs are attractive targets for development of neurotherapeutics. NMDAR channel blockers are currently the most clinically useful NMDAR-targeting drugs and show great promise in the treatment of multiple nervous system disorders, including neurodegenerative diseases, major depressive disorder, and

neuron death following ischemia (Krystal *et al.*, 1994; Parsons, Danysz, & Quack, 1999; Parsons *et al.*, 2007; Zhou *et al.*, 2011; Danysz & Parsons, 2012; Persson, 2013; Kafi *et al.*, 2014; Abdallah *et al.*, 2015; Kong *et al.*, 2017; Nair & Sahoo, 2019). NMDAR channel blockers display a strikingly diverse array of clinical effects, despite sharing overlapping binding sites and a similar general mechanism of inhibition ((Ferrer-Montiel *et al.*, 1998; Kashiwagi *et al.*, 2002); the putative blocking site for memantine is shown in Figure 2B,C). For example, the clinically relevant blockers memantine and ketamine share similar chemical properties and binding kinetics but possess vastly different effects on brain function. Ketamine is a drug of abuse and poorly tolerated, but possesses impressive efficacy in treating neuropathic pain and major depressive disorder (Noppers *et al.*, 2010; Zhou *et al.*, 2011; Persson, 2013; Miller *et al.*, 2014; Abdallah *et al.*, 2015). On the other hand, memantine possesses weaker efficacy in treatment of neuropathic pain and little to no effect on major depressive disorder, but is well-tolerated with few side effects and shows efficacy in the treatment of neurodegenerative disorders such as Alzheimer's disease (Parsons, Danysz, & Quack, 1999; Parsons *et al.*, 2007; Lipton, 2004; Chen & Lipton, 2006; Olivares *et al.*, 2012; Gideons *et al.*, 2014; Kafi *et al.*, 2014; Amidfar *et al.*, 2018).

Despite the clinical relevance of organic NMDAR channel blockers, the most important NMDAR channel blocker is undoubtably the inorganic cation Mg^{2+}. In 1984, Linda Nowak and the Ascher lab reported that the peculiar voltage sensitivity displayed by NMDARs was a consequence of channel block by endogenous extracellular Mg^{2+} ions (Nowak *et al.*, 1984), a discovery soon replicated by another research group (Mayer *et al.*, 1984). Channel block by Mg^{2+} is perhaps the most distinctive feature of NMDARs and has extreme impact on normal brain function. Mg^{2+} blocks NMDARs at resting membrane potentials and unbinds as the cell becomes depolarized. The voltage-dependence of Mg^{2+} block enables NMDARs to act as coincidence detectors that sense postsynaptic depolarization near-simultaneously with presynaptic glutamate release. The coincidence-detection ability of NMDARs is a key component of synaptic plasticity

as well as learning and memory (Malenka, 1994; Rudhard *et al.*, 2003; Chen, Errington, *et al.*, 2009; Lüscher & Malenka, 2012). Mg^{2+} block is also critical for proper excitation-inhibition balance and autonomic nervous system function, as deficiencies in Mg^{2+} block can lead to severe pathological phenotypes and death (Single *et al.*, 2000; Rudhard *et al.*, 2003; Chen, Errington, *et al.*, 2009; Lemke *et al.*, 2014).

Likely due to its vast physiological and clinical relevance, the biophysical underpinnings of NMDAR channel block have been extensively studied. Most, if not all, well-characterized NMDAR channel blockers with slow kinetics display some degree of use dependence and voltage-dependent binding. Most NMDAR channel blockers are monovalent or divalent cations and display far greater inhibition at negative than at positive membrane potentials (MacDonald *et al.*, 1991; Parsons *et al.*, 1995; Antonov & Johnson, 1996; Blanpied *et al.*, 1997; Sobolevsky *et al.*, 1999; Sobolevsky & Yelshansky, 2000; Bolshakov *et al.*, 2003; Gilling *et al.*, 2009). Nearly all known NMDAR channel blockers show some effect on channel gating (Johnson & Qian, 2002) and channel blockers are found to modulate nearly every aspect of gating (Wright & Nowak, 1992; Vorobjev & Sharonova, 1994; Costa & Albuquerque, 1994; Antonov *et al.*, 1995; Benveniste & Mayer, 1995; Antonov & Johnson, 1996; Li-Smerin & Johnson, 1996; Blanpied *et al.*, 1997, 2005; Chen & Lipton, 1997; Sobolevsky *et al.*, 1998, 1999; Sobolevsky & Yelshansky, 2000; Sobolevsky, 2000; Glasgow *et al.*, 2017). The striking diversity in the clinical effects of NMDAR channel blockers may in part arise from their diverse effects on channel gating.

1.4.1 Sequential blockers of NMDARs prevent channel closure and agonist dissociation

The sequential/foot-in-door blockers 9-aminoacridine (Table 1), tetrapentylammonium, and the amantadine derivative IEM-1857 are thought to force NMDARs to remain in open states by sterically prohibiting gate closure after entering the channel (Benveniste & Mayer, 1995;

Koshelev & Khodorov, 1995; Antonov & Johnson, 1996; Sobolevsky *et al.*, 1999; Sobolevsky, 2000). Importantly, occupancy of the channel by IEM-1857, tetrapentylammonium, or 9-aminoacridine also prevents agonist dissociation and channel desensitization (Benveniste & Mayer, 1995; Antonov & Johnson, 1996; Sobolevsky *et al.*, 1999), suggesting that blocker unbinding and subsequent channel closure are required for agonist dissociation. This finding is consistent with models of sequential channel block of nAChRs proposed by (Adams, 1975, 1976; Ruff, 1977; Neher & Steinbach, 1978). An experimental procedure used to test whether a channel blocker prevents channel closure and agonist dissociation is to determine if the blocker induces "tail currents". A tail current is a transient increase in receptor-mediated current observed upon rapid and simultaneous removal of blocker and agonist from the extracellular solution. If a blocker prevents channel closure, channels pass through the open, unblocked state following blocker unbinding, resulting in a tail current. However, any antagonist that unblocks more quickly than agonists unbind can induce tail currents; thus, observation of tail currents does not provide unambiguous evidence that a blocker acts via a sequential mechanism. More powerful evidence that a blocker prevents channel closure can be provided by (1) observation that a blocker chops single-channel currents into "bursts" of brief openings, and that the total channel open time during bursts is independent of blocker concentration (Neher & Steinbach, 1978), and (2) observation that the blocker concentration that inhibits responses by 50% (the IC_{50}) is inversely proportional to the receptor's P_{open}, a prediction that can be tested, e.g., by recording the IC_{50} of a blocker over a range of agonist concentrations (Johnson & Qian, 2002). The finding that channel occupation by sequential blockers prevents agonist unbinding as well as channel closing provided fundamental information on state transitions of ligand-gated ion channels.

Organic channel blocking compounds were remarkably useful in determining the location of the channel gate itself. The size of a blocking molecule is a key determinant of whether the blocker prevents channel closure or is trapped in the channel upon gate closure. Experiments

comparing block by IEM-1857 and the similar but smaller blocker IEM-1754 (Table 1) found that while binding of IEM-1857 prevented channel closure independent of voltage, IEM-1754 only prevented channel closure at relatively depolarized membrane potentials. At more hyperpolarized potentials, IEM-1754 is "pulled" by the membrane electric field deeper into the channel where it no longer prevents channel closure, instead acting as a trapping channel blocker (Antonov & Johnson, 1996). The voltage dependence of IEM-1754 block, as well as its interactions with permeant ions, demonstrated that IEM-1754 has two blocking modes, one in which the blocker associates with a shallower site and places the bulk of the molecule in the way of the gate, and a second in which the blocker associates with a deeper site and permits closure of the gate (Antonov & Johnson, 1996; Antonov *et al.*, 1998; Qian & Johnson, 2002). This finding strongly supported the idea that the NMDAR channel gate lies at the extracellular entrance to the channel, an idea that was recently validated by crystal and cryo-EM structures of ligand-bound NMDARs (Tajima *et al.*, 2016; Chou *et al.*, 2020).

1.4.2 Channel block by Mg^{2+} does not appear to affect NMDAR state transitions

The majority of NMDAR channel blockers affect gating, but at least one blocker exists as an exception to this rule: Mg^{2+} (Table 1). Binding of Mg^{2+} to the NMDAR channel does not prevent gate closure, agonist dissociation, or desensitization (Nowak *et al.*, 1984; Ascher & Nowak, 1988; Benveniste & Mayer, 1995; Sobolevsky & Yelshansky, 2000). Further evidence that Mg^{2+} has no effect on channel gating is provided by the relation between its equilibrium dissociation constant (K_d) and IC_{50}. The relation between K_d and IC_{50} directly depends on how a channel blocker affects channel transitions after binding. $K_d \approx IC_{50}$ suggests that a blocker has no effect on gating, $K_d > IC_{50}$ implies that a blocker stabilizes channel closed states, and $K_d < IC_{50}$ implies that a blocker stabilizes channel open states. The latter is the case for sequential blockers, which inhibit less

21

effectively as P_{open} decreases ($IC_{50} = K_d/P_{open}$; (Hille, 2001; Johnson & Qian, 2002)). Mg^{2+} boasts nearly equivalent K_d and IC_{50} (Qian *et al.*, 2002), suggesting that Mg^{2+} occupancy of the channel has no effect on state transitions.

The unusual ability of Mg^{2+} to block without altering gating could be due to its small size. A large conformational change in the extracellular region of the NMDAR channel is associated with gating, a conclusion supported by structural studies [(Chou *et al.*, 2020) and the observation that large organic blockers prevent channel closure. Although smaller organic blockers generally permit channel closure, stabilizing or destabilizing interactions with channel residues may alter channel gating kinetics. It is possible that the small size of Mg^{2+} (which is likely to be mostly dehydrated when blocking the channel (Mesbahi-Vasey *et al.*, 2017)), coupled with its limited interactions with channel residues outside of the ion selectivity filter (Mesbahi-Vasey *et al.*, 2017), allows binding in the NMDAR channel without affecting gating machinery. Also, in contrast to most organic blockers, Mg^{2+} has not been directly shown to act as a use-dependent open channel blocker or as a trapping blocker. Mg^{2+} displays extremely rapid binding and unbinding kinetics (Nowak *et al.*, 1984; Ascher & Nowak, 1988; Sobolevsky & Yelshansky, 2000), preventing accurate determination in whole-cell recordings of the rapid component of block or unblock, measurements required for demonstration of use dependence and trapping. Kinetic modeling studies, however, suggested that Mg^{2+} does indeed act as an open channel blocker (Sobolevsky & Yelshansky, 2000).

Despite the lack of effects of Mg^{2+} block on NMDAR gating, depolarization-induced Mg^{2+} unblock clearly depends on gating. Mg^{2+} unblock from GluN1/2A and GluN2B receptors displays a slow component as well as an extremely rapid component (Spruston *et al.*, 1995; Vargas-Caballero & Robinson, 2003; Kampa *et al.*, 2004; Clarke & Johnson, 2006, 2008; Clarke *et al.*, 2013). Although kinetic models in which Mg^{2+} block affects gating transitions and/or agonist binding rates reproduced slow Mg^{2+} unblock (Vargas-Caballero & Robinson, 2003; Kampa *et al.*,

22

2004), substantial experimental evidence demonstrated that Mg^{2+} does not affect NMDAR state transitions (Nowak *et al.*, 1984; Ascher & Nowak, 1988; Benveniste & Mayer, 1995; Sobolevsky & Yelshansky, 2000). This disagreement was reconciled by the discovery of the inherent (i.e., Mg^{2+}-independent) voltage-sensitivity of NMDAR gating, which underlies the slow component of Mg^{2+} unblock (Clarke & Johnson, 2008; Clarke *et al.*, 2013). Thus, the interplay between Mg^{2+} block and NMDAR gating is unidirectional, whereas Mg^{2+} block depends on NMDAR gating, but NMDAR gating is unaffected by Mg^{2+} block.

1.4.3 Trapping channel blockers modulate NMDAR state transitions

Trapping channel blockers display more subtle effects on gating than sequential blockers. Early studies using a combination of patch-clamp electrophysiology and kinetic modeling concluded that the amino-adamantane derivatives memantine and amantadine and the phencyclidine derivative NEFA have clear effects on channel gating (Blanpied *et al.*, 1997; Chen & Lipton, 1997; Dilmore & Johnson, 1998; Sobolevsky *et al.*, 1998). Initial proposals for the effects of amino-adamantane derivatives on NMDAR gating were wide-ranging, including models that suggested memantine and amantadine could stabilize open receptor states, as well as models that suggested memantine may stabilize closed receptor states (Blanpied *et al.*, 1997; Chen & Lipton, 1997; Sobolevsky *et al.*, 1998). It is possible that these discrepancies arose from the abilities of amino-adamantane derivatives to escape from some blocked channels after agonist removal (partial trapping), and to inhibit NMDARs via association with a site accessible in the absence of agonist (Blanpied *et al.*, 1997; Chen & Lipton, 1997; Sobolevsky *et al.*, 1998; Kotermanski *et al.*, 2009; Glasgow *et al.*, 2018).

Thorough evidence that amino-adamantane derivatives affect closed-state transitions came through investigation of the discrepancy between the K_d and IC_{50} of amantadine.

Amantadine's K_d (110 μM) is considerably greater than its IC_{50} (~35 μM; (Sobolevsky & Koshelev, 1998; Sobolevsky *et al.*, 1998; Bolshakov *et al.*, 2003; Blanpied *et al.*, 2005)). $K_d > IC_{50}$ implies that a blocker's mechanism of inhibition likely involves stabilization of channel closed states, either through decreasing the rate of channel opening, increasing the rate of channel closure, or both. Such blockers therefore have two inhibitory actions: (1) blocking current flow through open channels and (2) stabilization of closed channels. Amantadine is an example of such a dual-mechanism channel inhibitor. Investigation of amantadine block of single-channel and whole-cell NMDAR current revealed that binding of amantadine not only accelerates channel closure, but that this acceleration of channel closure is actually the predominant mechanism of inhibition by amantadine at concentrations lower than 100 μM (Blanpied *et al.*, 2005).
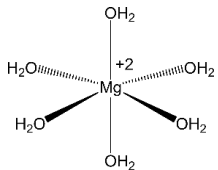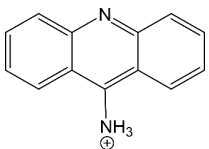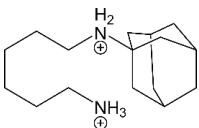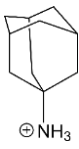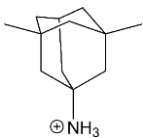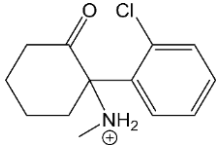
Recent studies reported additional drug-specific and NMDAR subtype-specific effects of channel blockers on gating transitions. Investigation of mechanisms by which memantine and ketamine preferentially target distinct populations of NMDARs led to the discovery that memantine and ketamine have differential, subtype-specific effects on NMDAR desensitization (Glasgow *et al.*, 2017). While ketamine accelerated recovery from desensitization of GluN1/2B receptors, memantine binding profoundly slowed recovery from desensitization of GluN1/2A receptors. The effect of memantine on GluN1/2A receptor desensitization was not observed in low-Ca^{2+} conditions, suggesting that memantine stabilizes a Ca^{2+}-dependent desensitized state of GluN1/2A receptors. A comparison of IC_{50} values measured in low and high Ca^{2+} conditions with K_d values predicted by a kinetic model found that in high Ca^{2+}, $K_d > IC_{50}$, whereas in low Ca^{2+}, $K_d \approx IC_{50}$, suggesting that memantine only alters GluN1/2A gating when Ca^{2+}-dependent desensitization can occur (Glasgow *et al.*, 2017).

Visualization of NMDARs bound to trapping channel blockers was provided by recent structural studies. Song et al. crystalized the closed GluN1/2B channel in complex with the high affinity blocker MK-801 and utilized long-timescale molecular dynamics to investigate the

mechanism of block by MK-801 and memantine (Song *et al.*, 2018). Both blockers were found to bind within the central cavity of the ion channel and promote closure of the channel gate, perhaps via a mechanism similar to amantadine (Blanpied *et al.*, 2005). Although this result may seem to contrast with the previous finding that memantine did not affect GluN1/2B receptor desensitization (Glasgow *et al.*, 2017), it is important to note that (1) memantine could affect GluN1/2B channel closure without affecting desensitization, and (2) the crystalized MK-801-NMDAR construct lacked both the ATD and CTD, which play key roles in gating and desensitization (Ehlers *et al.*, 1996; Krupp *et al.*, 1996, 1998, 2002; Villarroel *et al.*, 1998; Vissel *et al.*, 2002; Maki *et al.*, 2012; Chou *et al.*, 2020). Stabilization of closed channels by NMDAR channel blockers could have profound physiological implications by effectively increasing the potency of blockers under specific conditions.

Table 1. NMDAR channel blockers and their effects on gating.

Magnesium is depicted coordinating six water molecules (waters are replaced with the critical Asn residues when Mg^{2+} is blocking the channel), and all organic blockers are depicted in bond-line format. Blockers structures are scaled to depict approximate relative sizes.

Compound	Structure	Type of Blocker	Effects on Gating
Magnesium		Unclear - due to fast unblocking kinetics, trapping of Mg^{2+} has not been directly demonstrated.	None (Nowak *et al.*, 1984; Ascher & Nowak, 1988; Sobolevsky & Yelshansky, 2000; Johnson & Qian, 2002).
9-aminoacridine		Sequential (Benveniste & Mayer, 1995; Koshelev & Khodorov, 1995).	Stabilizes open state, prevents agonist dissociation (Benveniste & Mayer, 1995; Koshelev & Khodorov, 1995).
IEM-1754		Depolarized potentials: sequential. Strongly negative potentials: trapping (Antonov & Johnson, 1996).	Depolarized potentials: Stabilizes open state (Antonov & Johnson, 1996).
Amantadine		Partial trapping (Blanpied *et al.*, 1997; Sobolevsky & Yelshansky, 2000).	Accelerates channel closure of native NMDARs and GluN1/2B receptors (Blanpied *et al.*, 2005).
Memantine		Partial trapping (Blanpied *et al.*, 1997; Chen & Lipton, 1997; Mealing *et al.*, 1999; Kotermanski & Johnson, 2009; Kotermanski *et al.*, 2009).	Slows GluN1/2A receptor recovery from Ca^{2+}-dependent desensitization (Glasgow *et al.*, 2017).
Ketamine		Trapping (MacDonald *et al.*, 1987; Mealing *et al.*, 1999).	Accelerates GluN1/2B receptor recovery from desensitization (Glasgow *et al.*, 2017).

1.5 PHARMACOLOGICAL TARGETING OF SPECIFIC NMDARS STATES

Many NMDAR channel blockers, including amantadine and memantine, act by blocking and stabilizing NMDAR closed states (Blanpied *et al.*, 2005; Glasgow *et al.*, 2017). Stabilization of closed states by a channel blocker effectively enhances the potency of the blocker (Section 1.4.3). The ability to both block and modulate the gating of NMDAR receptors could lend additional specificity to channel blockers. Desensitized states are closed channel states the occupancy of which can vary by NMDAR subtype and physiological context (Benveniste *et al.*, 1990; Krupp *et al.*, 1996, 1998; Villarroel *et al.*, 1998; Glasgow *et al.*, 2017). Therefore, targeting specific receptor desensitized states could allow for preferential inhibition of select populations of NMDARs based on NMDAR subtype, physiological context, or both. This concept, known as state-specific or context-specific antagonism, is a rational strategy for the design of improved neurotherapeutic agents with reduced off-target and negative side effects. In this section, I will provide background on a context and subtype specific form of NMDAR desensitization, Ca^{2+}-dependent desensitization, and discuss the rationale behind the targeting of Ca^{2+}-dependent desensitized receptor states for neurotherapeutic purpose.

1.5.1 Targeting NMDA receptor desensitization

There are multiple distinct NMDAR desensitization processes, including glycine-dependent desensitization, Ca^{2+}-dependent desensitization, and glycine-and-Ca^{2+}-independent desensitization (Mayer *et al.*, 1989; Benveniste *et al.*, 1990; Lerma *et al.*, 1990; Lester *et al.*, 1990; Sather *et al.*, 1990; Legendre *et al.*, 1993; McBain & Mayer, 1994). Glycine-dependent desensitization can only occur in subsaturating glycine concentrations, and results from negative allosteric interaction between the glutamate and glycine binding sites in which the binding of

glutamate to the GluN2 subunit decreases the affinity of glycine to the GluN1 subunit. This reduction in affinity encourages glycine to unbind from the GluN1 subunit, which results in channel closure (Benveniste *et al.*, 1990; Lester *et al.*, 1993). Since the decay in the NMDAR response is a direct consequence of agonist unbinding, there is some debate as to whether glycine-dependent desensitization is a form of "true" desensitization (McBain & Mayer, 1994), as desensitization is canonically defined as a decrease in receptor P_{Open} while agonist is still bound (Katz & Thesleff, 1957). Mechanisms of glycine-and-Ca^{2+}-independent desensitization (Sather *et al.*, 1990) are less clear, but most evidence suggests that glycine-and-Ca^{2+}-independent desensitization is mediated through the extracellular NTD regions of GluN2 subunits in a subtype-dependent manner (Krupp *et al.*, 1998; Villarroel *et al.*, 1998).

Ca^{2+}-dependent desensitization results from an increase in $[Ca^{2+}]_i$, due either to NMDAR-mediated Ca^{2+} influx or Ca^{2+} from other sources (Legendre *et al.*, 1993; Vyklický, 1993; Medina *et al.*, 1994). The terms used to refer to desensitization processes that are Ca^{2+}-dependent has been inconsistent and include glycine-independent desensitization and the commonly-used Ca^{2+}-dependent inactivation (Legendre *et al.*, 1993; Tong & Jahr, 1994; Tong *et al.*, 1995; Krupp *et al.*, 2002; Iacobucci & Popescu, 2020). Regardless of name, all share the common features of (1) decreasing NMDAR P_{Open} while agonist is still bound and (2) dependence on elevation of $[Ca^{2+}]_i$. Therefore, unless otherwise stated, I will be referring to all desensitization processes regulated by $[Ca^{2+}]_i$ as Ca^{2+}-dependent desensitization (CDD) in this dissertation.

The mechanisms underlying CDD involve a combination of molecular interactions that are not yet fully understood, but the Ca^{2+}-binding/Ca^{2+}-activated proteins calmodulin (CaM), α-actinin, and calcineurin have all been implicated in CDD. CDD is certainly mediated, at least in part, through the binding of Ca^{2+}-bound CaM to the GluN1 C-terminal domain (CTD; (Ehlers *et al.*, 1996; Zhang *et al.*, 1998; Krupp *et al.*, 1999; Rycroft & Gibb, 2002)). α-actinin binds to the GluN1 CTD and has been proposed to stabilize an open, conducting NMDAR state (Wyszynski *et al.*,

1997; Krupp *et al.*, 1999). The interplay between CaM and α-actinin is complex, with evidence suggesting that Ca^{2+}-bound CaM displaces α-actinin from its binding site on the GluN1 CTD, promoting desensitization (Wyszynski *et al.*, 1997; Krupp *et al.*, 1999; Merrill *et al.*, 2007). Calcineurin has been suggested to interact with the GluN2A CTD and promote CDD through interaction with CaM (Tong *et al.*, 1995; Krupp *et al.*, 2002; Rycroft & Gibb, 2004). NMDAR CDD also depends on NMDAR subtype, but the mechanism underlying CDD in each subtype is unclear. CDD has been reported in GluN1/2A, GluN1/2B, and GluN1/2D receptors, but not GluN1/2C receptors (Krupp *et al.*, 1996; Medina *et al.*, 1996; Iacobucci & Popescu, 2020). GluN1/2A receptors are the only subtype to show CDD in all studies concerning NMDAR CDD, while studies of GluN1/2B receptor and GluN1/2D receptors have provided less consistent findings. Regardless of the underlying mechanisms, CDD is a key part of an endogenous negative-feedback loop that reduces Ca^{2+} influx through NMDARs in response to increases in $[Ca^{2+}]_i$ and thus protects neurons from excessive buildup of $[Ca^{2+}]_i$.

Dependence on context (i.e., increased $[Ca^{2+}]_i$) and NMDAR subtype make CDD an attractive target for pharmacological modulation. Indeed, previous data from our lab revealed that memantine stabilizes a Ca^{2+}-dependent desensitized state of GluN1/2A receptors (Glasgow *et al.*, 2017). Enhancement of CDD by memantine suggests a logical mechanism for neuroprotection: preferential inhibition of NMDARs in cellular populations subjected to pathological levels of Ca^{2+} influx, i.e., NMDARs likely to mediate excitotoxic cell death (Zorumski & Olney, 1993; Rothman & Olney, 1995; Okamoto *et al.*, 2009). In turn, characterization of the memantine-NMDAR complex may give insight into the structural underpinnings and mechanisms of CDD. The goals of the research presented in this dissertation are:

1. To characterize the relation between NMDAR CDD and channel block by memantine.

2. To investigate the structural basis of the relation between CDD and channel block.

3. To better understand mechanisms of channel block through characterization of novel NMDAR channel blockers.

2.0 CA^{2+}-DEPENDENT DESENSITIZATION REGULATES SUBTYPE-SPECIFIC BLOCK OF NMDA RECEPTORS BY MEMANTINE

2.1 OVERVIEW

N-methyl-D-aspartate receptors (NMDARs) are key mediators of neuronal Ca^{2+} influx. NMDAR-mediated Ca^{2+} influx plays a central role in synaptogenesis, synaptic plasticity, dendritic integration, and neuronal survival. However, excessive NMDAR activity can lead to buildup of pathological levels of Ca^{2+} inside neurons, which initiates cellular signaling pathways that result in neuronal death. Thus, drugs targeting NMDARs are of great clinical interest. The NMDAR channel blocker memantine is a well-tolerated Alzheimer's disease medication that also shows promise in treatment of other neurological disorders. Interestingly, memantine enhances desensitization of NMDARs in a subtype- and Ca^{2+}-dependent manner. Furthermore, memantine inhibits NMDARs more effectively in conditions that allow for increased Ca^{2+} influx and buildup, which suggests that memantine could preferentially target overactive NMDAR subpopulations. However, the direct effect of intracellular Ca^{2+} on NMDAR inhibition by memantine has not been systematically examined. Utilizing specially designed Ca^{2+}-buffering solutions and whole-cell patch-clamp recordings, we demonstrated that NMDAR channel block by memantine is directly related to intracellular Ca^{2+} concentration. We discovered that memantine potency increases alongside increasing intracellular Ca^{2+}, and that the effect of intracellular Ca^{2+} on memantine action depends on NMDAR subtype. These results present a previously unexamined form of state-specific antagonism, Ca^{2+}-dependent NMDAR channel block, that could have a profound impact on the design of drugs that selectively target NMDAR subpopulations involved in disease.

31

2.2 INTRODUCTION

NMDA receptors (NMDARs) are ionotropic glutamate receptors that possess a unique set of biophysical properties, including dependence of gating on co-agonism, voltage-dependent block by Mg^{2+}, high permeability to Ca^{2+}, and slow gating kinetics (Mayer *et al.*, 1984, 1987; Nowak *et al.*, 1984; Johnson & Ascher, 1987; Vicini *et al.*, 1998; Wyllie *et al.*, 1998; Traynelis *et al.*, 2010). This unique combination of properties allows NMDARs to control the magnitude and timing of Ca^{2+} influx during synaptic activity. Ca^{2+} influx due to NMDAR activity is vital to many aspects of neuronal function, including neuronal survival, synaptic development, and synaptic plasticity (Sheng *et al.*, 1994; Malenka & Bear, 2004; Hardingham, 2006; Akgül & McBain, 2016).

The magnitude of NMDAR-mediated Ca^{2+} influx is a crucial determinant of the signaling pathways elicited by NMDAR activity. Low levels of NMDAR activity sustain small, prolonged increases of intracellular Ca^{2+} concentration ($[Ca^{2+}]_i$), which supports signaling cascades involved in synaptic depression. In contrast, intense, transient NMDAR activation leads to brief bouts of high $[Ca^{2+}]_i$, which activates signaling cascades that drive synaptic potentiation (Lisman *et al.*, 2002; Lüscher & Malenka, 2012). Sustained high $[Ca^{2+}]_i$, however, initiates signaling cascades that result in neuronal death (Choi, 1987, 1992; Tymianski *et al.*, 1993; Lau & Tymianski, 2010). Cell death elicited by NMDAR overactivation, known as excitotoxicity, is a key feature of many nervous system disorders including Alzheimer's disease, Alzheimer's disease-related dementias, Huntington's disease, and cell death following stroke or ischemia (Zorumski & Olney, 1993; Lipton, 1999, 2004; Hynd *et al.*, 2004; Koutsilieri & Riederer, 2007; Dong *et al.*, 2009; Olivares *et al.*, 2012; Mota *et al.*, 2014; Gardoni & Di Luca, 2015; Wang & Reddy, 2017). Thus, NMDAR-mediated Ca^{2+} influx must be tightly regulated for proper nervous system function.

Although NMDARs are attractive targets for modulation by neurotherapeutic drugs, NMDAR pharmacology has proven remarkably complex. Due to the near-ubiquitous involvement

of NMDARs in normal neuronal function, arbitrary inhibition of NMDARs generates unacceptable side effects (Olney *et al.*, 1989; Zorumski & Olney, 1993; Krystal *et al.*, 1994; Muir, 2006). The specific inhibition of select subpopulations of NMDARs involved in disease may provide an avenue around the detrimental side effects of broad-scale NMDAR inhibition. A potential strategy for targeting specific NMDAR subpopulations is to target NMDARs based on subunit composition. NMDAR subunits are encoded by seven genes: a single GRIN1 gene encodes the GluN1 subunit, four GRIN2 genes encode GluN2A-GluN2D subunits, and two GRIN3 genes encode GluN3A-GluN3B subunits. To add to this broad subunit diversity, the GluN1 subunit also has 8 distinct splice variants (Traynelis *et al.*, 2010). NMDARs are heterotetrameric complexes typically assembled from two obligatory GluN1 subunits and two GluN2 subunits (Karakas & Furukawa, 2014; Lee *et al.*, 2014). The specific combination of GluN1 splice variants and GluN2 subunits governs many NMDAR characteristics including subcellular localization, intracellular signaling partners, and biophysical features such as agonist affinity, gating kinetics, channel block, and pharmacology (Hardingham & Bading, 2010; Siegler Retchless *et al.*, 2012; Paoletti *et al.*, 2013; Hansen *et al.*, 2014; Glasgow *et al.*, 2015; Stroebel *et al.*, 2018; Yi *et al.*, 2018).

Most attempts to selectively target NMDAR subpopulations have focused on developing drugs that can distinguish between NMDARs that contain different GluN2 subunits. In addition, most characterization of subtype-selective inhibitors of NMDAR has been performed on diheteromeric receptors composed of two GluN1 subunits and two identical GluN2 subunits. However, neurons can also co-express multiple different GluN2 subunits that can co-assemble to form complex triheteromeric receptors (Tovar *et al.*, 2013; Bhattacharya *et al.*, 2018; Stroebel *et al.*, 2018; Yi *et al.*, 2018), the pharmacology of which is poorly understood. Perhaps due to this vast subtype diversity, subtype-selective antagonism has not yet produced clinically useful drugs, although some compounds have shown promise (Preskorn *et al.*, 2008; Ibrahim *et al.*, 2012).

The most clinically successful NMDAR antagonists are channel blockers. Open channel blockers are drugs that bind in and prevent ion flux through open ion channels. However, most open channel blockers can elicit powerful and dangerous side effects, likely due to indiscriminate inhibition of large populations of NMDARs (Olney *et al.*, 1989; Zorumski & Olney, 1993; Krystal *et al.*, 1994). In stark contrast to other moderate and high-affinity NMDAR channel blockers, the adamantane derivative memantine is remarkably well-tolerated (Parsons, Danysz, & Quack, 1999; Chen & Lipton, 2006). Memantine is a clinically approved treatment for Alzheimer's disease (Witt *et al.*, 2004; Mecocci *et al.*, 2009; Danysz & Parsons, 2012) and shows promise in treating many other disorders including Parkinson's disease, Alzheimer's disease-related dementias, post-stroke cell death and dementia, schizophrenia, and disorders associated with rare *de novo* mutations of NMDAR subunits (Sonkusare *et al.*, 2005; Lipton, 2006; Parsons *et al.*, 2007; Berthier *et al.*, 2009; Olivares *et al.*, 2012; Pierson *et al.*, 2014; Johnson *et al.*, 2015; Di Iorio *et al.*, 2017; Zheng *et al.*, 2018). A leading hypothesis regarding the clinical safety of memantine is that memantine may preferentially inhibit subpopulations of NMDARs involved in disease (Zhao *et al.*, 2006; Léveillé *et al.*, 2008; Okamoto *et al.*, 2009; Xia *et al.*, 2010), which may arise from the ability of memantine to modulate NMDAR gating.

Memantine acts not only by blocking ion flux through NMDARs, but also by stabilizing a desensitized state of the NMDAR channel. Desensitized states are closed, agonist-bound states the occupancy of which can vary significantly by NMDAR subtype and physiological context (Benveniste *et al.*, 1990; Krupp *et al.*, 1996, 1998; Villarroel *et al.*, 1998; Glasgow *et al.*, 2017). We recently reported that memantine enhances NMDAR desensitization in a subtype- and context-specific manner (Glasgow *et al.*, 2017). Memantine profoundly slows recovery of GluN1/2A receptors, but not GluN1/2B receptors, from desensitization. The effect of memantine on desensitization was absent in low extracellular Ca^{2+}, and memantine inhibition of GluN1/2A receptors was shown to be more powerful in conditions supporting high levels of Ca^{2+} influx

(Glasgow *et al.*, 2017). These data suggest that memantine stabilizes a Ca^{2+}-dependent desensitized state of the GluN1/2A receptor. Ca^{2+}-dependent desensitization (CDD; also termed Ca^{2+}-dependent inactivation) is elicited by increases in $[Ca^{2+}]_i$ (Legendre *et al.*, 1993; Rozov & Burnashev, 2016; Iacobucci & Popescu, 2017, 2020) and acts as an endogenous negative-feedback loop by reducing NMDAR-mediated Ca^{2+} influx in response to increasing $[Ca^{2+}]_i$. Stabilization of a Ca^{2+}-dependent state by memantine offers a rational mechanism by which memantine can target specific NMDAR subpopulations involved in disease: preferential inhibition of NMDARs in neurons experiencing long durations of high Ca^{2+} influx, i.e. subpopulations of NMDARs involved in excitotoxicity. Selective inhibition of overactive NMDARs is an ideal property of a neuroprotective drug, and the elucidation of the mechanistic underpinnings of Ca^{2+}-dependent inhibition of NMDARs by memantine may aid in the design of more efficacious neuroprotectants.

Here we further investigated the relation between NMDAR CDD and the mechanism of action of memantine. Through electrophysiological recordings and manipulation of $[Ca^{2+}]_i$, we found that memantine inhibition of GluN2A-containing NMDARs is directly dependent on $[Ca^{2+}]_i$. This $[Ca^{2+}]_i$ dependence of memantine action is also dependent on the ability of the receptor to access a Ca^{2+}-dependent desensitized state. We found that although both GluN1/2A and GluN1/2A receptors exhibit CDD, $[Ca^{2+}]_i$-dependent inhibition by memantine is a GluN2A-specific phenomenon, suggesting that the relation between CDD and memantine inhibition is subtype-specific. Together, these results strongly support the hypothesis that memantine stabilizes a Ca^{2+}-dependent desensitized state of GluN2A-containing NMDARs and present a previously uncharacterized form of state-specific NMDAR antagonism.

2.3 MATERIALS AND METHODS

2.3.1 Cell culture and transfection

Experiments were performed in tsA201 cell cultures (European Collection of Authenticated Cell Cultures) or primary cortical neuron cultures. tsA201 cells were maintained as previously described (Glasgow & Johnson, 2014) in Dulbecco's modified Eagle's medium (DMEM) supplemented with 10% fetal bovine serum and 1% GlutaMAX (Thermo Fisher Scientific). Cells were plated at a density of 10^5 cells/dish in 35 mm petri dishes on 15 mm glass coverslips treated with poly D-lysine (0.1 mg/mL) and rat-tail collagen (0.1 mg/mL). 18-24 hours after plating, the cells were transfected using FuGENE 6 (Promega) with complementary DNA (cDNA) coding for enhanced green fluorescent protein (EGFP; Genbank ACS32473 in pCI-neo or pIRES) to identify transfected cells, WT rat GluN1-1a (GluN1; GenBank X63255 in pcDNA3.1 or U08261 in pCI-neo), and either GluN2A (GenBank M91561 in pcDNA1 or D13211 in pIRES), GluN2B (GenBank M91562 in pcDNA1), GluN2C (GenBank M91562 in pcDNA1), or GluN2D (GenBank L31611 in pcDNA1). EGFP was expressed using one of two plasmids: pCI-neo:EGFP:GluN1-1a or EGFP:pIRES:GluN2A, both kind gifts from Dr. Kasper Hansen. pCI-neo:EGFP:GluN1-1a was constructed by inserting cDNA encoding EGFP in pCI-neo under transcriptional control of the CMV promoter, between the CMV promoter and the GluN1 open reading frame (Yi *et al.*, 2018). EGFP:pIRES:GluN2A was constructed by inserting cDNA encoding EGFP between the CMV promoter and the GluN2A open reading frame in pIRES, with the internal ribosome entry site (i.e., the IRES) between the EGFP and GluN2A open reading frames. Both plasmids allow for co-expression of independent EGFP and NMDAR subunit proteins. For experiments with GluN1/2A receptors, cells were transfected with cDNA ratios of 1 GluN1: 1 GluN2. Cells were transfected with cDNA ratios of either 1 GluN1: 1 GluN2 or 1 GluN1: 2 GluN2 for experiments with GluN1/2B,

GluN1/2C, and GluN1/2D receptors. 200 µM of the competitive NMDAR antagonist dl-APV was added to medium at the time of transfection to prevent NMDAR-mediated cell death.

Primary cortical cultures (provided by Karen Harnett-Scott and Dr. Elias Aizenman of the University of Pittsburgh) were prepared from embryonic day 16 rats of both sexes. Pregnant rats (Charles River Laboratories) were sacrificed via CO_2 inhalation. Brains of embryonic rats were dissected, and cortices were dissociated with trypsin. Dissociated neurons were then plated at a density of 6.6 *10^5 to 7.0 * 10^5 cells/well on 15 mm glass coverslips in 6-well plates. Coverslips were acid-etched and treated with either poly-L-ornithine or poly-D-lysine prior to plating. Neurons were maintained in D10FC medium during days *in vitro* (DIV) 1-18. Non-neuronal cell proliferation inhibited on DIV 15 by adding 1-2 µM cytosine arabinosine (AraC) to D10FC. AraC and D10FC were removed on DIV18 and cells were maintained in D2C medium from DIV18 onward.

2.3.2 Electrophysiology

Patch-clamp electrophysiological experiments were performed in the whole-cell voltage-clamp configuration. Recordings from tsA201 cells were performed 18-30 hours after transfection. Recordings from cultured neurons were performed after DIV 15 to allow for adequate GluN2A subunit expression, which occurs after roughly two weeks *in vitro* (Zhong *et al.*, 1994; Li *et al.*, 1998; Sinor *et al.*, 2000). Pipettes were fabricated from borosilicate capillary tubing (outer diameter = 1.5 mm, inner diameter = 0.86 mm) using a Flaming Brown P-97 electrode puller (Sutter Instruments) and fire-polished to a resistance of 3.0 – 4.5 MΩ for tsA201 cell recordings or 3.5 – 5.0 MΩ for neuronal recordings. Whole-cell currents were amplified with Axopatch 1D or Axopatch 200A amplifiers and digitized using a Digidata 1440A digitizer (Molecular Devices). Current signals were low-pass filtered at 5 kHz and sampled at 20 kHz using pClamp10.7 (Molecular Devices). Series resistance was compensated between 85 – 90% in all experiments,

and data from cells with series resistance > 20 MΩ was excluded from analysis. In all experiments, an empirically determined liquid junction potential of -6 mV between the internal and external solutions was corrected. For experiments in Figures 4 – 7 and 10, data was collected 5 – 10 min after break-in.

Control bath solution (referred to as external solution) for tsA201 cell experiments contained (in mM): 140 NaCl, 2.8 KCl, 10 HEPES, 0.01 EDTA, 0.1 glycine, and either 0.1 or 1 $CaCl_2$. For all neuronal experiments, external solution contained 140 NaCl, 2.8 KCl, 10 HEPES, 0.01 EDTA, 0.01 glycine (lowered from tsA201 cell experiments to prevent activation of inhibitory glycine receptors), and 0.1 $CaCl_2$, with 0.2 µM tetrodotoxin (TTX) added to prevent synaptic events or action potential escape. Agonists and antagonists were added to external solutions on day of experiments. 1 mM glutamate (diluted from 1 M stock) was used for tsA201 cell experiments, and 10 µM NMDA (diluted from 10 mM stock) for neuronal experiments. Various concentrations of memantine and ketamine (both diluted from 10 mM stocks in dH_2O) were used for both tsA201 cell and neuronal experiments. For IC_{50} measurements, antagonist solutions were prepared via serial dilution. Control, agonist, and antagonist solutions were delivered to the patched cell via ten polyimide barrels using our in-house fabricated rapid-switching fast perfusion system (Glasgow & Johnson, 2014). Switches between solutions were performed by moving the barrel position relative to the patched cell with a voice-coil motor controlled by a custom program (Blanpied *et al.*, 1997). Solution flow rate was maintained at 1 – 2 mL/min for all experiments.

2.3.3 Intracellular solution preparation and determination of free [Ca^{2+}]

All intracellular (pipette) solutions contained 120 – 130 mM CsCl, 10 mM HEPES, and 4 mM MgATP and were pH balanced to 7.2 ± 0.05 with CsOH. To allow for study of the effects of known, constant [Ca^{2+}]$_i$ on channel block, each intracellular solution also contained calculated

concentrations of $CaCl_2$ and empirically determined concentrations of BAPTA, HEDTA, or NTA to buffer Ca^{2+} to desired concentrations. Because estimation of free Ca^{2+} concentrations ($[Ca^{2+}]_F$) in buffered solutions are subject to multiple sources of error (McGuigan *et al.*, 2016), we utilized the Ligand Optimization Method (LOM (McGuigan *et al.*, 1991, 2006)) to (1) aid in the design of intracellular solutions containing known concentrations of buffered $[Ca^{2+}]_F$ and (2) empirically determine $[Ca^{2+}]_F$ following solution preparation. The LOM is a multi-step process that obtains the best fit of the Nicolsky-Eisenman equation (Nicolsky *et al.*, 1967) to data measured with a Ca^{2+}-selective electrode by optimizing four parameters vital to accurate determination of $[Ca^{2+}]_F$: the slope of the electrode at $[Ca^{2+}] < 10$ μM (s), the lumped interference constant (Σ) describing the nonlinearity of the electrode at low $[Ca^{2+}]_F$, the total concentration of the Ca^{2+}-binding buffer ($[B]_T$), and the K_d of the buffer.

All solutions used for the LOM were prepared from a background solution containing 120 mM CsCl and 10 mM HEPES and balanced to pH 7.2 with CsOH. Ionic content of the background solution was designed to mimic our typical intracellular solutions. Seven calibration solutions, necessary for determination of s, were prepared by adding $CaCl_2$ to background solution to produce total $[Ca^{2+}]$ ($[Ca^{2+}]_T$) ranging from 0.5 - 10 mM. 10 Ca^{2+}-buffer solutions containing 10 mM of the calcium chelators BAPTA, HEDTA, or NTA (measured by weight) and known concentrations of $[Ca^{2+}]_T$ were prepared from background solution using the ratiometric method (McGuigan *et al.*, 2014). All measurements of $[Ca^{2+}]_F$ were made at 25° C using a Ca^{2+}-selective combination electrode that converts effective concentrations of free Ca^{2+} ions into electrical potentials according to the Nernst equation (Orion 9720BNWP, ThermoFisher) and a pH meter in mV mode (Accument AR15, ThermoFisher). To obtain values for fitting of the Nicolsky-Eisenman equation, electrical potentials of the calibration solutions were first measured in order of descending $[Ca^{2+}]_T$, followed by measurement of electrical potentials of the Ca^{2+}-buffer solutions in order of descending $[Ca^{2+}]_T$. Relative potentials (ΔE) for each solution were then calculated for

39

each solution by subtracting the potential measured in the $[Ca^{2+}]_T$ = 10 mM calibration solution. The relative potentials were then fit using the program CaSALE, a custom R script written specifically for use with the LOM (kindly provided by Dr. James Kay; (McGuigan *et al.*, 2014)) that automizes the iterative optimization of *s*, Σ, $[B]_T$, and K_d. Values of optimized parameters are listed in Table 2.

After LOM curves were obtained for each Ca^{2+} buffer (Figure 3), $[Ca^{2+}]_T$s required to give desired $[Ca^{2+}]_F$ in our intracellular solutions were calculated using the optimized $[B]_T$, and K_d values with **Equation 1**:

$$[Ca^{2+}]_T = \frac{([Ca^{2+}]_F)([B]_T + [Ca^{2+}]_F + K_d)}{[Ca^{2+}]_F + K_d}$$

Buffers with K_d closest to the target $[Ca^{2+}]_F$ were used for each solution: BAPTA (K_d = 144 nM) for $[Ca^{2+}]_F$ < 1 μM, HEDTA (K_d = 2.24 μM) for $[Ca^{2+}]_F$ 1 – 10 μM, and NTA (K_d = 81.5 μM) for $[Ca^{2+}]_F$ > 10 μM. The calculated $[Ca^{2+}]_T$ was added to background solution containing the specified buffer and 4 mM MgATP and the solution was pH balanced with CsOH. ΔE was then recorded for the prepared solution and was used, along with the optimized *s* and Σ values, to confirm the final $[Ca^{2+}]_F$ with **Equation 2**:

$$[Ca^{2+}]_F = 10^{\frac{\Delta E - E^o}{s}} - \Sigma$$

where E^0 represents the intrinsic potential of the recording system, a parameter determined by CaSALE calculations. Final $[Ca^{2+}]_F$ were confirmed to vary from the value predicted by the LOM curve by less than 2% on average (Table 3). All Ca^{2+}-buffer solutions were prepared using the LOM except for the $[Ca^{2+}]_F$ = 5 μM solution, which was prepared using the program MAXCHELATOR (Bers *et al.*, 2010) and later measured using the LOM. The original intention was to prepare a $[Ca^{2+}]_F$ = 10 μM solution using MAXCHELATOR estimates, but MAXCHELATOR does not account for buffer purity or the effect of background solution composition on buffer K_d

values (McGuigan *et al.*, 2016; Tran *et al.*, 2018). The HEDTA K_d value utilized by MAXCHELATOR is substantially higher than most measurements in solutions of similar composition to our intracellular solution (Tran *et al.*, 2018) as well as our LOM measurements (MAXCHELATOR K_d = 7.2 µM; LOM K_d = 2.24 µM) which resulted in preparation of a solution with substantially lower $[Ca^{2+}]_F$ than predicted (MAXCHELATOR predicted $[Ca^{2+}]_F$ = 10 µM; LOM measured $[Ca^{2+}]_F$ = 4.87 µM), illustrating the importance for precise measurement of $[Ca^{2+}]_F$ in buffered solutions.

2.3.4 Analysis

All electrophysiology data were analyzed with Clampfit 10.7 (Molecular Devices) and Prism 7-9 (Graphpad). Baseline current was subtracted from all current measurements. Concentration-inhibition relations for channel blockers were measured using the protocol shown in Figure 4A. Agonist was applied until current reached steady-state (I_{SS}), then sequentially increasing concentrations of antagonist were applied in the presence of constant [agonist]. Each antagonist solution was applied until a steady level of inhibition was reached (10 – 20 s for GluN1/2A receptors, 20 – 30 s for GluN1/2B GluN1/2C, and GluN1/2D receptors and in neuronal experiments). Antagonists were then removed and agonist alone was reapplied to allow recovery from channel block. Cells in which current did not recover to at least 85% of the steady-state current elicited by the initial agonist application were excluded from analysis. IC_{50} values were estimated by fitting concentration-inhibition data with the Hill equation, **Equation 3**:

$$\frac{I_{Drug}}{I_{Glu}} = \frac{1}{1 + (\frac{[Drug]}{IC_{50}})^{n_H}}$$

where I_{Drug} represents the mean I_{SS} over the final 1 s of drug application at a particular [Drug], I_{Glu} is the average of the mean I_{SS} over the final 1 s of the agonist application preceding drug application and the mean I_{SS} over the final 1 s of the agonist application following recovery from inhibition, and n_H is the Hill coefficient. IC_{50} and n_H were free parameters during fitting. The effect of $[Ca^{2+}]_i$ on memantine potency was quantified with a modified version of the Hill equation, **Equation 4**:

$$IC_{50} = minIC_{50} + \frac{maxIC_{50} - minIC_{50}}{1 + \left(\frac{[Ca_i^{2+}]}{CaEC_{50}}\right)^{n_H}}$$

where IC_{50} represents the memantine IC_{50} measured at each $[Ca^{2+}]_i$, $maxIC_{50}$ represents the maximal IC_{50} (the IC_{50} recorded at $[Ca^{2+}]_i < 1$ nM), $minIC_{50}$ represents the minimal IC_{50} value, $CaEC_{50}$ represents the $[Ca^{2+}]_i$ that elicits a half maximal effect on memantine potency, and n_H is the Hill coefficient. $CaEC_{50}$ and n_H were free parameters during fitting.

The time course of recovery from desensitization (RfD) for GluN1/2A receptors was measured using the protocol shown in Figure 5. Patched cells were subjected to repeated glutamate applications in the absence of antagonist or the presence of the indicated antagonist concentration following inter-application intervals of 1, 2, 5, 10, 20, 50, 100, and 200 s in random order or in order of increasing or decreasing duration. Figure 5 shows an example experiment using inter-application intervals of increasing length. Peak currents (I_{Peak}) following each inter-application interval were measured as the mean current over a 30 ms window centered around the peak absolute current. I_{peak}s were then normalized to the I_{Peak} following the 200 s inter-application interval to account for current rundown or changes in recording parameters. Cells where normalized I_{Peak} for any inter-application interval exceeded 1.2 were excluded from analysis. Plot of normalized I_{Peak}s as a function of inter-application interval were fit with either single or double exponential functions to determine time constants for RfD. To allow for

comparison with single exponential time constants (τ), double exponential time constants were converted to a weighted time constant (τ_w) using **Equation 5**:

$$\tau_w = \frac{(\tau_{fast} * A_{fast}) + (\tau_{slow} * A_{slow})}{A_{fast} + A_{slow}}$$

where τ_{fast}, A_{fast}, τ_{slow}, and A_{slow} represent the time constant and amplitude of the fast component and the time constant and amplitude of the slow component, respectively.

For experiments measuring the effect of $[Ca^{2+}]_i$ on desensitization, desensitization was quantified as a ratio of I_{ss} to I_{Peak}. I_{ss} was measured as in IC_{50} experiments. I_{Peak} was measured as in RfD experiments.

Table 2. Ligand Optimization Method parameters.

Optimized Parameter	BAPTA	HEDTA	NTA
s (mV/decade Ca^{2+})	28.7	28.8	28.3
Σ	$8.47 * 10^{-9}$	$7.64 * 10^{-18}$	$1.79 * 10^{-16}$
$[B]_T$ (M)	$9.49 * 10^{-3}$	$9.04 * 10^{-3}$	$8.71 * 10^{-3}$
K_d (M)	$1.44 * 10^{-7}$	$2.24 * 10^{-6}$	$8.15* 10^{-5}$
E^0 (mV)	57.4	57.5	56.5
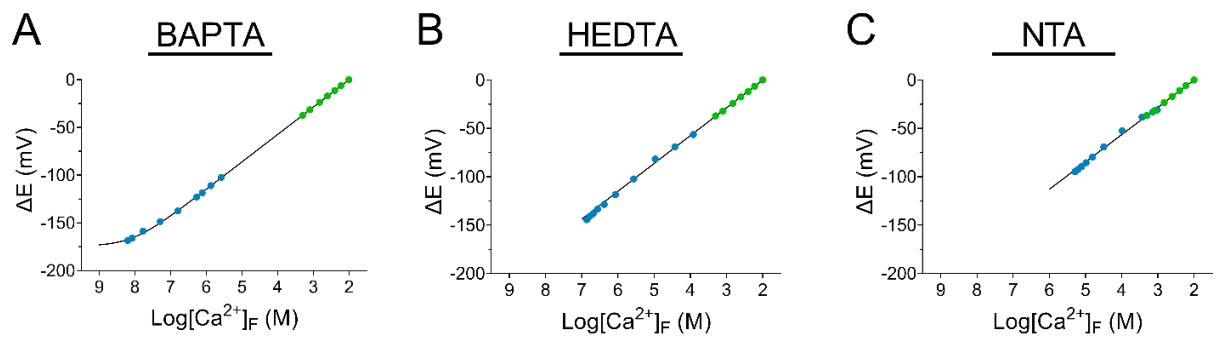
Figure 3. Ligand Optimization Method.

A-C, Ligand Optimization Method for BAPTA (A), HEDTA (B), and NTA (C). Line represents best fit of the Nicolsky-Eisenmann equation to ΔE values after final optimization of $[B]_T$, K_d, *s*, and Σ. Points represent measurements from calibration (green) or buffer (blue) solutions.

Table 3. Measured $[Ca^{2+}]_F$ values Ca^{2+}-Buffer solutions.

[#]5 μM solution prepared using MAXCHELATOR predictions, with $[Ca^{2+}]_F$ measured under the assumption that $[B]_T$ did not substantially vary between solutions. All other solutions prepared using LOM predictions. All $[Ca^{2+}]_F$ values measured using LOM after final solution preparation.

Target $[Ca^{2+}]_F$ (M)	Buffer	$[Ca^{2+}]_T$ (M)	Predicted ΔE (mV)	Measured ΔE (mV)	Measured $[Ca^{2+}]_F$ (M)
$1 * 10^{-8}$	BAPTA	$6.16 * 10^{-4}$	-164.58	-164.6	$9.98 * 10^{-9}$
$1 * 10^{-7}$	BAPTA	$3.89 * 10^{-3}$	-142.51	-142.5	$1.00 * 10^{-7}$
$1 * 10^{-6}$	HEDTA	$2.79 * 10^{-3}$	-115.07	-115.1	$9.98 * 10^{-7}$
[#]$5 * 10^{-6}$	HEDTA	$6.20 * 10^{-3}$	NA	-95.3	$4.87 * 10^{-6}$
$1 * 10^{-5}$	HEDTA	$7.39 * 10^{-3}$	-86.30	-86.3	$1.00 * 10^{-5}$
$5 * 10^{-5}$	NTA	$3.36 * 10^{-3}$	-64.99	-65.0	$5.01 * 10^{-5}$

2.4.1 Ca^{2+}-dependent block of GluN1/2A receptors by memantine

Memantine augments desensitization of GluN1/2A receptors by slowing recovery from, and therefore increasing occupancy of, a Ca^{2+}-dependent desensitized receptor state (Glasgow et al. 2017). To further parse the relation between memantine block and CDD, we used whole cell patch-clamp recordings to measure memantine potency while "clamping" [Ca^{2+}]$_i$ with Ca^{2+}-buffering pipette solutions containing known [Ca^{2+}]$_F$ and high concentrations of Ca^{2+} buffer. Estimation of [Ca^{2+}]$_F$ in buffered solutions is often performed using freely available software (Schoenmakers *et al.*, 1992; McGuigan *et al.*, 2006; Bers *et al.*, 2010) and requires the Ca^{2+}-binding affinity (K$_d$) and the purity of the buffer ([B]$_T$) to be known. However, reported K$_d$ values for commonly used Ca^{2+} buffers vary considerably and the purity of many Ca^{2+} buffers is reduced by binding to H$_2$O while in solid form (McGuigan *et al.*, 2016). Thus, accurate estimation of [Ca^{2+}]$_F$ in buffered solutions difficult. To avoid misestimation of [Ca^{2+}]$_F$ in our pipette solutions, we utilized the Ligand Optimization Method ((Luthi *et al.*, 1997; McGuigan *et al.*, 2006, 2007, 2016); see Methods section for details) to obtain accurate K$_d$ and [B]$_T$ values for each buffer used and empirically measure the [Ca^{2+}]$_F$ in our pipette solutions (Table 3). Furthermore, we performed recordings in low extracellular [Ca^{2+}] ([Ca^{2+}]$_e$ = 0.1 mM) to minimize the impact of Ca^{2+} influx on [Ca^{2+}]$_i$ and limit any confounding effects of [Ca^{2+}]$_e$ on NMDAR channel function (Ascher and Nowak 1988, Maki and Popescu 2014). Thus, we were able to isolate and examine the effect of [Ca^{2+}]$_i$ on memantine potency.

Recordings from transfected tsA201 cells expressing GluN1/2A diheteromers revealed a clear dependence of memantine potency on [Ca^{2+}]$_i$ (Figure 4A-D). Memantine inhibition was augmented by [Ca^{2+}]$_i$. Memantine IC$_{50}$ values significantly decreased as [Ca^{2+}]$_i$ increased,

47

culminating in a striking ~4-fold difference in potency between the lowest and highest $[Ca^{2+}]_i$ conditions (Figure 4C; $[Ca^{2+}]_i$ < 1 nM IC_{50} = 2.76 ± 0.27; $[Ca^{2+}]_i$ = 50 µM IC_{50} = 0.70 ± 0.06 µM, n = 5). This effect appeared to saturate at roughly $[Ca^{2+}]_i$ = 5 µM (Figure 4C,D). Memantine inhibition was sensitive not only to levels of $[Ca^{2+}]_i$ consistent with active signaling (1 µM) and pathological conditions (5 – 50 µM) in neurons, but also low $[Ca^{2+}]_i$'s at (100 nM) or even below (10 nM) resting levels, indicating that memantine potency is sensitive to $[Ca^{2+}]_i$ across a physiologically important range. To quantify the effect of $[Ca^{2+}]_i$ on inhibition by Mem, we fit the memantine IC_{50} data as a function of $[Ca^{2+}]_i$ using a modified version of the Hill equation (**Equation 4**). The relatively linear middle portion of the $[Ca^{2+}]_i$-Memantine IC_{50} curve spans the entire range of physiological $[Ca^{2+}]_i$ observed in neurons, with the half maximal effect of $[Ca^{2+}]_i$ reached at $[Ca^{2+}]_i$ = 54 nM (Figure 4D). These results suggest that memantine inhibition of GluN1/2A receptors is dynamically regulated by physiological fluctuations in $[Ca^{2+}]_i$.

Although it is likely that the primary effect of $[Ca^{2+}]_i$ on NMDARs in our experiments is modulation of CDD, manipulating $[Ca^{2+}]_i$ may alter other NMDAR channel properties that broadly affect channel block (Lan *et al.*, 2001; Skeberdis *et al.*, 2006; Murphy *et al.*, 2014). To determine whether the effect of $[Ca^{2+}]_i$ on memantine IC_{50} could be attributed to a general effect of $[Ca^{2+}]_i$ on channel block, we measured the effect of $[Ca^{2+}]_i$ on the IC_{50}s of the prototypical NMDAR channel blocker Mg^{2+} and of another clinically important organic channel blocker, ketamine. Neither Mg^{2+} IC_{50} (Figure 4E,F) nor ketamine IC_{50} (Figure 4G,H) showed any dependence on $[Ca^{2+}]_i$, suggesting that $[Ca^{2+}]_i$ has no broad effects on channel block. The $[Ca^{2+}]_i$-independent nature of ketamine potency is consistent with our previous findings that ketamine has no effect on CDD (Glasgow *et al.*, 2017), supporting the idea that the $[Ca^{2+}]_i$ dependence of memantine IC_{50} is inherently intertwined with CDD.
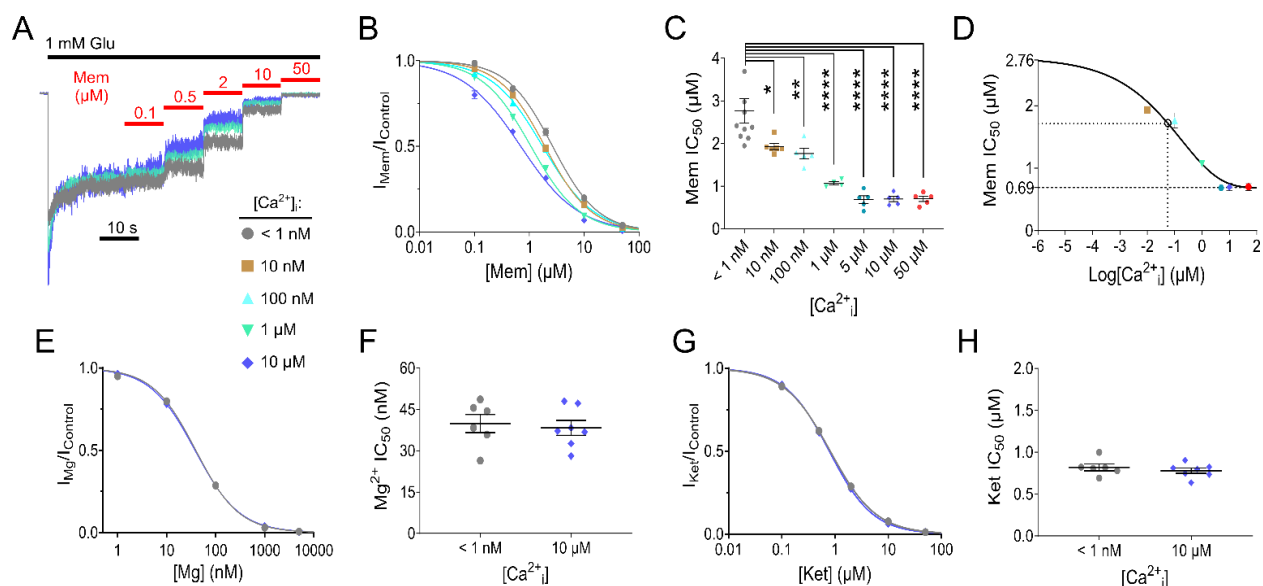
Figure 4. Ca^{2+}-dependent block of GluN1/2A receptors by memantine.

A, Overlay of WT GluN1/2A receptor currents used to measure memantine (Mem) concentration-inhibition curves during application of glutamate (Glu; black bar) and memantine (red bars) For visualization of differences in inhibition, only traces in conditions of [Ca^{2+}]$_i$ < 1 nM (grey), [Ca^{2+}]$_i$ = 1 μM (teal), and [Ca^{2+}]$_i$ = 10 μM (blue) are shown. [Ca^{2+}]$_e$ = 0.1 mM to prevent Ca^{2+} influx from altering [Ca^{2+}]$_i$. Currents are normalized to steady state current measured in 0 memantine. **B**, Memantine concentration-inhibition curves for [Ca^{2+}]$_i$ = 10 μM (blue), 1 μM (teal), 100 nM (light blue), 10 nM (gold), and < 1 nM (grey). Lines depict fit of Hill equation (**Equation 3**) to data. **C**, Summary of memantine IC$_{50}$ values measured at the indicated [Ca^{2+}]$_i$ (< 1 nM Ca^{2+}$_i$: IC$_{50}$ = 2.76 ± 0.27 μM, n = 9; 10 nM Ca^{2+}$_i$: IC$_{50}$ = 1.93 ± 0.07 μM, n = 6; 100 nM Ca^{2+}$_i$: IC$_{50}$ = 1.76 ± 0.12 μM, n = 5; 1 μM Ca^{2+}$_i$: IC$_{50}$ = 1.07 ± 0.04 μM, n = 4; 5 μM Ca^{2+}$_i$: IC$_{50}$ = 0.69 ± 0.06 μM, n = 5 10 μM Ca^{2+}$_i$: IC$_{50}$ = 0.69 ± 0.05 μM, n = 5; 50 μM Ca^{2+}$_i$: IC$_{50}$ = 0.70 ± 0.06 μM, n = 5). ANOVA with Sidak's post hoc test. *p < 0.05, **p < 0.01, ****p < 0.0001. **D,** Curve describing the effect of [Ca^{2+}]$_i$ on memantine IC$_{50}$. Line depicts fit of **Equation 4** to data. Memantine becomes more potent (i.e. IC$_{50}$ decreases) as [Ca^{2+}]$_i$ increases. Dashed line at memantine IC$_{50}$ = 0.69 μM depicts minimum IC$_{50}$. Dotted lines and open circle show the [Ca^{2+}]$_i$ required to induce a half-maximal effect on memantine IC$_{50}$ ([Ca^{2+}]$_i$ = 54 nM). **E**, Mg^{2+} concentration-inhibition curves for [Ca^{2+}]$_i$ < 1 nM (grey) and [Ca^{2+}]$_i$ = 10 μM (blue). Lines depict fit of Hill equation to data. **F**, Summary of Mg^{2+} IC$_{50}$ values measured at [Ca^{2+}]$_i$ of < 1 nM (grey; IC$_{50}$

49

= 39.9 ± 3.3 nM, n = 6) and 10 μM (blue; IC_{50} = 38.3 ± 2.7 nM, n = 7). 2-tailed Student t-test, p = 0.72. **G**,

Ketamine concentration-inhibition curves for $[Ca^{2+}]_i$ < 1 nM (grey) and $[Ca^{2+}]_i$ = 10 μM (blue). Lines depict

fit of Hill equation to data. **H**, Summary of ketamine IC_{50} values measured at $[Ca^{2+}]_i$ of < 1 nM (grey; IC_{50} =

0.82 ± 0.04, n = 6) and 10 μM (blue; IC_{50} = 0.78 ± 0.03 μM, n = 7). 2-tailed Student t-test, p = 0.46. For **C**,

F, and **H**, points represent individual values, bars and error bars depict mean ± SEM. For **B**, **D**, **E**, and **G**,

data are depicted as mean ± SEM and some error bars are smaller than symbols. Intracellular Ca^{2+}-

buffering conditions for each internal solution used (i.e. $[Ca^{2+}]_T$ and buffer) are given in Table 3, and $[B]_T$ for

each buffer is given in Table 2.

2.4.2 Ca²⁺-dependent desensitization is required for Ca²⁺-dependent block of GluN1/2A receptors by memantine

To determine whether memantine enhances GluN1/2A receptor desensitization by stabilizing a Ca^{2+}-dependent desensitized receptor state, we assessed the involvement of the GluN1 C-terminal domain (CTD) in two key phenomena: the effect of memantine on recovery of GluN1/2A receptors from desensitization, and the effect of $[Ca^{2+}]_i$ on memantine potency. The C0 region of the GluN1 CTD, a short sequence located ~30 amino acid resides after the transmembrane domain, is included in all GluN1 splice variants and is the primary structural mediator of NMDAR CDD via its interactions with calmodulin (Ehlers *et al.*, 1996; Zhang *et al.*, 1998; Krupp *et al.*, 1999). Truncation of the GluN1 subunit proximal to C0 (GluN1ΔCTD) eliminates CDD (Ehlers *et al.*, 1996; Zhang *et al.*, 1998; Krupp *et al.*, 1999) without affecting other desensitization mechanisms (Krupp *et al.*, 1998), allowing us to examine whether entry into a Ca^{2+}-dependent desensitized state is required for the effects of $[Ca^{2+}]_i$ on memantine action.

We measured the time course of recovery from desensitization (RfD) of GluN1/2A WT and GluN1ΔCTD/2A mutant receptors in the presence and absence of 3 µM memantine to assess whether the GluN1 CTD is involved in memantine's ability to stabilize a Ca^{2+}-dependent desensitized state. Consistent with previous results (Glasgow *et al.*, 2017), memantine greatly slowed RfD of WT GluN1/2A receptors in $[Ca^{2+}]_e$ = 1 mM (Figure 5A,B,E,G) but showed no effect on RfD in $[Ca^{2+}]_e$ = 0.1 mM (data not shown). The effect of memantine on RfD in $[Ca^{2+}]_e$ = 1 mM was ablated by truncation of the GluN1 CTD (Figure 5C,D,F,G). RfD of GluN1ΔCTD/2A mutant receptors showed no sensitivity to memantine and did not significantly differ from RfD of WT receptors in the absence of memantine (Figure 5G), confirming that the effect of memantine on GluN1/2A receptor desensitization requires accessibility of a Ca^{2+}-dependent desensitized state.

We then compared memantine IC_{50} values in $[Ca^{2+}]_e = 0.1$ mM for WT and GluN1ΔCTD mutant receptors in conditions of low ($[Ca^{2+}]_i <1$ nM) and high ($[Ca^{2+}]_i = 5$ μM) intracellular Ca^{2+}. WT receptors again displayed robust $[Ca^{2+}]_i$-dependence of block by memantine. However, $[Ca^{2+}]_i$ had no effect on block of GluN1ΔCTD/2A receptors (Figure 6). Additionally, GluN1ΔCTD mutant IC_{50} values in both conditions did not significantly differ from the WT value in the low $[Ca^{2+}]_i$ condition (Figure 6C), revealing that the sensitivity of memantine IC_{50} to $[Ca^{2+}]_i$ is entirely dependent on the GluN1 CTD. Consistent with our hypothesis, truncation of the GluN1 CTD also ablated CDD (Figure 6 D,E). Together, our results provide powerful evidence that the slowing of GluN1/2A receptor RfD by memantine and the $[Ca^{2+}]_i$ dependence of memantine inhibition both result from stabilization of a Ca^{2+}-dependent desensitized state.
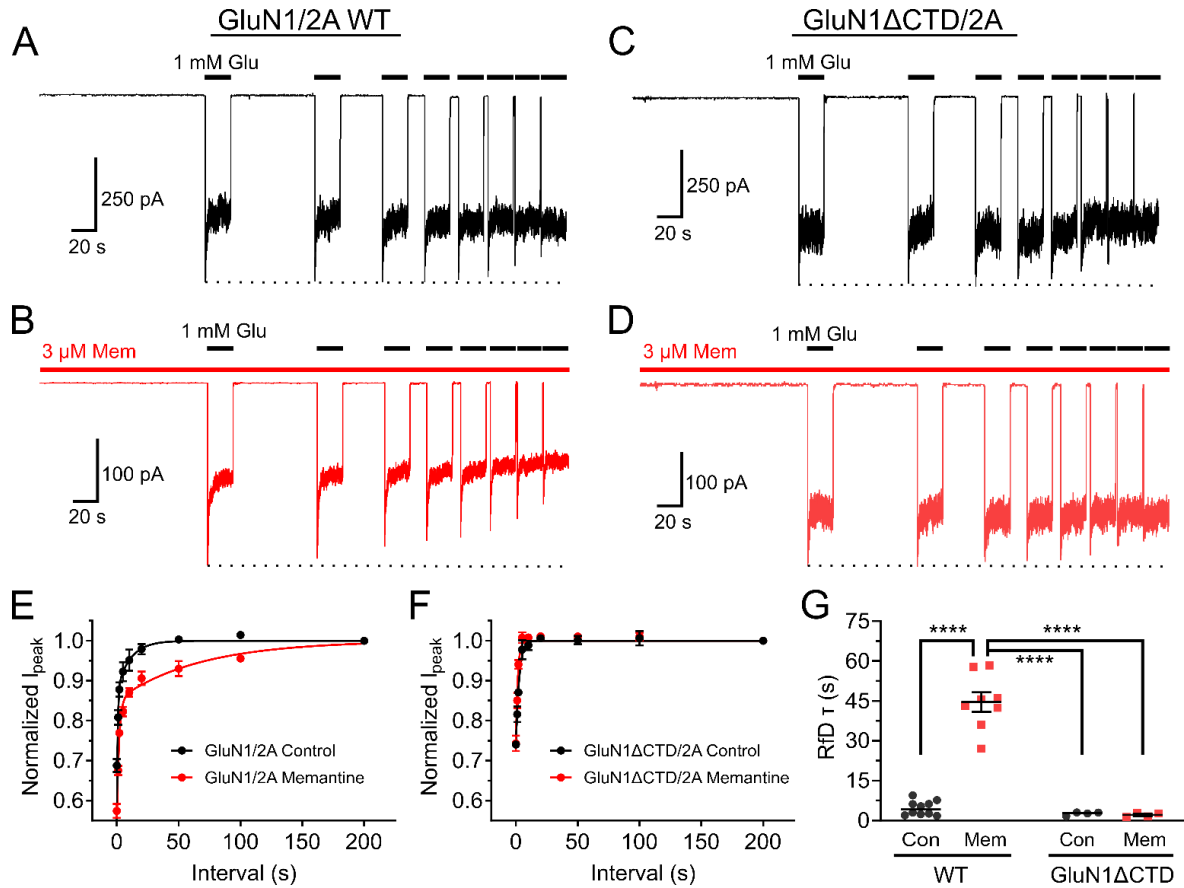
Figure 5. The GluN1 C-terminal domain is required for enhancement of GluN1/2A receptor Ca²⁺-dependent desensitization by memantine.

A-D, Representative current traces of WT GluN1/2A (**A**, **B**) and GluN1ΔCTD/2A receptor responses to 1 mM Glu (black bars) after inter-application intervals of decreasing duration in the absence (**A**, **C**) and presence (**B**, **D**) of 3 μM memantine (red bars). Dotted line placed at I_{Peak} after the 200 s inter-application interval to allow for visualization of differences between peaks. **E**, **F**, Exponential fits to time course of RfD data. Symbols depict normalized I_{Peak} values (see Section 2.3.4) for WT receptors (**E**) or GluN1ΔCTD/2A receptors (**F**). Data are depicted as mean ± SEM and some error bars are smaller than symbols. **G**, Summary and comparison of time constant of RfD values (WT Control τ = 4.66 ± 0.95 s, n = 8; WT Mem τw = 44.56 ± 3.46 s; GluN1ΔCTD Control τ = 2.58 ± 0.32 s; n = 4; GluN1ΔCTD Mem τ = 2.58 ± 0.32 s; n = 4). ANOVA with Tukey's post hoc test; ****p < 0.0001. Points represent individual values, bars and error bars depict mean ± SEM. Intracellular solutions contained 10 mM BAPTA and no added CaCl₂.

53
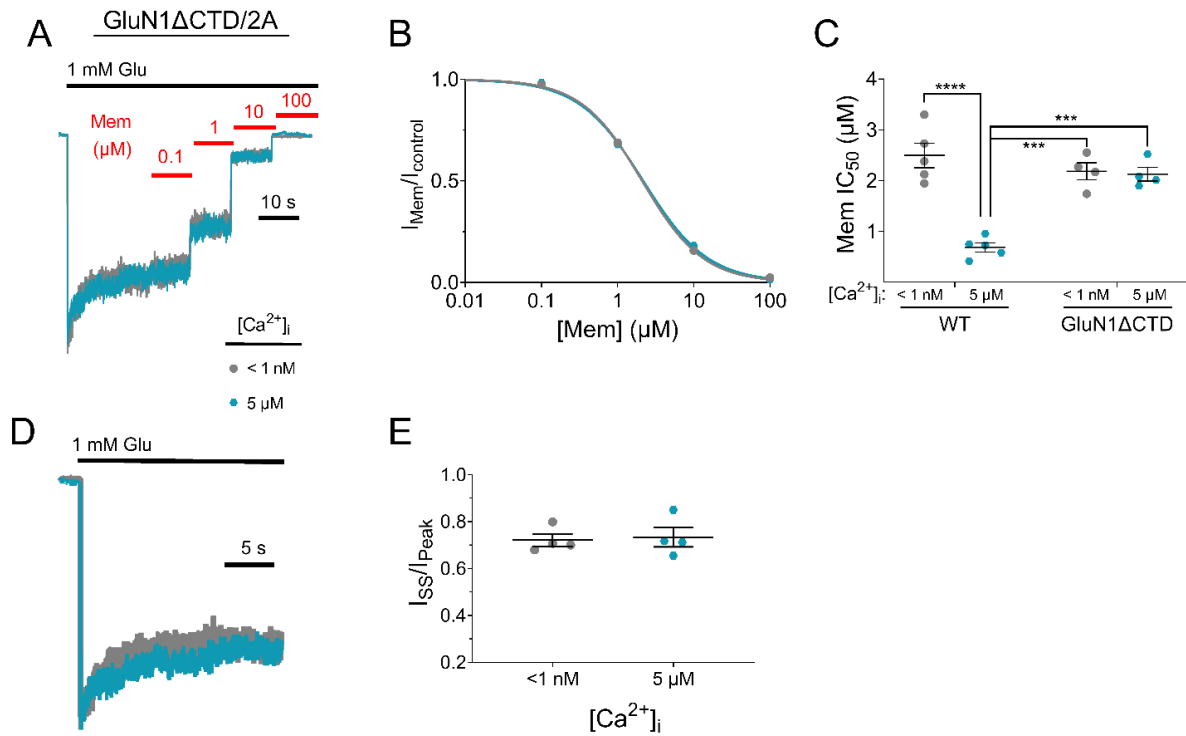
Figure 6. Ca^{2+}dependent block by memantine requires the GluN1 C-terminal domain.

A, Representative GluN1ΔCTD/2A receptor currents used to measure memantine concentration-inhibition relations in conditions of [Ca^{2+}]$_i$ = <1 nM (grey) and 5 μM (blue) in 0.1 mM Ca^{2+}$_e$. **B**, Concentration-inhibition curve for memantine at [Ca^{2+}]$_i$ = <1 nM and 5 μM. Points represent mean; error bars smaller than points. **C**, Summary of memantine IC$_{50}$ values for WT GluN1/2A and GluN1ΔCTD/2A receptors in conditions of [Ca^{2+}]$_i$ <1 nM and [Ca^{2+}]$_i$ = 5 μM. GluN1 CTD truncation ablates the effect of [Ca^{2+}]$_I$ on memantine IC$_{50}$ (for GluN1ΔCTD/2A receptors, [Ca^{2+}]$_i$ < 1 nM: 2.13 ± 0.27 μM, n = 4; [Ca^{2+}]$_i$ = 5 μM: 2.18 ± 0.34 μM, n = 4). 2-way ANOVA (interaction p < 0.001) with Tukey post hoc test for multiple comparisons (***p < 0.001, ****p < 0.0001). Points represent individual values, bars and error bars show mean ± SEM. **D**, Overlay of GluN1ΔCTD/2A receptor currents used to measure desensitization with [Ca^{2+}]$_i$ = <1 nM (grey) and 5 μM (blue) in 0.1 mM Ca^{2+}$_e$. Currents are normalized to I$_{Peak}$. **E**, Comparison of I$_{SS}$/I$_{Peak}$ values across conditions of [Ca^{2+}]$_i$ <1 and [Ca^{2+}]$_i$ = 5 μM. No difference in desensitization was observed (Student t-test). Intracellular Ca^{2+}-buffering conditions for each internal solution used (i.e. [Ca^{2+}]$_T$ and buffer) are given in Table 3, and [B]$_T$ for each buffer is given in Table 2.

54

2.4.3 [Ca^{2+}]$_i$-dependent block by memantine depends on receptor subtype

NMDARs display great diversity in subunit composition. The GluN2 subunit strongly influences many biophysical properties of NMDARs, including channel block and desensitization (Krupp *et al.*, 1996, 1998; Siegler Retchless *et al.*, 2012; Glasgow *et al.*, 2015, 2017). However, the dependence of CDD on GluN2 subunit identity, and therefore the dependence of [Ca^{2+}]$_i$-dependent block by memantine on GluN2 subunit identity, is still ambiguous. CDD has been reported in GluN1/2A, GluN1/2B, and GluN1/2D receptors, but not GluN1/2C receptors (Krupp *et al.*, 1996; Iacobucci & Popescu, 2020). However, while GluN1/2A CDD is well-characterized (Ehlers *et al.*, 1996; Krupp *et al.*, 1996, 1999, 2002; Zhang *et al.*, 1998; Iacobucci & Popescu, 2017, 2020), our understanding of GluN1/2B and GluN1/2D CDD is far less clear. GluN1/2A receptors display obvious CDD across a broad array of experimental conditions (Ehlers *et al.*, 1996; Krupp *et al.*, 1996; Iacobucci & Popescu, 2017, 2020). On the other hand, studies of CDD in GluN1/2B receptors have drawn inconsistent conclusions. GluN1/2B receptors were originally reported not to display CDD (Krupp *et al.*, 1996), but recent studies have detailed that CDD of GluN1/2B receptors can be achieved in conditions of very high [Ca^{2+}]$_i$ (Iacobucci & Popescu, 2020). Furthermore, we have previously shown that memantine enhances CDD of GluN1/2A receptors but has no effect on GluN1/2B receptor desensitization(Glasgow *et al.*, 2017), suggesting that either GluN1/2A and GluN1/2B receptors are differentially sensitive to Ca^{2+} or that distinct mechanisms underlie CDD of GluN1/2A and of GluN1/2B receptors. Furthermore, CDD of GluN1/2D receptors has only been investigated using experiments manipulating [Ca^{2+}]$_e$ (Krupp *et al.*, 1996; Iacobucci & Popescu, 2020). Therefore, we sought to further elucidate the link between CDD and [Ca^{2+}]$_i$-dependent block by memantine by investigating the effect of [Ca^{2+}]$_i$ on desensitization and memantine inhibition of each diheteromeric GluN1/2 receptor subtype.

We performed recordings from transfected tsA201 cells expressing GluN1/2A, GluN1/2B, GluN1/2C, or GluN1/2D receptors to measure desensitization and memantine potency in conditions of $[Ca^{2+}]_i$ <1 nM and $[Ca^{2+}]_i$ = 10 µM. As expected, GluN1/2A receptors exhibited both robust $[Ca^{2+}]_i$ dependence of block by memantine (Figure 7A,E,I) and strong CDD, showing substantially larger steady-state current/peak current ratios (I_{ss}/I_P) with $[Ca^{2+}]_i$ <1 nM than with $[Ca^{2+}]_i$ = 10 µM (Figure 7A,M). In contrast, GluN1/2B receptors displayed weak CDD (Figure 7B,N), but inhibition by memantine was entirely insensitive to $[Ca^{2+}]_i$ (Figure 7B,F,J). The lack of $[Ca^{2+}]_i$ dependence of memantine block of GluN1/2B receptors is consistent with our previous observations that memantine has no effect on GluN1/2B receptor RfD (Glasgow *et al.*, 2017). $[Ca^{2+}]_i$ had no effect on either desensitization or memantine inhibition of GluN1/2C (Figure 7C,G,K,O) or GluN1/2D receptors (Figure 7D,H,L,P). Interestingly, the GluN1/2A memantine IC_{50} for cells with $[Ca^{2+}]_i$ = 10 µM is nearly identical to the IC_{50} values in all other subtypes regardless of condition. Furthermore, inhibition of GluN1/2A receptors in cells with $[Ca^{2+}]_i$ < 1 nM was substantially weaker than memantine inhibition of any other NMDAR subtype tested, regardless of condition (Figure 7I-L). These finding suggests two intriguing possibilities. First, Ca^{2+}_i may drive the memantine binding site in the GluN1/2A channel into a conformation that resembles the binding site in the other NMDAR subtypes. Second, the GluN1/2A receptor may access a conformation in conditions of low $[Ca^{2+}]_i$ that is inaccessible by the other subtypes and exhibits weaker affinity for memantine. The accessibility of an additional state with weaker memantine affinity by GluN1/2A receptors may explain the discrepancies between memantine IC_{50} for GluN1/2A receptors and other GluN1/2 diheteromers reported previously (Parsons, Danysz, Bartmann, *et al.*, 1999; Dravid *et al.*, 2007).
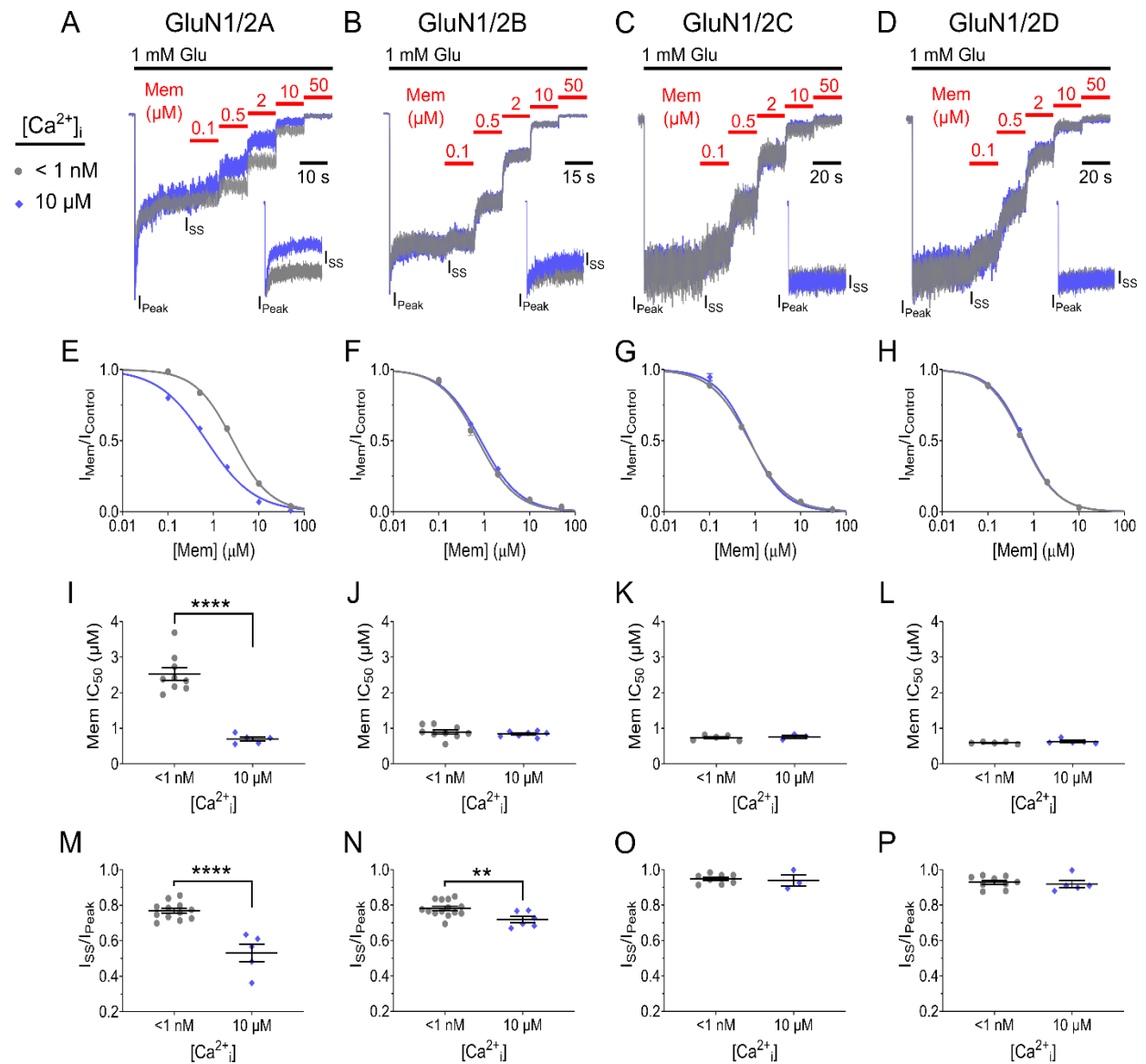
Figure 7. GluN2 subunit identity determines the effect of [Ca^{2+}]$_i$ on memantine potency and NMDAR desensitization.

A-D, Overlay of current traces used to measure memantine concentration-inhibition curves for indicated NMDAR subtype in cells with [Ca^{2+}]$_i$ < 1 nM (grey) and [Ca^{2+}]$_i$ = 10 μM (blue). [Ca^{2+}]$_e$ = 0.1 mM. Traces are normalized to I$_{SS}$ before application of memantine to facilitate comparison of inhibition between [Ca^{2+}]$_i$ conditions. Black bar depicts Glu application; red bars depict memantine applications. Insets depict overlay of response (normalized to I$_{Peak}$) to 1 mM Glu in the absence of memantine used to measure I$_{SS}$/I$_{Peak}$. **E-H**, Concentration-inhibition curves for indicated NMDAR subtype and [Ca^{2+}]$_i$. Points and error bars show mean

57

± SEM. Some error bars are smaller than points. **I-L**, Summary of IC_{50} values for indicated receptor subtype and $[Ca^{2+}]_i$. Inhibition of GluN1/2A receptors by memantine depends on $[Ca^{2+}]_i$. GluN1/2B, GluN1/2C, and GluN1/2D receptor inhibition is unaffected by $[Ca^{2+}]_i$. **M-P**, Summary of I_{SS}/I_{Peak} values for indicated receptor subtype and $[Ca^{2+}]_i$. GluN1/2A and GluN1/N2B receptors show CDD. Desensitization of GluN1/2C and GluN1/2D receptors does not depend on $[Ca^{2+}]_i$. Points represent individual values, bars and error bars show mean ± SEM; 2-tailed Student t-test, **$p < 0.01$, ***$p < 0.001$,****$p < 0.0001$. Intracellular Ca^{2+}-buffering conditions for each internal solution used (i.e. $[Ca^{2+}]_T$ and buffer) are given in Table 3, and $[B]_T$ for each buffer is given in Table 2. Memantine IC_{50} and I_{SS}/I_{Peak} numeric values for all subtypes are summarized in Table 4.

Table 4. Memantine block and desensitization of GluN1/2 diheteromeric receptors in low and high $[Ca^{2+}]_i$.

Values represent means ± sem (n).

NMDAR Subtype	Memantine IC$_{50}$ (µM)		I$_{SS}$/I$_{Peak}$	
	$[Ca^{2+}]_i$ <1 nM	$[Ca^{2+}]_i$ = 10 µM	$[Ca^{2+}]_i$ <1 nM	$[Ca^{2+}]_i$ = 10 µM
GluN1/2A	2.76 ± 0.27 (9)	0.69 ± 0.05 (5)	0.77 ± 0.02 (12)	0.53 ± 0.05 (5)
GluN1/2B	0.90 ± 0.06 (9)	0.83 ± 0.03 (7)	0.79 ± 0.01 (14)	0.72 ± 0.02 (6)
GluN1/2C	0.73 ± 0.03 (5)	0.76 ± 0.04 (3)	0.95 ± 0.01 (8)	0.94 ± 0.03 (3)
GluN1/2D	0.59 ± 0.02 (5)	0.63 ± 0.03 (5)	0.92 ± 0.02 (9)	0.93 ± 0.01 (5)

2.4.4 The relation between Ca^{2+}-dependent channel block and Ca^{2+}-dependent

      desensitization depends on NMDAR subtype

Why do we observe a relation between CDD and memantine block of GluN1/2A receptors, but not GluN1/2B receptors, in our experiments? First, in conditions of low $[Ca^{2+}]_i$ the GluN1/2A receptor channel may sample a conformation inaccessible to GluN1/2B receptors that exhibits weaker memantine affinity. Alternatively, GluN1/2B receptors could require greater buildup of Ca^{2+}_i and/or greater duration of exposure to high $[Ca^{2+}]_i$ to reach full desensitization, limiting expression of $[Ca^{2+}]_i$-dependent memantine block. To test this second possibility, we increased $[Ca^{2+}]_i$ to 50 µM and measured GluN1/2A and GluN1/2B receptor desensitization and memantine potency at intervals of 5, 10, and 15 min after whole-cell break-in. We found that although 50 µM Ca^{2+}_i did not elicit greater GluN1/2B desensitization than 10 µM Ca^{2+}_i at 5 min post break-in, both GluN1/2A (Figure 8A,B) and GluN1/2B (Figure 9A,B) desensitization greatly increased with duration of exposure to 50 µM Ca^{2+}_i. This increase in desensitization is similar to a previously described form of $[Ca^{2+}]_i$-and-time-dependent desensitization (Tong & Jahr, 1994; Krupp *et al.*, 2002).

Despite the substantial increase in desensitization over time, memantine IC_{50} remained stable at all time points for both GluN1/2A (Figure 8C) and GluN1/2B receptors (Figure 9C). As in previous experiments, memantine IC_{50} was dependent on $[Ca^{2+}]_i$ for GluN1/2A receptors (Figure 8D) but not GluN1/2B receptors (Figure 9D). Together, these results confirm that memantine block of GluN1/2B receptors is unaffected by $[Ca^{2+}]_i$ or desensitization. These results also confirm that the relation between CDD and memantine block of NMDARs is subtype-specific, and that Ca^{2+}-dependent memantine block is unique to GluN1/2A receptors.

To investigate the mechanism underlying this time-dependent form of CDD, we also measured GluN2B CDD at intervals of 5, 10, and 15 after whole-cell break-in while blocking kinase

activity with the SRC-family tyrosine kinase inhibitor dasatinib and the broad-spectrum kinase inhibitor staurosporine (500 nM each). Interestingly, although CDD was still observed (no kinase inhibition: $I_{SS}/I_{Peak} = 0.79 \pm 0.01$ at $[Ca^{2+}]_i < 1$ nM 5-10 min post break-in (Figure 7N); with kinase inhibition: $I_{ss}/I_{Peak} = 0.67 \pm 0.01$ at 50 µM $[Ca^{2+}]_i$ 5 min post break-in (Figure 9F)), the degree of desensitization did not increase with duration of exposure to high $[Ca^{2+}]_i$ (Figure 9E,F), suggesting that this time-dependent form of GluN1/2B receptor desensitization relies on kinase function.
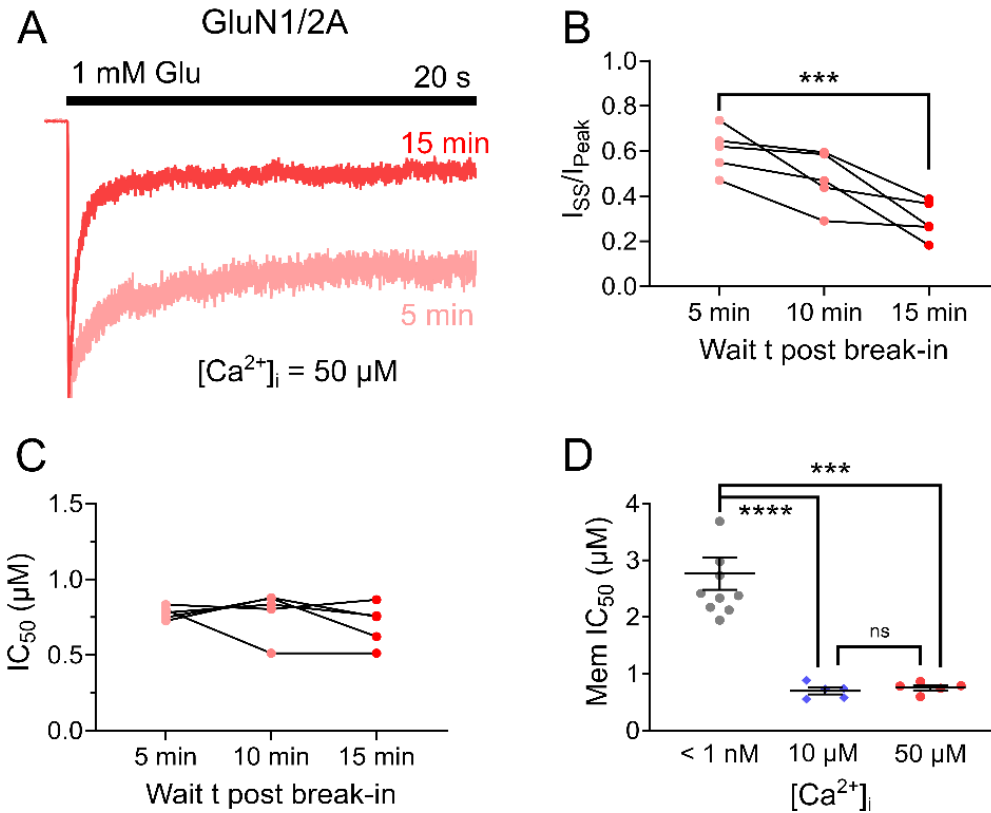
Figure 8. Desensitization, but not memantine inhibition, of GluN1/2A receptors depends on duration of exposure to high $[Ca^{2+}]_i$.

A, Overlay of GluN1/2A receptor responses in conditions of $[Ca^{2+}]_i = 50$ μM recorded at 5 (light red) and 15 (red) min after break-in. Currents are normalized to I_{Peak}. **B**, Progression of GluN1/2A receptor desensitization as a function of duration of exposure to $[Ca^{2+}]_i = 50$ μM. Desensitization greatly increases with duration of exposure to high $[Ca^{2+}]_i$ (5 min: $I_{ss}/I_{Peak} = 0.60 \pm 0.04$; 10 min: $I_{ss}/I_{Peak} = 0.48 \pm 0.06$; 15 min: $I_{ss}/I_{Peak} = 0.29 \pm 0.04$). Repeated measures one-way ANOVA with test for linear trend (***$p < 0.001$). **C**, Memantine IC_{50} plotted as a function of duration of exposure to $[Ca^{2+}]_i = 50$ μM. Memantine potency is not related to duration of exposure to high $[Ca^{2+}]_i$ (5 min: $IC_{50} = 0.73 \pm 0.02$ μM; 10 min: $IC_{50} = 0.74 \pm 0.07$ μM; 15 min: $IC_{50} = 0.70 \pm 0.06$ μM). Repeated measures one-way ANOVA with test for linear trend ($p = 0.29$). **D**, Summary and comparison of memantine IC_{50} values in conditions of $[Ca^{2+}]_i < 1$ nM ($IC_{50} = 2.76 \pm 0.27$), $[Ca^{2+}]_i = 10$ μM ($IC_{50} = 0.69 \pm 0.05$ μM), and $[Ca^{2+}]_i = 50$ μM (red; $IC_{50} = 0.70 \pm 0.06$ μM). Data replotted from Figure 4C. Data were recorded at 5 – 10 min post break-in for measurement of IC_{50} values plotted for

the $[Ca^{2+}]_i < 1$ nM and $[Ca^{2+}]_i = 10$ μM groups, and at 15 min post break-in for $[Ca^{2+}]_i = 50$ μM. Memantine potency in $[Ca^{2+}]_i = 50$ μM is stronger than in $[Ca^{2+}]_i < 1$ nM ($p^{***} < 0.001$) but does not differ from potency in $[Ca^{2+}]_i = 10$ μM; analysis same as reported in Figure 4C (one-way ANOVA with Tukey post hoc test). Points represent individual values, bars and error bars depict mean ± SEM. Intracellular Ca^{2+}-buffering conditions for each internal solution used (i.e. $[Ca^{2+}]_T$ and buffer) are given in Table 3, and $[B]_T$ for each buffer is given in Table 2.
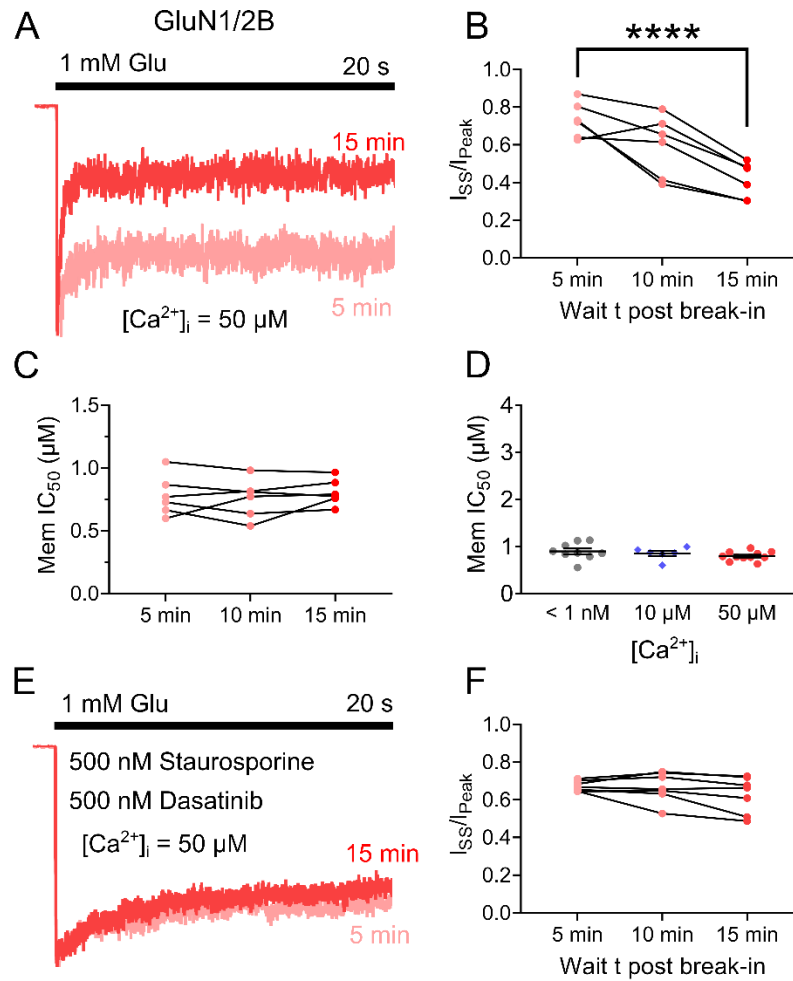
Figure 9. Desensitization, but not memantine inhibition, of GluN1/2B receptors depends on duration of exposure to high $[Ca^{2+}]_i$

A, Overlay of GluN1/2B receptor responses in conditions of $[Ca^{2+}]_i$ = 50 μM recorded at 5 (light red) and 15 (red) min after break-in. Currents are normalized to I_{Peak}. **B**, Progression of GluN1/2B receptor desensitization as a function of duration of exposure to $[Ca^{2+}]_i$ = 50 μM. Desensitization greatly increases with duration of exposure to high $[Ca^{2+}]_i$ (5 min: I_{ss}/I_{Peak} = 0.73 ± 0.04; 10 min: I_{ss}/I_{Peak}= 0.60 ± 0.07; 15 min: I_{ss}/I_{Peak} = 0.41 ± 0.04). Repeated measures one-way ANOVA with test for linear trend (****$p < 0.0001$). **C**, Memantine IC_{50} plotted as a function of duration of exposure to $[Ca^{2+}]_i$ = 50 μM. Memantine potency is not related to duration of exposure to high $[Ca^{2+}]_i$ (5 min: IC_{50} = 0.78 ± 0.07 μM; 10 min: IC_{50} = 0.76 ± 0.06 μM; 15 min: IC_{50} = 0.80 ± 0.04 μM). Repeated measures one-way ANOVA with test for linear trend ($p = 0.55$).

D, Summary of memantine IC_{50} values in conditions of $[Ca^{2+}]_i < 1$ nM ($IC_{50} = 0.90 \pm 0.06$), $[Ca^{2+}]_i = 10$ μM ($IC_{50} = 0.85 \pm 0.05$ μM), and $[Ca^{2+}]_i = 50$ μM ($IC_{50} = 0.79 \pm 0.05$ μM). Data were recorded at $5 - 10$ min post break-in for measurement of IC_{50} values plotted for the $[Ca^{2+}]_i < 1$ nM and $[Ca^{2+}]_i = 10$ μM groups, and at 15 min post break-in for $[Ca^{2+}]_i = 50$ μM. Memantine inhibition of GluN1/2B receptors does not depend on $[Ca^{2+}]_i$. One-way ANOVA with Tukey post hoc test. Points represent individual values, bars and error bars depict mean ± SEM. **E**, Overlay of GluN1/2B receptor responses recorded at 5 (light red) and 15 (red) min after break-in with $[Ca^{2+}]_i = 50$ μM and kinase activity inhibited. Currents are normalized to I_{Peak}. **F**, Progression of GluN1/2B receptor desensitization as a function of duration of exposure to $[Ca^{2+}]_i = 50$ μM with kinase activity inhibited. Kinase inhibition removed the dependence of desensitization on duration of exposure to high $[Ca^{2+}]_i$ (5 min: $I_{ss}/I_{Peak} = 0.67 \pm 0.01$; 10 min: $I_{ss}/I_{Peak} = 0.67 \pm 0.03$; 15 min: $I_{ss}/I_{Peak} = 0.63 \pm 0.04$). Repeated measures one-way ANOVA with test for linear trend ($p = 0.07$). Intracellular Ca^{2+}-buffering conditions for each internal solution used (i.e. $[Ca^{2+}]_T$ and buffer) are given in Table 3, and $[B]_T$ for each buffer is given in Table 2.

2.4.5 Ca^{2+}-dependent block of native NMDARs by memantine

We next examined whether memantine inhibition of native NMDARs is $[Ca^{2+}]_i$-dependent. Transfected cell lines offer the advantage of studying isolated NMDAR subtypes. However, properties of native NMDARs can differ from recombinant receptors due to differences in posttranslational modifications and interactions with distinct proteins or lipids (Chazot *et al.*, 1995; Kornau *et al.*, 1995; Standley & Baudry, 2000; Kloda *et al.*, 2007; Sornarajah *et al.*, 2008). Many, if not all, neurons also co-express multiple different GluN2 subunits, which can coassemble to form triheteromeric receptors (Stroebel *et al.*, 2018). To examine the effect of $[Ca^{2+}]_i$ on memantine block of native NMDARs, we performed IC_{50} measurements in cultured primary cortical neurons while clamping $[Ca^{2+}]_i$ at <1 nM or $[Ca^{2+}]_i$ = 50 µM using the same internal solutions as experiments with tsA201 cells. Our cortical neuronal cultures almost exclusively express GluN1, GluN2A, and GluN2B subunits (Qian *et al.*, 2005), with GluN2A subunit expression beginning at ~14 days *in vitro* (Zhong *et al.*, 1994; Li *et al.*, 1998; Sinor *et al.*, 2000). Therefore, all IC_{50} measurements in cultured neurons were performed after DIV 14. Since the GluN2B subunit is highly expressed in cortical neurons, and often co-assembles with GluN1 and GluN2A subunits to form GluN1/2A/2B triheteromers (Sheng *et al.*, 1994; Luo *et al.*, 1997; Gray *et al.*, 2011; Rauner & Köhr, 2011; Tovar *et al.*, 2013), we performed IC_{50} measurements in both the absence and presence of the highly selective GluN1/2B receptor antagonist CP101,606. At 1 µM, CP101,606 inhibits ~90% of GluN1/2B receptor currents while only inhibiting GluN1/2A/2B receptor currents by ~25% (Hansen *et al.*, 2014). Thus, experiments without CP101,606 allowed us to assess the effect of $[Ca^{2+}]_i$ on memantine block of the entire population of NMDARs, and experiments with CP101,606 allowed us to assess the effect of $[Ca^{2+}]_i$ on memantine block of native GluN2A-containing NMDARs.

Experiments without CP101,606 showed that memantine inhibition of native NMDARs strongly depends on $[Ca^{2+}]_i$, revealing a ~2-fold increase in memantine potency in conditions of $[Ca^{2+}]_i = 50$ µM relative to $[Ca^{2+}]_i < 1$ nM (Figure 10A-C). Potency of ketamine was again found to be $[Ca^{2+}]_i$-independent (Figure 10D,E). Surprisingly, the memantine IC_{50} value in $[Ca^{2+}]_i = 50$ µM and both ketamine IC_{50} values were skewed upward in comparison to experiments in tsA201 cells (Figure 4C,H). This could potentially be due to weaker space clamp of the larger, heavily branched neurons in comparison to the much more electrotonically compact tsA201 cells. In contrast, the memantine IC_{50} values in conditions of $[Ca^{2+}]_i < 1$nM, were roughly equivalent across our neuronal and tsA201 cell recordings (Figure 4C), suggesting that GluN1/2B receptors were also contributing to our observed IC_{50} values. Indeed, inhibition of GluN1/2B receptors with CP101,606 significantly increased the memantine IC_{50} measured in $[Ca^{2+}]_i < 1$ nM conditions (Figure 10C) without affecting IC_{50} values measured in $[Ca^{2+}]_i = 50$ µM, augmenting the dependence of memantine potency on $[Ca^{2+}]_i$. These results provide firm evidence that memantine inhibition of native GluN2A containing NMDARs heavily depends on $[Ca^{2+}]_i$.
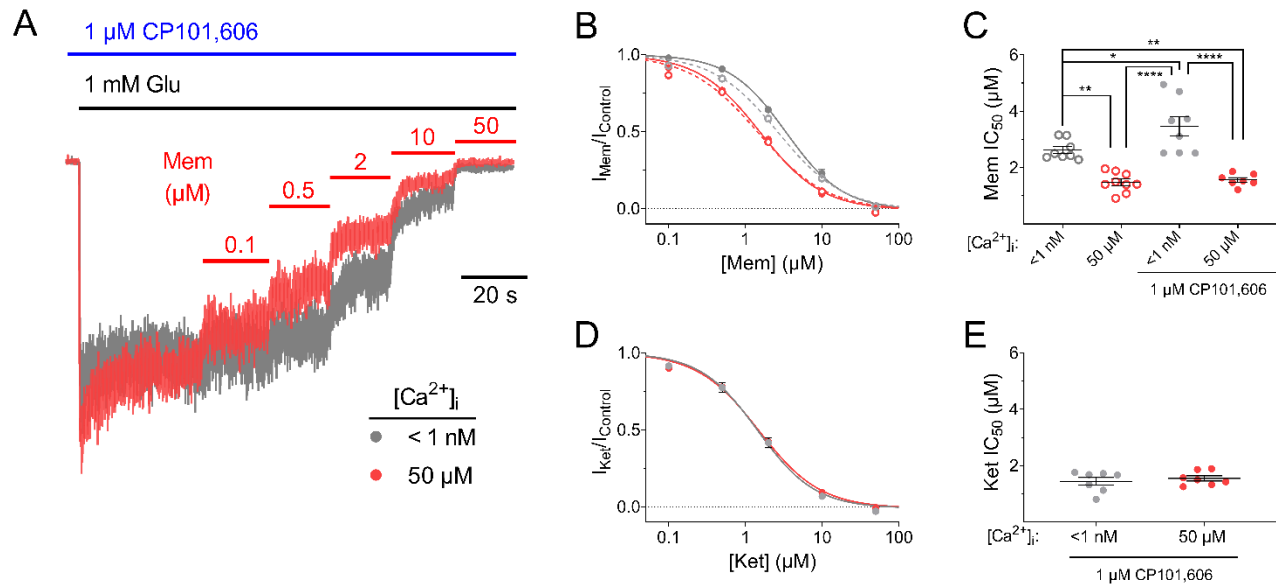
Figure 10. Memantine inhibition of native NMDARs is $[Ca^{2+}]_i$-dependent.

A, Overlay of current traces used to measure memantine concentration-inhibition curves from native NMDARs in cultured cortical neurons at $[Ca^{2+}]_i$ < 1 nM (grey) and $[Ca^{2+}]_i$ = 50 μM (red). Traces are normalized to steady-state current before application of memantine to facilitate comparison of inhibition between conditions. Black bar depicts Glu application; red bars depict memantine applications; blue bar depicts application of the selective GluN1/2B antagonist CP101,606 (1 μM). **B**, Memantine concentration-inhibition curves measured in conditions of $[Ca^{2+}]_i$ < 1 nM (gray) and $[Ca^{2+}]_i$ = 50 μM (red) in DIV 15-22 cultured cortical neurons. Curves and fractional current values measured in the absence of CP101,606 are depicted with dashed lines and open circles; curves and fractional current values measured in the presence of CP101,606 are depicted with solid lines and circles. **C**, Summary of memantine IC_{50} values measured at $[Ca^{2+}]_i$ of < 1 nM and 50 μM in the presence and absence of CP101,606. Memantine potency was significantly lower at $[Ca^{2+}]_i$ < 1 nM than $[Ca^{2+}]_i$ = 50 μM in the absence (2.63 ± 0.12 μM vs 1.48 ± 0.12 μM) and presence (3.46 ± 0.34 μM vs 1.56 ± 0.0.08 μM) of CP101,606. CP101,606 weakened memantine potency in conditions of $[Ca^{2+}]_i$ < 1 nM (3.46 ± 0.34 μM vs 2.63 ± 0.12 μM). One-way ANOVA with Tukey's post hoc test; *$p < 0.05$, **$p < 0.01$, ****$p < 0.0001$. **D**, Ketamine concentration-inhibition curves for $[Ca^{2+}]_i$ < 1 nM (grey) and $[Ca^{2+}]_i$ = 50 μM (red) in the presence of CP101,606. **E**, Summary of ketamine IC_{50} values measured at $[Ca^{2+}]_i$ of < 1 nM (grey; IC_{50} = 1.44 ± 0.14), and 50 μM (red; IC_{50} = 1.55 ± 0.09 μM). For **B** and

D, data are depicted as mean ± SEM and some error bars are smaller than symbols. For **C** and **E**, points represent individual values, bars and error bars depict mean ± SEM. Intracellular Ca^{2+}-buffering conditions for each internal solution used (i.e. $[Ca^{2+}]_T$ and buffer) are given in Table 3, and $[B]_T$ for each buffer is given in Table 2.

2.5 DISCUSSION

Preferential targeting of specific receptor states could have broad implications for the pharmacological profile of memantine. The state-specific nature of memantine inhibition allows memantine activity to be regulated by both physiological context and NMDAR subtype, which likely contributes to memantine's ability to inhibit select subpopulations of NMDARs. Here, we systematically investigated the relation between NMDAR desensitization and memantine inhibition. We uncovered a previously uncharacterized form of state-specific antagonism of NMDARs, $[Ca^{2+}]_i$-dependent channel block, that confers both context and subtype dependence to the action of memantine. We found that inhibition of GluN1/2A receptors by memantine is powerfully dependent on $[Ca^{2+}]_i$, with memantine potency increasing ~4-fold as $[Ca^{2+}]_i$ was raised from < 1 nM to 5 µM. Experiments utilizing mutant receptors that do not exhibit CDD revealed that the $[Ca^{2+}]_i$-dependence of memantine inhibition is intrinsically intertwined with CDD. Together, these results strongly support the hypothesis that the $[Ca^{2+}]_i$ dependence of memantine inhibition results from stabilization of a Ca^{2+}-dependent desensitized NMDAR state. Our findings demonstrate a logical mechanism by which memantine can preferentially target specific NMDAR subpopulations and act as a neuroprotectant: preferential inhibition of receptor subpopulations subjected to intense stimulation and prolonged durations of high $[Ca^{2+}]_i$, i.e., NMDARs mediating excitotoxicity.

Our findings mesh well with previous results detailing the effects of NMDAR activity level on memantine potency and the ability of memantine to enhance CDD (Glasgow *et al.*, 2017). Memantine inhibits GluN1/2A receptor responses to long duration glutamate exposures more effectively than responses to brief, synaptic-like applications (Glasgow *et al.*, 2017). This is consistent with our results, as long glutamate applications would allow for prolonged buildup of $[Ca^{2+}]_i$, resulting in higher occupancy of Ca^{2+}-dependent desensitized states, and therefore

increased memantine potency. Glasgow et al., 2017 also reported that memantine slows GluN1/2A receptor RfD in a $[Ca^{2+}]_e$-dependent manner, suggesting that memantine stabilizes a Ca^{2+}-dependent desensitized receptor state. We replicated these results and then expanded on the relation between CDD and the mechanism of action of memantine by directly testing whether receptor machinery required for CDD is also required for the effects of Ca^{2+} on memantine action. Truncation of the GluN1 CTD, a region required for CDD, ablates both the effect of memantine on RfD (Figure 5) and the effect of $[Ca^{2+}]_i$ on memantine potency (Figure 6), confirming that memantine action powerfully depends on CDD of GluN1/2A receptors.

Our findings also provide insight into mechanisms of NMDAR desensitization. NMDAR CDD is elicited by a complex series of molecular interactions involving calmodulin, α-actinin, and various kinases and phosphatases (Tong *et al.*, 1995; Wyszynski *et al.*, 1997; Zhang *et al.*, 1998; Krupp *et al.*, 1999; Rycroft & Gibb, 2002, 2004; Merrill *et al.*, 2007). However, whether multiple forms of CDD exist is currently unknown. Our investigation of the relation between memantine potency and CDD revealed that desensitization of GluN1/2A and GluN1/2B receptors is increased both by increasing $[Ca^{2+}]_i$ and by prolonging the duration of exposure of receptors to high $[Ca^{2+}]_i$. Our data showing that both GluN1/2A and GluN1/2B receptors exhibit CDD (Figure 7) is consistent with a recent study reporting that GluN1/2A and GluN1/2B receptors undergo CDD (Iacobucci & Popescu, 2020). Interestingly, although memantine potency for GluN1/2A receptors increased alongside increasing $[Ca^{2+}]_i$, memantine potency was unaffected by the progressive increase in desensitization elicited by prolonged exposure to $[Ca^{2+}]_i$ (Figure 8). Memantine potency for GluN1/2B receptors was also unrelated to this progressive, time-dependent increase in desensitization (Figure 9). In addition, the time-dependent desensitization we observed in Figure 8 & 9 experiments appears remarkably similar to a previously reported form of glycine-independent desensitization that depends on duration of exposure to $[Ca^{2+}]_i$ (Lieberman & Mody, 1994; Tong & Jahr, 1994; Medina *et al.*, 1995; Krupp *et al.*, 2002). Overall, our results suggest

that the $[Ca^{2+}]_i$-dependent and the $[Ca^{2+}]_i$-and-time-dependent phenomena we observe may represent different, separable forms of CDD. This conclusion is bolstered by our experiments testing the role of kinase activity on GluN1/2B receptor CDD. Although we still observed CDD of GluN1/2B receptors with kinase inhibitors in the pipette, the progressive time-dependent increase in desensitization was completely ablated (Figure 9). These results provide strong evidence for the existence of two separable forms of CDD with different underlying mechanisms.

Ketamine acts as a powerful negative control in our experiments. Unlike memantine, ketamine does not affect GluN1/2A desensitization (Glasgow *et al.*, 2017) and its potency shows no dependence on $[Ca^{2+}]_i$ in recombinant (Figure 4) or native NMDARs (Figure 10). This further supports our conclusion that the $[Ca^{2+}]_i$ dependence of memantine potency is derived from stabilization of a specific receptor state by memantine, and that the relation between CDD and channel block is not due to general effects of $[Ca^{2+}]_i$ on channel block. Differences between the effects of memantine and ketamine on NMDAR gating are particularly interesting. Memantine and ketamine, despite sharing overlapping binding sites in the NMDAR channel (Ferrer-Montiel *et al.*, 1998; Kashiwagi *et al.*, 2002), exhibit strikingly divergent clinical profiles (Krystal *et al.*, 1994; Parsons, Danysz, & Quack, 1999; Chen & Lipton, 2006; Johnson *et al.*, 2015). The difference we observe between the effects of $[Ca^{2+}]_i$ on memantine and ketamine potency could direct each drug to target distinct NMDAR subpopulations, a mechanism proposed to underpin some of the differences observed between the clinical profiles of memantine and ketamine (Gideons *et al.*, 2014; Johnson *et al.*, 2015; Kavalali & Monteggia, 2015).

NMDAR CDD and the effect of $[Ca^{2+}]_i$ on memantine potency both depend on NMDAR subunit composition (Figure 7). However, perhaps surprisingly, the expression of CDD by an NMDAR subtype does not necessitate that memantine block of that subtype is $[Ca^{2+}]_i$-dependent. We report that while both GluN1/2A receptors and GluN1/2B receptors exhibit CDD, only memantine block of GluN1/2A receptors is regulated by $[Ca^{2+}]_i$. Interestingly, the memantine IC_{50}

for GluN1/2A receptors in cells with $[Ca^{2+}]_i$ = 10 µM was nearly identical to the IC_{50} values measured in both low and high $[Ca^{2+}]_i$ conditions for the other NMDAR subtypes. In contrast, memantine inhibition of GluN1/2A receptors in cells with $[Ca^{2+}]_i$ < 1 nM was weaker than memantine inhibition of any other NMDAR subtype tested, regardless of condition. Therefore, our results suggest that GluN1/2A receptors, in conditions of low $[Ca^{2+}]_i$, exhibit a unique conformational state that (1) other subtypes are unable to access and (2) exhibits weaker affinity for memantine. The existence of a unique GluN1/2A receptor state with weaker affinity for memantine, and the ability of $[Ca^{2+}]_i$ to reduce occupancy of this state and increase memantine potency, may allow memantine to act somewhat like a low-pass filter for GluN1/2A receptor activity. In conditions of weak NMDAR stimulation, memantine would permit relatively normal activity of GluN1/2A receptors while limiting activity of GluN1/2B, GluN1/2C, and GluN1/2D NMDARs. As stimulation increases, buildup of $[Ca^{2+}]_i$ initiates CDD mechanisms that push GluN1/2A-containing receptor channels into a conformation that resembles the binding sites of other NMDAR subtypes, increasing memantine inhibition of GluN1/2A receptors. This filter-like action of memantine could contribute to its surprising combination of clinical efficacy and tolerability by permitting NMDAR activity in healthy neurons while limiting NMDAR activity in neurons subjected to pathological insults. Importantly, our experiments show that memantine inhibition of GluN1/2A receptors is dynamically regulated by fluctuations of $[Ca^{2+}]_i$ across both physiological and pathological ranges, and that memantine inhibition of a mixed population of native NMDARs containing both GluN2A- and GluN2B-containing receptors is $[Ca^{2+}]_i$-dependent. Thus, the $[Ca^{2+}]_i$ dependence of inhibition of NMDARs by memantine has the potential to profoundly impact the effects of memantine on neuronal function.

3.0 STRUCTURAL BASIS OF CA^{2+}-DEPENDENT CHANNEL BLOCK OF NMDA RECEPTORS BY MEMANTINE

3.1 OVERVIEW

N-methyl-D-aspartate receptors (NMDARs) are Ca^{2+}-permeable ligand-gated ion channels expressed at nearly all excitatory vertebrate synapses. NMDAR-mediated Ca^{2+} influx is essential for many critical neuronal functions and NMDAR dysfunction is implicated in numerous nervous system pathologies. Thus, drugs targeting NMDARs are of great clinical interest. Memantine and ketamine are both clinically useful NMDAR open channel blockers with similar pharmacological properties but paradoxically different clinical profiles. Recent work from our lab has revealed key biophysical differences in how memantine and ketamine act on NMDARs. Inhibition of NMDARs by memantine, but not ketamine, is dynamically regulated by intracellular Ca^{2+} concentration ($[Ca^{2+}]_i$), a phenomenon resulting from the ability of memantine to stabilize a Ca^{2+}-dependent desensitized NMDAR state. Here, we integrate molecular dynamics simulations with whole-cell recordings to identify differences in the memantine and ketamine binding sites and test the role of these differential interactions in the relation between channel blocker binding and NMDAR desensitization. We discovered that mutation of a single residue in the NMDAR pore alters memantine potency without affecting ketamine potency, greatly affects NMDAR desensitization, and influences the $[Ca^{2+}]_i$ dependence of memantine potency. These experiments provide evidence supporting the hypothesis that the differential effects of memantine and ketamine on NMDAR desensitization result from their differential interactions with residues in the NMDAR channel.

3.2 INTRODUCTION

NMDARs are ionotropic glutamate receptors involved in nearly every aspect of synaptic function including synaptogenesis, synaptic transmission, and synaptic plasticity. This ubiquitous involvement in synaptic function allows NMDARs to regulate neuronal function on a large scale by contributing to excitation/inhibition balance, neuronal oscillations, and dendritic integration. Unsurprisingly, aberrant NMDAR activity contributes to a wide breadth of neuronal dysfunctions that can drive nervous system disorders (Javitt, 2004; Zhou & Sheng, 2013). Modulating NMDAR activity with therapeutic drugs has proven to be excruciatingly complicated. The NMDAR open channel blockers memantine and ketamine provide two particularly interesting examples of the complex effects of NMDAR antagonism. Both memantine and ketamine show significant therapeutic utility, but despite sharing similar affinities, binding kinetics, and overlapping binding sites in the NMDAR transmembrane domain (TMD), possess wildly divergent clinical profiles (Ferrer-Montiel *et al.*, 1998; Parsons, Danysz, & Quack, 1999; Kashiwagi *et al.*, 2002; Chen & Lipton, 2006; Emnett *et al.*, 2013; Johnson *et al.*, 2015). Ketamine, but not memantine, shows great efficacy in the treatment of pain and major depressive disorder (Persson, 2013; Abdallah *et al.*, 2015; Kavalali & Monteggia, 2015) but is a drug of abuse and produces/exacerbates symptoms of schizophrenia (Krystal *et al.*, 2003; Bondi *et al.*, 2012; Corazza *et al.*, 2013). In contrast, Mem is well-tolerated, approved for treatment of Alzheimer's disease, and shows promise in treatment of other disorders including, paradoxically, schizophrenia (Chen & Lipton, 2006; Lipton, 2006; Parsons *et al.*, 2007; Danysz & Parsons, 2012; Parsons & Raymond, 2014; Di Iorio *et al.*, 2017). Our current understanding of the mechanisms of action of memantine and ketamine is unable to account for their divergent systemic effects.

Some clinical differences between memantine and ketamine, such as the hypnotic effect of ketamine (Chen, Shu, *et al.*, 2009), result from actions at different non-NMDAR targets.

However, there is substantial evidence that the effects of memantine and ketamine depend predominantly on inhibition of NMDARs ((Javitt, 2004; Wenk *et al.*, 2006; Parsons *et al.*, 2007; Bondi *et al.*, 2012), but see (Zanos *et al.*, 2016) for additional potential mechanisms of Ket in depression). Furthermore, differences between memantine and ketamine pharmacokinetics minimally contribute to the observed differences in their behavioral effects (Kotermanski *et al.*, 2013). Therefore, understanding the mechanisms underlying the differential effects of memantine and ketamine requires deeper insight into the biophysical action of each drug on NMDARs.

To this end, an attractive target of study is our discovery that inhibition of NMDAR by memantine, but not ketamine, is dynamically regulated by intracellular Ca^{2+} concentration ($[Ca^{2+}]_i$). In Chapter 2 we reported that increasing $[Ca^{2+}]_i$ increases memantine potency, and that the $[Ca^{2+}]_i$ dependence of memantine inhibition results from stabilization of a Ca^{2+}-dependent desensitized NMDAR state. This state specificity allows memantine to both block current flow through open receptors and stabilize closed receptors to varying degrees based on $[Ca^{2+}]_i$. Ca^{2+} dynamics and handling vary heavily by subcellular region and neuronal subtype (Schwaller, 2010; Higley & Sabatini, 2012), and desensitization of NMDARs plays a key role in shaping postsynaptic responses and plasticity (Jones & Westbrook, 1996; Urakubo *et al.*, 2008). Thus, the $[Ca^{2+}]_i$ dependence of memantine inhibition could provide a mechanism through which memantine preferentially targets different subpopulations of NMDARs than ketamine, potentially underpinning many of the striking dissimilarities observed between the two drugs. Additionally, the $[Ca^{2+}]_i$ dependence of memantine inhibition suggests an innovative, logical mechanism of neuroprotection: preferential inhibition of NMDARs that are exposed to large and prolonged increases of Ca^{2+}_i, i.e. receptors likely to mediate excitotoxic cell death (Zorumski & Olney, 1993; Rothman & Olney, 1995; Hasbani *et al.*, 1998; Hardingham & Bading, 2010; Wroge *et al.*, 2012; Zhou *et al.*, 2013).

The mechanism by which memantine stabilizes closed channels is currently unknown. Given that memantine and ketamine show differential effects on GluN1/2A receptor desensitization, it is likely that the structural interactions between each drug and the GluN1/2A channel also differ. However, despite their clinical relevance, there have been no direct comparisons of the memantine and ketamine binding sites. Here, we utilize a powerful combination of molecular simulations with atomistic GluN1/2A TMD models and whole-cell electrophysiology in transfected cells to investigate the relation between channel blocker-GluN1/2A channel interactions, desensitization, and the $[Ca^{2+}]_i$ dependence of memantine inhibition.

3.3 MATERIALS AND METHODS

3.3.1 Molecular modeling

All simulations were carried out using fully atomistic models of the GluN1/2A TMD. The GluN1/2A TMD model shown in Figure 11 (referred to as the 2017 model) and used for initial docking simulations for memantine and ketamine was developed in collaboration with the Kurnikova Lab of Carnegie Mellon University (Mesbahi-Vasey *et al.*, 2017). The 2017 model was initially constructed by homology modeling based on NaK (PDB 2AHY; (Shi *et al.*, 2006)) and AMPAR (PDB 3KG2; (Sobolevsky *et al.*, 2009)) crystal structures and was refined with targeted MD simulations to incorporate data from an NMDAR crystal structure (PDB 3KG2; (Lee *et al.*, 2014)). I developed and optimized models of memantine and ketamine using the software Gaussian 09 (M.J. Frisch, 2009). All docking simulations were carried out using the software Autodock Vina (Trott & Olson, 2010) with the assistance of Dr. Chamali Narangoda of the

Kurnikova Lab. For docking simulations, side chains of memantine and ketamine were allowed to rotate while protein side chains were held rigid. Memantine and ketamine were docked to 20 different snapshots of the closed 2017 model. Each docking simulation produced 9 predicted docking poses for each drug. The most commonly predicted poses were then assessed for consistency with experimental predictions of channel blocker binding sites, i.e. whether the charged amine group of the blocker was in close proximity to the critical asparagine residues GluN1 N616 and GluN2A N614, which are heavily implicated in NMDAR channel block (Burnashev, Schoepfer, *et al.*, 1992; Mori *et al.*, 1992; Kuner & Schoepfer, 1996; Ferrer-Montiel *et al.*, 1998; Kashiwagi *et al.*, 2002; Chen & Lipton, 2005; Mesbahi-Vasey *et al.*, 2017).

The GluN1/2A TMD model shown in Figure 14 (referred to as the 2019 model) and used for molecular dynamics (MD) simulations was developed from a cryo-EM density structure template (PDB 6MM9; (Jalali-Yazdi *et al.*, 2018)) by our collaborators Drs. Dhilon Patel and Maria Kurnikova of Carnegie Mellon University. After generation of the model, it was placed in an equilibrated 1-palmitoyl-2-oleoyl-sn-glycero-3-phosphocholine (POPC) bilayer, solvated with water, Na^+ and Cl^- ions, and equilibrated. Initial docking of memantine to this model was also performed with Autodock Vina. MD simulations were carried out with the MD software package Amber18 using the pmemd.cuda program (Case *et al.*, 2017). Pressure and temperature of the simulated system were maintained at 1 bar and 300 K, respectively. MD simulations of memantine binding to the NMDAR channel were carried out for WT as well as GluN1/2A(F641A) and GluN1/2A(F641W) receptors. Two 200 ns simulations were performed for each receptor-memantine complex. MD simulations were performed by Dr. Dhilon Patel with my assistance.

3.3.2 Cell culture and transfection

All experiments were performed in tsA201 cell cultures (European Collection of Authenticated Cell Cultures). tsA201 cells were maintained as previously described (Glasgow & Johnson, 2014) in Dulbecco's modified Eagle's medium (DMEM) supplemented with 10% fetal bovine serum and 1% GlutaMAX (Thermo Fisher Scientific). Cells were plated at a density of 10^5 cells/dish in 35 mm petri dishes on 15 mm glass coverslips treated with poly D-lysine (0.1 mg/ml) and rat-tail collagen (0.1 mg/ml). 18-24 hours after plating, the cells were transfected using FuGENE 6 (Promega) with complementary DNA (cDNA) coding for enhanced green fluorescent protein (EGFP; Genbank ACS32473 in pCI-neo) to identify transfected cells, WT rat GluN1-1a (GluN1; GenBank U08261 in pCI-neo), and either WT GluN2A (GenBank M91561 in pcDNA1) or GluN2A mutated at residue 641. Mutations were made using the Stratagene QuikChange II XL sited directed mutagenesis kit. EGFP was expressed using a specialty plasmid, pCI-neo:EGFP:GluN1-1a (a kind gift from Dr. Kasper Hansen), that allows for co-expression of independent EGFP and GluN1 subunit proteins. pCI-neo:EGFP:GluN1-1a was constructed by inserting cDNA encoding EGFP in pCI-neo under transcriptional control of the CMV promoter, between the CMV promoter and the GluN1 open reading frame (Yi *et al.*, 2018). Cells were transfected with cDNA ratios of 1 GluN1: 1 GluN2A. 200 µM of the competitive NMDAR antagonist dl-APV was added to medium at the time of transfection to prevent NMDAR-mediated cell death.

3.3.3 Electrophysiology

All patch-clamp electrophysiological experiments were performed in the whole-cell voltage-clamp configuration. Recordings from tsA201 cells were performed 18-30 hours after transfection. Pipettes were fabricated from as described in Chapter 2 (2.3.2). Whole-cell currents

were amplified with Axopatch 1D, 200A, or 200B amplifiers and digitized using a Digidata 1440A digitizer (Molecular Devices). Current signals were low-pass filtered at 5 kHz and sampled at 20 kHz using pCIamp10.7 (Molecular Devices). Series resistance was compensated between 85 – 90% in all experiments. An empirically determined liquid junction potential of -6 mV between the internal and external solutions was corrected for in all experiments.

Control bath solution (referred to as external solution) for tsA201 cell experiments contained (in mM): 140 NaCl, 2.8 KCl, 10 HEPES, 0.01 EDTA, 0.1 glycine, and either 0, 0.1 or 1 CaCl$_2$. Agonist (1 mM glutamate from 1 M stock) and antagonists (various memantine and ketamine concentrations from 10 mM stock in dH$_2$O) were added to external solutions on day of experiments. For IC$_{50}$ experiments, antagonist solutions were prepared via serial dilution. Control, agonist, and antagonist solutions were delivered to the patched cell via polyimide barrels using our in-house fabricated rapid-switching fast perfusion system (Glasgow & Johnson, 2014). Switches between solutions were performed by moving the barrel position relative to the patched cell with a voice-coil motor controlled by a custom program (Blanpied *et al.*, 1997). Solution flow rate was maintained at 1 – 2 mL/min for all experiments.

3.3.4 Intracellular solution preparation

All intracellular solutions contained 125 – 130 mM CsCl, 10 mM HEPES, and 4 mM MgATP and were pH balanced to 7.2 ± 0.05 with CsOH. For experiments in Figures 12, 13, 15, and 16, intracellular solutions contained 10 mM BAPTA. For experiments comparing the effects of [Ca^{2+}]$_i$ block and desensitization, we utilized the Ligand Optimization Method (LOM (McGuigan *et al.*, 1991, 2006)) as described in Chapter 2.3.3 to help prepare an intracellular solution containing an empirically determined [Ca^{2+}]$_F$ of 10 µM. For experiments in Figure 17, the [Ca^{2+}]$_i$ =

10 µM internal solution contained 10 mM HEDTA and 7.34 mM $CaCl_2$; the $[Ca^{2+}]_i$ < 1 nM contained 10 mM BAPTA and no added $CaCl_2$.

3.3.5 Analysis

All electrophysiologic data were analyzed with Clampfit 10.7 (Molecular Devices) and Prism 7-9 (Graphpad). Baseline current was subtracted from all current measurements. Concentration-inhibition relations for channel blockers were measured using the protocol shown in Figure 12A. Agonist was applied until current reached steady-state, then sequentially increasing concentrations of antagonist were applied the in the presence of constant [agonist]. Each [antagonist] was applied until a steady level of inhibition was reached (10 – 20 s). Antagonists were then removed and agonist alone was reapplied to allow recovery from channel block. Cells in which current did not recover to at least 85% of the steady-state current elicited by the initial agonist application were excluded from analysis. IC_{50} values were estimated as described in Chapter 2.3.4.

For experiments investigating the effects of Ca^{2+} and the GluN2A mutations on desensitization, desensitization was quantified as a ratio of steady-state current (I_{ss}) to peak current (I_{peak}) I_{ss} was measured as the mean current taken over the final 1 s of agonist application. I_{peak} was measured as the mean current over a 30 ms window set 5 ms centered on the peak absolute current. To allow for comparison of effects of mutations on CDD, I_{SS}/I_{Peak} in 1 mM extracellular Ca^{2+} (Ca^{2+}_e) was normalized to I_{SS}/I_{Peak} in 0.1 mM Ca^{2+}_e.

3.4 RESULTS

3.4.1 GluN2A residue 641 is predicted to interact with memantine, but not ketamine

The differential effects of memantine and ketamine on the stability of closed GluN1/2A channels suggests that the two channel blockers may differentially interact with channel residues. To assess whether memantine and ketamine interact with distinct channel residues, we utilized computational simulations to model the memantine and ketamine binding sites in the NMDAR channel. Using our recently published atomistic model of the GluN1/2A TMD (Mesbahi-Vasey *et al.*, 2017), we generated models of memantine and ketamine docked to a closed NMDAR channel using the software Autodock Vina (Trott & Olson, 2010). The most commonly predicted binding poses for memantine and ketamine placed them above the selectivity filter with their hydrophobic moieties nestled between the GluN1-GluN2A interface (Figure 11C,D). We then identified and compared residues within 3 Å of the predicted memantine and ketamine binding sites. Importantly, both memantine and ketamine were predicted to bind in close proximity to critical asparagine residues (GluN1 N616 and GluN2A N614; Figure 11E,F) that are key components of the NMDAR selectivity filter and heavily implicated in channel block (Burnashev, Schoepfer, *et al.*, 1992; Mori *et al.*, 1992; Kuner & Schoepfer, 1996; Ferrer-Montiel *et al.*, 1998; Kashiwagi *et al.*, 2002; Chen & Lipton, 2005; Mesbahi-Vasey *et al.*, 2017).

The predicted binding sites of memantine and ketamine heavily overlapped. Most residues within 3 Å of the docked blockers were identical. However, we identified a phenylalanine (F) residue in the M3 helix of the GluN2A subunit (F641) predicted to interact with memantine, but not ketamine (Figure 11E,F). To test the accuracy of this prediction, we experimentally investigated whether GluN2A 641 contributes to memantine or ketamine potency by making a relatively conservative phenylalanine to leucine mutation at GluN2A 641 and measuring

memantine and ketamine IC$_{50}$ (Figure 12A-F; Table 5). Interestingly, the GluN2A(F641L) mutation increased memantine potency relative to WT receptors (Figure 12G). The GluN2A(F641L) mutation had no effect on ketamine potency (Figure 12H). These results support the idea that memantine and ketamine form differential interactions with GluN1/2A channel residues.
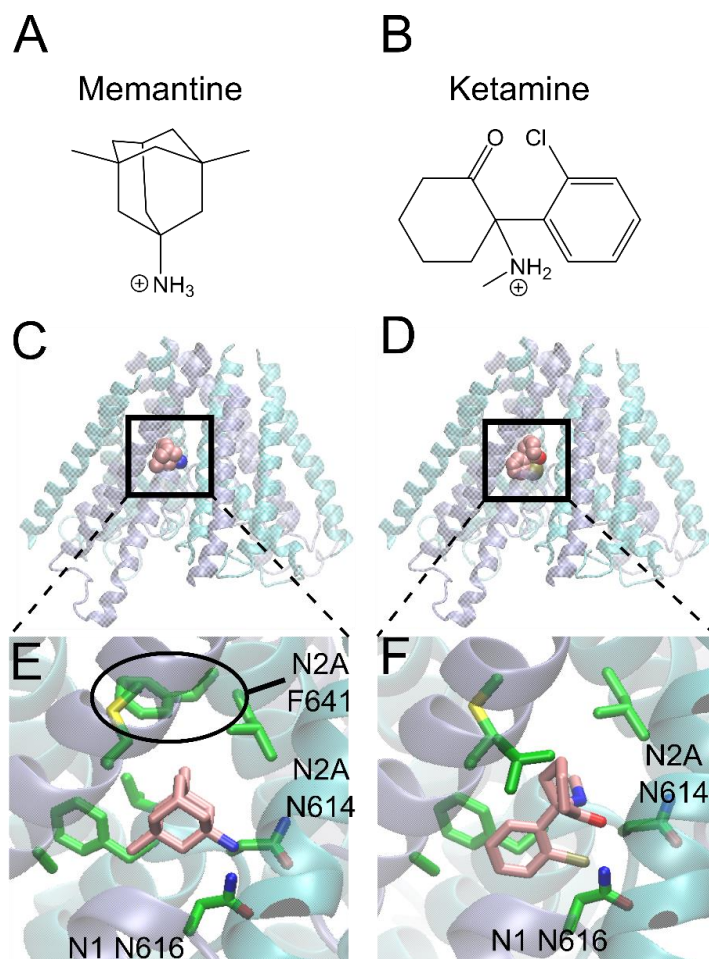
Figure 11. Docking of memantine and ketamine to 2017 GluN1/2A TMD model.

A, B, Bond-line structures of memantine (**A**) and ketamine (**B**) shown with protonated amines, the predominant form of each blocker at neutral pH (memantine pKa = 10.3 (Freudenthaler *et al.*, 1998); ketamine pKa = 7.5 (Budavari, 1989)). **C, D**, View of entire 2017 GluN1/2A TMD model (Mesbahi-Vasey *et al.*, 2017) with memantine (**C**) and ketamine (**D**) docked within the channel. GluN1 is depicted as gray-blue ribbons; GluN2A is depicted as cyan ribbons. Blockers are depicted as space-filling structures. Box depicts regions blown up in **E** and **F**. **E, F**, Magnified view of docking sites for memantine (**E**) and ketamine (**F**). Both blockers share close proximity with key asparagine residues and generated similar docking scores (memantine = - 7.1 kcal/mol; ketamine = - 8.8 kcal/mol). Residue N2A(F641) is predicted to be within 3 Å of memantine, but not ketamine. All other residues within 3 Å are shared. Colors: C = pink (drug), green (side chain); N = blue; O = red; S = yellow; Cl = gold.
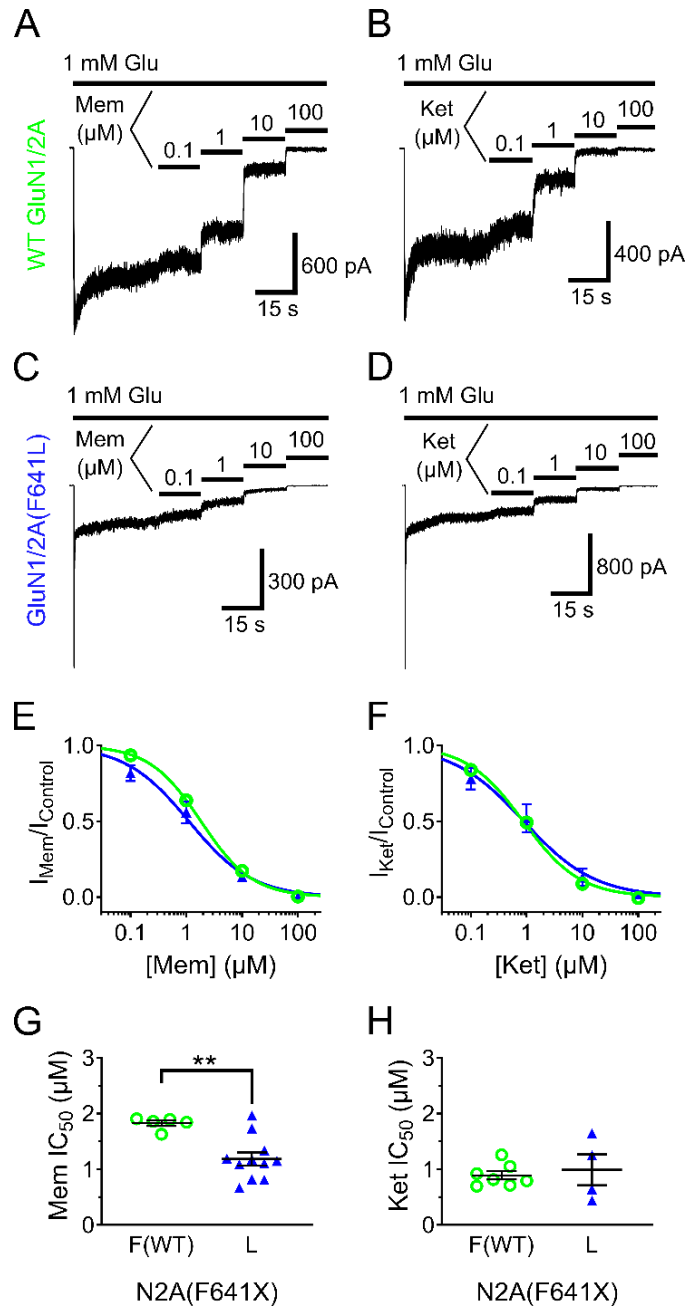
Figure 12. GluN2A F641 influences memantine potency but not ketamine potency.

A, B, Representative current traces for experiments measuring memantine (**A**) and ketamine (**B**) IC$_{50}$s for WT GluN1/2A receptors in [Ca^{2+}]$_e$ = 1 mM. **C, D**, Representative current traces for experiments measuring memantine (**C**) and ketamine (**D**) IC$_{50}$s for mutant GluN1/2A(F641L) receptors. Bars represent glutamate or memantine applications at indicated concentrations. **E, F**, IC$_{50}$ curves used to estimate memantine (**E**)

85

and ketamine (**F**) potency at WT GluN1/2A and mutant GluN1/2A(F641L) receptors. Green line and symbols represent values for WT receptors; blue line and symbols represent values for mutant receptors. Data are depicted as mean ± SEM; some error bars are smaller than symbols. Lines depict best fit of Hill equation (**Equation 3**) to data. **G, H**, Summary and comparison of IC_{50} values for memantine (**G**) and ketamine (**H**) at WT GluN1/2A and GluN1/2A(F641L) receptors. Memantine IC_{50} was significantly lower for GluN1/2A(F641L) receptors than WT receptors. Ketamine IC_{50} did not differ between groups. IC_{50} values are summarized in Table 5.

3.4.2 Size of GluN2A residue 641 influences inhibition by memantine, but not ketamine

Interestingly, the GluN2A(F641L) mutation reduced memantine IC_{50}. This effect could be due to multiple factors, including direct steric effects of the GluN2A F641 side chain on memantine binding, changes in receptor dynamics that contribute to memantine binding, or alteration of CDD. To further assess the contribution of GluN2A F641 to memantine potency, we generated additional mutant receptors with either a small residue (alanine; A) or a large aromatic residue (tryptophan; W) at position GluN2A F641 and measured memantine IC_{50} (Figure 13; Table 5). We found that mutations to smaller residues (A or L) significantly increased memantine potency (Figure 13A,B,I,K). Mutation to the larger W residue decreased memantine potency in comparison to GluN1/2A(F641A), GluN1/2A(F641L), and WT receptors (Figure 13C,D,I,K). Thus, size of GluN2A residue 641 influences memantine potency.

To ensure that the GluN1/2A(F641A) and GluN1/2A(F641W) mutations do not elicit changes in NMDAR dynamics that broadly affect channel block, we also measured and compared ketamine IC_{50}s. Importantly, none of the GluN2A F641 mutations altered ketamine potency (Figure 13 E-H,J,L; Table 5). These results confirm that mutation of GluN2A F641 does not broadly affect channel block and support the model predictions that GluN2A F641 specifically contributes to the memantine binding pocket.
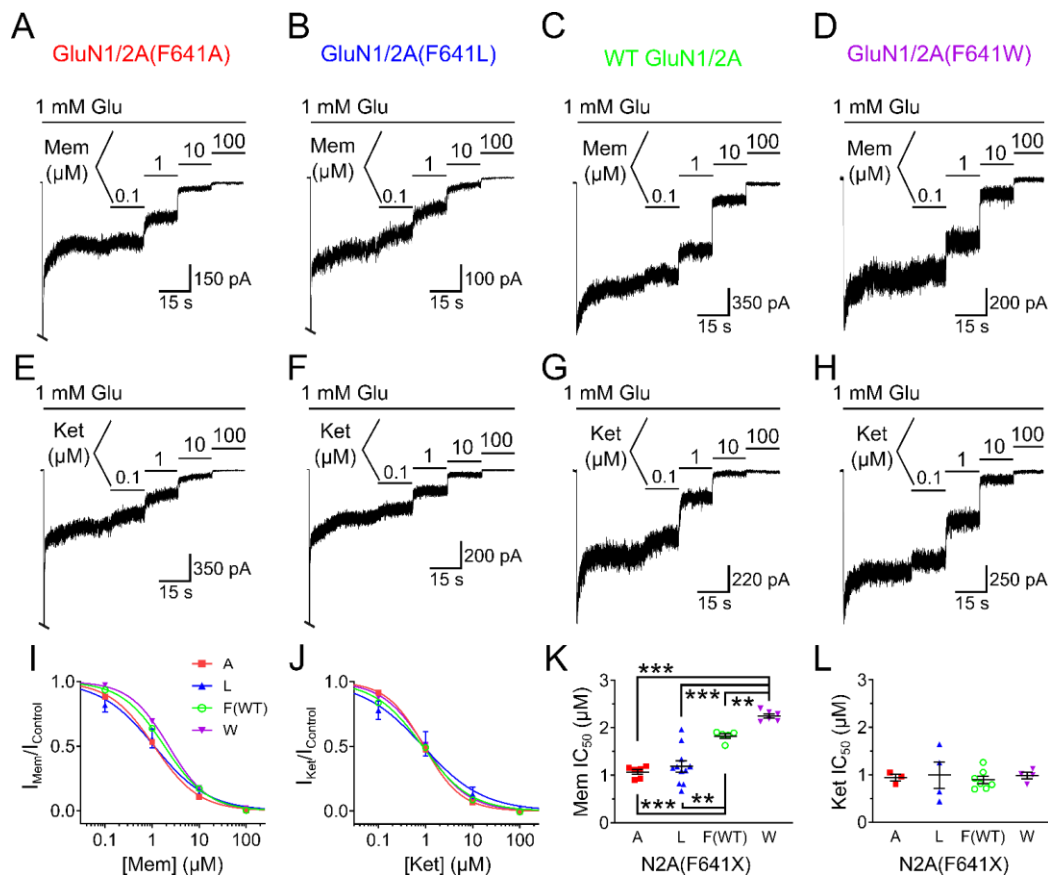
Figure 13. Size of GluN2A residue 641 influences memantine, but not ketamine, potency.

A-H, Representative GluN1/2A receptor currents used to measure memantine (**A-D**) and ketamine (**E-H**) concentration-inhibition relations in 1 mM Ca^{2+}_e. Traces are shown in order (Left → Right) of increasing residue size at position GluN2A 641. Peaks of Glu responses for GluN2A(F641A) and GluN2A(F641L) are truncated. **I, J**, Concentration-inhibition curves for memantine (**I**) and ketamine (**J**). Legend inset in I identifies amino acid residue at GluN2A position 641. Data expressed as mean ± SEM; error are bars smaller than symbols for WT, F641A, and F641W receptors. **K, L**, Summary of memantine IC_{50} values (**K**) and ketamine IC_{50} values (**L**). Memantine IC_{50} depends on residue size at GluN2A position 641, with IC_{50} decreasing with residue size (**K**). Ketamine IC_{50} does not depend on residue size at GluN2A position 641 (**L**). Points represent individual values, bar represents mean, and error bars depict SEM. **p < 0.01 , ***p < 0.001; ****p < 0.0001; one-way ANOVA with Tukey post hoc analysis. IC_{50} values are summarized in Table 5.

3.4.3 GluN2A residue 641 regulates memantine binding via inter-subunit interactions

Multiple possible mechanisms could account for the effect of GluN2A residue 641 size on memantine IC_{50}. Firstly, the large WT F and mutant W residues could form direct, energetically unfavorable interactions with memantine, limiting the stability of the TMD-memantine complex. Any steric hindrance generated by the larger residues would be removed by mutating GluN2A F641 to smaller residues (i.e., A or L), resulting in improved stability of memantine in the TMD. Another possibility is that GluN2A F641 may interact with other TMD residues that help form the memantine binding pocket, which could allow GluN2A F641 to indirectly affect memantine potency. However, our experimental data do not allow us to distinguish between direct and indirect contributions of GluN2A F641 to memantine binding. Therefore, we turned to molecular dynamics (MD) simulations to further investigate the role of GluN2A F641 in memantine binding. For MD simulations, we used an updated, more advanced NMDAR TMD model developed from a recent cryo-EM density structure of a GluN1/2A receptor (Jalali-Yazdi *et al.*, 2018). The 2019 model (Figure 14A,B) holds the advantage over the 2017 model (Figure 11; (Mesbahi-Vasey *et al.*, 2017) of being constructed based on an GluN1/2A receptor template rather than NaK, AMPAR, and GluN1/2B receptor channel templates. In addition, the 2019 model includes the linker residues connecting the first and second transmembrane helices (M1 and M2) as well as the helical pre-M1 region.

To investigate the role of GluN2A F641 on memantine binding, we docked memantine to the 2019 model using Autodock Vina (Trott & Olson, 2010) and used the docking positions as starting points for MD simulations. We then performed MD simulations with the memantine-TMD complex immersed in a POPC lipid bilayer (Figure 14A). Interestingly, we observed no direct interactions between GluN2A F641 and memantine in our simulations. Therefore, we performed *in silico* mutagenesis experiments to explore the mechanism by which the GluN2A(F641A) and

GluN2A(F641W) mutants affect memantine binding. Simulations with GluN2A(F641A) and GluN2A(F641W) mutants again did not show direct interaction of memantine with GluN2A residue 641. However, we instead observed that mutation of GluN2A F641 produced a pronounced change in an adjacent GluN1 residue, GluN1 M641.

Our simulations revealed that GluN1 M641 adopts one of two possible conformations depending on the size of GluN2A 641. In GluN1/2A(F641A) receptors, the GluN1 M641 side chain adopts a conformation projecting into the channel cavity, where it forms an energetically favorable interaction with memantine (Figure 14C). In contrast, the F641 residue of the WT GluN2A subunit forms an energetically favorable interaction with GluN1 M641, encouraging the side chain of GluN1 M641 to adopt a conformation projecting away from the channel cavity into a position where it is unlikely to interact with memantine (Figure 14D). In GluN1/2A(F641W) receptors, the interaction between GluN1 M641 and the large GluN2A W641 residue is strengthened, further restricting the movement of the GluN1 M641 side chain to this "outward" conformation and thus limiting its ability to interact with memantine (Figure 14E). In simpler terms, the large GluN2A F641 and mutant GluN2A W641 side chains can effectively compete with memantine for interaction with GluN1 M641. In contrast, the mutant GluN2A(F641A) residue is too small to strongly interact with GluN1 M641, allowing GluN1 M641 to preferentially adopt the "inward" conformation in which it favorably interacts with memantine. The results of our simulations mesh well with our experimental data showing that memantine potency depends on the size of GluN2A 641 (Figure 13). Thus, our modeling results suggest that GluN2A residue 641 indirectly regulates memantine binding via inter-subunit interactions.
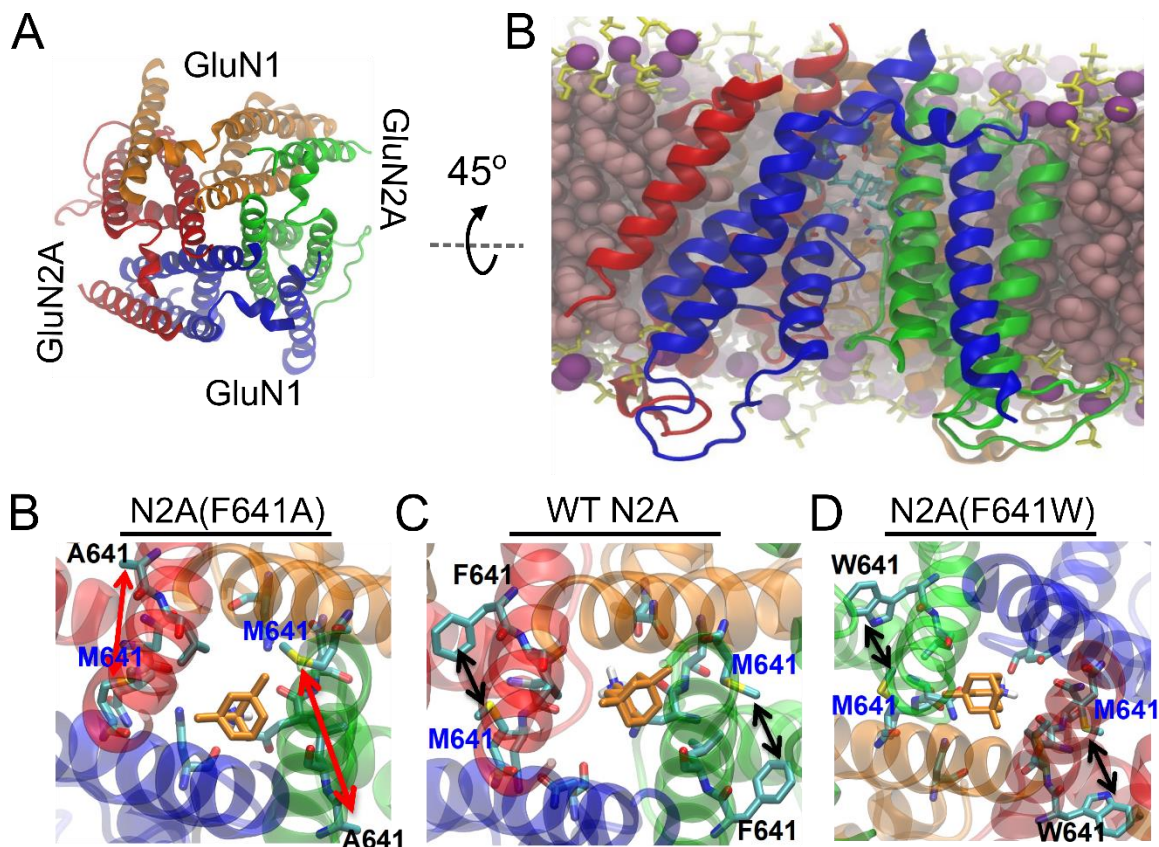
Figure 14. Mutation of GluN2A residue 641 affects dynamics of GluN1 M641.

A, Top-down view of 2019 GluN1/2A TMD model showing symmetry and central channel. For all panels, protein is depicted using a ribbon diagram; GluN1 subunits are blue and orange, GluN2A subunits are red and green. Memantine is shown as a stick model in the center of the channel. **B**, Snapshot of 2019 GluN1/2A TMD-memantine complex inserted into POPC bilayer. POPC head groups are shown as yellow sticks, with phosphates as purple spheres and fatty acid chains as pink spheres. **C**, Zoomed in top-down snapshot of memantine bound in GluN1/2A(F641A) receptor channel. Red arrows show large distance between GluN1 M641 and GluN2A A641. Due to lack of interaction with GluN2A(F641A), GluN1 M641 projects toward the center of the channel and engages in memantine binding. **D**, Zoomed in top-down snapshot of memantine binding site in WT GluN1/2A receptor channel. Black arrows show distance between GluN1 M641 and GluN2A F641. Due to interaction with GluN2A F641, GluN1 M641 adopts a conformation away from the center of the channel cavity, limiting favorable interactions with memantine. **E**, Zoomed in top-down snapshot of memantine binding site in GluN1/2A(F641W) receptor channel. Black

arrows show short distance between GluN1 M641 and GluN2A(F641W). Due to strong interaction with GluN2A(F641W), GluN1 M641 adopts a conformation away from the center of the channel cavity, preventing its favorable interaction with memantine.

Images adapted for this figure were generated by Dr. Dhilon Patel.

3.4.4 GluN2A residue 641 plays a key role in both Ca^{2+}-independent and Ca^{2+}-dependent desensitization of NMDARs

In addition to affecting memantine potency, mutation of GluN2A F641 has obvious effects on NMDAR desensitization (Figure 12C,D; Figure 13A,B,E,F). Given the link between memantine potency and CDD (Chapter 2), we next sought to investigate the role of GluN2A F641 in NMDAR desensitization. We measured desensitization of WT and mutant receptors in conditions of 0.1 and 1 mM Ca^{2+}_e to determine the effects of GluN1/2A F641 mutations on both Ca^{2+}-independent and Ca^{2+}-dependent desensitization. Experiments in 0.1 mM Ca^{2+}_e allowed us to assess effects of mutations specifically on Ca^{2+}-independent desensitization, while experiments in 1 mM Ca^{2+}_e allowed us to assess effects of mutants on total desensitization due to both Ca^{2+}-dependent and Ca^{2+}-independent mechanisms. GluN1/2A(F641A) and GluN1/2A(F641L) receptors exhibited robust desensitization in both 0.1 mM and 1 mM Ca^{2+}_e (Figure 15A,B). Interestingly, GluN1/2A(F641L) receptors exhibited stronger desensitization (i.e., smaller I_{ss}/I_{Peak}) than GluN1/2A(F641A) receptors in 0.1 mM Ca^{2+}_e (Figure 15C), despite showing similar I_{ss}/I_{Peak} in 1 mM Ca^{2+}_e (Figure 15D). This suggests that GluN1/2A(F641L) receptors undergo greater Ca^{2+}-independent desensitization than GluN1/2A(F641A) receptors. As expected, WT receptors displayed moderate desensitization in 1 mM Ca^{2+}_e and weak desensitization in 0.1 mM Ca^{2+}_e. GluN1/2A(F641W) mutants displayed weak desensitization in both conditions, and significantly weaker desensitization than WT receptors in 1 mM Ca^{2+}_e (Figure 15D). These results, similarly to our IC_{50} experiments, revealed a clear role of GluN2A residue 641 in desensitization, with desensitization in both 0.1 and 1 mM Ca^{2+} generally decreasing as residue size at position GluN2A 641 increases (Figure 15C,D).

We then assessed the effect of GluN2A 641 mutations on CDD by comparing I_{ss}/I_{Peak} values recorded in 0.1 and 1 mM Ca^{2+}_e. We found a clear relation between GluN2A 641 residue

size and CDD (Figure 16). GluN1/2A(F641A) (Figure 16A,E), GluN1/2A(F641L) (Figure 16B,F), and WT (Figure 16C,G) receptors displayed clear CDD, with GluN1/2A(F641A) receptors exhibiting robust CDD. In contrast, desensitization of GluN1/2A(F641W) receptors showed no dependence on $[Ca^{2+}]_e$ (Figure 16D,H). Interestingly, despite strongly affecting Ca^{2+}-independent desensitization (Figure 15C), the GluN1/2A(F641L) mutation had no effect on CDD in comparison to WT (Figure 16I). This surprising result may suggest that the structure of Ca^{2+}-dependent desensitized states may differ from Ca^{2+}-independent desensitized states. Overall, these experiments suggest that CDD, like memantine IC_{50} and nonspecific NMDAR desensitization, depends on the size of GluN2A residue 641, with CDD generally decreasing as residue size increases (Figure 16I). These results are consistent with our previous data supporting the idea that memantine IC_{50} and NMDAR desensitization are inherently intertwined.
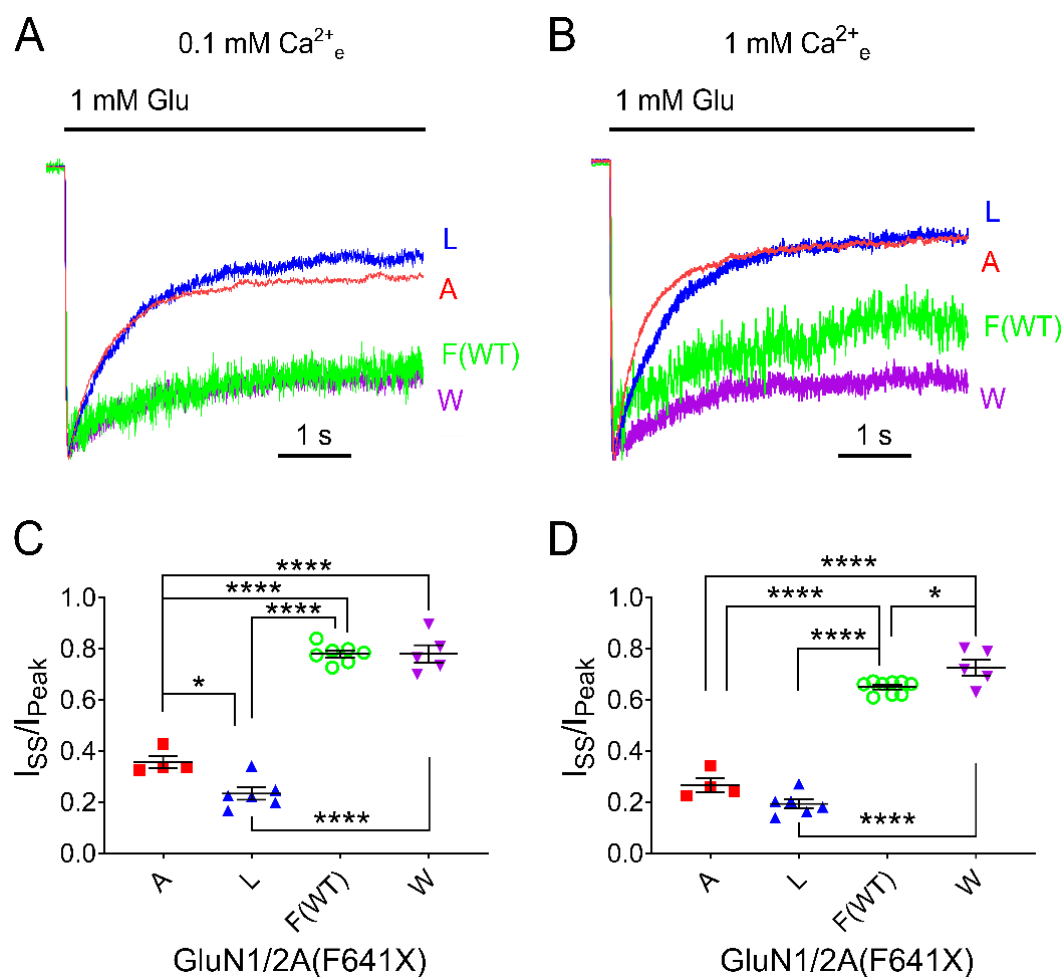
Figure 15. Mutation of GluN2A(F641) alters NMDAR desensitization.

A, B, Representative GluN1/2A receptor currents used to measure I_{SS}/I_{Peak} for WT receptors and indicated GluN2A F641 mutants in 0.1 mM Ca^{2+}_e (**A**) and 1 mM Ca^{2+}_e (**B**). Traces are normalized to I_{Peak} for visualization of differences in desensitization. **C, D**, Summary of values for WT receptors and GluN2A(F641) mutants in 0.1 mM Ca^{2+}_e (**C**) and 1 mM Ca^{2+}_e (**D**). Mutation of GluN1/2A(F641) significantly altered desensitization in both 0.1 mM Ca^{2+}_e and 1 mM Ca^{2+}_e. Points represent individual values, bar represents mean, and error bars depict SEM; *p < 0.05, ****p < 0.0001; one-way ANOVA with Tukey post hoc analysis. I_{SS}/I_{Peak} values summarized in Table 5.
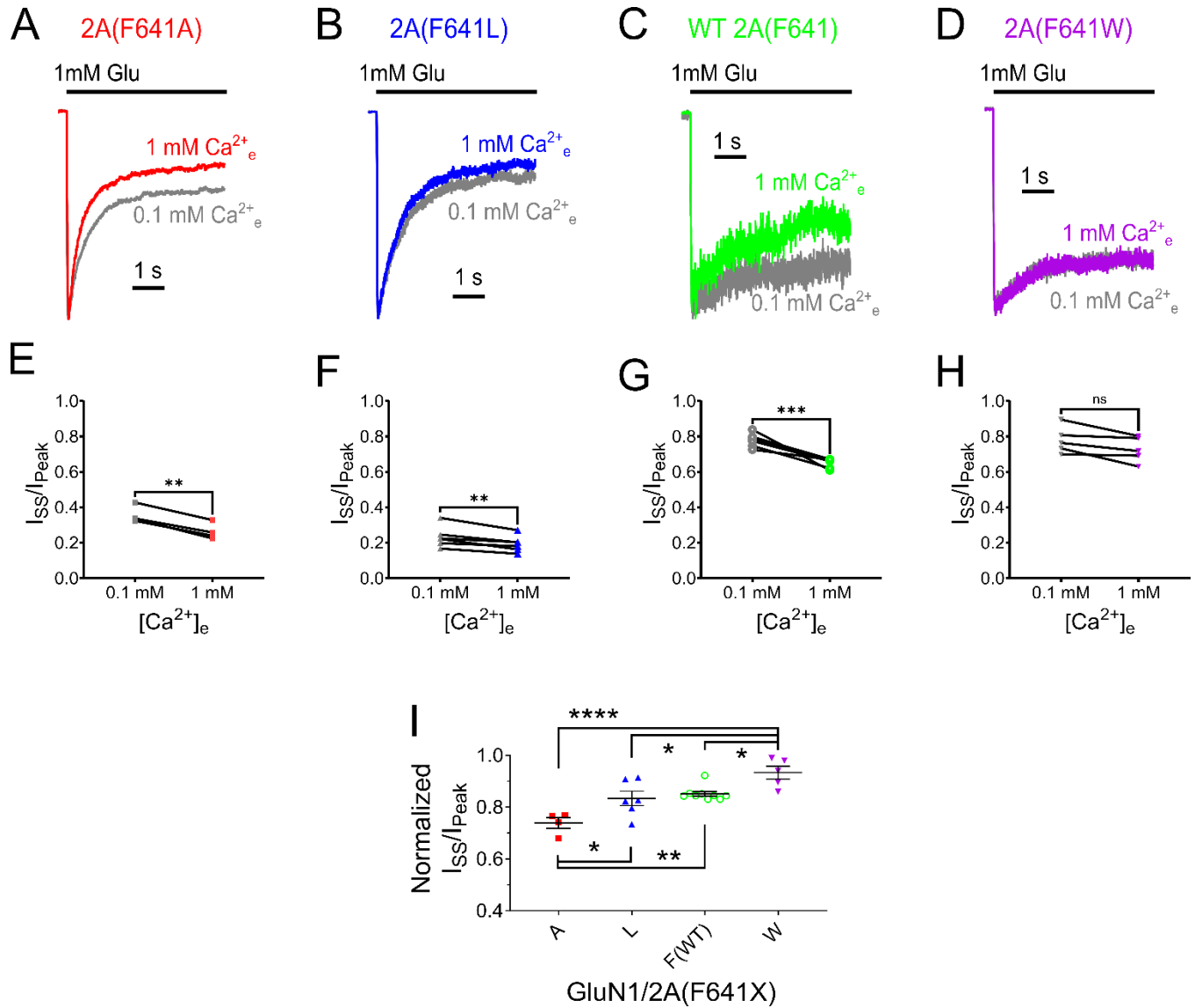
Figure 16. Size of GluN2A residue 641 plays a key role in $[Ca^{2+}]_i$-dependent desensitization.

A – D, Representative current traces from WT and mutant GluN1/2A(F641X) receptors used to measure I_{SS}/I_{Peak} in 0.1 (grey) and 1 mM Ca^{2+}_e (N2A(F641A), red; N2A(F641L), blue; WT, green; N2A(F641W), purple). Traces are shown in order (Left → Right) of increasing residue size at position GluN2A 641. Traces are normalized to I_{Peak} for visualization of differences in desensitization. **E – H**, Comparison of I_{SS}/I_{Peak} values measured in 0.1 and 1 mM Ca^{2+}_e for WT and mutant GluN1/2A(F641X) receptors. GluN1/2A(F641A) (**E**), GluN1/2A(F641L) (**F**), and WT (**G**) receptors all display significant CDD. GluN1/2A(F641W) receptors do not display CDD (**H**). Points represent individual values, connecting lines show pairs. Data analyzed with

paired t-test. **I**, Summary of normalized I_{SS}/I_{Peak} values (1 mM Ca^{2+}_e I_{SS}/I_{Peak} normalized to 0.1 mM Ca^{2+}_e I_{SS}/I_{peak}) for WT receptors and GluN2A(F641) mutants. CDD depends on residue size at GluN2A position 641, with the amount of CDD increasing as residue size decreases. Points represent individual values, bar represents mean, and error bars depict SEM; one-way ANOVA with Tukey post hoc analysis. For **E – I**, *, $p < 0.05$; **, $p < 0.01$; ***, $p < 0.001$; ****, $p < 0.0001$. I_{SS}/I_{Peak} and normalized I_{SS}/I_{Peak} values summarized in Table 5.

Table 5. Memantine block and desensitization of WT and GluN1/2A(F641) mutant receptors.

Values represent means ± sem (n).

Receptor	IC$_{50}$ (µM)		I$_{SS}$/I$_{Peak}$		Normalized I$_{SS}$/I$_{Peak}$
	Memantine	Ketamine	[Ca^{2+}]$_e$ = 0.1 mM	[Ca^{2+}]$_e$ = 1 mM	1/0.1 mM [Ca^{2+}]$_e$
GluN1/2A(F641A)	1.07 ± 0.05 (6)	0.94 ± 0.07 (3)	0.36 ± 0.02 (4)	0.27 ± 0.03 (4)	0.73 ± 0.02 (4)
GluN1/2A(F641L)	1.11 ± 0.12 (11)	0.99 ± 0.27 (4)	0.23 ± 0.02 (6)	0.19 ± 0.02 (6)	0.83 ± 0.02 (6)
WT	1.83 ± 0.05 (5)	0.89 ± 0.08 (7)	0.78 ± 0.01 (7)	0.65 ± 0.01 (9)	0.85 ± 0.01 (7)
GluN1/2A(F641W)	2.25 ± 0.05 (6)	0.98 ± 0.07 (4)	0.78 ± 0.03 (5)	0.73 ± 0.03 (5)	0.93 ± 0.03 (5)

3.4.5 GluN2A residue 641 contributes to the effects of $[Ca^{2+}]_i$ on desensitization and memantine inhibition of NMDARs

Given the role of GluN2A F641 in memantine potency and desensitization, we next assessed whether mutation of GluN2A F641 affects the $[Ca^{2+}]_i$ dependence of memantine inhibition. We measured desensitization and memantine IC_{50} for GluN2A(F641A), WT, and GluN2A(F641W) receptors while using specially prepared, Ca^{2+}-buffering pipette solutions to maintain $[Ca^{2+}]_i$ at either < 1 nM or 10 μM. We did not include GluN2A(F641L) receptors in these experiments, as the L mutation showed no effect on CDD (Figure 16I). Inhibition of GluN2A(F641A) and WT receptors by memantine was powerfully dependent on $[Ca^{2+}]_i$ (Figure 17A,B,E). Despite showing enhanced CDD in comparison to WT receptors, memantine inhibition of GluN2A(F641A) receptors did not exhibit greater dependence on $[Ca^{2+}]_i$, perhaps suggesting that the $[Ca^{2+}]_i$ dependence of memantine inhibition reaches a floor at $IC_{50} \approx 0.7$ μM (Figure 17E). Surprisingly, memantine inhibition of GluN1/2A(F641W) mutants also displayed some degree of $[Ca^{2+}]_i$ dependence. However, the effect of $[Ca^{2+}]_i$ on memantine block of GluN1/2A(F641W) mutants was much weaker than the effects observed in WT or GluN1/2A(F641A) receptors (Figure 17E), which is consistent with our previous data showing that the GluN2A(F641W) mutation weakens CDD (Figure 16D,H,I).

As expected, desensitization of both GluN1/2A(F641A) and WT receptors was augmented by high $[Ca^{2+}]_i$ (Figure 17F). However, in surprising contrast to experiments manipulating $[Ca^{2+}]_e$, desensitization of GluN2A(F641W) receptors was also dependent on $[Ca^{2+}]_i$. Furthermore, the magnitude of $[Ca^{2+}]_i$-dependent desensitization of GluN2A(F641W) receptors was similar to that exhibited by WT receptors (Figure 17F). This result seems inconsistent with the idea that the effects of the GluN2A(F641W) mutation on memantine potency are related to its effects on desensitization. However, it is possible that the desensitization elicited by our experiments

99

manipulating $[Ca^{2+}]_i$ may result from a different mechanism than our previous experiments manipulating $[Ca^{2+}]_e$ (Figure 16). Regardless of mechanism, it is clear that mutation of GluN2A F641 has profound implications for the $[Ca^{2+}]_i$ dependence of memantine inhibition of GluN1/2A receptors.
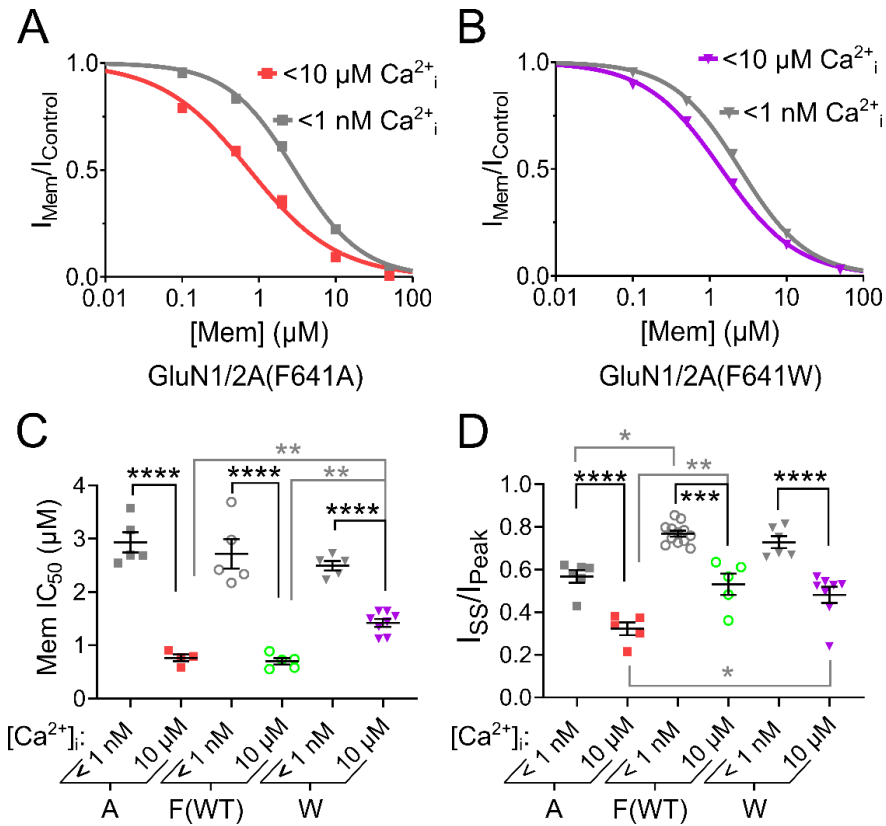
Figure 17. GluN2A residue 641 influences [Ca^{2+}]$_i$-dependent desensitization and the [Ca^{2+}]$_i$ dependence of memantine inhibition.

A, B, Concentration-inhibition curves for memantine inhibition of (A) GluN1/2A(F641A) and (B) GluN1/2A(F641W) receptors in conditions of [Ca^{2+}]$_i$ < 1 nM and [Ca^{2+}]$_i$ = 10 μM. Line depicts best fit of data to the Hill equation (**Equation 3**). Points and error bars show mean ± SEM. Some error bars are smaller than points. **C,** Summary of the [Ca^{2+}]$_i$ dependence of memantine IC$_{50}$ for WT receptors and GluN2A(F641) mutant receptors. IC$_{50}$ values are compared between conditions of [Ca^{2+}]$_i$ < 1 nM and [Ca^{2+}]$_i$ = 10 μM (black significance symbols and brackets) and across identity of GluN2A residue 641 (gray significance symbols and brackets). **D,** Summary of the [Ca^{2+}]$_i$ dependence of desensitization of WT receptors and GluN2A(F641) mutant receptors. I$_{SS}$/I$_{Peak}$ values are compared between conditions of [Ca^{2+}]$_i$ < 1 nM and [Ca^{2+}]$_i$ = 10 μM and across identity of GluN2A residue 641. Points represent individual values, bar represents mean, and error bars depict SEM. Data for **E** – **F** analyzed by way of two-way ANOVA with Tukey post hoc analysis; *, p < 0.05; **, p < 0.01; ***, p < 0.001; ****, p < 0.0001.

101

3.5 DISCUSSION

Inhibition of NMDARs by memantine, but not ketamine, is dynamically regulated by intracellular Ca^{2+} concentration ($[Ca^{2+}]_i$), a phenomenon resulting from the ability of memantine to stabilize a Ca^{2+}-dependent desensitized NMDAR state. In this chapter, we integrated computational simulations of NMDAR structure with electrophysiological experiments to investigate the role that differential blocker-NMDAR TMD interactions may play in the relation between NMDAR channel block and desensitization. We provide multiple lines of evidence in support of the hypothesis that the differential effects of memantine and ketamine on NMDAR desensitization result from their differential interactions with residues in the NMDAR channel, but significant caveats must be considered when interpreting modeling results and data from mutant receptors.

Our docking simulations identified a TMD residue, GluN2A F641, that was predicted to interact with memantine but not ketamine. Electrophysiological experiments supported this prediction, as mutation of GluN2A F641 altered memantine potency without affecting ketamine potency. However, docking simulations have significant limitations, such as use of rigid protein and ligand structure, and our electrophysiological data only test for functional effects of the mutations on memantine potency, not structural interactions. Indeed, our more sophisticated MD simulations suggested that GluN2A F641 does not form direct interactions with memantine. Our MD simulations instead describe a mechanism by which GluN2A F641 can indirectly influence memantine potency – by influencing the structure of the memantine binding site (Figure 14). Indirect effects of other residues on blocker potency have been previously reported (Siegler Retchless *et al.*, 2012), supporting the plausibility of this result. Interestingly, GluN1 M641, a residue predicted to be (1) involved in memantine binding and (2) influenced by GluN2A F641, was predicted by docking simulations to be in close proximity to both the memantine and ketamine

binding sites (Figure 11). However, GluN2A F641 does not contribute to ketamine potency (Figures 12 and 13), suggesting that memantine and ketamine may differentially interact with residues shared by their overlapping binding sites. A clear next step for the comparative analysis of the memantine and ketamine binding sites is experimentally testing the contribution of GluN1 M641 to memantine and ketamine potency.

An attractive interpretation of our data is that size of GluN2A residue 641 regulates desensitization, which in turn regulates memantine potency. Indeed, we found that mutation of GluN2A F641 to a smaller A residue enhances CDD and memantine potency, while mutation of GluN2A F641 to a larger W residue weakens desensitization and memantine potency (Figures 13, 15, and 16). Although the idea that GluN2A 641 residue size regulates memantine inhibition and NMDAR desensitization via a common mechanism is enticing, the effects of Ca^{2+} on memantine inhibition and desensitization of GluN2A(F641L) and GluN2A(F641W) mutants are complex.

GluN1/2A(F641L) mutant receptors display increased memantine potency (Figure 13) and Ca^{2+}-independent desensitization in comparison to WT receptors (Figure 15), but similar magnitudes of CDD (Figure 16). This finding argues against the idea that the effects of GluN2A F641 mutation on CDD underlies their differences in memantine potency. Interestingly, the data for GluN1/2A(F641L) mutants also shows far greater variability than data for other receptors tested, in nearly all experiments. It is possible that the relatively high flexibility of L contributes to the variability we see in its data as well as its differences from the other receptors. In contrast to WT and the other mutant GluN2A 641 residues, which are either large and rigid (W and F) or small with no meaningful rotatable bonds (A), L can sample a broad range of conformations. Therefore, the GluN1/2A(F641L) mutant may form unexpected contacts that stabilize or destabilize multiple states that we cannot easily resolve with electrophysiological experiments. Investigation of the effects of $[Ca^{2+}]_i$ on desensitization and memantine inhibition of

GluN1/2A(F641L) receptors would allow for further comparison with WT and the other mutant receptors, and *in silico* mutagenesis MD simulations may provide further insight into the role of residue flexibility on the electrophysiological characteristics of GluN1/2A(F641L) receptors.

The effects of Ca^{2+} on memantine inhibition and desensitization of GluN1/2A(F641W) mutant receptors are also intriguing. GluN2A(F641W) receptors did not exhibit CDD in experiments manipulating $[Ca^{2+}]_e$ (Figure 16), but both desensitization and memantine inhibition of GluN2A(F641W) receptors were dependent on $[Ca^{2+}]_i$ (Figure 17). This could be interpreted as evidence for the existence of multiple mechanisms of CDD, similar to our interpretation of Chapter 2 data (2.4.4) regarding the time dependence of $[Ca^{2+}]_i$-dependent desensitization. However the $[Ca^{2+}]_i$-and-time-dependent form of CDD, which is likely to be the form displayed by GluN1/2A(F641W) receptors due to the similarity in conditions for experiments in Figures 8 and 17 (high $[Ca^{2+}]_i$ internal solutions, 5-10 min wait time post-break in), showed no relation to the $[Ca^{2+}]_i$ dependence of memantine potency of WT receptors (Figure 8). Furthermore, desensitization of GluN2A(F641W) receptors in conditions of high $[Ca^{2+}]_i$ is comparable to that exhibited by WT receptors, but memantine inhibition of GluN2A(F641W) receptors was shown to be less dependent on $[Ca^{2+}]_i$ than inhibition of WT receptors (Figure 17). This reduction in sensitivity to $[Ca^{2+}]_i$ is consistent with the reduced CDD exhibited by GluN1/2A(F641W) receptors in experiments manipulating $[Ca^{2+}]_e$ (Figure 16), but inconsistent with results from experiments manipulating $[Ca^{2+}]_i$ (Figure 17). Therefore, although it is clear that GluN2A(F641W) receptors undergo some form of CDD, the relation between CDD and the $[Ca^{2+}]_i$ dependence of memantine inhibition of GluN1/2A(F641W) mutants remains unclear.

Interpretation of GluN2A(F641A) receptor data was far more straightforward, but not without some surprises. Despite exhibiting a lower memantine IC_{50} than WT receptors in conditions of 1 mM $[Ca^{2+}]_e$ with a 10 mM BAPTA internal solution (Figure 13) and displaying increased CDD in experiments manipulating $[Ca^{2+}]_e$ (Figure 16), memantine IC_{50} for

GluN2A(F641A) receptors did not differ from WT receptors in either $[Ca^{2+}]_i$ condition (Figure 17). This suggests that memantine inhibition of GluN2A(F641A) receptors and WT receptors is similarly sensitive to $[Ca^{2+}]_i$. However, it is equally possible that the IC_{50} values generated by our experiments, which utilized extremely low (< 1 nM) and high (10 µM) $[Ca^{2+}]_i$ conditions, may only represent the maximal and minimal memantine IC_{50} values for GluN2A(F641A) receptors, i.e. the floor and ceiling levels of the effect of $[Ca^{2+}]_i$ on memantine IC_{50}. Generation of a $[Ca^{2+}]_i$-memantine IC_{50} curve (as shown in Figure 4 for WT receptors) would allow for a more direct assessment of differences in the effect of $[Ca^{2+}]_i$ on memantine inhibition of GluN1/2A(F641A) and WT receptors.

4.0 ELECTROPHYSIOLOGICAL CHARACTERIZATION OF NOVEL NMDA RECEPTOR CHANNEL BLOCKING COMPOUNDS

Chapter 4 is adapted from Appendix B (Leiva *et al.*, 2018). Minor revisions were made to language and structure to facilitate integration of additional data.

4.1 OVERVIEW

NMDAR activity is critical for many types of synaptic plasticity and is a key player in memory formation and learning. Conversely, aberrant NMDAR activation is implicated in a variety of nervous system disorders. Excessive NMDAR activity can lead to build up of pathological levels of intracellular calcium and lead to cell death, a process known as excitotoxicity. Pharmacological targeting of NMDARs with channel blockers has shown therapeutic promise for protection from excitotoxicity as well as treatment of Alzheimer's disease. Despite sharing similarities in binding site and mechanism of inhibition, the clinical utility of NMDAR channel blockers with differing structure can vary dramatically. Further investigation into how channel blockers differentially affect receptor function may provide insight into their varying clinical efficacy and aid in future drug design. Here we characterize and compare the Alzheimer's disease drug memantine with four novel channel blockers. We find that subtle variation in channel blocker structure alters blocker characteristics. Excitingly, we show that potency of the novel channel blocker RL-208 depends on $[Ca^{2+}]_i$. The experiments and data detailed in this chapter lay the groundwork for future studies that will determine the structural determinants of $[Ca^{2+}]_i$-dependent channel block, potentially aiding in the design of more clinically efficacious NMDAR channel blocking drugs.

4.2 INTRODUCTION

NMDARs are expressed at nearly all vertebrate synapses and play key roles in neuronal development, plasticity, and survival. Ca^{2+} influx through NMDARs is a signal of paramount importance for synaptic plasticity, including long-term potentiation and long-term depression, physiological processes that are the cellular basis of many forms of learning and memory (Morris, 2013). However, NMDAR overstimulation triggers excessive Ca^{2+} influx and leads to excitotoxicity, which is the primary mediator of neuronal death following stroke and is believed to play a key role in the pathogenesis of neurodegenerative diseases, including Alzheimer's disease (AD) and Parkinson's disease (PD) (Zorumski & Olney, 1993; Lipton, 1999, 2004; Hynd *et al.*, 2004; Koutsilieri & Riederer, 2007; Dong *et al.*, 2009; Olivares *et al.*, 2012; Mota *et al.*, 2014; Gardoni & Di Luca, 2015; Wang & Reddy, 2017). Hence, NMDAR antagonists able to prevent overactivation of NMDARs are of interest as neuroprotective drugs.

Multiple types of NMDAR antagonists have been tested in clinical trials. Several competitive NMDAR antagonists failed trials for neurodegenerative disorders and related conditions, likely due to nonspecific NMDAR inhibition, i.e., the blocking of both physiological and pathological NMDAR activity, which leads to unacceptable side effects (Ikonomidou & Turski, 2002; Lipton, 2004; Muir, 2006). NMDAR open channel blocking antagonists have also been tested as therapeutic agents. In contrast to competitive antagonists, NMDAR channel blockers bind at sites that overlap with the Mg^{2+} binding site and can only bind and unbind when the channel is open (Blanpied *et al.*, 2005; Johnson & Kotermanski, 2006; Johnson *et al.*, 2015). Most NMDAR channel blockers also failed clinical trials, and several were found to be neurotoxic when administered at high doses to control animals (Olney *et al.*, 1989), including dizocilpine (MK-801), phencyclidine, and ketamine. Nevertheless, two adamantane derivatives, amantadine and memantine, which are low- (amantadine) and moderate- (memantine) affinity voltage-dependent

NMDAR channel blockers, have been found to be moderately effective for treatment of PD and AD (Danysz *et al.*, 1997; Lipton, 2006; Danysz & Parsons, 2012; Hubsher *et al.*, 2012; Alam *et al.*, 2017).

Several hypotheses have been proposed to explain the divergent clinical effects of NMDAR channel blockers. The kinetics of recovery from inhibition, which are much faster for memantine than dizocilpine, have been proposed to be a major determinant of clinical tolerability (Chen & Lipton, 2006; Lipton, 2006, 2007). Another hypothesis is that the utility of memantine may derive from an ability to preferentially inhibit extrasynaptic NMDARs, activation of which has been proposed to be especially neurotoxic (Hardingham & Bading, 2010; Gladding & Raymond, 2011; Parsons & Raymond, 2014). However, it is clear that overactivation of synaptic NMDARs also can be neurotoxic (Wroge *et al.*, 2012; Zhou *et al.*, 2013), so it unlikely that preferential inhibition of extrasynaptic NMDARs fully explains memantine's high tolerability. Another recent proposal is that clinical safety may be associated with preferential inhibition of NMDARs that undergo Ca^{2+}-dependent desensitization following exposure to high intracellular Ca^{2+}, a property exhibited by memantine but not ketamine (Glasgow *et al.*, 2017). The work presented in Chapter 2 of this dissertation further supports this idea, revealing that memantine inhibition depends on intracellular Ca^{2+} concentration ($[Ca^{2+}]_i$). The $[Ca^{2+}]_i$ dependence of memantine inhibition could provide a mechanism through which memantine preferentially targets different subpopulations of NMDARs than ketamine. It also suggests a logical mechanism of neuroprotection: preferential inhibition of NMDARs that are exposed to large and prolonged increases of Ca^{2+}_i, i.e. receptors likely to mediate excitotoxic cell death (Zorumski & Olney, 1993; Rothman & Olney, 1995; Hasbani *et al.*, 1998; Hardingham & Bading, 2010; Wroge *et al.*, 2012; Zhou *et al.*, 2013). Thus, many features of NMDAR channel blockers could potentially contribute to their clinical effects.

Unfortunately, although memantine is well-tolerated by patients, it possesses limited clinical efficacy (Matsunaga *et al.*, 2015). For this reason, new moderate-affinity NMDAR

antagonists with similar but distinct pharmacological properties are of interest (Chen & Lipton, 2006; Lipton, 2006, 2007). Thus, we began a project to design, synthesize, and characterize novel NMDAR channel blocking compounds to help us better understand mechanisms of channel block, with the end goal of developing new NMDAR-targeting neurotherapeutics with improved pharmacological profiles. In this chapter, I provide electrophysiological characterization of four novel channel blockers (Figure 18): the benzo-derivative EV-19 and the polycyclic amine memantine analogues RL-202, RL-208, and MFV-4.
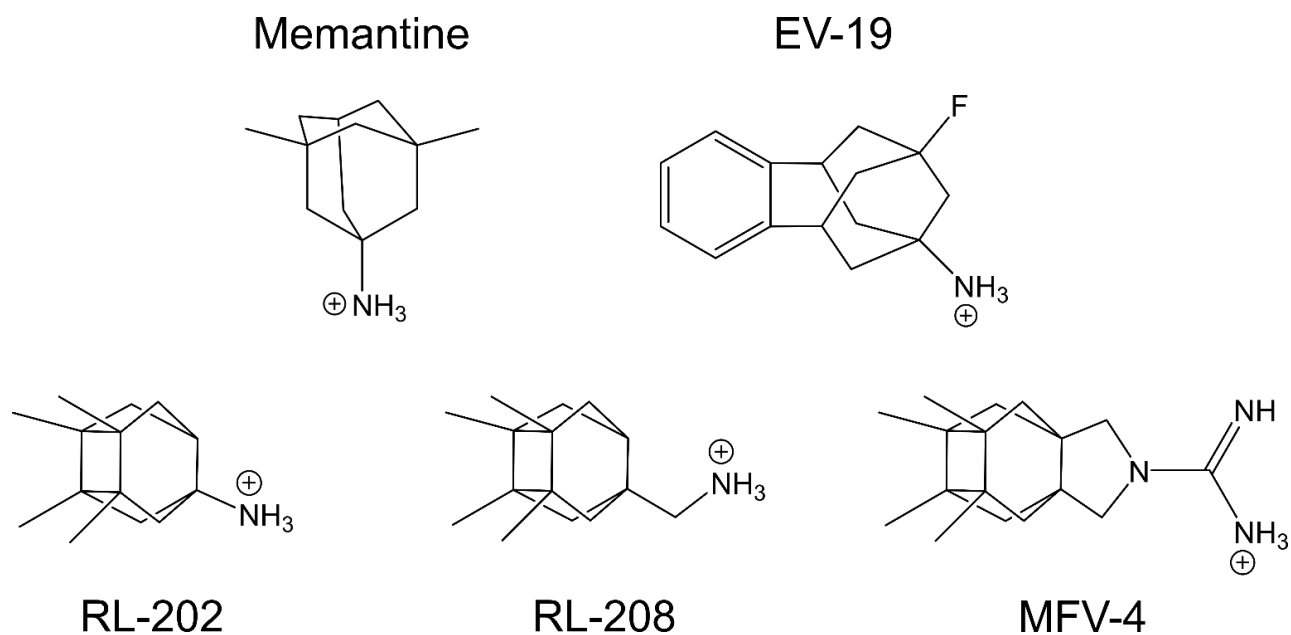
Figure 18. Structure of memantine and novel channel blockers.

Structures of organic channel blockers characterized in Chapter 4. All blockers are displayed in charged form and shown in bond-line format. EV-19, RL-202, RL-208, and MFV-4 were all designed and synthesized in the lab of our collaborator Dr. Santi Vázquez (University of Barcelona).

4.3 MATERIALS AND METHODS

4.3.1 Cell culture and transfection

All electrophysiological experiments were performed at room temperature using the tsA201 cell line (European Collection of Authenticated Cell Cultures). Cells were maintained as previously described (Glasgow & Johnson, 2014) in DMEM supplemented with 10% fetal bovine serum, 1% GlutaMAX (Thermo Fisher Scientific), and for some experiments 1% penicillin/streptomycin (Sigma). Cells were plated at 1×10^5 cells/dish in 35 mm petri dishes with three 15 mm glass coverslips treated with poly D-lysine (0.1 mg/ml) and rat-tail collagen (0.1 mg/ml, BD Biosciences).

12-24 hours after plating, tsA201 cells were transiently cotransfected (FuGENE 6 Transfection Reagent) with mammalian expression plasmids containing complementary DNA (cDNA) coding for enhanced green fluorescent protein (EGFP GenBank ACS32473 in pIRES) to identify transfected cells, WT rat GluN1-1a (GluN1; GenBank X63255 in pcDNA3.1), and GluN2A (D13211 in pIRES). EGFP was expressed using a specialty plasmid, EGFP:pIRES:GluN2A, gifted by Dr. Kasper Hansen. EGFP:pIRES:GluN2A was constructed by inserting cDNA encoding EGFP in pIRES between the CMV promoter and the GluN2A open reading frame, and allows for co-expression of independent EGFP and NMDAR subunit proteins. Cells were transfected with cDNA ratios of 1 GluN1: 1 GluN2A. Culture medium was supplemented with 200 µM dl-APV at the time of transfection to prevent NMDAR-mediated cell death.

4.3.2 Solution preparation

For experiments in Figures 19 - 23, intracellular pipette solution contained (in mM): 130 CsCl, 10 HEPES, 10 BAPTA, and 4 MgATP with pH balanced to 7.2 ± 0.05 with CsOH and an osmolality of 280 ± 10 mOsm. To allow for study of the effects of constant $[Ca^{2+}]_i$ on channel block by RL-208 (Figure 26), a high free Ca^{2+} (Ca^{2+}_F) internal solution containing 130 CsCl, 10 HEPES, 10 HEDTA, 6.2 $CaCl_2$, and 4 MgATP (pH balanced to 7.2 ± 0.05 with CsOH; osmolality = 280 ± 10 mOsm) was prepared using predictions from the program MAXCHELATOR (Bers *et al.*, 2010). The original intention was to $[Ca^{2+}]_F$ = 10 µM solution using MAXCHELATOR estimates, but MAXCHELATOR does not account for buffer purity or background solution composition and uses non-standardized buffer K_d values (McGuigan *et al.*, 2016; Tran *et al.*, 2018). Therefore, I empirically measured $[Ca^{2+}]_F$ using the Ligand Optimization Method (LOM; as described in Chapter 2.3.3) to gather an accurate estimate of $[Ca^{2+}]_F$ in this solution. We found that the HEDTA K_d value utilized by MAXCHELATOR is substantially higher than measurements made by the LOM for our solutions (MAXCHELATOR K_d = 7.2 µM; LOM K_d = 2.24 µM). This inaccuracy resulted in preparation of a solution with substantially lower $[Ca^{2+}]_F$ than predicted (MAXCHELATOR predicted $[Ca^{2+}]_F$ = 10 µM; LOM measured $[Ca^{2+}]_F$ = 4.89 µM). Therefore, $[Ca^{2+}]_F \approx 5$ µM for the high $[Ca^{2+}]_i$ internal solution used for experiments in Figure 26.

Extracellular recording solution contained (in mM) 140 NaCl, 2.8 KCl, 1 $CaCl_2$ (or 0.1 for experiments in Figure 26), 10 HEPES, 0.01 EDTA, and 0.1 glycine, and was balanced to pH 7.2 ± 0.05 with NaOH and to osmolality 290 ± 10 mOsm with sucrose. Channel blockers were diluted from concentrated stock solutions (memantine stock = 10 mM in dH_2O; $MgCl_2$ stock = 1 M in dH_2O; EV-19 stock = 10 mM in 140 mM NaCl and 2% DMSO; RL-202, RL-208, and MFV-4 stocks = 40 mM in 100% DMSO) in extracellular solution each day of experiments.

4.3.3 Electrophysiology

Whole-cell voltage-clamp recordings were performed 18 – 30 hours after transfection. Pipettes were pulled from borosilicate capillary tubing (OD = 1.5 mm, ID = 0.86 mm) using a Flaming Brown P-97 electrode puller (Sutter Instruments) and subsequently fire-polished to a resistance of 2.5 – 4.5 MΩ using an in-house fabricated microforge. Whole-cell currents were recorded using either an Axopatch 1D or Axopatch 200A patch-clamp amplifier (Molecular Devices). The current signal was low-pass filtered at 5 kHz and sampled at 20 kHz in pClamp 10 (Molecular Devices). Series resistance was compensated 80-90% in all experiments. A -6 mV liquid junction potential between the intracellular pipette solution and extracellular solution was corrected in all experiments. Glutamate and drug solutions were delivered to the cell via an in-house fabricated ten-barreled gravity-fed fast perfusion system (Glasgow & Johnson, 2014).

4.3.4 Analysis

Concentration-inhibition relations for EV-19 and Mg^{2+} were measured using the protocol shown in Figure 19A. Glutamate was applied until current reached steady state, then sequentially increasing concentrations of antagonist (channel blocker) were applied in the presence of constant [glutamate] until a steady level of inhibition was reached (10 – 20 s). Antagonists were then removed and agonist alone was reapplied to allow recovery from channel block. Concentration-inhibition relations for memantine, RL-202, RL-208, and MFV-4 were measured using the protocol shown in Figures 20 – 23, A and B. Glutamate was applied until current reached steady-state (20 s), then channel blocker at the plotted concentration was applied in the presence of constant [agonist] until a new steady-state current level was reached (30 s). Glutamate in the absence of drug was then reapplied for 30 s to allow drug unbinding and recovery from inhibition.

Cells in which recovery from inhibition did not reach 90% of steady-state current during initial glutamate application were excluded from analysis. IC_{50} and n_H (Hill coefficient) were estimated by fitting **Equation 3** to concentration-inhibition data as described in Chapter 2.3.4.

Voltage dependence of channel block by each blocker was measured using the protocol shown in Figures 19 – 23, C and D. Cells were subjected to voltage jumps from -65 mV to nine voltages ranging from -105 to +55 mV. The protocol at each voltage consisted of: a 4-s wait in extracellular solution following the voltage step; application of 1 mM glutamate for 10 s; application of drug with 1 mM glutamate for 15 s; application of 1 mM glutamate for 15 s to allow drug unbinding; application of extracellular solution for 2 s. Voltage was then returned to -65 mV for 4 s before the next voltage jump was made. ~2 times the IC_{50} of each drug was used in voltage dependence experiments. Voltage dependence of block was calculated using the Woodhull equation, **Equation 6**:

$$\frac{I_{Drug}}{I_{Glu}} = \frac{1}{1 + \dfrac{[Drug]}{IC_{50}(-65\ \text{mV})e^{\frac{V_m + 65}{V_0}}}}$$

where IC_{50}(–65 mV) is the IC_{50} at –65 mV calculated in concentration-inhibition experiments, and V_0 represents the change in voltage (in mV) that results in an *e*-fold change in the IC_{50} of the drug. I_{Drug}/I_{Glu} was calculated as described for concentration-inhibition data. V_0 was the only free parameter during fitting. An estimate of the fraction of the total membrane voltage field felt by the blocker at its binding site (δ;(Woodhull, 1973)) was calculated using **Equation 7**:

$$\delta = \frac{RT}{V_0 zF}$$

where R, T, z and F have their usual meanings. Note that, although δ is useful for comparing voltage dependence of blockers, voltage dependence of NMDAR channel block is influenced by

permeant ions (Antonov *et al.*, 1998). Therefore, δ should be used only as a rough estimate of binding site location in the voltage field.

4.3.5 Molecular modeling

The closed GluN1/2A TMD model used for docking simulations for memantine, RL-202, and RL-208 was developed in collaboration with the Kurnikova Lab of Carnegie Mellon University (Mesbahi-Vasey *et al.*, 2017) as described in Chapter 3.3.1. I developed and optimized models of memantine, RL-202, and RL-208 using the software Gaussian 09 (M.J. Frisch, 2009), and performed docking simulations using the software Autodock Vina (Trott & Olson, 2010) with the assistance of Dr. Chamali Narangoda as described in Chapter 3.3.1.

4.4 RESULTS

4.4.1 Characteristics of NMDAR inhibition by EV-19

We characterized NMDAR inhibition by EV-19 using whole-cell patch-clamp recordings from tsA201 cells expressing GluN1/2A receptors. Inhibition by EV-19 was measured as a function of drug concentration (Figure 19A) and used to calculate the EV-19 IC_{50} in cells held at -65 mV. The IC_{50} of EV-19 was found to be 4.40 ± 0.15 μM. (Figure 19B, C), well within the range of therapeutically beneficial NMDAR antagonists (e.g. ketamine IC_{50} ~ 1 μM; memantine IC_{50} ~ 1 – 2 μM; amantadine IC_{50} ~ 40 – 75 μM (Bresink *et al.*, 1996; Parsons *et al.*, 1996, 2007; Blanpied *et al.*, 1997, 2005; Parsons & Gilling, 2007; Kotermanski & Johnson, 2009; Otton *et al.*, 2011; Leiva *et al.*, 2018)).

NMDAR channel blockers share overlapping binding sites in the NMDAR channel (Burnashev, Schoepfer, *et al.*, 1992; Mori *et al.*, 1992; Kashiwagi *et al.*, 2002; Chen & Lipton, 2005). Thus, many organic NMDAR channel blockers (e.g. amantadine, memantine, and ketamine) show competitive binding with the endogenous blocker Mg^{2+} (MacDonald *et al.*, 1991; Kotermanski & Johnson, 2009; Otton *et al.*, 2011; Nikolaev *et al.*, 2012; Glasgow *et al.*, 2018). To ascertain whether EV-19 inhibits NMDARs via channel block, we tested the effect of extracellular Mg^{2+} on EV-19 potency. As predicted, the inclusion of 0.2 mM Mg^{2+} in the recording solution led to a substantial rightward shift in the EV-19 IC_{50} curve and a significant increase in EV-19 IC_{50} (IC_{50} = 4.40 ± 0.15 µM in 0 Mg^{2+} vs 21.41 ± 0.56 µM in 0.2 mM Mg^{2+}; $p < 0.0001$, two-sample Student t-test, n = 10 and 6, respectively; Figure 19B, C). This roughly 5-fold decrease in EV-19 potency suggests a competitive interaction between Mg^{2+} and EV-19 in the NMDAR channel.

We next determined the voltage dependence of inhibition by 10 µM (~2-fold IC_{50} at -65 mV) EV-19. As predicted of a positively charged channel blocker, inhibition by EV-19 was markedly weaker at depolarized potentials (Figure 19D-F). **Equation 6** and **Equation 7** were used to quantify V_0, the change in voltage (in mV) that results in an e-fold change in the IC_{50} of a drug, and δ, an estimate of the fraction of the total transmembrane voltage field felt by the blocker at its binding site (Woodhull, 1973). Inhibition of GluN1/2A receptors by EV-19 is strongly voltage-dependent, as reflected by the drug's small V_0 (25.43 ± 0.54 mV) and large δ (1.01 ± 0.02). The EV-19 V_0 and δ values are similar to previously reported values for monovalent organic channel blockers (e.g. V_0 ~ 26 – 30 mV, δ ~ 0.8 – 1.0 for memantine, ketamine, and recently synthesized polycyclic amines (Blanpied *et al.*, 1997; Parsons, Danysz, & Quack, 1999; Gilling *et al.*, 2009; Otton *et al.*, 2011; Leiva *et al.*, 2018)). The profound dependence of EV-19 inhibition on $[Mg^{2+}]$ and on membrane potential strongly supports the conclusion that EV-19 inhibits NMDARs by binding in and blocking the NMDAR channel.
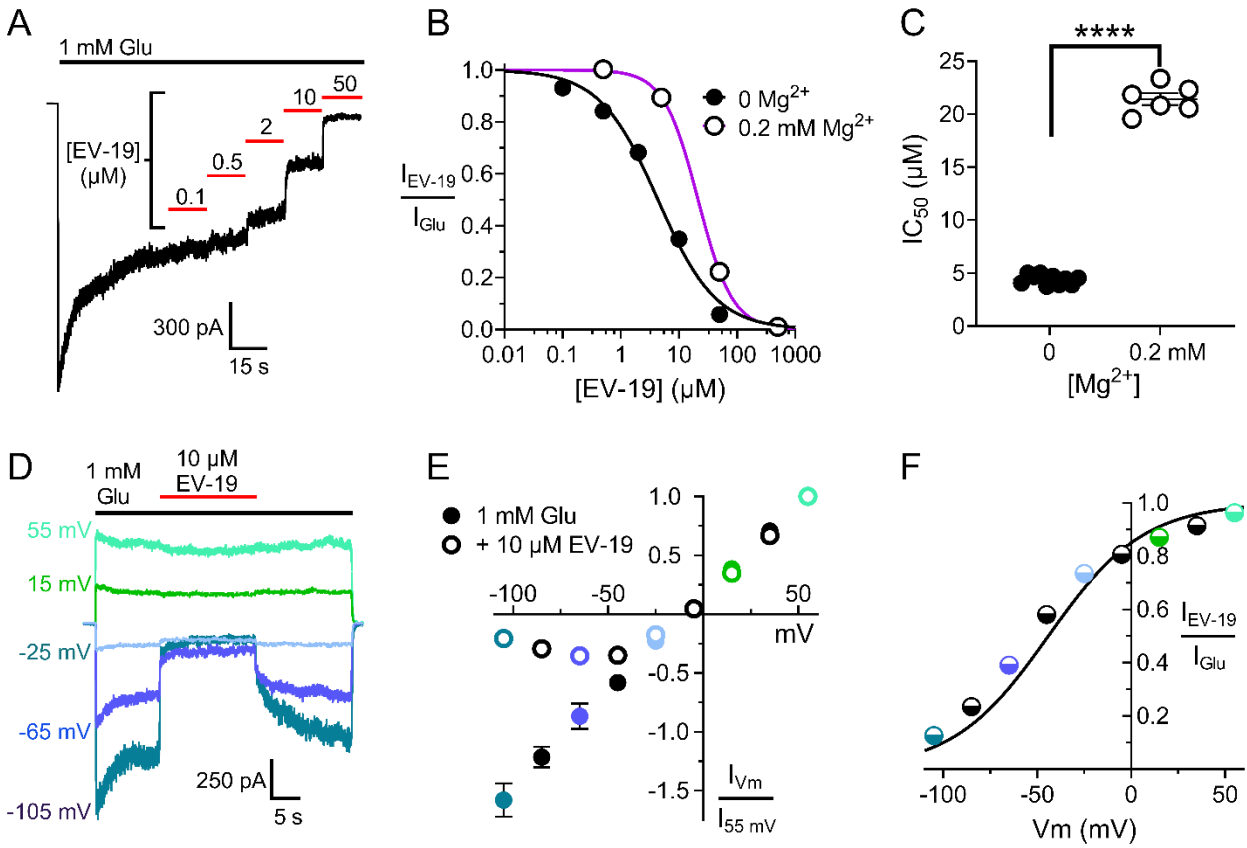
Figure 19. Characteristics of GluN1/2A receptor channel block by EV-19.

A, Representative current trace from one cell depicting inhibition of GluN1/2A receptors by EV-19 at -65 mV. Current evoked by application of 1 mM glutamate (Glu; black bars) was reduced as [EV-19] (red bars) increased. **B**, Concentration-inhibition relation for EV-19 in 0 Mg^{2+} (black line, filled symbols) and in 0.2 mM Mg^{2+} (purple line, open symbols). Symbols represent means, error bar are smaller than symbols. Lines show best fits of **Equation 3** to data. **C**, Comparison of IC_{50} values in 0 and 0.2 mM Mg^{2+}. 0.2 mM Mg^{2+} greatly reduces EV-19 potency (IC_{50} = 4.40 ± 0.15 μM in 0 Mg $^{2+}$ vs 21.41 ± 0.56 μM in 0.2 mM Mg^{2+}; n = 10 and 6, respectively; p < 0.0001, two-sample Student t-test, n = 10 and 6, respectively). Data shown as individual values, line and error bars depict mean ± SEM. **D**, Representative current traces from one cell depicting the voltage dependence of inhibition by 10 μM EV-19. For clarity, traces from only five of the tested membrane potentials are displayed. **E**, Current-voltage relation for GluN1/2A receptors in 1 mM Glu (filled symbols) and 1 mM Glu + 10 μM EV-19 (open symbols). Current at each voltage (I_{Vm}) was normalized

117

to current at 55 mV ($I_{55\ mV}$) for each cell. Symbols represent means, error bars represent SEM; some error bars are smaller than symbols. **F**, Mean current-voltage relation data replotted as fractional current in the presence of 10 µM EV-19. Solid line shows best fit of **Equation 6** to estimate V_0 (25.43 ± 0.54 mV; n = 7). V_0 was subsequently used to calculate δ (1.01 ± 0.02; n = 7) with **Equation 7**. Error bars in F are smaller than symbols. Colors of symbols in E and F correspond to colors of example traces in D; black symbols represent measurements at voltages not shown in D. Summary of IC_{50}, V_0, and δ values are given in Table 6.

4.4.2 Concentration and voltage dependence of NMDAR inhibition by memantine

analogues

Whole-cell patch-clamp recordings from tsA201 cells expressing GluN1/2A receptors were used to assess the pharmacological properties of three promising memantine analogues, primary amines RL-202 and RL-208 and guanidine MFV-4. Experiments measuring the IC_{50} and voltage-dependence of block by compound memantine were performed for comparison. In cells held at -65 mV, inhibition by each drug was measured at increasing drug concentrations (Figures 20 - 23, A) and used to calculate the IC_{50} and Hill coefficient (n_H, which reflects the steepness of the concentration-inhibition curve; **Equation 3**). The IC_{50} value and Hill coefficient measured for memantine (Figure 20B) are similar to previously-reported values measured under similar conditions (Gilling *et al.*, 2007, 2009; Glasgow *et al.*, 2017). RL-202, RL-208 and MFV-4 were found to have moderate IC_{50} values (Figures 21 – 23, B). The IC_{50}s of RL-208 (1.01 ± 0.13 µM) and MFV-4 (0.48 ± 0.09 µM) were significantly lower than the IC_{50}s of memantine (1.84 ± 0.39 µM) or RL-202 (2.78 ± 0.25 µM), and the IC_{50} of memantine was significantly lower than the IC_{50} of RL-202 (Figure 24A). There were no significant differences between the n_H of the drugs, i.e., 1.07 ± 0.27, 0.98 ± 0.08, 1.01 ± 0.11, and 1.00 ± 0.03 for memantine, RL-202, RL-208 and MFV-4, respectively.

To measure voltage dependence of inhibition by memantine, RL-202, RL-208 and MFV-4, inhibition elicited by roughly twice the IC_{50} of each drug was measured at 9 different voltages (examples from 5 voltages are shown in Figures 20 - 23, C). The inhibition produced by the drugs decreased as voltage was depolarized (Figures 20 - 23, C and D), as expected of positively charged channel blockers. Fitting of **Equation 6** to current-voltage data was used to quantify V_0, the change in voltage (in mV) that results in an *e*-fold change in the IC_{50} of a drug. **Equation 7** was used to calculate δ, an estimate of the fraction of the total transmembrane voltage field felt

119

by the blocker at its binding site. The value of δ is calculated from the value of V_0; strong voltage dependence is reflected by a large δ and a small V_0. All compounds displayed strongly voltage-dependent block, i.e., for **memantine,** $V_0 = 28.0 \pm 2.2$ mV and $\delta = 0.91 \pm 0.08$; for RL-202, $V_0 = 26.5 \pm 1.8$ mV and $\delta = 0.99 \pm 0.05$; for RL-208, $V_0 = 29.9 \pm 1.9$ mV and $\delta = 0.87 \pm 0.05$; for MFV-4, $V_0 = 33.6 \pm 1.5$ mV and $\delta = 0.76 \pm 0.03$ (Figures **20 – 23, D**). The voltage dependence of inhibition was found to be significantly weaker for MFV-4 than for either **memantine** or RL-202 (Figure 24B).
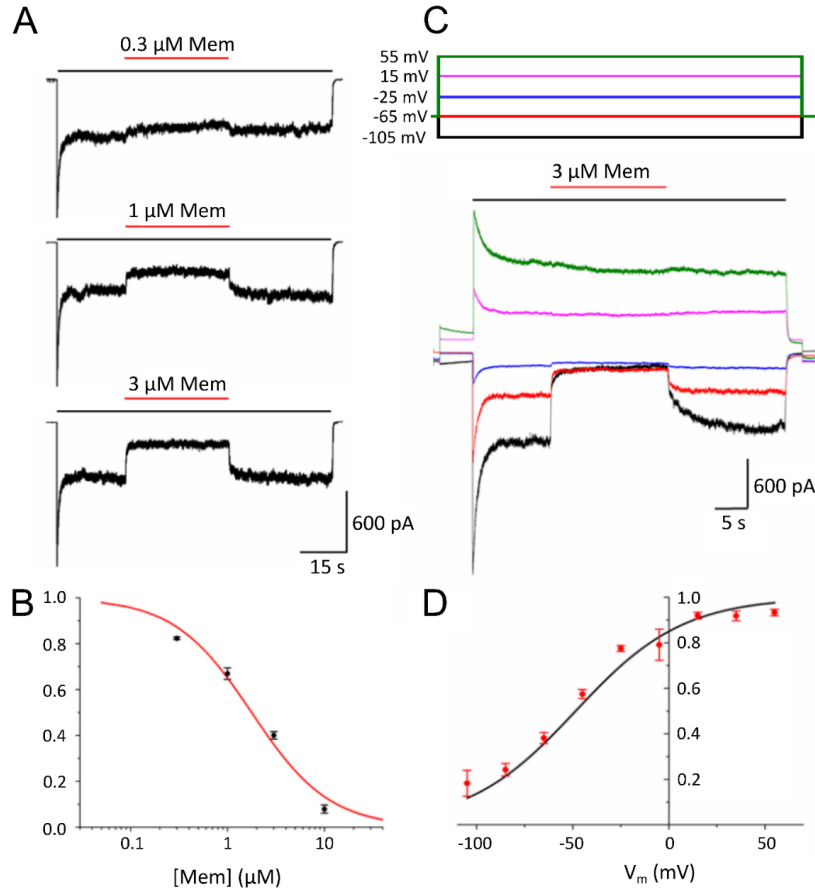
Figure 20. Concentration and voltage dependence of NMDAR inhibition by memantine.

A, Representative current traces from one cell depicting effect of memantine on GluN1/2A receptor currents. Application of 1 mM Glu (black bars) elicited an inward current that was antagonized by application of memantine (red bars). **B**, Concentration-inhibition relation for memantine. Line shows best fit of **Equation 3** (IC_{50} = 1.84 ± 0.39 µM, n_H = 1.07 ± 0.27; n=5). **C**, Representative voltage (V_m; top) and current (bottom) traces depicting effect of membrane potential upon inhibition by 3 µM memantine. Traces from 5 of the 9 membrane potentials tested are displayed for clarity. **D**, Current-voltage relation of inhibition by memantine. Line shows best fit of **Equation 6** (V_0 = 28.0 ± 2.2; n=5). Points in B and D represent mean fractional currents measured at each concentration (B) or voltage (D); error bars represent SEM and are sometimes smaller than symbols. Comparison of the concentration and voltage dependence of NMDAR inhibition by memantine, RL-202, RL-208 and MFV-4 is shown in Figure 24. Summary of IC_{50}, V_0, and δ values are given in Table 6.
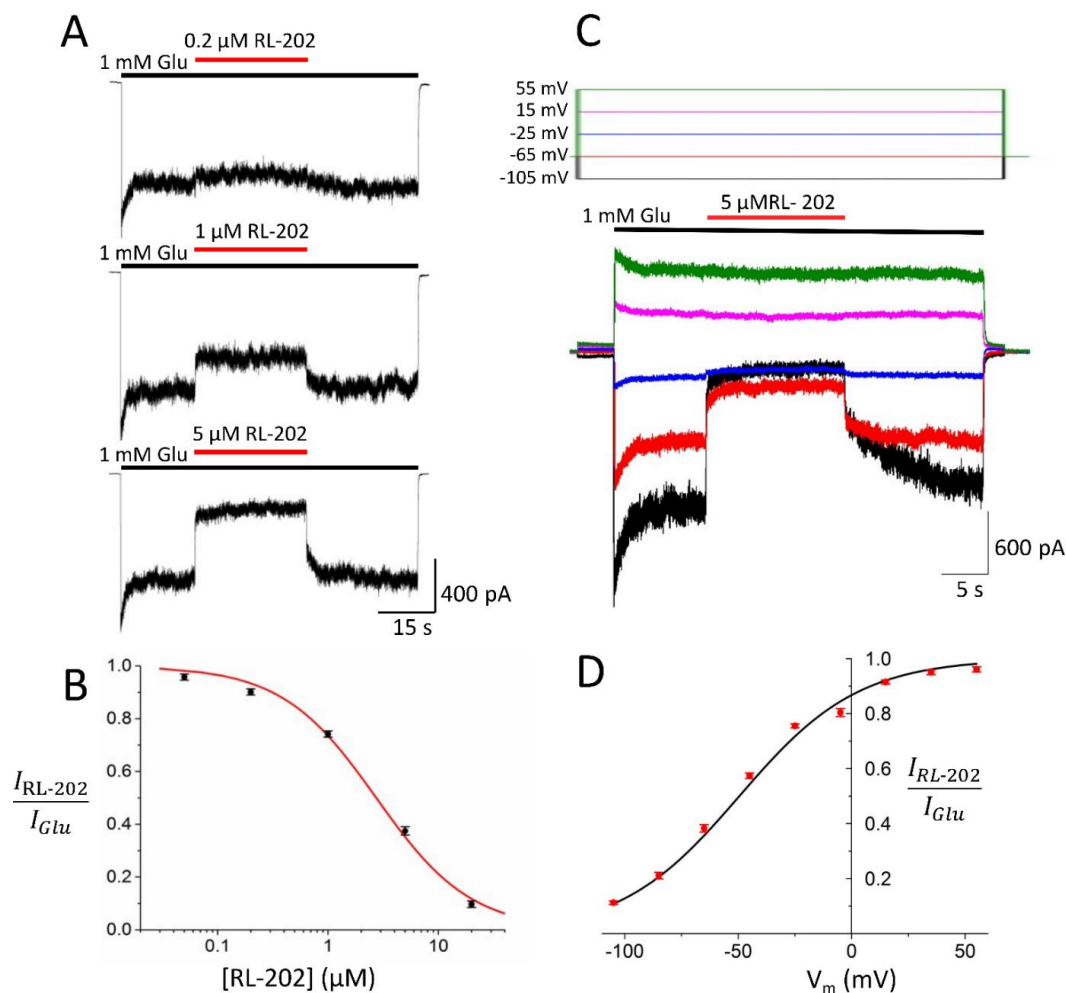
Figure 21. Concentration and voltage dependence of NMDAR inhibition by RL-202.

A, **B**, Same as Figure 20A, B, except concentration-inhibition measurements made using RL-202. Line in B shows best fit of **Equation 3** (IC_{50} = 2.78 ± 0.25 µM, n_H = 0.98 ± 0.08; n=7). **C**, **D**, Same as Figure 20C, D, except measurements of voltage-dependence made using 5 µM RL-202. Line in D shows best fit of **Equation 6** (V_0 = 26.5 ± 1.8; n=7). Comparison of the concentration and voltage dependence of NMDAR inhibition by memantine, RL-202, L-208 and MFV-4 is shown in Figure 24. Summary of IC_{50}, V_0, and δ values are given in Table 6.
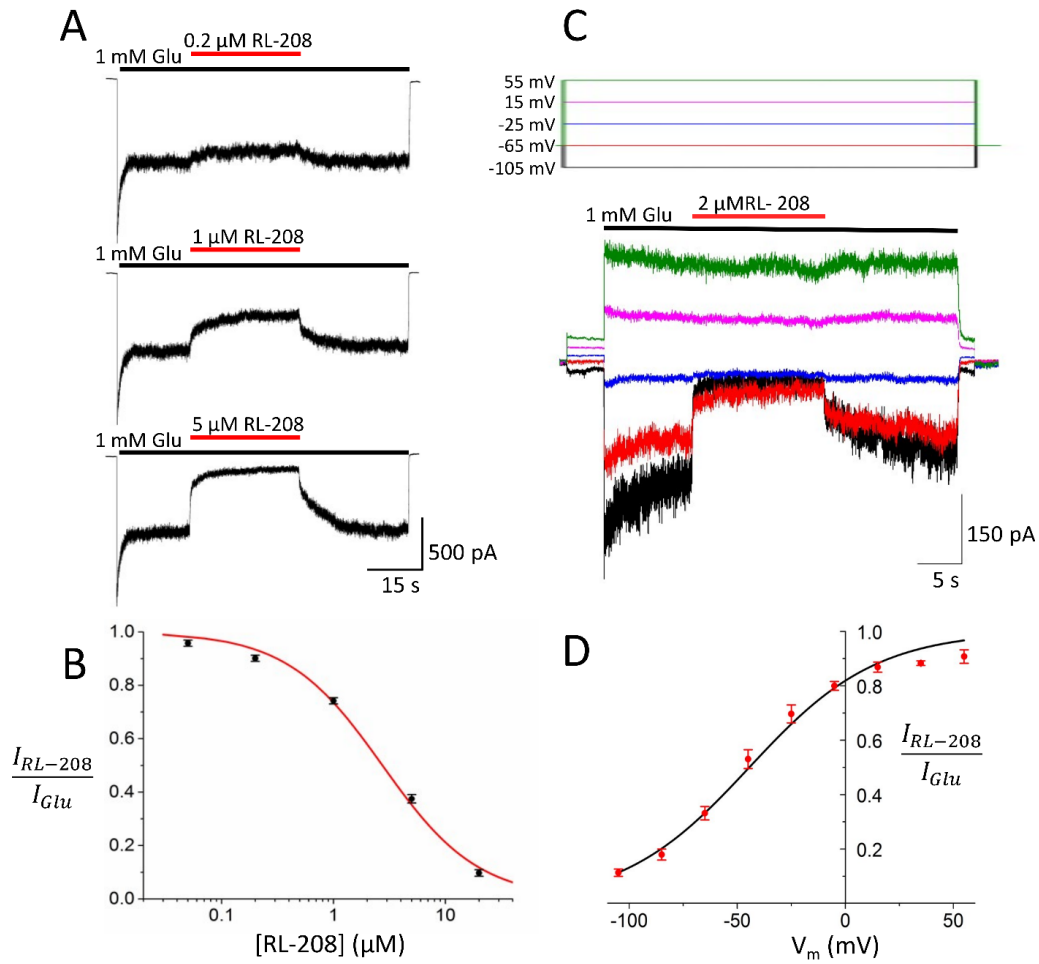
Figure 22. Concentration and voltage dependence of NMDAR inhibition by RL-208.

A, **B**, Same as Figure 20A, B, except concentration-inhibition measurements made using RL-208. Line in

B shows best fit of **Equation 3** (IC_{50} = 1.01 ± 0.13 µM, n_H = 1.01 ± 0.11; n=7). **C**, **D**, Same as Figure 20C,

D, except measurements of voltage-dependence made using 2 µM RL-208. Line in D shows best fit of

Equation 6 (V_0 = 29.9 ± 1.9; n=8). Comparison of the concentration and voltage dependence of NMDAR

inhibition by memantine, RL-202, RL-208 and MFV-4 is shown in Figure 24. Summary of IC_{50}, V_0, and δ

values are given in Table 6.
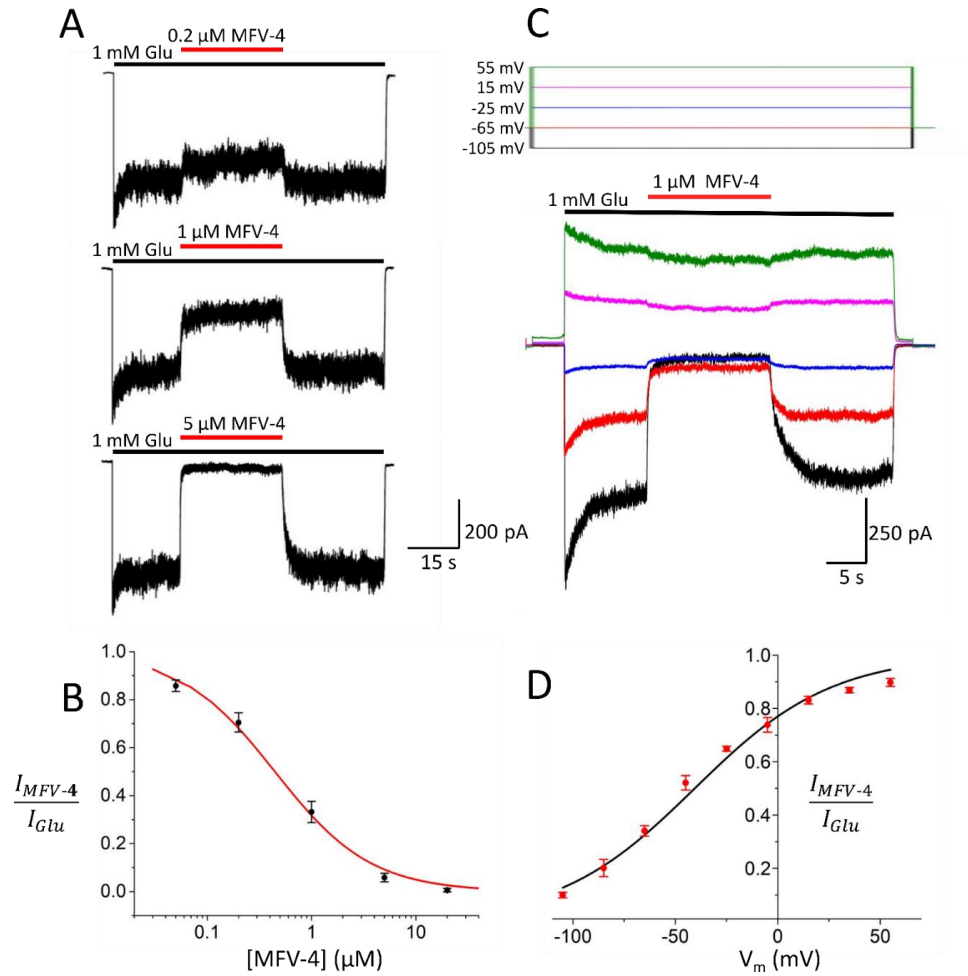
Figure 23. Concentration and voltage dependence of NMDAR inhibition by MFV-4.

A, **B**, Same as Figure 20A, B, except concentration-inhibition measurements made using MFV-4. Line in B shows best fit of **Equation 3** ($IC_{50} = 0.48 \pm 0.09$ µM, $n_H = 1.00 \pm 0.03$; n=4). **C**, **D**, Same as Figure 20C, D, except measurements of voltage-dependence made using 1 µM MFV-4. Line in D shows best fit of **Equation 6** ($V_0 = 33.6 \pm 1.5$; n=4). Comparison of the concentration and voltage dependence of NMDAR inhibition by memantine, RL-202, RL-208 and MFV-4 is shown in Figure 24. Summary of IC_{50}, V_0, and δ values are given in Table 6.
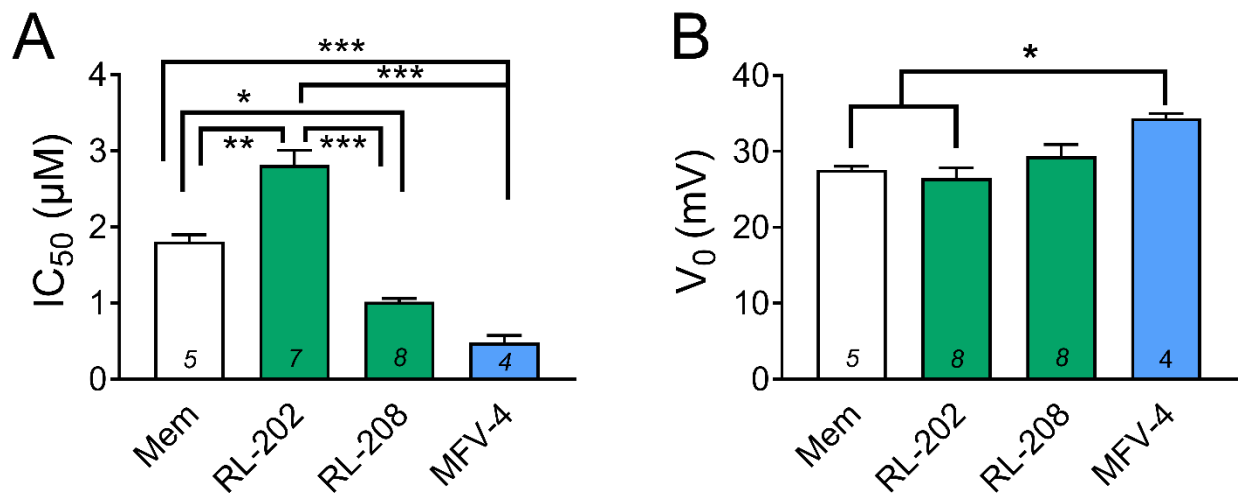
Figure 24. Comparison of NMDAR channel blocker properties.

A, Comparison of blocker IC_{50} values measured at -65 mV. **B**, Comparison of voltage dependence of inhibition by the blockers. All comparisons made by one-way ANOVA with Tukey *post hoc* analysis; *p<0.01, **p<0.001, ***p<0.0001. Sample size denoted by number inside column.

Table 6. IC$_{50}$ and voltage dependence of inhibition for memantine and novel channel blockers.

Values represent means ± sem (n).

Channel blocker	IC$_{50}$ (µM)	V$_0$ (mV)	δ
Memantine	1.84 ± 0.39 (5)	28.0 ± 2.2 (5)	0.91 ± 0.08 (5)
EV-19	4.40 ± 0.15 (10)	25.43 ± 0.54 (7)	1.01 ± 0.02 (7)
RL-202	2.78 ± 0.25 (7)	26.5 ± 1.8 (8)	0.99 ± 0.05 (8)
RL-208	1.01 ± 0.13 (8)	29.9 ± 1.9 (8)	0.87 ± 0.05 (8)
MFV-4	0.48 ± 0.09 (4)	33.6 ± 1.5 (4)	0.76 ± 0.03 (4)

4.4.3 Docking predicts overlapping binding sites for RL compounds and memantine

To provide insight into the binding sites of the novel polycyclic amines, we performed and compared docking simulations of memantine, RL-202, and RL-208. Docking simulations of memantine predicted a binding pose in the channel between the GluN1 and GluN2A subunits (Figure 25A,D) and in close proximity to GluN1 residue M641 and critical asparagine residues (GluN1 N616 and GluN2A N614) that are key components of the NMDAR selectivity filter and heavily implicated in channel block ((Burnashev, Schoepfer, *et al.*, 1992; Mori *et al.*, 1992; Kuner & Schoepfer, 1996; Ferrer-Montiel *et al.*, 1998; Kashiwagi *et al.*, 2002; Mesbahi-Vasey *et al.*, 2017); Figure 25G). This predicted memantine binding pose is identical to previous docking simulations (shown in Figure 11), highlighting the consistency of Autodock Vina simulations. RL-202 and RL-208 were also predicted to bind in the channel above the selectivity filter, between the GluN1 and GluN2A subunits (Figure 25B,C,E,F). Nearly all residues predicted to be in close proximity with the RL compounds were shared with memantine (Figure 15G,H,I). The "R-group" containing the primary amine of RL-208 is predicted to project slightly farther out into the channel than the R-groups of memantine and RL-202, potentially allowing it to interact with an additional critical asparagine (GluN1 614; Figure 25I), and memantine is predicted to interact with additional hydrophobic residues GluN2A F641 and GluN1 A627. The similarities between the predicted binding sites is consistent with our data showing the general similarities between the electrophysiological characteristics of memantine and the RL compounds.
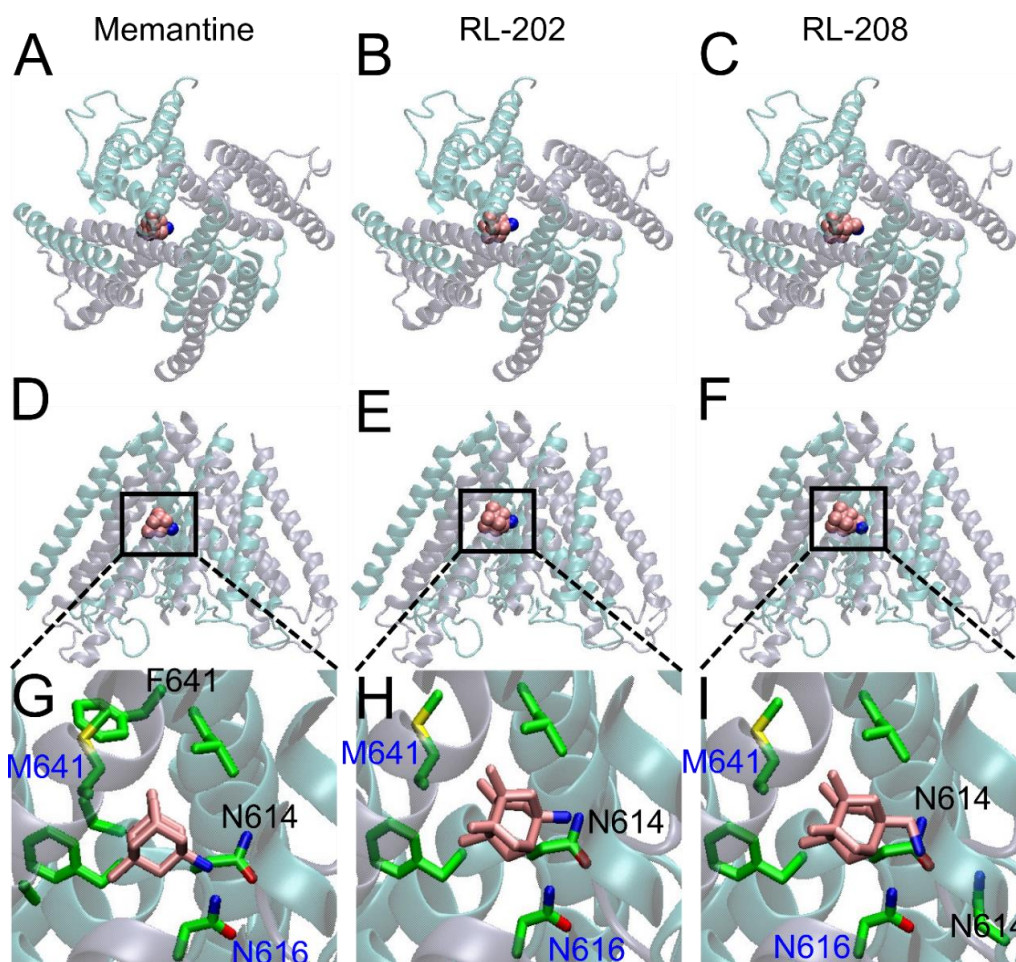
Figure 25. Predicted binding sites of memantine, RL-202, and RL-208.

A – C, Top-down view of memantine (**A**), RL-202 (**B**), and RL-208 (**C**) docked to the GluN1/2A channel. **D – F**, Full scale view of memantine (**D**), RL-202 (**E**), and RL-208 (**F**) docked within the GluN1/2A receptor channel model (Mesbahi-Vasey *et al.*, 2017). GluN1 is depicted as gray-blue ribbons; GluN2A is depicted as cyan ribbons. Blockers are depicted as space-filling structures. Boxes in (**D**) – (**F**) depicts regions blown up in (**G**) – (**I**). **G – I**, Magnified view of docking sites for memantine (**G**), RL-202 (**H**), and RL-208 (**I**). Residues are shown as stick models. All three blockers are predicted to bind in close proximity with key asparagine residues. Memantine, but not the RL compounds, is predicted to bind in close proximity to residues GluN1 A627, GluN2A F641 (labeled in G), and GluN2A V612. RL-208 is predicted to interact with GluN1 N614 of both GluN1 subunits. All other residues within 3 Å are shared. Drug C = pink (drug) or green (amino acid side chain); N = blue; O = red; S = yellow.

128

4.4.4 $[Ca^{2+}]_i$ dependence of inhibition by RL-208

Given the similarities between both the electrophysiological characteristics and the predicted binding sites of memantine and the RL compounds, we next tested whether inhibition of GluN1/2A receptors by RL-208 depended on $[Ca^{2+}]_i$. We measured the RL-208 IC_{50} in conditions of low (< 1 nM) and high (5 μM) $[Ca^{2+}]_i$ and found that inhibition of RL-208 was heavily dependent on $[Ca^{2+}]_i$. RL-208 potency was roughly 3-fold higher in conditions of $[Ca^{2+}]_i = 5$ μM than conditions of $[Ca^{2+}]_i$ < 1 nM (Figure 26). The degree of $[Ca^{2+}]_i$-dependence of RL-208 potency is similar to that observed for memantine (Figure 4).
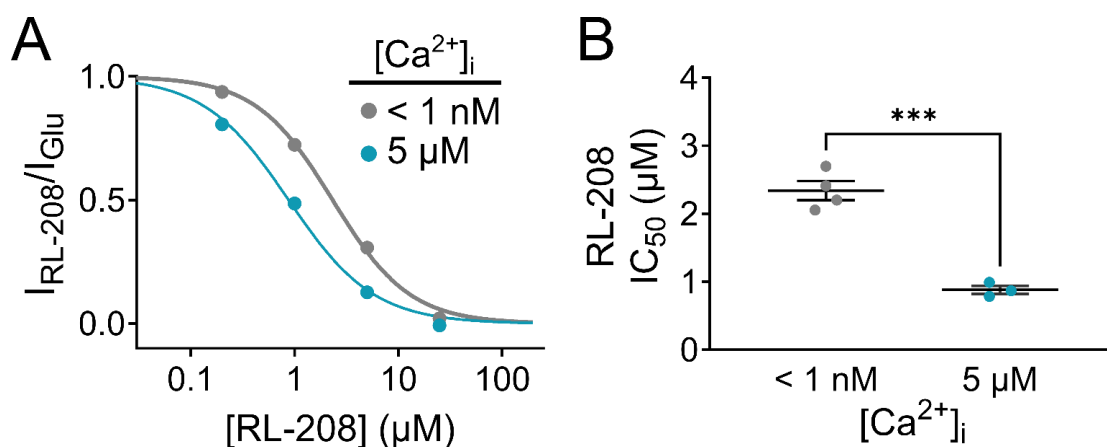
Figure 26. Inhibition by RL-208 depends on $[Ca^{2+}]_i$.

A, Concentration-inhibition curve for RL-208 at $[Ca^{2+}]_i$ <1 nM and $[Ca^{2+}]_i$ = 5 µM, measured using recordings from recombinant GluN1/2A receptors. Points represent mean; error bars smaller than points. **B,** Summary of RL-208 IC_{50} values for GluN1/2A receptors in conditions of $[Ca^{2+}]_i$ = <1 and 5 µM. RL-208 potency depends on $[Ca^{2+}]_i$ ($[Ca^{2+}]_i$ < 1 nM: 2.34 ± 0.14 µM; $[Ca^{2+}]_i$ = 5 µM: 0.88 ± 0.06 µM). Unpaired Student's t-test, ***p < 0.001.

4.5 DISCUSSION

NMDAR channel blockers are clinically useful therapeutic drugs, but their clinical profiles can be surprisingly diverse and difficult to predict. Amongst channel blockers, memantine is particularly interesting due to its combination of clinically efficacy and high tolerability (Parsons, Danysz, & Quack, 1999; Lipton, 2004; Parsons & Gilling, 2007; Parsons *et al.*, 2007; Johnson *et al.*, 2015). Here we characterize and compare with memantine four novel NMDAR antagonists, the benzo-derivative EV-19 and the novel memantine analogues RL-202, RL-208, and MFV-4. All drugs tested displayed IC_{50}s well within the $0.5 - 75$ μM range of therapeutically beneficial NMDAR antagonists (Bresink *et al.*, 1996; Parsons *et al.*, 1996, 2007; Blanpied *et al.*, 1997, 2005; Parsons & Gilling, 2007; Kotermanski & Johnson, 2009; Otton *et al.*, 2011; Leiva *et al.*, 2018). Multiple lines of evidence support the conclusion that EV-19, RL-202, RL-208, and MFV-4 all act as channel blockers. EV-19 potency is greatly reduced in the presence of the prototypical NMDAR channel blocker Mg^{2+} (Figure 19), suggesting competition for binding. Docking simulations predict that RL-202 and RL-208 share nearly identical binding sites to memantine (Figure 25), which is known to bind in the NMDAR channel. Finally, inhibition by all four drugs is voltage-dependent (Figures 19, 21-24), which is a hallmark of positively charged channel blockers.

Interestingly, subtle differences between the memantine analogues had substantial influence on their potency. RL-202, despite having the most similar structure to memantine out of the novel compounds tested, was found to have a 1.5-fold higher IC_{50} than memantine. Even more impressively, RL-208 was found to have a > 2.5-fold lower IC_{50} than RL-202, despite differing by only a single CH_2. MFV-4, which possesses multiple additional carbons and nitrogens in comparison to memantine and the RL compounds, was the most potent blocker tested. It is possible that guanidine group of MFV-4 allows for easier coordination by the critical asparagine residues, or the additional carbons form additional energetically favorable interactions with

131

hydrophobic residues surrounding the pore, resulting in increased potency. Sophisticated MD simulations would provide crucial insight into the mechanism of interaction between each novel compound and the GluN1/2A TMD, giving us a strong starting point for experiments that further probe the effect of blocker structure on potency.

Unlike potency, structure had little influence over the voltage dependence of inhibition by each blocker. Even the benzodiazepine derivative EV-19, despite its slightly higher IC_{50} and vastly different structure, exhibited comparable V_0 and δ values to memantine and the memantine analogs (will tabulate values). MFV-4 was the only blocker to show a significant difference in voltage dependence, displaying slightly weaker voltage dependence than memantine and RL-202. This could be related to the ability of MFV-4's guanidine R-group to easily delocalize its positive charge due to resonance, in contrast to the other blockers which possess primary amine R-groups. Although the mechanisms underlying the pharmacological differences between memantine, its analogs, and EV-19 are still unclear, our data provides strong evidence that even small differences in NMDAR channel blocker structure can greatly influence potency.

It is important to note that we observed differences between EV-19 IC_{50}s measured using intracellular Ca^{2+} measurements from cerebellar granule neurons (1.93 ± 0.21 μM, personal communication with Santi Vazquez of University of Barcelona) and patch-clamp recordings from tsA201 cells expressing GluN1/2A receptors (Figure 19). We also observed a similar trend In previous comparisons of NMDAR channel blocker IC_{50}s across these two experimental preparations, with intracellular Ca^{2+} measurements from cerebellar granule neurons again generating lower IC_{50} values for memantine, the RL compounds, and MFV-4 than whole-cell recordings (Leiva *et al.*, 2018). This discrepancy may result from inherent differences between the recording techniques and/or from expression of GluN2 subunits other than GluN2A by cerebellar granule neurons. Further investigation of EV-19, RL-203, RL-208, and MFV-4 potency

132

across NMDAR subtype and in cultured neurons will help us further understand the subtle differences between these compounds.

Excitingly, our data shows that inhibition of GluN1/2A receptors by RL-208 depends on $[Ca^{2+}]_i$. RL-208 is the first channel blocker other than memantine to display $[Ca^{2+}]_i$-dependent channel block. This is perhaps unsurprising, given the similarities in the predicted memantine and RL-208 binding sites. The $[Ca^{2+}]_i$ dependence of RL-208 potency suggests that RL-208 also stabilizes a Ca^{2+}-dependent desensitized receptor state, and may preferentially target receptors exposed to high $[Ca^{2+}]_i$ for prolonged durations. A clear next step is to test whether RL-202 potency is also $[Ca^{2+}]_i$-dependent. An ideal neuroprotective drug would show weak interaction with receptors unaffected by pathological insults while strongly inhibiting receptors involved in neurotoxicity. Thus, the weaker potency of RL-202 could make it a strong candidate for a neuroprotectant if its potency shows strong $[Ca^{2+}]_i$ dependence. Furthermore, investigation of the $[Ca^{2+}]_i$ dependence of EV-19, RL-202, MFV-4 potency would lay the groundwork for future studies that determine the structural determinants $[Ca^{2+}]_i$-dependent channel block. Understanding the structural bases of the mechanisms of action of channel blockers will improve our understanding of how channel blockers affect NMDAR gating and may help guide the development of more clinically efficacious NMDAR-targeting neurotherapeutics.

5.0 GENERAL DISCUSSION

The work presented in this dissertation focuses on the interplay between the effects of intracellular Ca^{2+} (Ca^{2+}_i) on NMDAR channel block and desensitization. Through investigation of the relation between NMDAR desensitization and channel block, we discovered that potency of the clinically efficacious channel blocker memantine was powerfully dependent on $[Ca^{2+}]_i$. In contrast, potency of neither the endogenous channel blocker Mg^{2+} nor another clinically useful channel blocker, ketamine, was found to be $[Ca^{2+}]_i$-dependent. Utilizing this discrepancy, we then further probed the mechanism underlying the relation between memantine block and NMDAR desensitization by comparing the memantine and ketamine binding sites. We identified a residue in the GluN2A transmembrane domain (TMD) that strongly contributes to NMDAR desensitization and memantine potency, providing insight into how memantine may interact with the NMDAR channel. Finally, we characterized novel NMDAR channel blockers to help us better understand how blocker structure contributes to the pharmacological characteristics of channel block. Excitingly, we discovered that potency of a memantine derivative was also dependent on $[Ca^{2+}]_i$, providing optimism for the directed design of future NMDAR channel blockers with improved therapeutic benefits. This chapter discusses the implications of our findings on our understanding of NMDAR desensitization, the relation between channel block and NMDAR gating, and the utility of memantine and other state-specific NMDAR-targeting antagonists for treatment of nervous system pathologies.

5.1 MULTIPLE MECHANISMS OF, AND NAMES FOR, CA^{2+}-DEPENDENT DESENSITIZATION

Despite a wealth of research, the mechanisms underlying CDD have been the subject of much debate. The confusion surrounding CDD mechanisms is due, in part, to the lack of consistent definitions and terminology used to refer to CDD processes that are potentially driven by distinct mechanisms. The data presented in this dissertation, particularly from experiments addressing the relation between desensitization and NMDAR block by memantine, provide new evidence that helps delineate different CDD mechanisms.

There are likely, at minimum, two separable forms of CDD: a fast mechanism that occurs over the course of 0.01 – 5 s, and a slow mechanism that takes minutes to develop. A rapid reduction in NMDAR activity caused by NMDAR-mediated Ca^{2+} influx was first reported by Mayer and Westbrook in 1985 and was referred to as desensitization (Mayer & Westbrook, 1985). Eight years later, the Westbrook lab revisited the effect of intracellular Ca^{2+} on rapid NMDAR desensitization and termed it Ca^{2+}-dependent inactivation (CDI) to "avoid confusion with other forms of NMDA receptor desensitization" (Legendre *et al.*, 1993). Other studies reported slower forms of NMDAR desensitization, referred to as glycine-insensitive desensitization or "Ca^{2+}-dependent activation of NMDAR desensitization", that were regulated by Ca^{2+} and related to the duration of elevated [Ca^{2+}]$_i$ (Sather *et al.*, 1992; Lieberman & Mody, 1994; Tong & Jahr, 1994; Tong *et al.*, 1995). Despite being observed under different experimental conditions (i.e. outside-out patches vs whole cell recordings, long recordings vs short recordings, etc.), these desensitization processes were eventually absorbed by the monolithic term CDI (Iacobucci & Popescu, 2017, 2020).

Many interactions between NMDARs and downstream signaling molecules, predominantly the Ca^{2+}-binding/Ca^{2+}-activated proteins calmodulin (CaM) and α-actinin, have

135

been implicated in processes referred to as CDI (Ehlers *et al.*, 1996; Wyszynski *et al.*, 1997; Zhang *et al.*, 1998; Krupp *et al.*, 1999; Rycroft & Gibb, 2002; Iacobucci & Popescu, 2017). The most complete hypothesis for a CDI mechanism posits that buildup of $[Ca^{2+}]_i$ leads to activation of CaM, which displaces α-actinin from its binding site on the GluN1 CTD, releasing the channel from the actin cytoskeleton (Zhang *et al.*, 1998; Krupp *et al.*, 1999). The displacement of α-actinin by CaM could even lead to desensitization by itself, since the α-actinin-GluN1 interaction is thought to stabilize an open NMDAR state (Wyszynski *et al.*, 1997; Krupp *et al.*, 1999). Some evidence suggests that direct binding of Ca^{2+} by α-actinin can drive the dissociation of α-actinin from GluN1 without the need for CaM (Krupp *et al.*, 1999), but it is well-accepted that direct interaction of CaM with the GluN1 CTD is the primary driver of CDI (Ehlers *et al.*, 1996; Zhang *et al.*, 1998; Rycroft & Gibb, 2002, 2004; Iacobucci & Popescu, 2017). Thus, CDI is most accurately defined as a fast CDD process that depends on the direct binding of CaM to the GluN1 CTD.

Our understanding of the slower form of CDD is far less advanced. Slow CDD, originally referred to as a glycine-independent desensitization mechanism, can be broadly defined as a progressive increase in desensitization following whole-cell break-in or outside-out patch formation (Sather *et al.*, 1992; Lieberman & Mody, 1994; Tong & Jahr, 1994; Villarroel *et al.*, 1998). Glycine-independent desensitization, or at least a form of it, was shown to depend on Ca^{2+} by experiments that prevented rises of $[Ca^{2+}]_i$ either through chelation of Ca^{2+} by high intracellular [BAPTA] or through manipulation of NMDAR-mediated Ca^{2+} influx (Lieberman & Mody, 1994; Tong & Jahr, 1994; Medina *et al.*, 1995; Krupp *et al.*, 2002). There are clear kinetic differences between this Ca^{2+}-dependent, glycine-independent desensitization process and the CaM-binding-dependent CDI. CDI occurs over the course of milliseconds (Legendre *et al.*, 1993; Ehlers *et al.*, 1996; Zhang *et al.*, 1998; Krupp *et al.*, 1999). In contrast, this Ca^{2+}-dependent, glycine-independent desensitization develops over the course of minutes (Lieberman & Mody, 1994; Tong & Jahr, 1994; Medina *et al.*, 1995; Krupp *et al.*, 2002). Despite this obvious difference in time-

scale, the slower form of CDD has also been referred to as CDI (Iacobucci & Popescu, 2017, 2020).

The molecular mechanisms underlying slow CDD are unclear. The most heavily implicated driver of slow CDD is calcineurin, a Ca^{2+}-CaM-activated serine/threonine protein phosphatase. Calcineurin has been reported to regulate NMDAR desensitization in response to prolonged elevations of $[Ca^{2+}]_i$ or transient synaptic Ca^{2+} influx (Lieberman & Mody, 1994; Tong & Jahr, 1994; Tong et al., 1995; Krupp et al., 2002; Rycroft & Gibb, 2004). Inhibition of calcineurin has been reported to ablate the time-dependent, Ca^{2+} dependent increase in desensitization following whole-cell break-in or outside-out patch formation (Lieberman & Mody, 1994; Tong & Jahr, 1994; Krupp et al., 2002). Krupp et al. 2002 further narrowed down the mechanism of slow CDD by showing that (1) dephosphorylation of multiple sites on the GluN2A CTD by calcineurin is necessary for slow CDD and (2) that truncation of the GluN1 CTD had no effect on slow CDD, fully distinguishing slow CDD from CDI. However, a recent study (Iacobucci & Popescu, 2017) reported that calcineurin inhibition had no effect on desensitization elicited by prolonged exposure to $[Ca^{2+}]_i$ (high $[Ca^{2+}]_F$ in pipette, 15 min post-break-in). To further complicate matters, Iacobucci & Popescu 2017 (who refer to this Ca^{2+}-dependent, progressive increase in desensitization as CDI) also reported that truncation of the GluN1 CTD ablated the sensitivity of all forms of NMDAR desensitization to $[Ca^{2+}]_i$. These inconsistencies make it difficult to definitively state that the slow and fast CDD processes are mediated by distinct mechanisms.

Through investigating the mechanisms underlying the $[Ca^{2+}]_i$ dependence of memantine potency, we uncovered evidence supporting the existence of distinct Ca^{2+}-dependent desensitized states. Our data support the hypothesis that the $[Ca^{2+}]_i$ dependence of memantine potency arises from the ability of memantine to stabilize a Ca^{2+}-dependent desensitized GluN1/2A receptor state. Stabilization of a receptor state by memantine necessitates an energetically favorable interaction between memantine and that state, or in other terms, increased affinity of

memantine for that state. Both memantine potency and NMDAR desensitization increase with increasing $[Ca^{2+}]_i$, and ablating CDD also ablates the effect of $[Ca^{2+}]_i$. This suggests that memantine has a higher affinity for this Ca^{2+}-dependent desensitized state. We also found that desensitization of GluN1/2A receptors is further increased by prolonging the duration that receptors are subjected to high $[Ca^{2+}]_i$. However, memantine inhibition of GluN1/2A receptors does not progressively increase alongside this progressive $[Ca^{2+}]_i$-and-time-dependent increase in desensitization. Therefore, our data suggest there are at least two distinct Ca^{2+}-dependent desensitized conformational states: one conformation with a higher affinity for memantine, and one conformation with unchanged affinity for memantine.

Our data makes a strong case for the existence of two distinct desensitized conformational states, both dependent on $[Ca^{2+}]_i$, with different interactions with memantine. However, it is difficult to conclude definitively which mechanisms underlie which desensitization process. It is almost certain that the desensitization process that produces the state stabilized by memantine is relatively fast. This conclusion is supported by our data showing that the $[Ca^{2+}]_i$ dependence of memantine potency does not depend on duration of exposure to $[Ca^{2+}]_i$, as well as by previous data from our lab showing that memantine potency increases in conditions that allow for increased buildup of $[Ca^{2+}]_i$ via NMDAR-mediated influx over short timescales (Glasgow *et al.*, 2017). Notably, in our experiments, both the $[Ca^{2+}]_i$ dependence of memantine potency and a form of CDD are reliant on the presence of the GluN1 CTD. This suggests that the mechanism of CDD related to memantine potency is likely similar to the "canonical" CDI mechanism, which requires interactions between CaM, α-actinin, and the GluN1 CTD (Zhang *et al.*, 1998; Krupp *et al.*, 1999). The slower $[Ca^{2+}]_i$-and-time-dependent desensitization in our experiments is similar to the slow form of CDD previously reported by the Jahr and Westbrook labs (Tong & Jahr, 1994; Krupp *et al.*, 2002). This conclusion, however, is complicated by conflicting data from the Westbrook and Popescu labs regarding the roles of calcineurin and the GluN1 CTD in the slow

mechanism of CDD (Krupp *et al.,* 2002; Iacobucci & Popescu, 2017). Future experiments assessing the role of calcineurin in the $[Ca^{2+}]_i$ dependence of memantine potency and the role of the GluN1 CTD in $[Ca^{2+}]_i$-and-time-dependent desensitization will help clarify the mechanism underlying the slow form of CDD observed in our experiments.

5.2 STRUCTURAL UNDERPINNINGS OF $[CA^{2+}]_i$-DEPENDENT CHANNEL BLOCK

Our results support the idea that the $[Ca^{2+}]_i$ dependence of memantine potency arises from the ability of memantine to stabilize a Ca^{2+}-dependent desensitized GluN1/2A receptor state, which suggests that memantine has a higher affinity for receptors in this state. This finding has the potential to deepen our understanding of the structural features underlying the conformational changes that occur during NMDAR state transitions. Understanding the structural features that govern the relation between memantine potency and CDD may also aid in the design of future channel blockers that more selectively target specific receptors states. Our experiments have identified several key structural features that contribute to both the $[Ca^{2+}]_i$ dependence of memantine potency and CDD.

The most obvious structural feature of the NMDAR that contributes to both the $[Ca^{2+}]_i$ dependence of memantine potency and CDD is the GluN1 CTD. Both the $[Ca^{2+}]_i$ dependence of memantine potency and CDD require the GluN1 CTD. However, the GluN1 CTD is relatively distant from regions making up the NMDAR pore. Therefore, in order to reach the conformation stabilized by memantine, the channel must receive some long-distance allosteric signal from the GluN1 CTD. NMDARs are particularly notorious for long-distance allosteric transduction between receptor domains (Paoletti *et al.*, 1997, 2000; Zheng *et al.*, 1998, 2001; Rachline *et al.*, 2005; Gielen *et al.*, 2008, 2009; Siegler Retchless *et al.*, 2012; Tajima *et al.*, 2016; Sun *et al.*, 2017;

139

Jalali-Yazdi *et al.,* 2018; Esmenjaud *et al.*, 2019; Vyklicky *et al.*, 2021). Unfortunately, how conformational changes in the GluN1 CTD contribute to channel gating is unknown, and there are currently no NMDAR crystal or cryo-EM structures that include the GluN1 CTD (or any other NMDAR subunit CTD). Improved structural models may provide further insight into the role of TMD-CTD coupling in CDD and the $[Ca^{2+}]_i$ dependence of memantine potency.

Our investigation into the role of the GluN2 subunit in the effects of $[Ca^{2+}]_i$ on memantine potency also provided insights into the structural underpinnings of the relation between memantine potency and CDD. The identity of the GluN2 subunit determines the effects of $[Ca^{2+}]_i$ on desensitization and memantine potency. $[Ca^{2+}]_i$ dependence of memantine inhibition is a GluN2A subunit-specific phenomenon; block of GluN1/2B, GluN1/2C, and GluN1/2D receptors by memantine is $[Ca^{2+}]_i$-independent. Memantine inhibition of GluN1/2A receptors in cells with $[Ca^{2+}]_i$ < 1 nM was significantly weaker than memantine inhibition of any other NMDAR subtype tested, regardless of condition. This suggests that GluN1/2A receptors can sample a unique channel conformation, inaccessible to other subtypes, with weak memantine affinity. In contrast, the memantine IC_{50} measured for GluN1/2A receptors with $[Ca^{2+}]_i$ = 10 μM was nearly identical to the IC_{50} values measured for all other NMDAR subtypes, regardless of condition. This finding suggests that Ca^{2+}_i drives the GluN1/2A channel, and its memantine binding site, into a conformation that is similar to the other receptor subtypes. The high degree of sequence homology in the pore-lining regions of the GluN2 subunits (Traynelis *et al.*, 2010; Siegler Retchless *et al.*, 2012) suggests that that variations in channel conformations between the subtypes result from differences in regions outside the channel. Furthermore, given that the GluN1 CTD is an essential determinant of CDD and the Ca^{2+} dependence of memantine potency, it is highly likely that differences in inter-subunit interactions govern the subtype-dependent differences in the effects of $[Ca^{2+}]_i$ on desensitization and memantine potency. Indeed, Vissel et al. 2002 identified a region in the GluN2A M2-M3 loop that was critical for CDD perhaps due to

interaction with residues 834 – 843 of the GluN1 CTD C0 region (Vissel *et al.*, 2002). Investigation of the role of the GluN2A M2-M3 loop in memantine potency may provide further insight into the structural interactions governing the $[Ca^{2+}]_i$ dependence of GluN1/2A receptor inhibition by memantine.

Little is known about conformational changes or residue-residue interactions at the level of the TMD during NMDAR desensitization. Our simulations and experiments in Chapter 3 identified residues in the NMDAR TMD, GluN1 M641 and GluN2A F641, that may play key roles in NMDAR desensitization and the $[Ca^{2+}]_i$ dependence of memantine potency. We found that both desensitization and memantine inhibition of GluN1/2A receptors is influenced by a residue in the GluN2A M3 helix, GluN2A F641. Mutation of GluN2A F641 had powerful effects on NMDAR desensitization, with mutation of the WT F residue to smaller residues (A or L) in comparison to the larger WT F residue greatly increasing desensitization. Interestingly, though both mutations enhanced desensitization, the GluN2A(F641A) and GluN2A(F641L) mutations displayed key differences in which type of desensitization they enhanced. GluN1/2A(F641L) receptors only enhanced Ca^{2+}-independent desensitization, while GluN1/2A(F641A) receptors enhanced both Ca^{2+}-independent desensitization and CDD in comparison to WT receptors. These finding suggests intriguing possibilities for the role of GluN2A F641 in desensitization. Firstly, our data suggests that GluN2A F641 is likely involved in interactions that affect the relative stability of open and closed states of the NMDAR channel. Secondly, the differential ability of the GluN2A(F641A) and GluN2A(F641L) mutations to stabilize different desensitized states suggests that different desensitized states have different conformations at the level of the TMD. This idea is further supported by our finding that memantine stabilizes a specific Ca^{2+}-dependent desensitized receptor state rather than broadly stabilizing all closed states. Using MD simulations to identify channel residues that differentially interact with GluN2A(F641A) and GluN2A(F641L), and then experimentally testing the role of these residues in desensitization, may be a fruitful strategy for

141

determining structural differences between Ca^{2+}-independent and Ca^{2+}-dependent desensitized states.

Interestingly, our results do not suggest that mutation of GluN2A F641 influences memantine inhibition simply by affecting NMDAR desensitization. Although our MD simulations did not suggest a direct interaction between GluN2A F641 and memantine, the simulations suggested that GluN2A F641 instead regulated memantine potency through interaction with GluN1 M641. GluN1 M641 was predicted to form energetically favorable interactions with both memantine and GluN2A F641. Simulations suggested that the size of GluN2A residue 641 contributes to its strength of interaction with GluN1 M641, with larger residues forming stronger interactions. Stronger interaction of GluN1 M641 with GluN2A F641 reduces interaction of GluN1 M641 with memantine, increasing memantine IC_{50} in comparison to the IC_{50} for GluN1/2A(F641A) receptors. This modeling prediction is supported by our experimental data, which show that size of the residue at GluN2A 641 is correlated with memantine IC_{50}. Thus, our simulations suggest that memantine and GluN2A F641 compete for interaction with GluN1 M641. It is important to note, however, that neither our simulations nor our experiments rule out the possibility that interaction of GluN2A F641 with GluN1 M641 could regulate desensitization. Larger GluN2A 641 residues and stronger interaction with GluN1 M641 may aid in stabilizing a receptor open state, reducing desensitization, while mutation of GluN2A 641 to smaller residues may remove this interaction with GluN1 M641, allowing for stronger interaction of GluN1 M641 with memantine and stabilization of a receptor closed/desensitized state. This prediction could be tested by experimentally investigating the effects of GluN1 M641 mutations on desensitization, memantine potency, and the Ca^{2+} dependence of memantine potency.

Excitingly, we found that memantine is not the only channel blocker that displays $[Ca^{2+}]_i$-dependent potency. Inhibition of GluN1/2A receptors by the novel memantine analog RL-208 increased 2-3-fold between conditions of $[Ca^{2+}]_i < 1$ nM and $[Ca^{2+}]_i = 5$ μM, which suggests that

RL-208 also stabilizes a Ca^{2+}-dependent desensitized receptor state. There are clear structural similarities between memantine and RL-208. Both memantine and RL-208 (see Figure 18) are essentially polycyclic carbon balls with multiple methyl groups and a primary amine. It is likely that these general structural features govern the ability of memantine and RL-208 to stabilize a Ca^{2+}-dependent desensitized receptor state. Further structural comparison of memantine and RL-208 with ketamine (see Figure 11 for structure), which does not display $[Ca^{2+}]_i$-dependent potency, reveals several notable differences that may contribute to the differential interactions these drugs have with desensitized states.

Both memantine and RL-208 (Figure 18) are primary amines, while ketamine (Figure 11) is a secondary amine. It is possible that the additional methyl group attached to the ketamine nitrogen forms interactions with residues near the critical Asn residues that are unable to be reached by memantine and RL-208. Ketamine is much "flatter" and more flexible than memantine and RL-208. Ketamine consists of two 6-carbon rings - a phenyl chloride and a cyclohexanone - adjoined by a single C-C bond. In comparison to the polycyclic carbon balls that make up the bulk of memantine and RL-208, the flatter rings of ketamine can more easily form energetically favorable interactions with hydrophilic or aromatic residues in the channel pore (Dougherty, 2007). Additionally, the single C-C bond that connect the ketamine rings is rotatable, allowing ketamine to adopt a greater number of conformations than memantine and RL-208. In contrast, the rigid, bulky, and relatively symmetric memantine and RL-208 molecules have a greater potential to favorably coordinate with hydrophobic residues. Indeed, simulations and structural modeling performed by Song et al. 2018 suggested that memantine may stabilize a closed channel state by coordinating with hydrophobic residues near the bundle crossing (Song *et al.*, 2018), a TMD region critically involved in iGluR gating (Chang & Kuo, 2008; Sobolevsky *et al.*, 2009; Twomey & Sobolevsky, 2018). A clear next step is to investigate the dependence of RL-202, MFV-4, and EV-19 potency on $[Ca^{2+}]_i$, which will allow us to further examine the structural features that dictate

143

whether a channel blocker can stabilize a Ca^{2+}-dependent desensitized receptor state. In addition, by expanding our structural comparison of the binding sites beyond the conservative range used for Chapter 3 experiments, we can identify additional TMD residues that differentially contribute to the binding of the memantine analogs and ketamine. This may lead us toward identification of additional residues involved in CDD. Thus, although the structural underpinnings of $[Ca^{2+}]_i$-dependent channel block are still unresolved, memantine, ketamine, and the novel channel blockers should serve as effective experimental probes for interrogating the structure of a Ca^{2+}-dependent desensitized state and, subsequently, the mechanisms underlying $[Ca^{2+}]_i$-dependent channel block.

5.3 LIMITATIONS OF MOLECULAR MODELING

Molecular modeling can aid in the interpretation of complicated electrophysiological data and facilitate the development of novel hypotheses. However, results of simulations are easy to overinterpret and both our docking and MD simulations are subject to notable limitations. Docking simulations, when used alone, have many weaknesses. The predominant limitation of docking simulations is the use of rigid protein structures. We utilized a stochastic conformational search method in which rotatable bonds in the ligand (i.e., the channel blocker) can be rotated by the program to give the most favorable conformations, as determined by a predefined scoring function, for docking to specific regions of the protein (Trott & Olson, 2010). Though this allowed us to partially account for the conformational dynamics of the blockers, the protein was held static during docking. Therefore, our docking simulations were limited to static snapshots of the GluN1/2A TMD taken from an MD simulation. In addition, scoring functions used to determine favorable docking sites are only general approximations of the free energy of the ligand-protein

144

complex (Sousa *et al.*, 2006; Gaillard, 2018). Therefore, Autodock Vina simulations alone are unable to distinguish between resides that directly contribute to the binding of a ligand and residues that are merely in close proximity to a ligand's predicted binding site. Autodock Vina also does not account for solvent molecules, which can play key roles in NMDAR channel block (Mesbahi-Vasey *et al.*, 2017). Thus, Autodock simulations are best used as a preliminary tool to predict the general site of ligand-protein interactions before experimental validation.

To overcome some of the limitations of docking simulations, we utilized atomistic MD simulations to further model interactions of memantine with the GluN1/2A TMD. Our MD simulations highlighted a weakness of Autodock Vina simulations, suggesting that a residue predicted to contribute to the memantine binding site by Autodock Vina (GluN2A F641) did not directly interact with memantine. In addition, these simulations provided a logical explanation for the effect of GluN1/2A F641 mutations on memantine IC_{50} that was consistent with our electrophysiological data. However, our MD simulations are limited in scope. We are currently limited to only modeling TMD dynamics. NMDAR desensitization is heavily modulated by regions distal to the TMD, primarily the NTD and the CTD (Ehlers *et al.*, 1996; Krupp *et al.*, 1996, 1998, 2002; Villarroel *et al.*, 1998; Vissel *et al.*, 2002; Thomas *et al.*, 2006). However, the impact of these distal regions on the structural dynamics of the TMD is not incorporated into our current model. This limitation is predominantly due to the lack of knowledge concerning how long-range conformational signaling affects TMD structure, as well as the computational burden associated with atomistic simulation of large-scale conformational changes.

It is also important to note that we are simulating the binding of memantine to a closed channel state of unknown identity. Since there are no crystal or cryoEM structures of NMDARs in confirmed desensitized states, little is known about the conformational differences between different closed states. However, the ability of memantine to stabilize only a specific desensitized state suggests that different closed states have different conformations at the level of the TMD.

145

Furthermore, as noted previously, our models do not contain the GluN1 CTD, a structural component necessary for CDD and $[Ca^{2+}]_i$-dependent memantine block. Therefore, it is possible that our MD simulations do not capture interactions between memantine and the TMD that are relevant to CDD. Despite these limitations, our simulations provided interesting insights into the structure of the memantine binding site, demonstrating the power of integrating theoretical and experimental approaches.

5.4 THERAPEUTIC RELEVANCE OF STATE-SPECIFIC NMDAR INHIBITION

Indiscriminate inhibition of NMDARs can generate deleterious side effects in patients, including sedation, psychosis, and even neurotoxicity (Olney *et al.*, 1989; Zorumski & Olney, 1993; Krystal *et al.*, 1994, 2003; Chen & Lipton, 2006). Therefore, for an NMDAR antagonist to be clinically acceptable, it must somehow inhibit NMDARs involved in pathological processes while leaving NMDAR activity involved in normal physiology relatively intact. State-specific inhibition, the targeting of specific receptor states, could allow for preferential inhibition of select populations of NMDARs and thus limit off-target and negative side effects. In this dissertation, we present multiple lines of evidence that memantine acts not only by blocking ion flux through NMDARs, but also by stabilizing a desensitized state of the NMDAR channel. Thus, our results strongly support the idea that memantine is a state-specific inhibitor of GluN1/2A receptors.

The ability to stabilize a Ca^{2+}dependent desensitized receptor state enables memantine to differentially target NMDARs based on a combination of physiological context (i.e. activity level) and subunit composition. Indeed, our experiments revealed that memantine inhibition of GluN1/2A receptors is dynamically regulated by fluctuations of $[Ca^{2+}]_i$ in both physiological and pathological ranges, with higher $[Ca^{2+}]_i$ leading to greater memantine inhibition. These results

have clear implications for neuroprotection. The $[Ca^{2+}]_i$ dependence of memantine potency should allow memantine to inhibit NMDARs in cellular populations subjected to pathological levels of Ca^{2+} influx, i.e., NMDARs likely to mediate excitotoxic cell death (Zorumski & Olney, 1993; Rothman & Olney, 1995; Okamoto *et al.*, 2009; Hardingham & Bading, 2010), more readily than NMDARs involved in normal physiological signaling. Thus, our results provide a logical explanation for how memantine may preferentially target subpopulations of NMDARs involved in disease, which has long been a leading hypothesis regarding the unique clinical safety of memantine (Zhao *et al.*, 2006; Léveillé *et al.*, 2008; Okamoto *et al.*, 2009; Xia *et al.*, 2010).

In addition to clear implications for neuroprotection, the subtype- and context-specificity of memantine action may allow memantine to preferentially target specific subpopulations of neurons. GluN2A-containing receptors are likely the most prevalent NMDARs expressed by neurons in the adult hippocampus and cortex (Rauner & Köhr, 2011; Tovar *et al.*, 2013; Stroebel *et al.*, 2018). However, while mature excitatory pyramidal cells almost exclusively express GluN2A and GluN2B subunits, inhibitory interneurons strongly express GluN2A as well as GluN2C and GluN2D subunits (Monyer *et al.*, 1994; Kinney *et al.*, 2006). The differential subunit expression pattern observed between excitatory neurons and inhibitory neurons has major implications for channel block. GluN1/2A and GluN1/2B receptors, and GluN1/2A/2B triheteromeric receptors, are much more sensitive to Mg^{2+} block than GluN1/2C and GluN1/2D receptors (Monyer *et al.*, 1994; Kuner & Schoepfer, 1996; Hansen *et al.*, 2014). The subtype-dependence of Mg^{2+} block has a profound effect on the subtype selectivity of memantine. Given that memantine and Mg^{2+} compete for binding in the NMDAR channel, memantine inhibits GluN1/2C and GluN1/2D receptors more effectively than GluN1/2A and GluN1/2B receptors in physiological $[Mg^{2+}]$ (Kotermanski & Johnson, 2009). Therefore, the high expression level of GluN2C and GluN2D by inhibitory in comparison to excitatory neurons should direct memantine to preferentially inhibit NMDAR responses in inhibitory neurons. Indeed, experiments recording from prefrontal cortex

slices have reported that memantine inhibits spiking activity of inhibitory interneurons more effectively than excitatory neurons (Povysheva & Johnson, 2016).

The GluN2A specificity of the $[Ca^{2+}]_i$ dependence of memantine inhibition likely compounds with the effect of Mg^{2+} competition on subtype selectivity of memantine. Data presented in Chapter 2 suggest that GluN1/2A receptors, in conditions of low $[Ca^{2+}]_i$, sample a unique conformational state that exhibits weaker affinity for memantine and cannot be accessed by GluN1/2B, GluN1/2C, or GluN1/2D receptors. Therefore, in the absence of strong excitation, memantine potency for GluN1/2A receptors is greatly reduced by both Mg^{2+} competition and the $[Ca^{2+}]_i$ dependence of memantine potency. Furthermore, endogenous Ca^{2+}-buffering capacity and dynamics can vary greatly between neuronal class due to differential expression of Ca^{2+}-buffering proteins. In particular, parvalbumin interneurons exhibit fast spiking activity and unique Ca^{2+} dynamics that allow for prolonged elevations of Ca^{2+}_i (Schwaller, 2010). Thus, the GluN2 expression pattern, high-frequency activity, and slow, large Ca^{2+} transients displayed by many inhibitory interneurons make them prime targets for preferential inhibition by memantine.

The ability of memantine to preferentially target inhibitory neurons could contribute to its neurotherapeutic benefits, particularly for Alzheimer's disease. Alzheimer's patients have been reported to have decreased cortical activity, reduced metabolism in the prefrontal cortex, and strong degeneration of excitatory neurons in comparison to inhibitory neurons (Hof *et al.*, 1991; Rombouts *et al.*, 2000; Hof & Morrison, 2004; Schroeter *et al.*, 2012). Therefore, evidence suggests that the excitation/inhibition (E/I) balance of cortical activity is altered by the progression of Alzheimer's disease, with a shift toward inhibition. By preferentially inhibiting inhibitory neurons, memantine would allow for increased excitatory neuron activity and lead to a shift of the E/I balance back toward physiological levels.

Many NMDAR channel blockers are thought to preferentially target inhibitory interneurons and increase cortical excitation (Moghaddam *et al.*, 1997; Sharp *et al.*, 2001; Jackson *et al.*, 2004;

Homayoun & Moghaddam, 2007; Widman & McMahon, 2018). However, excessive inhibition of inhibitory neurons and subsequent runaway excitation has been proposed to be the mechanism by which poorly tolerated NMDAR channel blockers such as ketamine, MK-801, and phencyclidine produce psychotomimetic effects and kill neurons (Sharp *et al.*, 2001; Homayoun & Moghaddam, 2007). Why, then, does memantine not produce these unacceptable side effects? It is possible that the $[Ca^{2+}]_i$ dependence of memantine inhibition of GluN1/2A receptors acts as a fail-safe preventing runaway excitation. Under normal conditions, memantine may preferentially target GluN1/2C and GluN1/2D receptors on inhibitory neurons over GluN1/2A and GluN1/2B receptors on excitatory neurons due to differences in Mg^{2+} block. Then, as excitatory neuron activity increases due to disinhibition, Mg^{2+} block of GluN1/2A receptors is relieved and $[Ca^{2+}]_i$ increases in excitatory neurons. As $[Ca^{2+}]_i$ increases, memantine inhibition of GluN1/2A receptors in excitatory neurons increases to levels similar to that of GluN1/2B, GluN1/2C, and GluN1/2D receptors. This increase in memantine potency at GluN1/2A receptors, when coupled with Mg^{2+} unblock, could weaken the preference of memantine for inhibitory interneurons. Thus, the $[Ca^{2+}]_i$ dependence of memantine inhibition of GluN1/2A receptors could allow memantine to subtly increase cortical excitability while preventing runaway excitation. Though this hypothesis is likely oversimplified, it highlights that subtle mechanistic differences in pharmacodynamics may have substantial impact on the clinical profiles of channel blockers.

5.5 FUTURE DIRECTIONS

In this dissertation, we present the first characterization of a novel form of state-specific NMDAR antagonism, $[Ca^{2+}]_i$-dependent channel block of GluN1/2A receptors by memantine. Through examination of the $[Ca^{2+}]_i$ dependence of memantine potency, we also gathered insights

into NMDAR desensitization and the structure of the memantine binding site. Lastly, we characterized the electrophysiological properties of newly synthesized NMDAR channel blockers, and discovered that potency of a memantine analog is also dependent on $[Ca^{2+}]_i$. This section will highlight additional questions generated by our data that have not yet been addressed.

The experiments presented in Chapter 2 only scratch the surface of the effects of $[Ca^{2+}]_i$ on desensitization and memantine inhibition of triheteromeric NMDARs and native NMDAR populations. GluN1/2A/2B receptors are likely to be the most prevalent form of NMDAR expressed in the adult neocortex and hippocampus (Sheng *et al.*, 1994; Luo *et al.*, 1997; Gray *et al.*, 2011; Rauner & Köhr, 2011; Paoletti *et al.*, 2013; Tovar *et al.*, 2013; Stroebel *et al.*, 2018). Although we showed that memantine inhibition of a mixed population of native NMDARs containing both GluN2A- and GluN2B-containing receptor is $[Ca^{2+}]_i$-dependent, we have not directly tested whether memantine inhibition of triheteromeric NMDARs is $[Ca^{2+}]_i$-dependent. As mentioned previously, isolation of triheteromeric receptors is difficult. Current methods that allow for investigation of triheteromeric NMDARs in transfected cells rely on modifications to receptor regions involved in either Mg^{2+} (Hatton & Paoletti, 2005) block or desensitization (Hansen *et al.*, 2014; Stroebel *et al.*, 2014), and thus are unsuitable for our purposes. Development of new methods for isolation of triheteromeric NMDARs will be critical for evaluating the relation between desensitization and channel block of GluN1/2A/2B receptors.

The $[Ca^{2+}]_i$ dependence of memantine potency may contribute to the preferential targeting of inhibitory interneurons. Previous work from our lab has shown that memantine inhibition of synaptic NMDAR responses in excitatory neurons is enhanced in conditions allowing for buildup of Ca^{2+}_i (Glasgow *et al.*, 2017). However, the effect of $[Ca^{2+}]_i$ on memantine inhibition of inhibitory neurons has not been directly tested, nor compared with the effect of $[Ca^{2+}]_i$ on memantine inhibition of excitatory neurons. Furthermore, different types of inhibitory neurons express distinct Ca^{2+}-binding proteins and exhibit different Ca^{2+}-buffering dynamics (Schwaller, 2010). Thus,

150

future experiments comparing the effects of $[Ca^{2+}]_i$ on desensitization and memantine inhibition of different types of inhibitory neurons may provide insight into the effects of endogenous Ca^{2+} buffers on CDD and memantine inhibition.

Our simulations and experiments in Chapter 3 provided insight into the structure of the memantine binding site. However, interpretations of our simulation results are limited due to our lack of knowledge about structures of NMDAR desensitized states and our inability to model long-distance domain-domain interactions. Future studies could ameliorate some of these issues through utilization of elastic network models (ENMs). Elastic network models treat the protein backbone as harmonic springs between Cα atoms, greatly reducing the computational requirements for simulations (Atilgan *et al.*, 2001; Bahar *et al.*, 2010). Due to this reduction in computational cost, ENMs are particularly useful for modeling long-range conformational changes that are typically beyond the scope of atomistic MD simulations. Although ENMs are coarse-grained models that lack the resolution of atomistic MD simulations, simulations with ENMs have been successfully integrated with atomistic MD simulations to provide interesting insights into the conformational dynamics of iGluRs (Dutta *et al.*, 2015; Krieger *et al.*, 2015, 2019; Lee *et al.*, 2019). Therefore, integration of our MD simulations with ENM simulations may be a useful strategy for investigating the role of non-TMD regions in CDD and memantine binding.

We have so far only identified two blockers, memantine and RL-208, that show $[Ca^{2+}]_i$-dependent potency. However, we have only examined the effects of $[Ca^{2+}]_i$ on potencies of four channel blockers in total: memantine, RL-208, ketamine, and Mg^{2+}. Characterization of the effects of $[Ca^{2+}]_i$ on the potencies of EV-19, RL-202, and MFV-4 will provide further insight into the structural properties that determine whether a blocker stabilizes a Ca^{2+}-dependent desensitized GluN1/2A receptor state. Atomistic simulations of blocker binding will also provide further insight into the structural mechanisms governing GluN1/2A receptor CDD and channel block. Overall, the concepts presented in this dissertation will hopefully guide future research utilizing this

powerful combination of experimental and computational/theoretical approaches to ultimately aid in the future design of more clinically efficacious NMDAR-targeting neurotherapeutics and deepen our understanding of NMDAR structure and channel block.

APPENDIX A INTERPLAY BETWEEN GATING AND BLOCK OF LIGAND-GATED ION

CHANNELS

Phillips, M.B., Nigam, A., & Johnson, J.W. (2020) Interplay between Gating and Block of Ligand Gated Ion Channels. *Brain Sci.*, **10**.

Interplay between Gating and Block of Ligand-Gated Ion Channels

Matthew B. Phillips [1,2], Aparna Nigam [1] and Jon W. Johnson [1,2,*]

[1] Department of Neuroscience, University of Pittsburgh, Pittsburgh, PA 15260, USA;
   matt.phillips@pitt.edu (M.B.P.); apn20@pitt.edu (A.N.)

[2] Center for Neuroscience, University of Pittsburgh, Pittsburgh, PA 15260, USA

* Correspondence: jjohnson@pitt.edu; Tel.: +1-(412)-624-4295

Abstract: Drugs that inhibit ion channel function by binding in the channel and preventing current flow, known as channel blockers, can be used as powerful tools for analysis of channel properties. Channel blockers are used to probe both the sophisticated structure and basic biophysical properties of ion channels. Gating, the mechanism that controls the opening and closing of ion channels, can be profoundly influenced by channel blocking drugs. Channel block and gating are reciprocally connected; gating controls access of channel blockers to their binding sites, and channel-blocking drugs can have profound and diverse effects on the rates of gating transitions and on the stability of channel open and closed states. This review synthesizes knowledge of the inherent intertwining of block and gating of excitatory ligand-gated ion channels, with a focus on the utility of channel blockers as analytic probes of ionotropic glutamate receptor channel function.

1. Introduction

Neuronal information processing depends on the distribution and properties of the ion channels found in neuronal membranes. Channel gating, perhaps the most basic characteristic of ion channels, refers to the ability of ion channels to either open and allow transmembrane ion flux or to close and prevent ion flux. The gating mechanisms employed by ligand-gated ion channels are divided into three general categories, namely, activation, deactivation, and desensitization. Activation refers to the transition of ion channels from closed to open states following application of agonist. Deactivation refers to the transition of channels from open to closed states following removal of agonist. Desensitization is canonically defined as a decrease in the fraction of channels that are in the open state (termed open probability, or P_{open}) in the maintained presence of agonist [1]. Desensitization is typically a direct consequence of agonist binding. A fourth gating mechanism that resembles desensitization but is not driven by agonist binding was referred to both as desensitization and inactivation [2–4], although inactivation is a term typically used to describe a different mechanism employed by voltage-gated channels [5]. Although driven by different underlying mechanisms, both desensitization and inactivation ultimately describe nonconducting channel states that do not respond to typical activating stimuli [1,5]. Gating mechanisms of ion channels are finely tuned and are essential to normal nervous system function, with even minor aberrations of channel gating often resulting in disease. While most known channelopathies involve dysfunction of voltage-gated channels, naturally occurring genetic variants that alter the gating of ligand-gated ion channels are increasingly associated with neurological disorders, including epilepsy, intellectual disability, and autism [6].

Studies of drugs that inhibit channel function provide valuable insight into ion channel gating mechanisms. Channel blockers, antagonists that bind in and prevent ion flux through ion channels, have been successfully used to probe both the structure of ion channel pores and the kinetics of channel gating. Channel gating requires conformational changes in or near the channel pore (i.e., the transmembrane ion

conduction pathway), and channel blockers are known to interact differentially with channels in open, closed, inactivated, and desensitized states [3,7–10]. Thus, channel blockers are exceptionally well-positioned, both figuratively and literally, for use as analytic probes in studies of channel gating. Here, we discuss the interaction between channel block and channel gating of excitatory ligand-gated ion channels, with a focus on ionotropic glutamate receptors.

Reciprocal Interactions between Channel Block and Channel Gating

Channel gating can profoundly influence channel block, and channel block can profoundly influence channel gating. The initial binding of channel blockers often depends on gating state. Most blockers of ligand-gated ion channels can only enter and bind to the channel while agonist is bound and the channel is in the open state (Figure 1A). Such blockers are descriptively named open channel blockers and are the focus of this review. In some cases, open channel blockers are also termed "use-dependent" [11]. A blocker is termed use-dependent if inhibition by the blocker (1) requires activation of the channel, and (2) increases with duration of channel activation until an equilibrium between blocker binding and unbinding is reached (Figure 1A). The actions of almost all known ligand-gated ion channel blockers have been found to be at least partially dependent on channel opening, binding either exclusively or with much faster kinetics when the channel is open.

Channel blocker unbinding also depends on gating transitions. If closure of the channel gate and agonist unbinding can occur while the blocker is bound, the blocker may become "trapped" in the channel (Figure 1C,D), unable to unbind until agonist is reapplied. Interestingly, some trapping blockers display the ability to escape from a fraction of blocked channels even after removal of agonist, a phenomenon termed "partial trapping" that is not fully understood [12–16]. On the other hand, sequential or "foot-in-door" channel blockers physically occlude closure of the channel gate (Figure 1E). The depth of the blocking site, size of the channel blocker, location of the channel gate, and gating-associated conformational changes all contribute to whether channels can close while the blocker is bound. These features dictate the structural interactions between channel blockers and the receptor's gating machinery, which in turn determine the influence that the channel blocker can reciprocally exert on gating transitions.

Bound channel blockers can affect gating transitions in three general ways. Blockers can:
4. Alter agonist binding and/or unbinding kinetics;
5. Stabilize channel open states;
6. Stabilize channel closed states.

For example, the binding of large sequential blockers to open channels prevents both transition of channels into closed states (Figure 1E) and agonist unbinding [7,17–20]. In contrast, smaller trapping blockers can interact with either open or closed channel states and can therefore have many possible effects on channel gating (Figure 1D). For example, trapping blockers can stabilize open or closed channels and/or facilitate entry into or recovery from desensitized states [3,8,21]. The inherent intertwining of channel gating and block allows channel blockers to be leveraged as powerful tools for the study of ion channel structure and function.

Figure 1. Interplay between channel gating and open channel block. (**A**) Schematic depicting inhibition of current (black line) by a prototypical open channel blocker. Three agonist applications (green bars) are shown. The first agonist application in the absence of blocker shows the control response. The second agonist application, which follows the application and removal of a blocker (red bar), shows that the blocker cannot access its binding site when the channel is closed. The third agonist application, which is made in the presence of a blocker, shows that the blocker can access its binding site and inhibit agonist-activated current when the channel is in the open state. Entry of a blocker into open channels accelerates the apparent decay of the response and decreases the steady state response. Because the blocker cannot bind until the channel opens, peak current in response to the first agonist application in the presence of the blocker may be unaffected, as shown here. However, if blocker binding is fast relative to current activation kinetics, the peak response may be reduced. (**B**) Ion channels can transition between open, ion permeable states and closed, impermeable states. k_c is transition rate into closed state and k_o is transition rate into open state. (**C–E**) The

156

size of channel blocking compounds (red) and depth of the blocking site affects blocker interactions with the channel gate. (**C**) Small channel blockers, such as inorganic cations, can block open channels without preventing channel closure or affecting gating transitions. k_{on} is blocker binding rate and k_{off} is blocker unbinding rate. When the channel is blocked by a blocker that does not interact with the gate, channel closing rate is k'_c and channel opening rate is k'_o. (**D**) Small-to-intermediate-sized organic channel blockers can block open channels without preventing channel closure, but nevertheless can interact with the channel gate, either accelerating or decelerating gating transitions. When the channel is blocked by a blocker that interacts with the gate, channel closing rate is k''_c and channel opening rate is k''_o. (**E**) Large, organic, sequential/foot-in-door blockers can block open channels and prevent channel closure. k'''_c is channel closing rate when the channel is blocked by a sequential/foot-in-the-door blocker.

Nicotinic Acetylcholine Receptors

Since the turn of the 20th century, the study of nicotinic acetylcholine receptors (nAChRs) has played a critical role in our understanding of ionotropic receptor biophysics and pharmacology. The very concept of transmitter receptors arose from the observation that application of nicotine to denervated striated muscle elicited muscle contraction, resulting in John Newport Langley's inference of the presence of a "receptive substance" on muscle fibers [22]. The nAChR has served as the prototypical ion channel since its discovery, being the first ion channel to be isolated, characterized, structurally imaged, and cloned [23–31]. nAChRs additionally served as the subject for the first kinetic models of ion channel function [1,32] and for the development of patch-clamp electrophysiology [33,34]. Consistent with their vast historical importance, nAChRs mediate neuromuscular transmission and play key roles in nervous system function. Cholinergic signaling through nAChRs heavily modulates excitatory and inhibitory transmission in hippocampal and mesolimbic circuits, and thus is vital in shaping synaptic plasticity and learning [35–40]. Unsurprisingly, aberrant expression or activation of nAChRs is heavily implicated in many neurological and neuromuscular disorders, including addiction, schizophrenia, epilepsy, Alzheimer's disease, myasthenia gravis, and Lambert–Eaton myasthenic syndrome, making nAChRs a major neurotherapeutic target [41–49].

nAChRs are excitatory, cation-selective members of the Cys-loop receptor superfamily, a major class of ligand-gated ion channels named for a conserved loop of 13 amino acid residues formed by disulfide-bonded cysteine residues in their extracellular domain. Other members of the Cys-loop family include the cation-selective serotonin (5-HT$_3$) and zinc-activated (ZAC) receptors, as well as the anion-selective γ-aminobutyric acid (GABA$_A$) and glycine (Gly) receptors [50]. Like all Cys-loop receptors, nAChRs are pentameric protein complexes with broad subunit diversity. nAChRs are assembled from a large catalog of subunits consisting of 10 α subunits (α1–10; although α8 is only expressed in avian species), four β subunits (β1–4), and the singular γ, δ, and ε subunits. This high subunit diversity is augmented further by the "sidedness" of each subunit, which allows the specific order in which subunits assemble to affect the receptor's biophysical properties, resulting in more than 1000 possible nAChR subtypes [38]. All neuromuscular junction (NMJ) nAChRs are heteropentameric, composed of α1, β1, γ, and either δ or ε subunits at a respective ratio of 2:1:1:1. Neuronal nAChRs, on the other hand, assemble either as α-homomers or as heteromers composed of α(2–10) subunits complexed with β(2–4) subunits. Homomeric α7 and heteromeric α4β2 (2 α4, 3 β2) are the most commonly expressed nAChR subtypes in the brain [51–53].

All nAChR subunits possess a modular structure composed of a large extracellular N-terminal domain (NTD; the location of the Cys-loop), three-membrane spanning regions (M1-M3), a variable intracellular loop, another transmembrane region (M4), and a short extracellular C-terminal domain. Although most nAChR subtypes possess two acetylcholine (ACh) binding sites formed within the NTD at the interface between α subunits and their neighboring subunits, the precise location and properties of agonist binding

sites differs broadly depending on subunit composition. For NMJ nAChRs, binding sites form at the α–γ or α–ε and at the α–δ subunit interfaces. Neuronal nAChRs again show greater diversity, with heteromeric receptors typically possessing two ACh binding sites located at α–β interfaces and homomeric receptors possessing five potential ACh binding sites [54–56]. The transmembrane regions (M1-M4) form a central, water-filled pore lined by the M2 transmembrane region that serves as a conduction pathway for the permeable cations Na^+, K^+, and Ca^{2+} [57,58]. Gating of nAChRs is initiated by binding of agonist in the extracellular domain, which begins a series of conformational changes that propagate to the transmembrane region and induce opening of the channel gate. Gating transitions of nAChRs are also heavily dependent on receptor subtype, but cycle through three basic states, namely, a resting closed state, an open state, and a desensitized state. nAChRs pass through multiple additional states after agonist binding prior to channel opening [59] and display many desensitized states. In fact, desensitization was first defined by Katz and Thesleff through the study of NMJ nAChR currents [1].

Channel Block of nAChRs

As with nearly every aspect of ion channel research, nAChRs were also the first ion channels to be investigated using antagonists. Experiments utilizing the arrow poison curare and the snake venom α-bungarotoxin produced thorough descriptions of competitive antagonism and served as the starting point for the isolation of nAChRs and characterization of their function [29,60,61]. Early studies using channel blockers to investigate gating of ligand-gated ion channels also largely focused on nAChRs. Local anesthetics and barbiturates act as nonselective nAChR blockers (but also target voltage-gated Na^+ channels [5] and GABA$_A$ receptors [62], respectively) and were among the first drugs used to probe ligand-gated ion channel block. Treatment of muscle fibers with local anesthetics (most notably, the lidocaine derivatives QX-222 and QX-314) converted the normally single exponential decay of motor endplate currents into a double exponential decay [63,64], an effect also observed with the barbiturates thiopentone, amylobarbitone, and methohexitone [65,66]. These observations served as the basis of a slew of studies that characterized the basic features of ion channel block. Adams provided the first extensive characterization of use-dependent ligand-gated ion channel block, providing (1) compelling evidence that nAChR channel blockade was strongly voltage-dependent, suggesting that the blocker binding site was within the membrane electric field, and (2) the first model of sequential channel block of a ligand-gated ion channel (Figure 1E; [65–67]). Around the same time, Ruff proposed a similar conceptual model for sequential channel block of nAChRs [19]. This model was soon validated by Neher and Steinback, who used single-channel recordings to show that binding of QX-222 blocked current flow and that open, blocked channels could not close (Figure 1E; [20]). These pioneering studies laid the groundwork for the use of channel blockers as experimental probes for the study of ion channel gating and function.

More recent studies of nAChR-channel blocker interactions provided further insight into nAChR gating mechanisms. Block of nAChRs by choline and millimolar concentrations of ACh prolong channel open times without affecting desensitization [10,68,69]. These findings led to the development of the "dual-gate" hypothesis of nAChR gating, which posits that nAChR activation and desensitization are mediated by distinct gates. Photolabeling experiments utilizing chlorpromazine further supported this dual-gate model, showing that (1) chlorpromazine has multiple binding sites in the nAChR channel and (2) the state of the receptor (i.e., desensitized, activated, or non-activated) directs the binding of chlorpromazine to specific sites in the channel [9,70–72]. Structural and functional evidence supporting the dual-gate model of activation and desensitization have been further found for an array of other pentameric ion channels [73], providing yet another example of the power of channel blockers as analytic tools.

Ionotropic Glutamate Receptors

Ionotropic glutamate receptors (iGluRs) are members of the pore loop superfamily of ion channels, integral membrane proteins that mediate the majority of ion flux across neuronal membranes [5]. Fast excitatory synaptic transmission in the central nervous system is primarily mediated by iGluRs, and proper functioning of iGluRs is vital to synaptogenesis, synaptic plasticity, signal integration, and information transfer [74,75]. Due to the integral roles iGluRs play in neuronal function and their ubiquitous expression, aberrant iGluR activity contributes to a wide variety of neuronal dysfunctions that can drive nervous system disorders [6,76–82].

iGluRs are divided into three main classes by structure: α-amino-3-hydroxyl-5-methyl-4-isoxazole-propionate receptors (AMPARs), kainate receptors (KARs), and N-methyl-D-aspartate receptors (NMDARs). A fourth division of the iGluR family, δ receptors, shares substantial sequence homology with other iGluR subtypes. Surprisingly, despite forming functional ion channels [83–85], δ receptors show no ligand-gated ion channel function [86–89] and are therefore not discussed in this review. All iGluRs assemble as complexes of four membrane-spanning subunits that form a central pore. Each iGluR subunit contributes exclusively to one subtype of iGluR: GluA1–4 form AMPARs, GluN1, GluN2A-D, and GluN3A-B form NMDARs, and GluK1–5 form KARs. Despite this wide diversity, all iGluR subunits possess a similar general structure (shown in Figure 2A using an NMDAR as an example) consisting of four discrete, semiautonomous domains, namely, an extracellular amino-terminal domain (ATD), an extracellular ligand-binding domain (LBD), a transmembrane domain (TMD), and an intracellular carboxy-terminal domain (CTD, which was deleted from the structure shown in Figure 2). Unlike nAChRs, each iGluR subunit possesses an agonist-binding site located within the LBD. The four TMDs of iGluRs form the pore, and thus the site of channel blocker binding (Figure 2B). Within the TMD lies the glutamine (Q) – arginine (R) – asparagine (N) (QRN) site, a site found at the tip of the re-entrant loop (M2 loop) in the iGluR pore (Figure 2C) that helps form the selectivity filter and plays a crucial role in the differential cation selectivity and channel block of the three iGluR classes [90–93]. Recent mid- and high-resolution structures of AMPAR [94–97] and NMDAR [21,98] TMDs provided great insight into iGluR gating transitions and channel block.
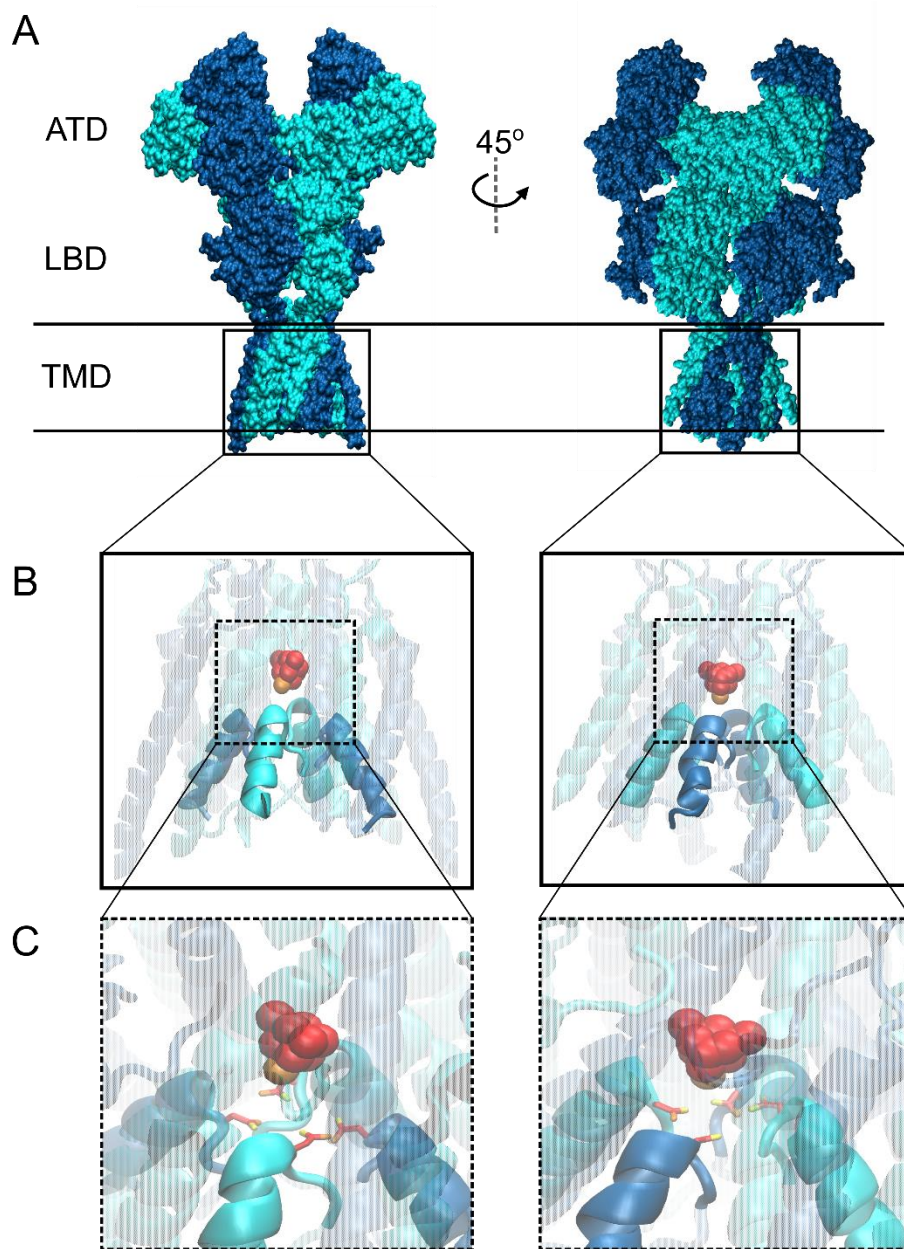
Figure 2. General N-methyl-D-aspartate (NMDA) receptor structure and putative blocking site. (**A**) Recently published structure of N-methyl-D-aspartate receptor (NMDAR) in an "active" state showing domain topology shared by all iGluR subtypes (ATD, amino-terminal domain; LBD, ligand-binding domain; TMD, transmembrane domain; Protein Data Bank (PDB) code 6WHT; [98]). GluN1 subunit is depicted in dark blue and GluN2B in cyan. Horizontal lines show the approximate locations of the outer and inner surfaces of the membrane. (**B**) Blow-up of NMDAR TMD (boxes in A) with docked channel blocker memantine (space-filled; carbons are red, nitrogen is orange) displaying typical site of channel block. Most channel blocking compounds show intimate interaction with the external tip of the iGluR selectivity filter formed by the re-entrant M2 loops of each subunit (opaque; M1, M3, and M4 transmembrane helices are transparent for visualization of blocking site). (**C**) Magnified view of memantine coordination by the QRN site asparagine residues GluN1 N616 and GluN2B N615, which are critically involved in NMDAR channel blocker binding

[99–103]. Autodock Vina was used for molecular docking of memantine to PDB 6WHT, and structural images were prepared using the program Visual Molecular Dynamics (VMD) [98,104,105].

Characteristics of AMPA and Kainate Receptor Block

AMPARs and KARs display a number of common characteristics not shared with NMDARs. AMPARs and KARs can form both homomers and heteromers that possess four glutamate binding sites. Gating of AMPARs and KARs does not require all four subunits to be bound to an agonist, allowing single-channel currents to show multiple conductance levels depending on LBD occupancy [106–108]. Gating transitions of AMPARs and KARs are also very fast compared to NMDARs. Channel deactivation occurs within 5–10 ms of agonist removal and desensitization generates a >90% decrease in current within 20 ms of channel opening in the continued presence of an agonist [75]. These rapid gating transitions allow AMPARs and KARs to mediate the time course of the fast component of synaptic transmission [109].

Channel Block of AMPAR and KAR is Regulated by Channel Gating

Channel block of AMPARs and KARs is remarkably similar and is primarily governed by RNA editing at the QRN site in the channel pore. While the exons for all AMPAR and KAR subunits code for an uncharged glutamine (Q) at this site, RNA for the GluA2, GluK1, and GluK2 subunits can be edited, resulting in a change from the conserved glutamine to a positively charged arginine (R; [110–112]). GluA2-lacking AMPARs and GluK1/2-lacking KARs, which contain the unedited Q at the QRN site, are permeable to calcium (Ca^{2+}) and are readily blocked by endogenous intracellular polyamines such as spermine [91,92,111,113–116]. However, incorporation of a single edited GluA2, GluK1, or GluK2 subunit into an AMPAR or KAR, i.e., a subunit with a positively charged R at the QRN site, abolishes Ca^{2+} permeability as well as polyamine block [113–115]. Interestingly, editing at the QRN site also controls inhibition of KARs by fatty acids, with only fully edited KARs displaying sensitivity to fatty acid inhibition [117]. Although fatty acid inhibition is only weakly voltage-dependent and may involve interactions with residues outside the pore [118], the involvement of the QRN site suggests a possible interaction within the pore. For the remainder of this section, we focus on AMPARs and KARs with Q at the QRN site of each subunit.

Polyamine block of iGluRs is strongly voltage-dependent and at least partially use-dependent [115,119,120]. Both AMPARs and KARs show birectifying responses in the presence of cytoplasmic polyamines [115], suggesting a common block mechanism. Recent cryo-electron microscopy (cryo-EM) structures of unedited GluA2(Q) receptors revealed the location and structure of the polyamine binding site in the pore [95,96]. Just below the QRN site lies a strongly electronegative portion of the channel, which likely contributes to both the cation selectivity of AMPARs [96] and the local membrane electric field [119,121,122]. Relief of polyamine block of AMPARs and KARs occurs via two separate mechanisms, i.e., permeation through the channel, which occurs at high positive voltages, and unblock to the cytoplasm, which occurs at negative voltages [115,123]. Polyamines are also trapping channel blockers and thus can only readily unbind when the channel is open [96,119]. Although trapping of polyamines seems counterintuitive, since they can unbind to either the intracellular or extracellular space, recent cryo-EM experiments provided compelling structural evidence of polyamine trapping. AMPAR structures produced by Twomey et al. suggested that closure of a gate near the extracellular entrance to the channel prevents polyamine permeation, while constriction of the selectivity filter prevents unbinding to the intracellular space by "pinching" the tail of the bound polyamine [96]. Thus, the gating state of AMPARs and KARs governs channel block by endogenous polyamines.

Effects of Auxiliary Proteins on Gating of AMPARs and KARs Modulates Block by Endogenous Polyamines

The interplay between gating and block of AMPARs and KARs is further regulated by the interaction of AMPARs and KARs with auxiliary proteins. Beginning with the discovery of the transmembrane AMPA

receptor regulatory protein (TARP) stargazin [124], a wealth of studies identifying and characterizing additional auxiliary proteins have greatly increased our understanding of AMPAR and KAR regulation. Auxiliary proteins play an integral role in the trafficking, synaptic targeting, and gating of non-NMDAR iGluRs [121,122,125–131], and several in-depth reviews have been written concerning their function [131–138].

Through their regulation of channel gating, auxiliary proteins necessarily regulate channel block of AMPARs and KARs. Many auxiliary proteins, including stargazin, cornichon-3, and members of the CKAMP/Shisa family, substantially augment AMPAR currents by slowing desensitization and increasing mean channel conductance [122,139–146]. Similarly, the KAR auxiliary proteins Neto1 and Neto2 increase KAR currents by decreasing desensitization and increasing peak P_{open} ([121,129–131], but see [128]). Interaction with auxiliary proteins that increase channel conductance and/or P_{open} greatly attenuates polyamine block of AMPARs and KARs. Increasing P_{open} reduces the time that the channel spends in closed states, which in turn reduces polyamine trapping and facilitates permeation. Indeed, association of AMPARs with stargazin or cornichon-3 and KARs with Neto1/2 greatly increases polyamine permeation [121,122]. Although increasing P_{open} would also be expected to allow polyamines to more readily access their binding sites, AMPAR-auxiliary protein interactions were surprisingly found to slow the onset of polyamine block at negative voltages [147]. The enhancement of blocker permeation at positive voltages and reduction onset of block at negative voltages combine to profoundly weaken polyamine block. Association of AMPARs with stargazin or cornichon-3 attenuates polyamine block by 3–15-fold [122,140,146,147], and KAR association with Neto1/2 reduces block by 8- to 20-fold [121,148]. In contrast, the AMPAR auxiliary protein GSG1L reduces channel conductance while increasing polyamine-dependent rectification [125]. The structural underpinnings of this intrinsic relation between polyamine block and the regulation of AMPAR and KAR gating by auxiliary proteins are yet to be elucidated. Possible explanations include auxiliary protein-induced stabilization of receptor open states [146,149], alteration of pore structure due to interactions of auxiliary subunits with the AMPAR/KAR TMD [96,138,144], or interactions between auxiliary protein C-terminal domains and AMPAR/KAR intracellular domains [140,148].

Effects of Polyamine Block on Gating Transitions of AMPARs and KARs

Although much is known about how channel gating regulates AMPAR and KAR blockade by polyamines, there is a dearth of knowledge about how polyamine occupancy of the channel affects AMPAR or KAR gating. To our knowledge, there are no reports of modulation of KAR gating by polyamine block. Polyamine block of AMPARs is known to contribute to frequency-dependent synaptic facilitation, but this effect appears unrelated to polyamine effects on gating. Instead, at negative potentials, repetitive stimulation of AMPARs can cause an increase in the rate of polyamine unblock without a concomitant increase in the rate of block [119,120,150]. However, there is some evidence that polyamine binding may stabilize or accelerate entry into AMPAR closed states [119]. The presence of trapped spermine in the channel of unedited GluA2(Q) receptors causes a delay in channel activation upon presentation of agonist, suggesting that spermine stabilizes a closed receptor state. Furthermore, kinetic models suggest that the observed acceleration of channel deactivation in the presence of spermine could be explained by a doubling of the rate of channel closure [119]. Acceleration of channel closure could potentially result from polyamines emptying and excluding other permeant ions from the pore, an effect observed in studies of voltage-gated potassium channel block [151]. Stabilization of a channel closed state by polyamines could also be due to allosteric modulation, a mechanism suggested for certain blockers of Cys-loop receptors [73]. Given the roles Ca^{2+}-permeable, non-NMDAR iGluRs play in both normal physiological and disease states [138,152–155], it is important to further our understanding of AMPAR and KAR block not only to better understand neuronal information processing, but also to aid in the design of more efficacious therapeutics.

Characteristics of NMDAR Channel Block

NMDARs display myriad biophysical properties unique amongst the iGluR family, including high Ca^{2+} permeability, slow gating kinetics, dependence on co-agonism for gating, and voltage-dependent block by magnesium (Mg^{2+}) ions [75,156–161]. These characteristics allow NMDARs to control the magnitude and timing of Ca^{2+} influx during synaptic activity and therefore play a pivotal role in synaptic development and plasticity [162–164]. NMDARs are obligate heterotetramers, typically composed of two GluN1 subunits (eight splice variants), which bind glycine or d-serine, and two GluN2 subunits (GluN2A–GluN2D), which bind glutamate. A third group of subunits, GluN3A/B, also bind glycine/d-serine (although d-serine acts only as a partial agonist [165]) and can assemble with GluN1 and GluN2 subunits to form NMDARs activated by glutamate and glycine/d-serine. Interestingly, GluN3 subunits can also assemble just with GluN1 subunits to form unconventional NMDARs activated solely by glycine/d-serine. However, these GluN1/3 receptors only pass weak currents in physiological conditions, so their role in neuronal function is largely unknown [165]. Conventional NMDARs consisting of two GluN1 subunits and two GluN2 subunits rely on the binding of both glutamate and glycine/d-serine for activation [156,166] and, unlike AMPARs and KARs, require all four agonist binding domains to be occupied for the channel to transition to the open state [167–169]. Additionally, conventional NMDARs possess a conserved asparagine at the QRN site (Figure 2C) that confers high Ca^{2+} permeability even relative to Ca^{2+}-permeable AMPAR and KARs, as well as sensitivity to block by Mg^{2+} [90,101,123].

Channel block of NMDARs has been extensively studied. Known, well-characterized NMDAR channel blockers with slow kinetics displayed some degree of use dependence. Another highly conserved key feature of NMDAR channel blockers is voltage dependence. Most NMDAR channel blockers are monovalent or divalent cations and display far greater inhibition at negative than at positive membrane potentials [12,13,15,17,170–173]. Due to their many roles in normal and pathological brain function, NMDARs are attractive targets for development of neurotherapeutics. NMDAR channel blockers are currently the most clinically useful NMDAR-targeting drugs and show great promise in the treatment of multiple nervous system disorders, including neurodegenerative diseases, major depressive disorder, and neuron death following ischemia [174–182].

NMDAR channel blockers display a strikingly diverse array of clinical effects, despite sharing overlapping binding sites and a similar general mechanism of inhibition ([99,183]; the putative blocking site for memantine is shown in Figure 2B,C). For example, the clinically relevant blockers memantine and ketamine share similar chemical properties (Table 1) and binding kinetics but possess vastly different effects on brain function. Ketamine is a drug of abuse and poorly tolerated, but possesses impressive efficacy in treating neuropathic pain and major depressive disorder [176,180,184,185]. On the other hand, memantine possesses weaker efficacy in treatment of neuropathic pain and little to no effect on major depressive disorder, but is well-tolerated with few side effects and shows efficacy in the treatment of neurodegenerative disorders such as Alzheimer's disease [177,179,186–190]. The striking diversity in the clinical effects of NMDAR channel blockers may in part arises from their diverse effects on channel gating. Nearly all known NMDAR channel blockers show some effect on channel gating [191] and channel blockers are found to modulate nearly every aspect of gating [3,7,8,12,13,17,173,192–200].

Sequential Blockers of NMDARs Prevent Channel Closure and Agonist Dissociation

The sequential/foot-in-door blockers 9-aminoacridine (Table 1), tetrapentylammonium, and the amantadine derivative IEM-1857 (synthesized at the Institute of Experimental Medicine (IEM), St. Petersburg, Russia) are thought to force NMDARs to remain in open states by sterically prohibiting gate closure after entering the channel [7,17,173,195,201]. Importantly, occupancy of the channel by IEM-1857,

tetrapentylammonium, or 9-aminoacridine also prevents agonist dissociation and channel desensitization [7,17,173], suggesting that blocker unbinding and subsequent channel closure are required for agonist dissociation. This finding is consistent with models of sequential channel block of nAChRs proposed by [19,20,66,67]. An experimental procedure used to test whether a channel blocker prevents channel closure and agonist dissociation is to determine if the blocker induces "tail currents". A tail current is a transient increase in receptor-mediated current observed upon rapid and simultaneous removal of blocker and agonist from the extracellular solution. If a blocker prevents channel closure, channels pass through the open, unblocked state following blocker unbinding, resulting in a tail current. However, any antagonist that unbinds more quickly than agonists can induce tail currents; thus, observation of tail currents does not provide unambiguous evidence that a blocker acts via a sequential mechanism. More powerful evidence that a blocker prevents channel closure can be provided by (a) observation that a blocker chops single-channel currents into "bursts" of brief openings, and that the total channel open time during bursts is independent of blocker concentration [20], and (b) observation that the blocker concentration that inhibits responses by 50% (the IC_{50}) is inversely proportional to the receptor's P_{open}, a prediction that can be tested, e.g., by recording the IC_{50} of a blocker over a range of agonist concentrations [191]. The finding that channel occupation by sequential blockers prevents agonist unbinding as well as channel closing provided fundamental information on state transitions of ligand-gated ion channels.

Table 1. NMDAR channel blockers and their effects on gating.

Compound	Structure	Type of Blocker	Effects on Gating
Magnesium		Unclear—due to fast unblocking kinetics, trapping of Mg^{2+} has not been directly demonstrated.	None [13,202].
9-aminoacridine		Sequential [7,201].	Stabilizes open state [7,201]. Prevents agonist dissociation [7,201].
IEM-1754		Depolarized potentials: sequential [173]. Strongly negative potentials: trapping [173].	Depolarized potentials: Stabilizes open state [173].
Amantadine		Partial trapping [12,13].	Accelerates channel closure of native NMDARs and GluN1/2B receptors [8].
Memantine		Partial trapping [8,16,197,203,204].	Slows GluN1/2A receptor recovery from Ca^{2+}-dependent desensitization [3].
Ketamine		Trapping [204].	Accelerates GluN1/2B receptor recovery from desensitization [3].

Magnesium is depicted coordinating six water molecules, and all organic blockers are depicted in bond-line format. Blockers structures are scaled to depict approximate relative sizes.

Organic channel blocking compounds were remarkably useful in determining the location of the channel gate itself. The size of a blocking molecule is a key determinant of whether the blocker prevents channel closure or is trapped in the channel upon gate closure. Experiments comparing block by IEM-1857 and the similar but smaller blocker IEM-1754 (Table 1) found that while binding of IEM-1857 prevented channel closure independent of voltage, IEM-1754 only prevented channel closure at relatively depolarized membrane potentials. At more hyperpolarized potentials, IEM-1754 is "pulled" by the membrane electric field deeper into the channel where it no longer prevents channel closure, instead acting as a trapping channel blocker [173]. The voltage dependence of IEM-1754 block, as well as its interactions with permeant ions, demonstrated that IEM-1754 has two blocking modes, one that associates with a shallower site and places the bulk of the molecule in the way of the gate, and a second that associates with a deeper site and permits closure of the gate [173,205,206]. This finding strongly supported the idea that the NMDAR channel gate lies at the extracellular entrance to the channel, an idea that was recently validated by crystal and cryo-EM structures of ligand-bound NMDARs [98,207].

Trapping Channel Blockers Modulate NMDAR State Transitions

Trapping channel blockers display more subtle effects on gating than sequential blockers. Early studies using a combination of patch-clamp electrophysiology and kinetic modeling concluded that the amino-adamantane derivatives memantine and amantadine and the phencyclidine derivative NEFA have clear effects on channel gating [12,192,193,197]. Initial proposals for the effects of amino-adamantane derivatives on NMDAR gating were wide-ranging, including models that suggested memantine and amantadine could stabilize open receptor states, as well as models that suggested memantine may stabilize closed receptor states [12,192,197]. It is possible that these discrepancies arose from the abilities of amino-adamantane derivatives to escape from some blocked channels after agonist removal (partial trapping) and to inhibit NMDARs via association with a site accessible in the absence of agonist [12,16,192,197,208,209].

Thorough evidence that amino-adamantane derivatives affect closed-state transitions came through investigation of the discrepancy between the equilibrium dissociation constant (K_d) and potency (represented by IC_{50}) of amantadine. The relation between K_d and IC_{50} depends directly on how a channel blocker affects channel transitions after binding. $K_d < IC_{50}$ implies that a blocker stabilizes channel open states. This is the case for sequential blockers, which inhibit less effectively as P_{open} decreases ($IC_{50} = K_d/P_{open}$, see Section 6.1; [5,191]). In contrast, $K_d > IC_{50}$ implies that a blocker's mechanism of inhibition likely involves stabilization of channel closed states, either through decreasing the rate of channel opening, increasing the rate of channel closure, or both. Such blockers therefore have two inhibitory actions: (1) blocking current flow through open channels and (2) stabilization of closed channels. Amantadine is an example of such a dual-mechanism channel inhibitor. Amantadine's K_d (110 μM) is considerably greater than its IC_{50} (~35 μM; [8,15,192,210]). Investigation of amantadine block of single-channel and whole-cell NMDAR current revealed that binding of amantadine not only accelerates channel closure, but that this acceleration of channel closure is actually the predominant mechanism of inhibition by amantadine at concentrations lower than 100 μM [8].

Recent studies reported additional drug-specific and NMDAR subtype-specific effects of channel blockers on gating transitions. Investigation of mechanisms by which memantine and ketamine preferentially target distinct populations of NMDARs led to the discovery that memantine and ketamine have differential, subtype-specific effects on NMDAR desensitization [3]. While ketamine accelerated recovery from desensitization of GluN1/2B receptors, memantine binding profoundly slowed recovery from desensitization of GluN1/2A receptors. The effect of memantine on GluN1/2A receptor desensitization was not observed in low-Ca^{2+} conditions, suggesting that memantine stabilizes a Ca^{2+}-dependent desensitized state of GluN1/2A receptors. A comparison of IC_{50} values measured in low and high Ca^{2+} conditions with K_d values predicted by a kinetic model found that in high Ca^{2+}, $K_d > IC_{50}$, whereas in low Ca^{2+}, $K_d \approx IC_{50}$, suggesting that memantine only alters GluN1/2A gating when Ca^{2+}-dependent desensitization can occur [3].

Visualization of NMDARs bound to trapping channel blockers was provided by recent structural studies. Song et al. crystalized the closed GluN1/2B channel in complex with the high affinity blocker MK-801 and utilized long-timescale molecular dynamics to investigate the mechanism of block by MK-801 and memantine [21]. Both blockers were found to bind within the central cavity of the ion channel and promote closure of the channel gate [21], perhaps via a mechanism similar to amantadine [8]. Although this result may seem to contrast with the previous finding that memantine did not affect GluN1/2B receptor desensitization [3], it is important to note that (1) memantine could affect GluN1/2B channel closure without affecting desensitization, and (2) the crystalized MK-801-NMDAR construct lacked both the ATD and CTD, which play key roles in gating and desensitization [98,211–215]. Stabilization of closed channels by NMDAR channel blockers could have profound physiological implications by effectively increasing the potency of blockers under certain conditions. For example, the ability of memantine to stabilize a Ca^{2+}-dependent desensitized state suggests a logical mechanism for neuroprotection: Preferential inhibition of

NMDARs in cellular populations subjected to pathological levels of Ca^{2+} influx, i.e., NMDARs likely to mediate excitotoxic cell death [79,216–218].

Channel Block by Mg^{2+} Does Not Appear to Affect NMDAR State Transitions

The majority of NMDAR channel blockers affect gating, but at least one blocker exists as an exception to this rule: Mg^{2+} (Table 1). Binding of Mg^{2+} to the NMDAR channel does not prevent gate closure, agonist dissociation, or desensitization [7,13,157,219]. Mg^{2+} boasts nearly equivalent K_d and IC_{50} values [202], further suggesting that Mg^{2+} occupancy of the channel has no effect on state transitions. The unusual ability of Mg^{2+} to block without altering gating could be due to its small size. A large conformational change in the extracellular region of the NMDAR channel is associated with gating, a conclusion supported by structural studies [98] and the observation that large organic blockers prevent channel closure. Although smaller organic blockers generally permit channel closure, stabilizing or destabilizing interactions with channel residues may alter channel gating. It is possible that the small size of Mg^{2+} (which is likely to be mostly dehydrated when blocking the channel [103]), coupled with its limited interactions with channel residues outside of the ion selectivity filter [103], allows binding in the NMDAR channel without affecting gating machinery. Also, in contrast to most organic blockers, Mg^{2+} has not been directly shown to act as a use-dependent open channel blocker or as a trapping blocker. Mg^{2+} displays extremely rapid binding and unbinding kinetics [157,219], preventing accurate determination in whole-cell recordings of the rapid component of block or unblock, measurements required for demonstration of use dependence and trapping. Kinetic modeling studies, however, suggested that Mg^{2+} does indeed act as an open channel blocker [13].

Despite the lack of effects of Mg^{2+} block on NMDAR gating, depolarization-induced Mg^{2+} unblock clearly depends on gating. Mg^{2+} unblock from GluN1/2A and GluN2B receptors displays a slow component as well as an extremely rapid component [220–225]. Although kinetic models in which Mg^{2+} block affects gating transitions and/or agonist binding rates reproduced slow Mg^{2+} unblock [222,224], substantial experimental evidence demonstrated that Mg^{2+} does not affect NMDAR state transitions [7,13,157,219]. This disagreement was reconciled by the discovery of the inherent (i.e., Mg^{2+}-independent) voltage-sensitivity of NMDAR gating, which underlies the slow component of Mg^{2+} unblock [221,225]. Thus, the interplay between Mg^{2+} block and NMDAR gating is unidirectional, whereby Mg^{2+} block depends on NMDAR gating, but NMDAR gating is unaffected by Mg^{2+} block.

Conclusions

Channel blockers are invaluable tools for the study of channel gating. The diverse array of effects that blockers exert on gating have facilitated numerous seminal discoveries into both the structure and the function of receptor channel gating machinery. The abilities to alter the rate of gating transitions and stabilize/destabilize channel states enable blockers to act as dual-mechanism drugs, both inhibiting current flow and modulating receptor function. The stabilization of specific receptor states also may contribute to the surprising diversity in the clinical effects of channel blockers. Future research determining the structural mechanisms by which channel blockers influence gating may aid in the directed design of more clinically efficacious neurotherapeutics.

Conflicts of Interest: The authors declare no conflict of interest.

References

1. Katz, B.; Thesleff, S. A study of the desensitization produced by acetylcholine at the motor end-plate. *J. Physiol. (Lond.)* **1957**, *138*, 63–80, doi:10.1113/jphysiol.1957.sp005838.
2. Mayer, M.L.; Westbrook, G.L. The action of N-methyl-D-aspartic acid on mouse spinal neurones in culture. *J. Physiol. (Lond.)* **1985**, *361*, 65–90, doi:10.1113/jphysiol.1985.sp015633.
3. Glasgow, N.G.; Povysheva, N.V.; Azofeifa, A.M.; Johnson, J.W. Memantine and ketamine differentially alter NMDA receptor desensitization. *J. Neurosci.* **2017**, *37*, 9686–9704, doi:10.1523/JNEUROSCI.1173-17.2017.
4. Legendre, P.; Rosenmund, C.; Westbrook, G.L. Inactivation of NMDA channels in cultured hippocampal neurons by intracellular calcium. *J. Neurosci.* **1993**, *13*, 674–684.
5. Hille, B. *Ion Channels of Excitable Membranes*, 3rd ed.; Sinauer Associates Is an Imprint of Oxford University Press: Sunderland, MA, USA, 2001.
6. Yuan, H.; Low, C.-M.; Moody, O.A.; Jenkins, A.; Traynelis, S.F. Ionotropic GABA and glutamate receptor mutations and human neurologic diseases. *Mol. Pharmacol.* **2015**, *88*, 203–217, doi:10.1124/mol.115.097998.
7. Benveniste, M.; Mayer, M.L. Trapping of glutamate and glycine during open channel block of rat hippocampal neuron NMDA receptors by 9-aminoacridine. *J. Physiol. (Lond.)* **1995**, *483 Pt 2*, 367–384, doi:10.1113/jphysiol.1995.sp020591.
8. Blanpied, T.A.; Clarke, R.J.; Johnson, J.W. Amantadine inhibits NMDA receptors by accelerating channel closure during channel block. *J. Neurosci.* **2005**, *25*, 3312–3322, doi:10.1523/JNEUROSCI.4262-04.2005.
9. Heidmann, T.; Changeux, J.P. Characterization of the transient agonist-triggered state of the acetylcholine receptor rapidly labeled by the noncompetitive blocker [3H]chlorpromazine: Additional evidence for the open channel conformation. *Biochemistry* **1986**, *25*, 6109–6113, doi:10.1021/bi00368a041.
10. Purohit, Y.; Grosman, C. Block of muscle nicotinic receptors by choline suggests that the activation and desensitization gates act as distinct molecular entities. *J. Gen. Physiol.* **2006**, *127*, 703–717, doi:10.1085/jgp.200509437.
11. Courtney, K.R. Mechanism of frequency-dependent inhibition of sodium currents in frog myelinated nerve by the lidocaine derivative GEA. *J. Pharmacol. Exp. Ther.* **1975**, *195*, 225–236.
12. Blanpied, T.A.; Boeckman, F.A.; Aizenman, E.; Johnson, J.W. Trapping channel block of NMDA-activated responses by amantadine and memantine. *J. Neurophysiol.* **1997**, *77*, 309–323, doi:10.1152/jn.1997.77.1.309.
13. Sobolevsky, A.I.; Yelshansky, M.V. The trapping block of NMDA receptor channels in acutely isolated rat hippocampal neurones. *J. Physiol. (Lond.)* **2000**, *526 Pt 3*, 493–506, doi:10.1111/j.1469-7793.2000.t01-2-00493.x.
14. Mealing, G.A.; Lanthorn, T.H.; Small, D.L.; Murray, R.J.; Mattes, K.C.; Comas, T.M; Morley P. Structural modifications to an N-methyl-D-aspartate receptor antagonist result in large differences in trapping block. *J. Pharmacol. Exp. Ther.* **2001**, *297*, 906–914.
15. Bolshakov, K.V.; Gmiro, V.E.; Tikhonov, D.B.; Magazanik, L.G. Determinants of trapping block of N-methyl-d-aspartate receptor channels. *J. Neurochem.* **2003**, *87*, 56–65, doi:10.1046/j.1471-4159.2003.01956.x.
16. Kotermanski, S.E.; Wood, J.T.; Johnson, J.W. Memantine binding to a superficial site on NMDA receptors contributes to partial trapping. *J. Physiol. (Lond.)* **2009**, *587*, 4589–4604, doi:10.1113/jphysiol.2009.176297.
17. Sobolevsky, A.I.; Koshelev, S.G.; Khodorov, B.I. Probing of NMDA channels with fast blockers. *J. Neurosci.* **1999**, *19*, 10611–10626.
18. Armstrong, C.M. Interaction of tetraethylammonium ion derivatives with the potassium channels of giant axons. *J. Gen. Physiol.* **1971**, *58*, 413–437, doi:10.1085/jgp.58.4.413.
19. Ruff, R.L. A quantitative analysis of local anaesthetic alteration of miniature end-plate currents and end-plate current fluctuations. *J. Physiol. (Lond.)* **1977**, *264*, 89–124, doi:10.1113/jphysiol.1977.sp011659.
20. Neher, E.; Steinbach, J.H. Local anaesthetics transiently block currents through single acetylcholine-receptor channels. *J. Physiol. (Lond.)* **1978**, *277*, 153–176, doi:10.1113/jphysiol.1978.sp012267.

21. Song, X.; Jensen, M.Ø.; Jogini, V.; Stein, R.A.; Lee, C.-H.; Mchaourab, H.S; Shaw D.E.; Gouaux E. Mechanism of NMDA receptor channel block by MK-801 and memantine. *Nature* **2018**, *556*, 515–519, doi:10.1038/s41586-018-0039-9.

22. Langley, J.N. On the reaction of cells and of nerve-endings to certain poisons, chiefly as regards the reaction of striated muscle to nicotine and to curari. *J. Physiol. (Lond.)* **1905**, *33*, 374–413, doi:10.1113/jphysiol.1905.sp001128.

23. Noda, M.; Takahashi, H.; Tanabe, T.; Toyosato, M.; Kikyotani, S.; Furutani, Y; Hirose T.; Takashima H.; Inayama S.; Miyata T.; Numa S. Structural homology of Torpedo californica acetylcholine receptor subunits. *Nature* **1983**, *302*, 528–532, doi:10.1038/302528a0.

24. Devillers-Thiery, A.; Giraudat, J.; Bentaboulet, M.; Changeux, J.P. Complete mRNA coding sequence of the acetylcholine binding alpha-subunit of Torpedo marmorata acetylcholine receptor: A model for the transmembrane organization of the polypeptide chain. *Proc. Natl. Acad. Sci. USA* **1983**, *80*, 2067–2071, doi:10.1073/pnas.80.7.2067.

25. Claudio, T.; Ballivet, M.; Patrick, J.; Heinemann, S. Nucleotide and deduced amino acid sequences of Torpedo californica acetylcholine receptor gamma subunit. *Proc. Natl. Acad. Sci. USA* **1983**, *80*, 1111–1115, doi:10.1073/pnas.80.4.1111.

26. Cartaud, J.; Benedetti, E.L.; Cohen, J.B.; Meunier, J.C.; Changeux, J.P. Presence of a lattice structure in membrane fragments rich in nicotinic receptor protein from the electric organ of Torpedo marmorata. *FEBS Lett.* **1973**, *33*, 109–113, doi:10.1016/0014-5793(73)80171-1.

27. Miledi, R.; Molinoff, P.; Potter, L.T. Isolation of the cholinergic receptor protein of Torpedo electric tissue. *Nature* **1971**, *229*, 554–557, doi:10.1038/229554a0.

28. Karlin, A.; Prives, J.; Deal, W.; Winnik, M. Affinity labeling of the acetylcholine receptor in the electroplax. *J. Mol. Biol.* **1971**, *61*, 175–188, doi:10.1016/0022-2836(71)90214-2.

29. Changeux, J.P.; Kasai, M.; Lee, C.Y. Use of a snake venom toxin to characterize the cholinergic receptor protein. *Proc. Natl. Acad. Sci. USA* **1970**, *67*, 1241–1247, doi:10.1073/pnas.67.3.1241.

30. Changeux, J.-P. The nicotinic acetylcholine receptor: The founding father of the pentameric ligand-gated ion channel superfamily. *J. Biol. Chem.* **2012**, *287*, 40207–40215, doi:10.1074/jbc.R112.407668.

31. Miyazawa, A.; Fujiyoshi, Y.; Unwin, N. Structure and gating mechanism of the acetylcholine receptor pore. *Nature* **2003**, *423*, 949–955, doi:10.1038/nature01748.

32. Colquhoun, D.; Hawkes, A.G. Relaxation and fluctuations of membrane currents that flow through drug-operated channels. *Proc. R. Soc. Lond. B Biol. Sci.* **1977**, *199*, 231–262, doi:10.1098/rspb.1977.0137.

33. Neher, E.; Sakmann, B. Single-channel currents recorded from membrane of denervated frog muscle fibres. *Nature* **1976**, *260*, 799–802, doi:10.1038/260799a0.

34. Hamill, O.P.; Marty, A.; Neher, E.; Sakmann, B.; Sigworth, F.J. Improved patch-clamp techniques for high-resolution current recording from cells and cell-free membrane patches. *Pflugers Arch.* **1981**, *391*, 85–100, doi:10.1007/BF00656997.

35. Caillé, S.; Guillem, K.; Cador, M.; Manzoni, O.; Georges, F. Voluntary nicotine consumption triggers in vivo potentiation of cortical excitatory drives to midbrain dopaminergic neurons. *J. Neurosci.* **2009**, *29*, 10410–10415, doi:10.1523/JNEUROSCI.2950-09.2009.

36. Mao, D.; Gallagher, K.; McGehee, D.S. Nicotine potentiation of excitatory inputs to ventral tegmental area dopamine neurons. *J. Neurosci.* **2011**, *31*, 6710–6720, doi:10.1523/JNEUROSCI.5671-10.2011.

37. Levin, E.D. Nicotinic receptor subtypes and cognitive function. *J. Neurobiol.* **2002**, *53*, 633–640, doi:10.1002/neu.10151.

38. Dani, J.A. Neuronal nicotinic acetylcholine receptor structure and function and response to nicotine. *Int. Rev. Neurobiol.* **2015**, *124*, 3–19, doi:10.1016/bs.irn.2015.07.001.

39. Ji, D.; Lape, R.; Dani, J.A. Timing and location of nicotinic activity enhances or depresses hippocampal synaptic plasticity. *Neuron* **2001**, *31*, 131–141, doi:10.1016/S0896-6273(01)00332-4.

40. McKay, B.E.; Placzek, A.N.; Dani, J.A. Regulation of synaptic transmission and plasticity by neuronal nicotinic acetylcholine receptors. *Biochem. Pharmacol.* **2007**, *74*, 1120–1133, doi:10.1016/j.bcp.2007.07.001.

41. Bertrand, S.; Weiland, S.; Berkovic, S.F.; Steinlein, O.K.; Bertrand, D. Properties of neuronal nicotinic acetylcholine receptor mutants from humans suffering from autosomal dominant nocturnal frontal lobe epilepsy. *Br. J. Pharmacol.* **1998**, *125*, 751–760, doi:10.1038/sj.bjp.0702154.

42. Vallés, A.S.; Borroni, M.V.; Barrantes, F.J. Targeting brain $\alpha 7$ nicotinic acetylcholine receptors in Alzheimer's disease: Rationale and current status. *CNS Drugs* **2014**, *28*, 975–987, doi:10.1007/s40263-014-0201-3.

43. Yakel, J.L. Cholinergic receptors: Functional role of nicotinic ACh receptors in brain circuits and disease. *Pflugers Arch.* **2013**, *465*, 441–450, doi:10.1007/s00424-012-1200-1.

44. Martínez-Hernández, R.; Bernal, S.; Also-Rallo, E.; Alías, L.; Barceló, M.J.; Hereu, M; Esquerda J.E.; Tizzano E.F. Synaptic defects in type I spinal muscular atrophy in human development. *J. Pathol.* **2013**, *229*, 49–61, doi:10.1002/path.4080.

45. Steinlein, O.K.; Bertrand, D. Neuronal nicotinic acetylcholine receptors: From the genetic analysis to neurological diseases. *Biochem. Pharmacol.* **2008**, *76*, 1175–1183, doi:10.1016/j.bcp.2008.07.012.

46. Leonard, S.; Mexal, S.; Freedman, R. Smoking, genetics and schizophrenia: Evidence for self medication. *J. Dual Diagn.* **2007**, *3*, 43–59, doi:10.1300/J374v03n03_05.

47. Lindstrom, J. Autoimmune diseases involving nicotinic receptors, *J. Neurobiol.* **2002**, *53*, 656–665, doi:10.1002/neu.10106.

48. Tarr, T.B.; Malick, W.; Liang, M.; Valdomir, G.; Frasso, M.; Lacomis, D; Reddel S.W.; Garcia-Ocano A.; Wipf P.; Meriney S.D. Evaluation of a novel calcium channel agonist for therapeutic potential in Lambert-Eaton myasthenic syndrome. *J. Neurosci.* **2013**, *33*, 10559–10567, doi:10.1523/JNEUROSCI.4629-12.2013.

49. Tarr, T.B.; Wipf, P.; Meriney, S.D. Synaptic Pathophysiology and Treatment of Lambert-Eaton Myasthenic Syndrome. *Mol. Neurobiol.* **2015**, *52*, 456–463, doi:10.1007/s12035-014-8887-2.

50. Thompson, A.J.; Lester, H.A.; Lummis, S.C.R. The structural basis of function in Cys-loop receptors. *Q. Rev. Biophys.* **2010**, *43*, 449–499, doi:10.1017/S0033583510000168.

51. Séguéla, P.; Wadiche, J.; Dineley-Miller, K.; Dani, J.A.; Patrick, J.W. Molecular cloning, functional properties, and distribution of rat brain alpha 7: A nicotinic cation channel highly permeable to calcium. *J. Neurosci.* **1993**, *13*, 596–604.

52. Cooper, E.; Couturier, S.; Ballivet, M. Pentameric structure and subunit stoichiometry of a neuronal nicotinic acetylcholine receptor. *Nature* **1991**, *350*, 235–238, doi:10.1038/350235a0.

53. Wada, E.; Wada, K.; Boulter, J.; Deneris, E.; Heinemann, S.; Patrick, J; Swanson L.W.. Distribution of alpha 2, alpha 3, alpha 4, and beta 2 neuronal nicotinic receptor subunit mRNAs in the central nervous system: A hybridization histochemical study in the rat. *J. Comp. Neurol.* **1989**, *284*, 314–335, doi:10.1002/cne.902840212.

54. Palma, E.; Bertrand, S.; Binzoni, T.; Bertrand, D. Neuronal nicotinic alpha 7 receptor expressed in Xenopus oocytes presents five putative binding sites for methyllycaconitine. *J. Physiol. (Lond.)* **1996**, *491 Pt 1*, 151–161, doi:10.1113/jphysiol.1996.sp021203.

55. Taly, A.; Corringer, P.-J.; Guedin, D.; Lestage, P.; Changeux, J.-P. Nicotinic receptors: Allosteric transitions and therapeutic targets in the nervous system. *Nat. Rev. Drug Discov.* **2009**, *8*, 733–750, doi:10.1038/nrd2927.

56. Fasoli, F.; Gotti, C. Structure of neuronal nicotinic receptors. *Curr. Top. Behav. Neurosci.* **2015**, *23*, 1–17, doi:10.1007/978-3-319-13665-3_1.

57. Vernino, S.; Amador, M.; Luetje, C.W.; Patrick, J.; Dani, J.A. Calcium modulation and high calcium permeability of neuronal nicotinic acetylcholine receptors. *Neuron* **1992**, *8*, 127–134, doi:10.1016/0896-6273(92)90114-s.

58. Dani, J.A.; Eisenman, G. Monovalent and divalent cation permeation in acetylcholine receptor channels. Ion transport related to structure. *J. Gen. Physiol.* **1987**, *89*, 959–983, doi:10.1085/jgp.89.6.959.

59. Auerbach, A. Agonist activation of a nicotinic acetylcholine receptor. *Neuropharmacology* **2015**, *96*, 150–156, doi:10.1016/j.neuropharm.2014.10.004.

60. Dale, H. Chemical transmission of the effects of nerve impulses. *Br. Med. J.* **1934**, *1*, 835–841, doi:10.1136/bmj.1.3827.835.

61. Chang, C.C.; Lee, C.Y. Isolation of neurotoxins from the venom of bungarus multicinctus and their modes of neuromuscular blocking action. *Arch. Int. Pharm. Ther.* **1963**, *144*, 241–257.

62. Löscher, W.; Rogawski, M.A. How theories evolved concerning the mechanism of action of barbiturates. *Epilepsia* **2012**, *53* (Suppl. 8), 12–25, doi:10.1111/epi.12025.

63. Steinbach, A.B. Alteration by xylocaine (lidocaine) and its derivatives of the time course of the end plate potential. *J. Gen. Physiol.* **1968**, *52*, 144–161, doi:10.1085/jgp.52.1.144.

64. Steinbach, A.B. A kinetic model for the action of xylocaine on receptors for acetylcholine. *J. Gen. Physiol.* **1968**, *52*, 162–180, doi:10.1085/jgp.52.1.162.

65. Adams, P.R. Voltage jump analysis of procaine action at frog end-plate. *J. Physiol. (Lond.)* **1977**, *268*, 291–318, doi:10.1113/jphysiol.1977.sp011858.

66. Adams, P.R. Drug blockade of open end-plate channels. *J. Physiol. (Lond.)* **1976**, *260*, 531–552, doi:10.1113/jphysiol.1976.sp011530.

67. Adams, P.R. A model for the procaine end-plate current. *J. Physiol. (Lond.)* 1975, 246, 61P–63P.

68. Auerbach, A.; Akk, G. Desensitization of mouse nicotinic acetylcholine receptor channels. A two-gate mechanism. *J. Gen. Physiol.* **1998**, *112*, 181–197, doi:10.1085/jgp.112.2.181.

69. Lape, R.; Krashia, P.; Colquhoun, D.; Sivilotti, L.G. Agonist and blocking actions of choline and tetramethylammonium on human muscle acetylcholine receptors. *J. Physiol. (Lond.)* **2009**, *587*, 5045–5072, doi:10.1113/jphysiol.2009.176305.

70. Chiara, D.C.; Hamouda, A.K.; Ziebell, M.R.; Mejia, L.A.; Garcia, G.; Cohen, J.B. [(3)H]chlorpromazine photolabeling of the torpedo nicotinic acetylcholine receptor identifies two state-dependent binding sites in the ion channel. *Biochemistry* **2009**, *48*, 10066–10077, doi:10.1021/bi901271w.

71. Giraudat, J.; Dennis, M.; Heidmann, T.; Chang, J.Y.; Changeux, J.P. Structure of the high-affinity binding site for noncompetitive blockers of the acetylcholine receptor: Serine-262 of the delta subunit is labeled by [3H]chlorpromazine. *Proc. Natl. Acad. Sci. USA* **1986**, *83*, 2719–2723, doi:10.1073/pnas.83.8.2719.

72. Revah, F.; Galzi, J.L.; Giraudat, J.; Haumont, P.Y.; Lederer, F.; Changeux, J.P. The noncompetitive blocker [3H]chlorpromazine labels three amino acids of the acetylcholine receptor gamma subunit: Implications for the alpha-helical organization of regions MII and for the structure of the ion channel. *Proc. Natl. Acad. Sci. USA* **1990**, *87*, 4675–4679, doi:10.1073/pnas.87.12.4675.

73. Gielen, M.; Corringer, P.-J. The dual-gate model for pentameric ligand-gated ion channels activation and desensitization. *J. Physiol. (Lond.)* **2018**, *596*, 1873–1902, doi:10.1113/JP275100.

74. Paoletti, P.; Bellone, C.; Zhou, Q. NMDA receptor subunit diversity: Impact on receptor properties, synaptic plasticity and disease. *Nat. Rev. Neurosci.* **2013**, *14*, 383–400, doi:10.1038/nrn3504.

75. Traynelis, S.F.; Wollmuth, L.P.; McBain, C.J.; Menniti, F.S.; Vance, K.M.; Ogden, K.K; Hansen K.B.; Yuan H.; Myers S.J.; Dingledine R. Glutamate receptor ion channels: Structure, regulation, and function. *Pharmacol. Rev.* **2010**, *62*, 405–496, doi:10.1124/pr.109.002451.

76. Burnashev, N.; Szepetowski, P. NMDA receptor subunit mutations in neurodevelopmental disorders. *Curr. Opin. Pharmacol.* **2015**, *20*, 73–82, doi:10.1016/j.coph.2014.11.008.

77. Salpietro, V.; Dixon, C.L.; Guo, H.; Bello, O.D.; Vandrovcova, J.; Efthymiou, S.; Maroofian R.; Heimer G.; Burglen L.; Valence S.; et al. AMPA receptor GluA2 subunit defects are a cause of neurodevelopmental disorders. *Nat. Commun.* **2019**, *10*, 3094, doi:10.1038/s41467-019-10910-w.

78. Lee, E.-J.; Choi, S.Y.; Kim, E. NMDA receptor dysfunction in autism spectrum disorders. *Curr. Opin. Pharmacol.* **2015**, *20*, 8–13, doi:10.1016/j.coph.2014.10.007.

79. Zorumski, C.F.; Olney, J.W. Excitotoxic neuronal damage and neuropsychiatric disorders. *Pharmacol. Ther.* **1993**, *59*, 145–162.

80. Lau, C.G.; Zukin, R.S. NMDA receptor trafficking in synaptic plasticity and neuropsychiatric disorders. *Nat. Rev. Neurosci.* **2007**, *8*, 413–426, doi:10.1038/nrn2153.

81. Javitt, D.C. Glutamate as a therapeutic target in psychiatric disorders. *Mol. Psychiatry* **2004**, *9*, 984–997, 979, doi:10.1038/sj.mp.4001551.

82. Bowie, D. Ionotropic glutamate receptors & CNS disorders. *CNS Neurol. Disord. Drug Targets* **2008**, *7*, 129–143.

83. Benamer, N.; Marti, F.; Lujan, R.; Hepp, R.; Aubier, T.G.; Dupin, A.A.M; Frébourg G.; Pons S.; Maskos U.; Faure P.; et al. GluD1, linked to schizophrenia, controls the burst firing of dopamine neurons. *Mol. Psychiatry* **2018**, *23*, 691–700, doi:10.1038/mp.2017.137.

84. Ady, V.; Perroy, J.; Tricoire, L.; Piochon, C.; Dadak, S.; Chen, X.; Dusart I.; Fagni L.; Lambolez B.; Levenes C. Type 1 metabotropic glutamate receptors (mGlu1) trigger the gating of GluD2 delta glutamate receptors. *EMBO Rep.* **2014**, *15*, 103–109, doi:10.1002/embr.201337371.

85. Gantz, S.C.; Moussawi, K.; Hake, H.S. Delta glutamate receptor conductance drives excitation of mouse dorsal raphe neurons. *eLife* **2020**, *9*, e56054, doi:10.7554/eLife.56054.

86. Araki, K.; Meguro, H.; Kushiya, E.; Takayama, C.; Inoue, Y.; Mishina, M. Selective expression of the glutamate receptor channel delta 2 subunit in cerebellar Purkinje cells. *Biochem. Biophys. Res. Commun.* **1993**, *197*, 1267–1276, doi:10.1006/bbrc.1993.2614.

87. Lomeli, H.; Sprengel, R.; Laurie, D.J.; Köhr, G.; Herb, A.; Seeburg, P.H; Wisden W. The rat delta-1 and delta-2 subunits extend the excitatory amino acid receptor family. *FEBS Lett.* **1993**, *315*, 318–322, doi:10.1016/0014-5793(93)81186-4.

88. Yamazaki, M.; Araki, K.; Shibata, A.; Mishina, M. Molecular cloning of a cDNA encoding a novel member of the mouse glutamate receptor channel family. *Biochem. Biophys. Res. Commun.* **1992**, *183*, 886–892, doi:10.1016/0006-291x(92)90566-4.

89. Orth, A.; Tapken, D.; Hollmann, M. The delta subfamily of glutamate receptors: Characterization of receptor chimeras and mutants. *Eur. J. Neurosci.* **2013**, *37*, 1620–1630, doi:10.1111/ejn.12193.

90. Premkumar, L.S.; Auerbach, A. Identification of a high affinity divalent cation binding site near the entrance of the NMDA receptor channel. *Neuron* **1996**, *16*, 869–880, doi:10.1016/s0896-6273(00)80107-5.

91. Hume, R.I.; Dingledine, R.; Heinemann, S.F. Identification of a site in glutamate receptor subunits that controls calcium permeability. *Science* **1991**, *253*, 1028–1031, doi:10.1126/science.1653450.

92. Sommer, B.; Köhler, M.; Sprengel, R.; Seeburg, P.H. RNA editing in brain controls a determinant of ion flow in glutamate-gated channels. *Cell* **1991**, *67*, 11–19, doi:10.1016/0092-8674(91)90568-j.

93. Burnashev, N.; Schoepfer, R.; Monyer, H.; Ruppersberg, J.P.; Günther, W.; Seeburg, P.H; Sakmann B. Control by asparagine residues of calcium permeability and magnesium blockade in the NMDA receptor. *Science* **1992**, *257*, 1415–1419, doi:10.1126/science.1382314.

94. Twomey, E.C.; Yelshanskaya, M.V.; Grassucci, R.A.; Frank, J.; Sobolevsky, A.I. Channel opening and gating mechanism in AMPA-subtype glutamate receptors. *Nature* **2017**, *549*, 60–65, doi:10.1038/nature23479.

95. Twomey, E.C.; Sobolevsky, A.I. Structural mechanisms of gating in ionotropic glutamate receptors. *Biochemistry* **2018**, *57*, 267–276, doi:10.1021/acs.biochem.7b00891.

96. Twomey, E.C.; Yelshanskaya, M.V.; Vassilevski, A.A.; Sobolevsky, A.I. Mechanisms of Channel Block in Calcium-Permeable AMPA Receptors. *Neuron* **2018**, *99*, 956–968.e4, doi:10.1016/j.neuron.2018.07.027.

97. Nakagawa, T. Structures of the AMPA receptor in complex with its auxiliary subunit cornichon. *Science* **2019**, *366*, 1259–1263, doi:10.1126/science.aay2783.

98. Chou, T.-H.; Tajima, N.; Romero-Hernandez, A.; Furukawa, H. Structural basis of functional transitions in mammalian NMDA receptors. *Cell* **2020**, *182*, 357–371.e13, doi:10.1016/j.cell.2020.05.052.

99. Ferrer-Montiel, A.V.; Merino, J.M.; Planells-Cases, R.; Sun, W.; Montal, M. Structural determinants of the blocker binding site in glutamate and NMDA receptor channels. *Neuropharmacology* **1998**, *37*, 139–147, doi:10.1016/S0028-3908(98)00007-0.

100. Fedele, L.; Newcombe, J.; Topf, M.; Gibb, A.; Harvey, R.J.; Smart, T.G. Disease-associated missense mutations in GluN2B subunit alter NMDA receptor ligand binding and ion channel properties. *Nat. Commun.* **2018**, *9*, 957, doi:10.1038/s41467-018-02927-4.

101. Mori, H.; Masaki, H.; Yamakura, T.; Mishina, M. Identification by mutagenesis of a Mg(2+)-block site of the NMDA receptor channel. *Nature* **1992**, *358*, 673–675, doi:10.1038/358673a0.

102. Lemke, J.R.; Hendrickx, R.; Geider, K.; Laube, B.; Schwake, M.; Harvey, R.J; James V.M.; Pepler A.; Steiner I.; Hörtnagel K.; et al. GRIN2B mutations in West syndrome and intellectual disability with focal epilepsy. *Ann. Neurol.* **2014**, *75*, 147–154, doi:10.1002/ana.24073.

103. Mesbahi-Vasey, S.; Veras, L.; Yonkunas, M.; Johnson, J.W.; Kurnikova, M.G. All atom NMDA receptor transmembrane domain model development and simulations in lipid bilayers and water. *PLoS ONE* **2017**, *12*, e0177686, doi:10.1371/journal.pone.0177686.

104. Trott, O.; Olson, A.J. AutoDock Vina: Improving the speed and accuracy of docking with a new scoring function, efficient optimization, and multithreading. *J. Comput. Chem.* **2010**, *31*, 455–461, doi:10.1002/jcc.21334.

105. Humphrey, W.; Dalke, A.; Schulten, K. VMD: Visual molecular dynamics. *J. Mol. Graph.* **1996**, *14*, 33–38, 27, doi:10.1016/0263-7855(96)00018-5.

106. Smith, T.C.; Howe, J.R. Concentration-dependent substate behavior of native AMPA receptors. *Nat. Neurosci.* **2000**, *3*, 992–997, doi:10.1038/79931.

107. Jin, R.; Banke, T.G.; Mayer, M.L.; Traynelis, S.F.; Gouaux, E. Structural basis for partial agonist action at ionotropic glutamate receptors. *Nat. Neurosci.* **2003**, *6*, 803–810, doi:10.1038/nn1091.

108. Rosenmund, C.; Stern-Bach, Y.; Stevens, C.F. The tetrameric structure of a glutamate receptor channel. *Science* **1998**, *280*, 1596–1599, doi:10.1126/science.280.5369.1596.

109. Trussell, L.O.; Fischbach, G.D. Glutamate receptor desensitization and its role in synaptic transmission. *Neuron* **1989**, *3*, 209–218, doi:10.1016/0896-6273(89)90034-2.

110. Higuchi, M.; Single, F.N.; Köhler, M.; Sommer, B.; Sprengel, R.; Seeburg, P.H. RNA editing of AMPA receptor subunit GluR-B: A base-paired intron-exon structure determines position and efficiency. *Cell* **1993**, *75*, 1361–1370, doi:10.1016/0092-8674(93)90622-w.

111. Rosenthal, J.J.C.; Seeburg, P.H. A-to-I RNA editing: Effects on proteins key to neural excitability. *Neuron* **2012**, *74*, 432–439, doi:10.1016/j.neuron.2012.04.010.

112. Melcher, T.; Maas, S.; Higuchi, M.; Keller, W.; Seeburg, P.H. Editing of alpha-amino-3-hydroxy-5-methylisoxazole-4-propionic acid receptor GluR-B pre-mRNA in vitro reveals site-selective adenosine to inosine conversion. *J. Biol. Chem.* **1995**, *270*, 8566–8570, doi:10.1074/jbc.270.15.8566.

113. Hollmann, M.; Hartley, M.; Heinemann, S. Ca²⁺ permeability of KA-AMPA—Gated glutamate receptor channels depends on subunit composition. *Science* **1991**, *252*, 851–853, doi:10.1126/science.1709304.

114. Burnashev, N.; Monyer, H.; Seeburg, P.H.; Sakmann, B. Divalent ion permeability of AMPA receptor channels is dominated by the edited form of a single subunit. *Neuron* **1992**, *8*, 189–198, doi:10.1016/0896-6273(92)90120-3.

115. Bowie, D.; Mayer, M.L. Inward rectification of both AMPA and kainate subtype glutamate receptors generated by polyamine-mediated ion channel block. *Neuron* **1995**, *15*, 453–462, doi:10.1016/0896-6273(95)90049-7.

116. Kamboj, S.K.; Swanson, G.T.; Cull-Candy, S.G. Intracellular spermine confers rectification on rat calcium-permeable AMPA and kainate receptors. *J. Physiol. (Lond.)* **1995**, *486 Pt 2*, 297–303, doi:10.1113/jphysiol.1995.sp020812.

117. Wilding, T.J.; Zhou, Y.; Huettner, J.E. Q/R site editing controls kainate receptor inhibition by membrane fatty acids. *J. Neurosci.* **2005**, *25*, 9470–9478, doi:10.1523/JNEUROSCI.2826-05.2005.

118. Wilding, T.J.; Chen, K.; Huettner, J.E. Fatty acid modulation and polyamine block of GluK2 kainate receptors analyzed by scanning mutagenesis. *J. Gen. Physiol.* **2010**, *136*, 339–352, doi:10.1085/jgp.201010442.

119. Bowie, D.; Lange, G.D.; Mayer, M.L. Activity-dependent modulation of glutamate receptors by polyamines. *J. Neurosci.* **1998**, *18*, 8175–8185.

120. Rozov, A.; Zilberter, Y.; Wollmuth, L.P.; Burnashev, N. Facilitation of currents through rat Ca²⁺-permeable AMPA receptor channels by activity-dependent relief from polyamine block. *J. Physiol. (Lond.)* **1998**, *511 Pt 2*, 361–377, doi:10.1111/j.1469-7793.1998.361bh.x.

121. Brown, P.M.G.E.; Aurousseau, M.R.P.; Musgaard, M.; Biggin, P.C.; Bowie, D. Kainate receptor pore-forming and auxiliary subunits regulate channel block by a novel mechanism. *J. Physiol. (Lond.)* **2016**, *594*, 1821–1840, doi:10.1113/JP271690.

122. Brown, P.M.G.E.; McGuire, H.; Bowie, D. Stargazin and cornichon-3 relieve polyamine block of AMPA receptors by enhancing blocker permeation. *J. Gen. Physiol.* **2018**, *150*, 67–82, doi:10.1085/jgp.201711895.

123. Burnashev, N.; Zhou, Z.; Neher, E.; Sakmann, B. Fractional calcium currents through recombinant GluR channels of the NMDA, AMPA and kainate receptor subtypes. *J. Physiol. (Lond.)* **1995**, *485 Pt 2*, 403–418, doi:10.1113/jphysiol.1995.sp020738.

124. Chen, L.; Chetkovich, D.M.; Petralia, R.S.; Sweeney, N.T.; Kawasaki, Y.; Wenthold, R.J; Bredt D.S.; Nicoll R.A. Stargazin regulates synaptic targeting of AMPA receptors by two distinct mechanisms. *Nature* **2000**, *408*, 936–943, doi:10.1038/35050030.

125. McGee, T.P.; Bats, C.; Farrant, M.; Cull-Candy, S.G. Auxiliary Subunit GSG1L Acts to Suppress Calcium-Permeable AMPA Receptor Function. *J. Neurosci.* **2015**, *35*, 16171–16179, doi:10.1523/JNEUROSCI.2152-15.2015.

126. Wang, R.; Walker, C.S.; Brockie, P.J.; Francis, M.M.; Mellem, J.E.; Madsen, D.M; Maricq A.V. Evolutionary conserved role for TARPs in the gating of glutamate receptors and tuning of synaptic function. *Neuron* **2008**, *59*, 997–1008, doi:10.1016/j.neuron.2008.07.023.

127. Zhang, W.; St-Gelais, F.; Grabner, C.P.; Trinidad, J.C.; Sumioka, A.; Morimoto-Tomita, M.; Kim K.S.; Straub C.; Burlingame A.L.; Howe J.R.; et al. A transmembrane accessory subunit that modulates kainate-type glutamate receptors. *Neuron* **2009**, *61*, 385–396, doi:10.1016/j.neuron.2008.12.014.

128. Copits, B.A.; Robbins, J.S.; Frausto, S.; Swanson, G.T. Synaptic targeting and functional modulation of GluK1 kainate receptors by the auxiliary neuropilin and tolloid-like (NETO) proteins. *J. Neurosci.* **2011**, *31*, 7334–7340, doi:10.1523/JNEUROSCI.0100-11.2011.

129. Straub, C.; Hunt, D.L.; Yamasaki, M.; Kim, K.S.; Watanabe, M.; Castillo, P.E; Tomita S. Distinct functions of kainate receptors in the brain are determined by the auxiliary subunit Neto1. *Nat. Neurosci.* **2011**, *14*, 866–873, doi:10.1038/nn.2837.

130. Tang, M.; Pelkey, K.A.; Ng, D.; Ivakine, E.; McBain, C.J.; Salter, M.W; McInnes R.R. Neto1 is an auxiliary subunit of native synaptic kainate receptors. *J. Neurosci.* **2011**, *31*, 10009–10018, doi:10.1523/JNEUROSCI.6617-10.2011.

131. Tomita, S.; Castillo, P.E. Neto1 and Neto2: Auxiliary subunits that determine key properties of native kainate receptors. *J. Physiol. (Lond.)* **2012**, *590*, 2217–2223, doi:10.1113/jphysiol.2011.221101.

132. Jackson, A.C.; Nicoll, R.A. The expanding social network of ionotropic glutamate receptors: TARPs and other transmembrane auxiliary subunits. *Neuron* **2011**, *70*, 178–199, doi:10.1016/j.neuron.2011.04.007.

133. Haering, S.C.; Tapken, D.; Pahl, S.; Hollmann, M. Auxiliary subunits: Shepherding AMPA receptors to the plasma membrane. *Membranes* **2014**, *4*, 469–490, doi:10.3390/membranes4030469.

134. Greger, I.H.; Watson, J.F.; Cull-Candy, S.G. Structural and Functional Architecture of AMPA-Type Glutamate Receptors and Their Auxiliary Proteins. *Neuron* **2017**, *94*, 713–730, doi:10.1016/j.neuron.2017.04.009.

135. Howe, J.R. Modulation of non-NMDA receptor gating by auxiliary subunits. *J. Physiol. (Lond.)* **2015**, *593*, 61–72, doi:10.1113/jphysiol.2014.273904.

136. Copits, B.A.; Swanson, G.T. Dancing partners at the synapse: Auxiliary subunits that shape kainate receptor function. *Nat. Rev. Neurosci.* **2012**, *13*, 675–686, doi:10.1038/nrn3335.

137. Bissen, D.; Foss, F.; Acker-Palmer, A. AMPA receptors and their minions: Auxiliary proteins in AMPA receptor trafficking. *Cell Mol. Life Sci.* **2019**, *76*, 2133–2169, doi:10.1007/s00018-019-03068-7.

138. Bowie, D. Polyamine-mediated channel block of ionotropic glutamate receptors and its regulation by auxiliary proteins. *J. Biol. Chem.* **2018**, *293*, 18789–18802, doi:10.1074/jbc.TM118.003794.

139. Klaassen, R.V.; Stroeder, J.; Coussen, F.; Hafner, A.-S.; Petersen, J.D.; Renancio, C.; Schmitz L.J.; Normand E.; Lodder J.C.; Rotaru D.C.; et al. Shisa6 traps AMPA receptors at postsynaptic sites and prevents their desensitization during synaptic activity. *Nat. Commun.* **2016**, *7*, 10682, doi:10.1038/ncomms10682.

140. Soto, D.; Coombs, I.D.; Gratacòs-Batlle, E.; Farrant, M.; Cull-Candy, S.G. Molecular mechanisms contributing to TARP regulation of channel conductance and polyamine block of calcium-permeable AMPA receptors. *J. Neurosci.* **2014**, *34*, 11673–11683, doi:10.1523/JNEUROSCI.0383-14.2014.

141. Ben-Yaacov, A.; Gillor, M.; Haham, T.; Parsai, A.; Qneibi, M.; Stern-Bach, Y. Molecular mechanism of AMPA receptor modulation by tarp/stargazin. *Neuron* **2017**, *93*, 1126–1137.e4, doi:10.1016/j.neuron.2017.01.032.

142. Coombs, I.D.; Soto, D.; Zonouzi, M.; Renzi, M.; Shelley, C.; Farrant, M.; Cull-Candy, S.G. Cornichons modify channel properties of recombinant and glial AMPA receptors. *J. Neurosci.* **2012**, *32*, 9796–9804, doi:10.1523/JNEUROSCI.0345-12.2012.

143. Coombs, I.D.; MacLean, D.M.; Jayaraman, V.; Farrant, M.; Cull-Candy, S.G. Dual Effects of TARP γ-2 on Glutamate Efficacy Can Account for AMPA Receptor Autoinactivation. *Cell Rep.* **2017**, *20*, 1123–1135, doi:10.1016/j.celrep.2017.07.014.

144. Chen, S.; Zhao, Y.; Wang, Y.; Shekhar, M.; Tajkhorshid, E.; Gouaux, E. Activation and Desensitization Mechanism of AMPA Receptor-TARP Complex by Cryo-EM. *Cell* **2017**, *170*, 1234–1246.e14, doi:10.1016/j.cell.2017.07.045.

145. Twomey, E.C.; Yelshanskaya, M.V.; Grassucci, R.A.; Frank, J.; Sobolevsky, A.I. Elucidation of AMPA receptor-stargazin complexes by cryo-electron microscopy. *Science* **2016**, *353*, 83–86, doi:10.1126/science.aaf8411.

146. Jackson, A.C.; Milstein, A.D.; Soto, D.; Farrant, M.; Cull-Candy, S.G.; Nicoll, R.A. Probing TARP modulation of AMPA receptor conductance with polyamine toxins. *J. Neurosci.* **2011**, *31*, 7511–7520, doi:10.1523/JNEUROSCI.6688-10.2011.

147. Soto, D.; Coombs, I.D.; Kelly, L.; Farrant, M.; Cull-Candy, S.G. Stargazin attenuates intracellular polyamine block of calcium-permeable AMPA receptors. *Nat. Neurosci.* **2007**, *10*, 1260–1267, doi:10.1038/nn1966.

148. Fisher, J.L.; Mott, D.D. The auxiliary subunits Neto1 and Neto2 reduce voltage-dependent inhibition of recombinant kainate receptors. *J. Neurosci.* **2012**, *32*, 12928–12933, doi:10.1523/JNEUROSCI.2211-12.2012.

149. Shelley, C.; Farrant, M.; Cull-Candy, S.G. TARP-associated AMPA receptors display an increased maximum channel conductance and multiple kinetically distinct open states. *J. Physiol. (Lond.)* **2012**, *590*, 5723–5738, doi:10.1113/jphysiol.2012.238006.

150. Rozov, A.; Zakharova, Y.; Vazetdinova, A.; Valiullina-Rakhmatullina, F. The Role of Polyamine-Dependent Facilitation of Calcium Permeable AMPARs in Short-Term Synaptic Enhancement. *Front. Cell Neurosci.* **2018**, *12*, 345, doi:10.3389/fncel.2018.00345.

151. Baukrowitz, T.; Yellen, G. Use-dependent blockers and exit rate of the last ion from the multi-ion pore of a K+ channel. *Science* **1996**, *271*, 653–656, doi:10.1126/science.271.5249.653.

152. Weiss, J.H. Ca permeable AMPA channels in diseases of the nervous system. *Front. Mol. Neurosci.* **2011**, *4*, 42, doi:10.3389/fnmol.2011.00042.

153. Wright, A.; Vissel, B. The essential role of AMPA receptor GluR2 subunit RNA editing in the normal and diseased brain. *Front. Mol. Neurosci.* **2012**, *5*, 34, doi:10.3389/fnmol.2012.00034.

154. Lerma, J.; Marques, J.M. Kainate receptors in health and disease. *Neuron* **2013**, *80*, 292–311, doi:10.1016/j.neuron.2013.09.045.

155. Deng, W.; Rosenberg, P.A.; Volpe, J.J.; Jensen, F.E. Calcium-permeable AMPA/kainate receptors mediate toxicity and preconditioning by oxygen-glucose deprivation in oligodendrocyte precursors. *Proc. Natl. Acad. Sci. USA* **2003**, *100*, 6801–6806, doi:10.1073/pnas.1136624100.

156. Johnson, J.W.; Ascher, P. Glycine potentiates the NMDA response in cultured mouse brain neurons. *Nature* **1987**, *325*, 529–531, doi:10.1038/325529a0.

157. Nowak, L.; Bregestovski, P.; Ascher, P.; Herbet, A.; Prochiantz, A. Magnesium gates glutamate-activated channels in mouse central neurones. *Nature* **1984**, *307*, 462–465, doi:10.1038/307462a0.

158. Mayer, M.L.; Westbrook, G.L.; Guthrie, P.B. Voltage-dependent block by Mg^{2+} of NMDA responses in spinal cord neurones. *Nature* **1984**, *309*, 261–263, doi:10.1038/309261a0.

159. Mayer, M.L.; MacDermott, A.B.; Westbrook, G.L.; Smith, S.J.; Barker, J.L. Agonist- and voltage-gated calcium entry in cultured mouse spinal cord neurons under voltage clamp measured using arsenazo III. *J. Neurosci.* **1987**, *7*, 3230–3244.

160. Vicini, S.; Wang, J.F.; Li, J.H.; Zhu, W.J.; Wang, Y.H.; Luo, J.H; Wolfe B.B.; Grayson D.R. Functional and pharmacological differences between recombinant N-methyl-D-aspartate receptors. *J. Neurophysiol.* **1998**, *79*, 555–566, doi:10.1152/jn.1998.79.2.555.

161. Wyllie, D.J.; Béhé, P.; Colquhoun, D. Single-channel activations and concentration jumps: Comparison of recombinant NR1a/NR2A and NR1a/NR2D NMDA receptors. *J. Physiol. (Lond.)* **1998**, *510 Pt 1*, 1–18.

162. Malenka, R.C.; Bear, M.F. LTP and LTD: An embarrassment of riches. *Neuron* **2004**, *44*, 5–21, doi:10.1016/j.neuron.2004.09.012.

163. Akgül, G.; McBain, C.J. Diverse roles for ionotropic glutamate receptors on inhibitory interneurons in developing and adult brain. *J. Physiol. (Lond.)* **2016**, *594*, 5471–5490, doi:10.1113/JP271764.

164. Sheng, M.; Cummings, J.; Roldan, L.A.; Jan, Y.N.; Jan, L.Y. Changing subunit composition of heteromeric NMDA receptors during development of rat cortex. *Nature* **1994**, *368*, 144–147, doi:10.1038/368144a0.

165. Grand, T.; Gerges, S.A.; David, M.; Diana, M.A.; Paoletti, P. Unmasking GluN1/GluN3A excitatory glycine NMDA receptors. *Nat. Commun.* **2018**, *9*, 4769, doi:10.1038/s41467-018-07236-4.

166. Mothet, J.P.; Parent, A.T.; Wolosker, H.; Brady, R.O.; Linden, D.J.; Ferris, C.D; Rogawski M.A.; Snyder S.H. D-serine is an endogenous ligand for the glycine site of the N-methyl-D-aspartate receptor. *Proc. Natl. Acad. Sci. USA* **2000**, *97*, 4926–4931, doi:10.1073/pnas.97.9.4926.

167. Benveniste, M.; Mayer, M.L. Kinetic analysis of antagonist action at N-methyl-D-aspartic acid receptors. Two binding sites each for glutamate and glycine. *Biophys. J.* **1991**, *59*, 560–573, doi:10.1016/S0006-3495(91)82272-X.

168. Clements, J.D.; Westbrook, G.L. Activation kinetics reveal the number of glutamate and glycine binding sites on the N-methyl-D-aspartate receptor. *Neuron* **1991**, *7*, 605–613, doi:10.1016/0896-6273(91)90373-8.

169. Schorge, S.; Elenes, S.; Colquhoun, D. Maximum likelihood fitting of single channel NMDA activity with a mechanism composed of independent dimers of subunits. *J. Physiol. (Lond.)* **2005**, *569*, 395–418, doi:10.1113/jphysiol.2005.095349.

170. Gilling, K.E.; Jatzke, C.; Hechenberger, M.; Parsons, C.G. Potency, voltage-dependency, agonist concentration-dependency, blocking kinetics and partial untrapping of the uncompetitive N-methyl-D-aspartate (NMDA) channel blocker memantine at human NMDA (GluN1/GluN2A) receptors. *Neuropharmacology* **2009**, *56*, 866–875, doi:10.1016/j.neuropharm.2009.01.012.

171. Parsons, C.G.; Quack, G.; Bresink, I.; Baran, L.; Przegalinski, E.; Kostowski, W.; Krzascik P.; Hartmann S.; Danysz W. Comparison of the potency, kinetics and voltage-dependency of a series of uncompetitive NMDA receptor antagonists in vitro with anticonvulsive and motor impairment activity in vivo. *Neuropharmacology* **1995**, *34*, 1239–1258, doi:10.1016/0028-3908(95)00092-k.

172. MacDonald, J.F.; Bartlett, M.C.; Mody, I.; Pahapill, P.; Reynolds, J.N.; Salter, M.W; Schneiderman J.H.; Pennefather P.S. Actions of ketamine, phencyclidine and MK-801 on NMDA receptor currents in cultured mouse hippocampal neurones. *J. Physiol. (Lond.)* **1991**, *432*, 483–508, doi:10.1113/jphysiol.1991.sp018396.

173. Antonov, S.M.; Johnson, J.W. Voltage-dependent interaction of open-channel blocking molecules with gating of NMDA receptors in rat cortical neurons. *J. Physiol. (Lond.)* **1996**, *493 Pt 2*, 425–445, doi:10.1113/jphysiol.1996.sp021394.

174. Krystal, J.H.; Karper, L.P.; Seibyl, J.P.; Freeman, G.K.; Delaney, R.; Bremner, J.D; Heninger G.R.; Bowers M.B.; Charney D.S. Subanesthetic effects of the noncompetitive NMDA antagonist, ketamine, in humans. Psychotomimetic, perceptual, cognitive, and neuroendocrine responses. *Arch. Gen. Psychiatry* **1994**, *51*, 199–214, doi:10.1001/archpsyc.1994.03950030035004.

175. Persson, J. Ketamine in pain management. *CNS Neurosci. Ther.* **2013**, *19*, 396–402, doi:10.1111/cns.12111.

176. Zhou, H.-Y.; Chen, S.-R.; Pan, H.-L. Targeting N-methyl-D-aspartate receptors for treatment of neuropathic pain. *Expert Rev. Clin. Pharmacol*. **2011**, *4*, 379–388.

177. Kafi, H.; Salamzadeh, J.; Beladimoghadam, N.; Sistanizad, M.; Kouchek, M. Study of the neuroprotective effects of memantine in patients with mild to moderate ischemic stroke. *Iran. J. Pharm. Res.* **2014**, *13*, 591–598.

178. Danysz, W.; Parsons, C.G. Alzheimer's disease, β-amyloid, glutamate, NMDA receptors and memantine—Searching for the connections. *Br. J. Pharmacol.* **2012**, *167*, 324–352, doi:10.1111/j.1476-5381.2012.02057.x.

179. Parsons, C.G.; Danysz, W.; Quack, G. Memantine is a clinically well tolerated N-methyl-D-aspartate (NMDA) receptor antagonist—A review of preclinical data. *Neuropharmacology* **1999**, *38*, 735–767, doi:10.1016/s0028-3908(99)00019-2.

180. Abdallah, C.G.; Averill, L.A.; Krystal, J.H. Ketamine as a promising prototype for a new generation of rapid-acting antidepressants. *Ann. N. Y. Acad. Sci.* **2015**, *1344*, 66–77, doi:10.1111/nyas.12718.

181. Kong, M.; Ba, M.; Ren, C.; Yu, L.; Dong, S.; Yu, G.; Liang H. An updated meta-analysis of amantadine for treating dyskinesia in Parkinson's disease. *Oncotarget* **2017**, *8*, 57316–57326, doi:10.18632/oncotarget.17622.

182. Nair, A.S.; Sahoo, R.K. Efficacy of memantine hydrochloride in neuropathic pain. *Indian J. Palliat. Care* **2019**, *25*, 161–162, doi:10.4103/IJPC.IJPC_189_18.

183. Kashiwagi, K.; Masuko, T.; Nguyen, C.D.; Kuno, T.; Tanaka, I.; Igarashi, K.; Williams K. Channel blockers acting at N-methyl-D-aspartate receptors: Differential effects of mutations in the vestibule and ion channel pore. *Mol. Pharmacol.* **2002**, *61*, 533–545.

184. Miller, O.H.; Yang, L.; Wang, C.-C.; Hargroder, E.A.; Zhang, Y.; Delpire, E.; Hall B.J. GluN2B-containing NMDA receptors regulate depression-like behavior and are critical for the rapid antidepressant actions of ketamine. *eLife* **2014**, *3*, e03581, doi:10.7554/eLife.03581.

185. Noppers, I.; Niesters, M.; Aarts, L.; Smith, T.; Sarton, E.; Dahan, A. Ketamine for the treatment of chronic non-cancer pain. *Expert Opin. Pharmacother.* **2010**, *11*, 2417–2429, doi:10.1517/14656566.2010.515978.

186. Amidfar, M.; Réus, G.Z.; Quevedo, J.; Kim, Y.-K. The role of memantine in the treatment of major depressive disorder: Clinical efficacy and mechanisms of action. *Eur. J. Pharmacol.* **2018**, *827*, 103–111, doi:10.1016/j.ejphar.2018.03.023.

187. Gideons, E.S.; Kavalali, E.T.; Monteggia, L.M. Mechanisms underlying differential effectiveness of memantine and ketamine in rapid antidepressant responses. *Proc. Natl. Acad. Sci. USA* **2014**, *111*, 8649–8654, doi:10.1073/pnas.1323920111.

188. Chen, H.-S.V.; Lipton, S.A. The chemical biology of clinically tolerated NMDA receptor antagonists. *J. Neurochem.* **2006**, *97*, 1611–1626, doi:10.1111/j.1471-4159.2006.03991.x.

189. Parsons, C.G.; Stöffler, A.; Danysz, W. Memantine: A NMDA receptor antagonist that improves memory by restoration of homeostasis in the glutamatergic system—Too little activation is bad, too much is even worse. *Neuropharmacology* **2007**, *53*, 699–723, doi:10.1016/j.neuropharm.2007.07.013.

190. Lipton, S.A. Paradigm shift in neuroprotection by NMDA receptor blockade: Memantine and beyond. *Nat. Rev. Drug Discov.* **2006**, *5*, 160–170, doi:10.1038/nrd1958.

191. Johnson, J.W.; Qian, A. Interaction between channel blockers and channel gating of NMDA receptors. *Biol. Membr.* **2002**, *19*, 110–115.

192. Sobolevsky, A.I.; Koshelev, S.G.; Khodorov, B.I. Interaction of memantine and amantadine with agonist-unbound NMDA-receptor channels in acutely isolated rat hippocampal neurons. *J. Physiol. (Lond.)* **1998**, *512 Pt 1*, 47–60, doi:10.1111/j.1469-7793.1998.047bf.x.

193. Dilmore, J.G.; Johnson, J.W. Open channel block and alteration of N-methyl-D-aspartic acid receptor gating by an analog of phencyclidine. *Biophys. J.* **1998**, *75*, 1801–1816, doi:10.1016/S0006-3495(98)77622-2.

194. Wright, J.M.; Nowak, L.M. Effects of low doses of bicuculline on N-methyl-D-aspartate single-channel kinetics are not evident in whole-cell currents. *Mol. Pharmacol.* **1992**, *41*, 900–907.

195. Sobolevsky, A.I. Quantitative analysis of tetrapentylammonium-induced blockade of open N-methyl-D-aspartate channels. *Biophys. J.* **2000**, *79*, 1324–1335, doi:10.1016/S0006-3495(00)76385-5.

196. Antonov, S.M.; Johnson, J.W.; Lukomskaya, N.Y.; Potapyeva, N.N.; Gmiro, V.E.; Magazanik, L.G. Novel adamantane derivatives act as blockers of open ligand-gated channels and as anticonvulsants. *Mol. Pharmacol.* **1995**, *47*, 558–567.

197. Chen, H.S.; Lipton, S.A. Mechanism of memantine block of NMDA-activated channels in rat retinal ganglion cells: Uncompetitive antagonism. *J. Physiol. (Lond.)* **1997**, *499 Pt 1*, 27–46, doi:10.1113/jphysiol.1997.sp021909.

198. Costa, A.C.; Albuquerque, E.X. Dynamics of the actions of tetrahydro-9-aminoacridine and 9-aminoacridine on glutamatergic currents: Concentration-jump studies in cultured rat hippocampal neurons. *J. Pharmacol. Exp. Ther.* **1994**, *268*, 503–514.

199. Vorobjev, V.S.; Sharonova, I.N. Tetrahydroaminoacridine blocks and prolongs NMDA receptor-mediated responses in a voltage-dependent manner. *Eur. J. Pharmacol.* **1994**, *253*, 1–8, doi:10.1016/0014-2999(94)90750-1.

200. Li-Smerin, Y.; Johnson, J.W. Effects of intracellular Mg^{2+} on channel gating and steady-state responses of the NMDA receptor in cultured rat neurons. *J. Physiol. (Lond.)* **1996**, *491 Pt 1*, 137–150, doi:10.1113/jphysiol.1996.sp021202.

201. Koshelev, S.G.; Khodorov, B.I. Blockade of open NMDA channel by tetrabutylammonium, 9-aminoacridine and tacrine prevents channels closing and desensitization. *Membr. Cell Biol. C/C Biol. Membr.* **1995**, *9*, 93–110.

202. Qian, A.; Antonov, S.M.; Johnson, J.W. Modulation by permeant ions of Mg^{2+} inhibition of NMDA-activated whole-cell currents in rat cortical neurons. *J. Physiol. (Lond.)* **2002**, *538*, 65–77, doi:10.1113/jphysiol.2001.012685.

203. Kotermanski, S.E.; Johnson, J.W. Mg^{2+} imparts NMDA receptor subtype selectivity to the Alzheimer's drug memantine. *J. Neurosci.* **2009**, *29*, 2774–2779, doi:10.1523/JNEUROSCI.3703-08.2009.

204. Mealing, G.A.; Lanthorn, T.H.; Murray, C.L.; Small, D.L.; Morley, P. Differences in degree of trapping of low-affinity uncompetitive N-methyl-D-aspartic acid receptor antagonists with similar kinetics of block. *J. Pharmacol. Exp. Ther.* **1999**, *288*, 204–210.

205. Antonov, S.M.; Gmiro, V.E.; Johnson, J.W. Binding sites for permeant ions in the channel of NMDA receptors and their effects on channel block. *Nat. Neurosci.* **1998**, *1*, 451–461, doi:10.1038/2167.

206. Qian, A.; Johnson, J.W. Channel gating of NMDA receptors. *Physiol. Behav.* **2002**, *77*, 577–582, doi:10.1016/s0031-9384(02)00906-x.

207. Tajima, N.; Karakas, E.; Grant, T.; Simorowski, N.; Diaz-Avalos, R.; Grigorieff, N.; et al. Activation of NMDA receptors and the mechanism of inhibition by ifenprodil. *Nature* **2016**, *534*, 63–68, doi:10.1038/nature17679.

208. Glasgow, N.G.; Wilcox, M.R.; Johnson, J.W. Effects of Mg^{2+} on recovery of NMDA receptors from inhibition by memantine and ketamine reveal properties of a second site. *Neuropharmacology* **2018**, *137*, 344–358, doi:10.1016/j.neuropharm.2018.05.017.

209. Wilcox, M.R.; Glasgow, N.G.; Mesbahi-Vasey, S.; Nigam, A.; Phillips, M.B.; Turcu, A.L; Narangoda C.; Kurnikova M.G.; Vazquez S.; Johnson J.W. *A Hydrophobic Path Allows Drug Access to the NMDA Receptor Channel*. Program No. 370.16.; 2018 Neuroscience Meeting Planner. San Diego, CA: Society for Neuroscience, 2018. Online.

210. Sobolevsky, A.; Koshelev, S. Two blocking sites of amino-adamantane derivatives in open N-methyl-D-aspartate channels. *Biophys. J.* **1998**, *74*, 1305–1319, doi:10.1016/S0006-3495(98)77844-0.

211. Maki, B.A.; Aman, T.K.; Amico-Ruvio, S.A.; Kussius, C.L.; Popescu, G.K. C-terminal domains of N-methyl-D-aspartic acid receptor modulate unitary channel conductance and gating. *J. Biol. Chem.* **2012**, *287*, 36071–36080, doi:10.1074/jbc.M112.390013.

212. Krupp, J.J.; Vissel, B.; Heinemann, S.F.; Westbrook, G.L. N-terminal domains in the NR2 subunit control desensitization of NMDA receptors. *Neuron* **1998**, *20*, 317–327, doi:10.1016/s0896-6273(00)80459-6.

213. Krupp, J.J.; Vissel, B.; Thomas, C.G.; Heinemann, S.F.; Westbrook, G.L. Calcineurin acts via the C-terminus of NR2A to modulate desensitization of NMDA receptors. *Neuropharmacology* **2002**, *42*, 593–602, doi:10.1016/s0028-3908(02)00031-x.

214. Villarroel, A.; Regalado, M.P.; Lerma, J. Glycine-independent NMDA receptor desensitization: Localization of structural determinants. *Neuron* **1998**, *20*, 329–339, doi:10.1016/S0896-6273(00)80460-2.

215. Ehlers, M.D.; Zhang, S.; Bernhadt, J.P.; Huganir, R.L. Inactivation of NMDA receptors by direct interaction of calmodulin with the NR1 subunit. *Cell* **1996**, *84*, 745–755, doi:10.1016/s0092-8674(00)81052-1.

216. Rothman, S.M.; Olney, J.W. Excitotoxicity and the NMDA receptor—Still lethal after eight years. *Trends Neurosci.* **1995**, *18*, 57–58, doi:10.1016/0166-2236(95)93869-y.

217. Okamoto, S.; Pouladi, M.A.; Talantova, M.; Yao, D.; Xia, P.; Ehrnhoefer, D.E.; Zaidi R.; Clemente A.; Kaul M.; Graham R.K.; et al. Balance between synaptic versus extrasynaptic NMDA receptor activity influences inclusions and neurotoxicity of mutant huntingtin. *Nat. Med.* **2009**, *15*, 1407–1413, doi:10.1038/nm.2056.

218. Hardingham, G.E.; Bading, H. Synaptic versus extrasynaptic NMDA receptor signalling: Implications for neurodegenerative disorders. *Nat. Rev. Neurosci.* **2010**, *11*, 682–696, doi:10.1038/nrn2911.

219. Ascher, P.; Nowak, L. The role of divalent cations in the N-methyl-D-aspartate responses of mouse central neurones in culture. *J. Physiol. (Lond.)* **1988**, *399*, 247–266.

220. Clarke, R.J.; Johnson, J.W. NMDA receptor NR2 subunit dependence of the slow component of magnesium unblock. *J. Neurosci.* **2006**, *26*, 5825–5834, doi:10.1523/JNEUROSCI.0577-06.2006.

221. Clarke, R.J.; Glasgow, N.G.; Johnson, J.W. Mechanistic and structural determinants of NMDA receptor voltage-dependent gating and slow Mg^{2+} unblock. *J. Neurosci.* **2013**, *33*, 4140–4150, doi:10.1523/JNEUROSCI.3712-12.2013.

222. Vargas-Caballero, M.; Robinson, H.P.C. A slow fraction of Mg^{2+} unblock of NMDA receptors limits their contribution to spike generation in cortical pyramidal neurons. *J. Neurophysiol.* **2003**, *89*, 2778–2783, doi:10.1152/jn.01038.2002.

223. Spruston, N.; Jonas, P.; Sakmann, B. Dendritic glutamate receptor channels in rat hippocampal CA3 and CA1 pyramidal neurons. *J. Physiol. (Lond.)* **1995**, *482 Pt 2*, 325–352, doi:10.1113/jphysiol.1995.sp020521.

224. Kampa, B.M.; Clements, J.; Jonas, P.; Stuart, G.J. Kinetics of Mg^{2+} unblock of NMDA receptors: Implications for spike-timing dependent synaptic plasticity. *J. Physiol. (Lond.)* **2004**, *556*, 337–345, doi:10.1113/jphysiol.2003.058842.

225. Clarke, R.J.; Johnson, J.W. Voltage-dependent gating of NR1/2B NMDA receptors. *J. Physiol. (Lond.)* **2008**, *586*, 5727–5741, doi:10.1113/jphysiol.2008.160622.

Publisher's Note: MDPI stays neutral with regards to jurisdictional claims in published maps and institutional affiliations.

APPENDIX B PHARMACOLOGICAL AND ELECTROPHYSIOLOGICAL

CHARACTERIZATION OF NOVEL NMDA RECEPTOR ANTAGONISTS

Leiva, R., Phillips, M.B., Turcu, A.L., Gratacòs-Batlle, E., León-García, L., Sureda, F.X., Soto, D., Johnson, J. W., & Vázquez, S. (2018) Pharmacological and electrophysiological characterization of novel NMDA receptor antagonists. *ACS Chem. Neurosci.*, **9**, 2722–2730.

Pharmacological and electrophysiological characterization of novel NMDA receptor antagonists

Rosana Leiva,[†,∥] Matthew B. Phillips,[‡,∥] Andreea L. Turcu,[†,‡] Esther Gratacòs-Batlle,[‡] Lara León-García,[#] Francesc X. Sureda,[#] David Soto,[‡] Jon W. Johnson,[‡,]* Santiago Vázquez[†,]*

[†]Laboratori de Química Farmacèutica (Unitat Associada al CSIC), Facultat de Farmàcia i Ciències de l'Alimentació i Institut de Biomedicina (IBUB), Universitat de Barcelona, Av. Joan XXIII, 27-31, 08028 Barcelona, Spain.

[‡]Department of Neuroscience and Center for Neuroscience, University of Pittsburgh, Pittsburgh, Pennsylvania 15260, United States.

[‡]Neurophysiology Laboratory, Physiology Unit, Department of Biomedicine, Medical School Universitat de Barcelona, August Pi i Sunyer Biomedical Research Institute (IDIBAPS), Barcelona, and Institut of Neurosciences, 08036 Barcelona, Spain.

[#]Pharmacology Unit, Faculty of Medicine and Health Sciences, Universitat Rovira i Virgili, C./St. Llorenç 21, 43201 Reus (Tarragona), Spain.

ABSTRACT. This work reports the synthesis, and pharmacological and electrophysiological evaluation of new *N*-methyl-*D*-aspartic acid receptor (NMDAR) channel blocking antagonists

181

featuring polycyclic scaffolds. Changes in the chemical structure modulate the potency and voltage dependence of inhibition. Two of the new antagonists display properties comparable to those of memantine, a clinically approved NMDAR antagonist.

INTRODUCTION

The amino acid L-glutamate[1-2] is the main excitatory neurotransmitter in the central nervous system and activates a wide diversity of receptors comprising ionotropic (iGluRs) as well as metabotropic glutamate receptors. iGluRs, ligand-gated ion channels composed of four subunits, can be subdivided into three classes based on their subunit composition and their selective activation by the agonists (S)-2-amino-3-(3-hydroxy-5-methylisoxazol-4-yl)propionic acid (AMPA), kainate and N-methyl-D-aspartic acid (NMDA).[3-5] Among iGluRs, the NMDA receptor (NMDAR) possesses unique properties including co-agonism, a high permeability for Ca^{2+} ions, and voltage-dependent channel blockade by Mg^{2+}, which has to be relieved to allow ion flow through the channel.[6-8]

NMDARs are heterotetrameric complexes derived from three main types of subunits, namely GluN1, GluN2 and GluN3, of which GluN1 is obligatory.[9-14] Usually a single NMDAR is composed of two glycine-binding GluN1 subunits plus two glutamate-binding GluN2 subunits. There are eight known splice variants of the GluN1 subunit, four GluN2 subunit subtypes (A-D), and two GluN3 subunit subtypes (A,B).[8,15-17]

NMDARs are expressed at nearly all vertebrate synapses and play key roles in neuronal development, plasticity, and survival. Ca^{2+} influx through NMDARs is a signal of paramount importance for synaptic plasticity, including long-term potentiation and long-term depression, physiological processes that are the cellular basis of many forms of learning and memory.[18] However, NMDAR overstimulation triggers excessive Ca^{2+} influx and leads to excitotoxicity,

which is the primary mediator of neuronal death following stroke and is believed to play a key role in the pathogenesis of neurodegenerative diseases, including Alzheimer's disease (AD) and Parkinson's disease (PD).[9-20] Hence, NMDAR antagonists able to prevent overactivation of NMDARs are of interest as neuroprotective drugs.

Multiple types of NMDAR antagonists have been tested in clinical trials. Several competitive NMDAR antagonists failed trials for neurodegenerative disorders and related conditions, possibly because they blocked the physiological as well 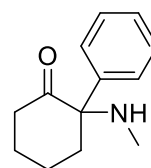as the pathological effects of NMDARs, leading to severe adverse effects.[21-23] NMDAR open channel blocking antagonists have also been tested as therapeutic agents. In contrast to competitive antagonists, NMDAR channel blockers bind at sites that overlap with the Mg^{2+} site and can only bind and unbind when the channel is open.[24-26] Most NMDAR channel blockers also failed clinical trials, and several were found to be neurotoxic when administered at high doses to control animals,[27] including dizocilpine (MK-801), phencyclidine, and ketamine (compounds **1**, **2**, and **3**, respectively, in Figure 1). Nevertheless, two adamantane derivatives, amantadine and memantine (compounds **4** and **5**, respectively, in Figure 1), which are low- (amantadine) and moderate- (memantine) affinity voltage-dependent NMDAR channel blockers, have found moderately effective for treatment of PD and AD, respectively.[28-32]
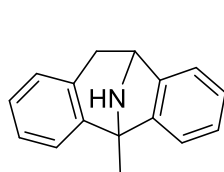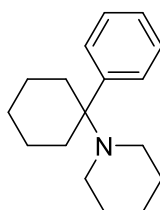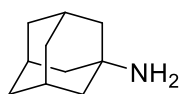

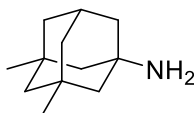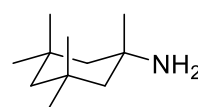**1**, dizocilpine   **2**, phencyclidine   **3**, ketamine

4, amantadine   **5**, memantine   **6**, neramexane

Figure 1. Structures of NMDAR channel blocking antagonists **1-6**.

Several hypotheses have been proposed to explain the divergent clinical effects of NMDAR channel blockers. The kinetics of recovery from inhibition, which are much faster for memantine than dizocilpine, have been proposed to be a major determinant of clinical tolerability.[29,33-34] An alternative hypothesis is that the utility of memantine may derive from an ability to preferentially inhibit extrasynaptic NMDARs, activation of which has been proposed to be especially neurotoxic.[35-37] It is clear, however, that overactivation of synaptic NMDARs also can be neurotoxic.[38,39] Another recent proposal is that clinical safety may be associated with preferential inhibition of NMDARs that undergo Ca^{2+}-dependent desensitization following exposure to high intracellular Ca^{2+}, a property exhibited by **5** but not **3**.[40]

Although memantine is well-tolerated by AD patients, it possesses limited clinical efficacy.[41] For this reason, new moderate-affinity NMDAR antagonists with similar but distinct pharmacological properties are of interest.[29,33-34] Thus, we recently started a project aimed to design, synthesize, and characterize new polycyclic amines as analogues of **5** with improved pharmacological profiles.

Taking into account that carbocyclic amines other than **4** and **5** display similar affinity to NMDARs (e.g, neramexane, **6** in Figure 1),[42-45] and that the methyl groups of memantine are critical for optimal potency at NMDARs (memantine is roughly fifty-fold more potent than amantadine),[46-47] we envisaged the synthesis of polycyclic amine **7** (Figure 2) and a few selected analogues. These new analogues included amines **8**, for considering the impact of the distance between the polcyclic cage and the amino group; **9** and **10**, for assessing the effect of conformational freedom; and guanidine **11**, for evaluating the effect of basicity.
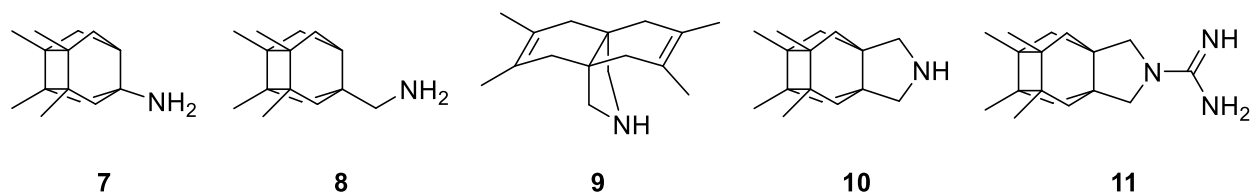
Figure 2. Chemical structures of new putative NMDAR antagonists **7-11**.

RESULTS AND DISCUSSION

Chemical synthesis. Compounds **9**, **10** and **11** were prepared using procedures previously reported by our group.[48-49] Primary amines **7** and **8** were synthesized following the sequence shown in Scheme 1, starting from known anhydride **12**.[50] Briefly, treatment of anhydride **12** with an excess of methanol at reflux furnished hemiester **13** in quantitative yield. Barton's decarboxylation procedure led to ester **14**, which upon hydrolysis yielded carboxylic acid **15**. From this key intermediate, Curtius rearrangement led to primary amine **7**. Finally, amine **8** was obtained by reduction of amide **16**, in turn obtained from **15**. Both target amines **7** and **8** were fully characterized as their corresponding hydrochlorides.

Scheme 1. Synthesis of primary amines **7** and **8.**
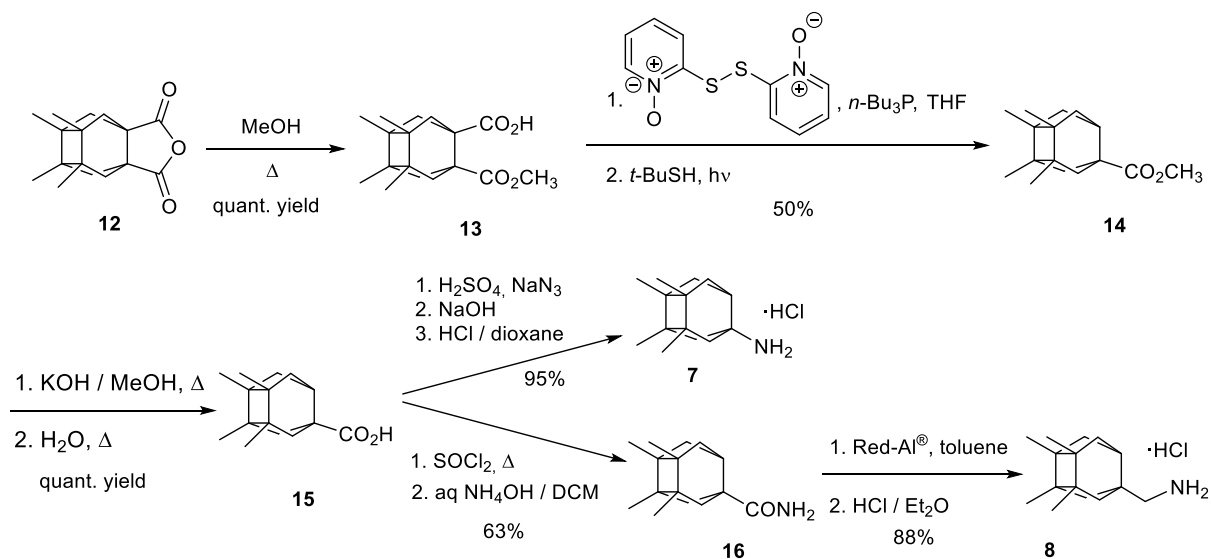
Pharmacology and Structure-Activity Relationships. To evaluate if the new compounds were able to antagonize NMDARs, we measured their effect on the increase in intracellular Ca^{2+} evoked by application of NMDA (100 μM, in the presence of 10 μM of glycine) to cultured rat cerebellar granule neurons.[51] Pleasingly, inspection of the results shown in Table 1 reveals that all the new compounds were clearly more potent than amantadine (IC_{50} = 92 μM) with values of IC_{50} in the low micromolar range. Although differences are small, it seems that conformationally restricted secondary amines **9** (5.8 ± 1.0 μM) and **10** (5.1 ± 1.0 μM) are less potent than secondary amine **8** (2.8 ± 1.1 μM), while directly joining the polar amino group to the polycyclic ring slightly reduces the potency (compare **7** *vs* **8**). Overall, guanidine **11** and primary amine **8** were the more potent compounds, with IC_{50} values (2.7 ± 0.4 and 2.8 ± 1.1 μM, respectively) only slightly higher than that of memantine (1.5 ± 0.1 μM).

Table 1. IC_{50} (μM) values for amantadine, memantine and new analogs **7-11** as NMDAR antagonists.[a]

Compound	NMDA (100 μM) IC$_{50}$ (μM)
4	92 ± 29
5	1.5 ± 0.1
7	4.1 ± 1.7
8	2.8 ± 1.1
9	5.8 ± 1.0
10	5.1 ± 1.0
11	2.7 ± 0.4

[a]IC$_{50}$ is the concentration of a compound that inhibits the measured response by 50%. Data were obtained from primary cultures of cerebellar granule neurons as described in Methods by measuring the intracellular Ca^{2+} concentration. Cells were exposed to 100 μM NMDA plus 10 μM glycine. Data shown are means ± SEM of at least three separate experiments carried out on three different batches of cultured cells.

Functional block of NMDARs by polycyclic compounds 7-11. We next evaluated electrophysiologically the functional ability of compounds **7-11** to block NMDARs. To carry out these studies, we performed whole-cell experiments on tsA201 cells transfected with expression plasmids codifying rat GluN1 and GluN2A subunits to measure the properties of the newly synthesized polycyclic amines. We clamped the cells at -60 mV and then evoked NMDAR currents by applying 100 μM NMDA plus 10 μM glycine. After the NMDAR-evoked current reached a steady state, we rapidly applied a given blocking compound by means of piezoelectric translation of a double-barreled theta glass tubing (<1 ms exchange between solutions). By doing so, we could compare the percentage of block for each tested compound. Figure 3 shows a typical example of an experiment for the compounds tested (**5** and **7-11**). Compound **5** at 10 μM blocked nearly 90% of the activated current while the percentage of block by the newly synthetized compounds varied amongst them. Compounds **7** and **8** at 10 μM displayed degree of NMDAR block similar to **5**, i.e., 82.5 ± 3.2 % for **7** and 88.3 ± 3.7 % for **8** *vs* 89.2 ± 1.0 % for **5** (Figure 4A). Compounds **9** and **10** at 10 μM induced less inhibition than **5**, i.e., 71.9 ± 3.8 % for **9** and 70.4 ± 5.6 % for **10** *vs* 89.2 ±

1.0 % for **5**; (Figure 4A). On the other hand, 10 μM of compound **11** induced more inhibition than **5**, although the difference was not significant, i.e., 97.9 ± 1.9 % for **11** *vs* 89.2 ± 1.0 % for **5**. Thus, compounds **7**, **8** and **11** appeared to block NMDARs with potency similar to that of memantine.

We also evaluated the ability of the newly synthesized blockers to unbind from the channel pore upon drug removal. Unbinding was measured by rapidly removing the blocker in the continuous presence of agonists (100 μM NMDA plus 10 μM glycine). Unblock (Fig. 4B) was calculated as the percentage of current recovery after a 30-s application of agonists without blocker, when the current was at or very near steady state. All tested compounds showed similar abilities to unbind from the pore compared with **5**, i.e., 94.9 ± 2.2 %, 90.6 ± 3.5 %, 92.5 ± 5.9, 92.3 ± 3.0 % and 93.5 ± 3.4 % for compounds **7**, **8**, **9**, **10** and **11**, respectively, *vs* 94.2 ± 2.1 % for **5** (Figure 4B).

Finally we assessed the voltage dependence of channel block by the compounds. During the recordings we applied two positive pulses to +60 mV for 0.5 s during the sustained NMDA- and glycine-evoked current. The first pulse was applied in the presence of the blocking compound at 10 μM and a second +60 mV pulse was applied in the absence of the blocker. Hence, we could extract the percentage block at +60 mV. Compound **11**, which appeared to be the most potent compound when tested at -60 mV, also displayed the greatest inhibition at +60 mV, i.e., 73.0 ± 3.6 % block for **11** *vs* 8.1 ± 4.0 % for **5** (Figure 4C). Compounds **7-10** had similar blocking percentages at +60 mV to **5**, i.e., 2.4 ± 5.1 %, 14.7 ± 4.5 %, 9.0 ± 3.6 % and 10.4 ± 6.4 % for compounds 7, 8, 9, and 10, respectively; (Figure 4C).
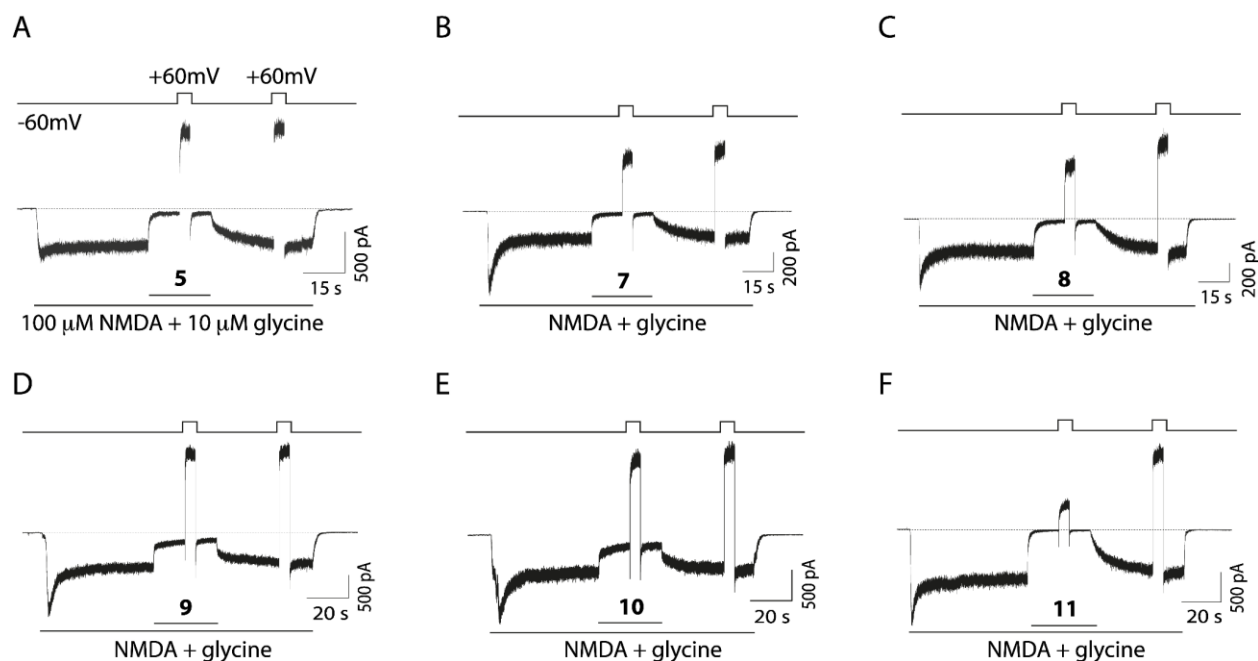
Figure 3. Block, unblock and voltage dependence of compounds **5**, **7-11**. **A.** Example recording showing the protocol used to study the degree of channel block, the voltage dependence and the unblocking percentage of compound **5**. Whole-cell currents were evoked in tsA201 cells expressing GluN1/2A NMDARs by bath application of 100 μM NMDA plus 10 μM glycine. Compound **5** was rapidly applied at 10 μM. **B-F.** Example traces in the same conditions as described in A but for compounds **7**, **8**, **9**, **10** and **11**, respectively. All compounds were used at 10 μM.
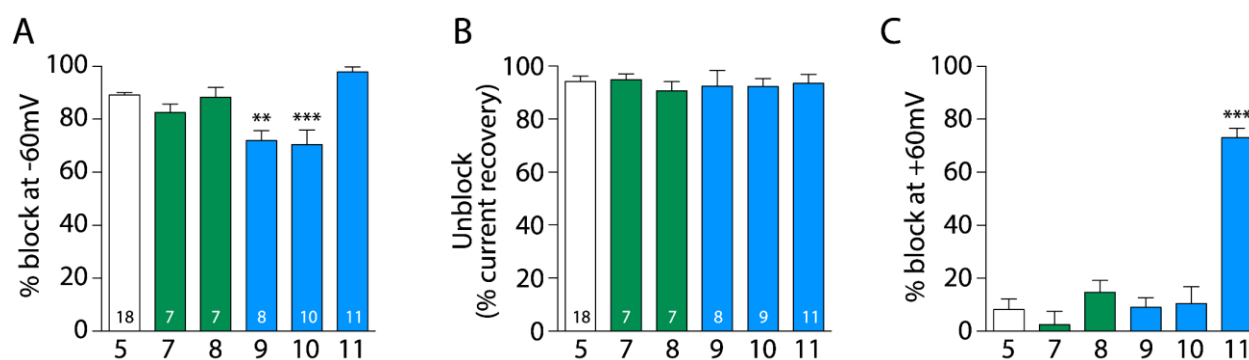
Figure 4. Quantification of block, unblock and percentage of block at +60mV of compounds **5, 7-11**. **A.** Summary of the blocking percentage at the holding potential of -60 mV for the different compounds tested. Asterisks identify mean values with statistically significant differences. The number of asterisks indicates the magnitude of the p-value, the probability of measuring by chance a difference equal to or greater than the observed difference between indicated mean values. **p<0.01 and ***p<0.001 *vs* compound **5**; one-way ANOVA with Tukey post hoc analysis. Numbers inside bars denote the number of experiments. **B.** Degree of unblock, measured as the percentage of current recovery after removal of the blocker; no differences between compounds was observed (p>0.05 for all compounds compared with compound **5**). Numbers inside bars denote the number of experiments. **C.** Percentage of block at +60 mV for the studied compounds. ***p<0.0001 *vs* compounds **5, 7, 8, 9**, and **10**; one-way ANOVA with Tukey post hoc analysis; n=17, 7, 7, 8, 10 and 10 for compounds **5, 7, 8, 9, 10** and **11**, respectively.

**Concentration and voltage dependence of NMDAR inhibition by 5, 7, 8, and 11.** Whole-cell patch-clamp recordings from tsA201 cells expressing GluN1/2A receptors were used to further assess the pharmacological properties of three promising derivatives, primary amines **7, 8**, and **11**. Experiments measuring the IC_{50} and voltage-dependence of block by compound **5** were performed for comparison. In cells held at -65 mV, inhibition by each drug was measured at increasing drug concentrations (Figures 5–8, A) and used to calculate the IC_{50} and Hill coefficient (n_H, which reflects the steepness of the concentration-inhibition curve; see Equation 2). The IC_{50} value and Hill coefficient measured for **5** (Fig. 5B) are similar to previously-reported values measured under the same conditions.[42] Compounds **7, 8**, and **11** were found to have moderate IC_{50} values (Figures 6–8, B). The IC_{50}s of compounds **8** (1.01 ± 0.13 μM) and **11** (0.48 ± 0.09 μM) were significantly

lower than the IC$_{50}$s of **5** (1.84 ± 0.39 µM) or **7** (2.78 ± 0.25 µM), and the IC$_{50}$ of **5** was significantly lower than the IC$_{50}$ of **7** (Fig. 9A). There were no significant differences between the n$_{H}$ of the drugs, i.e., 1.07 ± 0.27, 0.98 ± 0.08, 1.01 ± 0.11, and 1.00 ± 0.03 for compounds **5, 7, 8**, and **11,** respectively. Modest differences between IC$_{50}$s measured using intracellular Ca^{2+} measurements from cerebellar granule neurons (Table 1) and patch-clamp recordings from tsA201 cells expressing GluN1/2A receptors (Figs. 5 – 9) were observed. The differences may have resulted from expression of GluN2 subunits other than GluN2A in cerebellar granule neurons, and from differences in recording technique.

To measure voltage dependence of inhibition by **5, 7, 8,** and **11**, inhibition elicited by roughly twice the IC$_{50}$ of each drug was measured at 9 different voltages (examples from 5 voltages are shown in Figures 5–8, C). The inhibition produced by the drugs decreased as voltage was depolarized (Figures 5–8, C and D), as expected of positively charged channel blockers. Fitting of Equation 3 to current-voltage data was used to quantify V$_{0,}$ the change in voltage (in mV) that results in an *e*-fold change in the IC$_{50}$ of a drug. Equation 4 was used to calculate δ, an estimate of the fraction of the total transmembrane voltage field felt by the blocker at its binding site.[52] The value of δ is calculated from the value of V$_{0}$ (Equation 4); strong voltage dependence is reflected by a large δ and a small V$_{0}$. All compounds displayed strongly voltage-dependent block ,i.e., for **5,** V$_{0}$ = 28.0 ± 2.2 mV and δ = 0.91 ± 0.08; for **7,** V$_{0}$ = 26.5 ± 1.8 mV and δ = 0.99 ± 0.05; for **8,** V$_{0}$ = 29.9 ± 1.9 mV and δ = 0.87 ± 0.05; for **11,** V$_{0}$ = 33.6 ± 1.5 mV and δ = 0.76 ± 0.03 (Figures 5–8, D). The voltage dependence of inhibition was found to be significantly weaker for **11** than for either **5** or **7** (Fig. 9B).
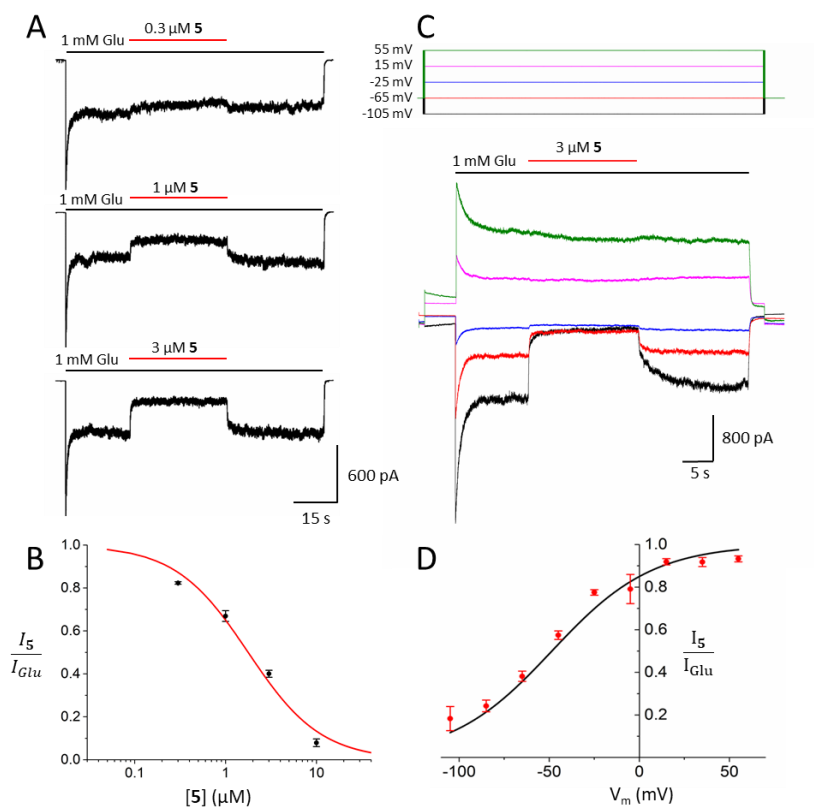
Figure 5. Concentration and voltage dependence of NMDAR inhibition by **5**. **A.** Representative current traces from one cell depicting effect of **5** on GluN1/2A receptor currents. Application of 1 mM Glu (black bars) elicited an inward current that was antagonized by application of **5** (red bars). **B.** Concentration-inhibition relation for **5**. Line shows best fit of Equation 2 ($IC_{50} = 1.84 \pm 0.39$ μM, $n_H = 1.07 \pm 0.27$; n=5). **C.** Representative voltage (V_m; top) and current (bottom) traces depicting effect of membrane potential upon inhibition by 3 μM **5**. Traces from 5 of the 9 membrane potentials tested are displayed for clarity. **D.** Current-voltage relation of inhibition by **5**. Line shows best fit of Equation 3 ($V_0 = 28.0 \pm 2.2$; n=5). Points in B and D represent mean fractional currents measured at each concentration (B) or voltage (D); error bars represent SEM and are sometimes smaller than symbols. Comparison of the concentration and voltage dependence of NMDAR inhibition by compounds 5, 7, 8, and 11 is shown in Figure 9.
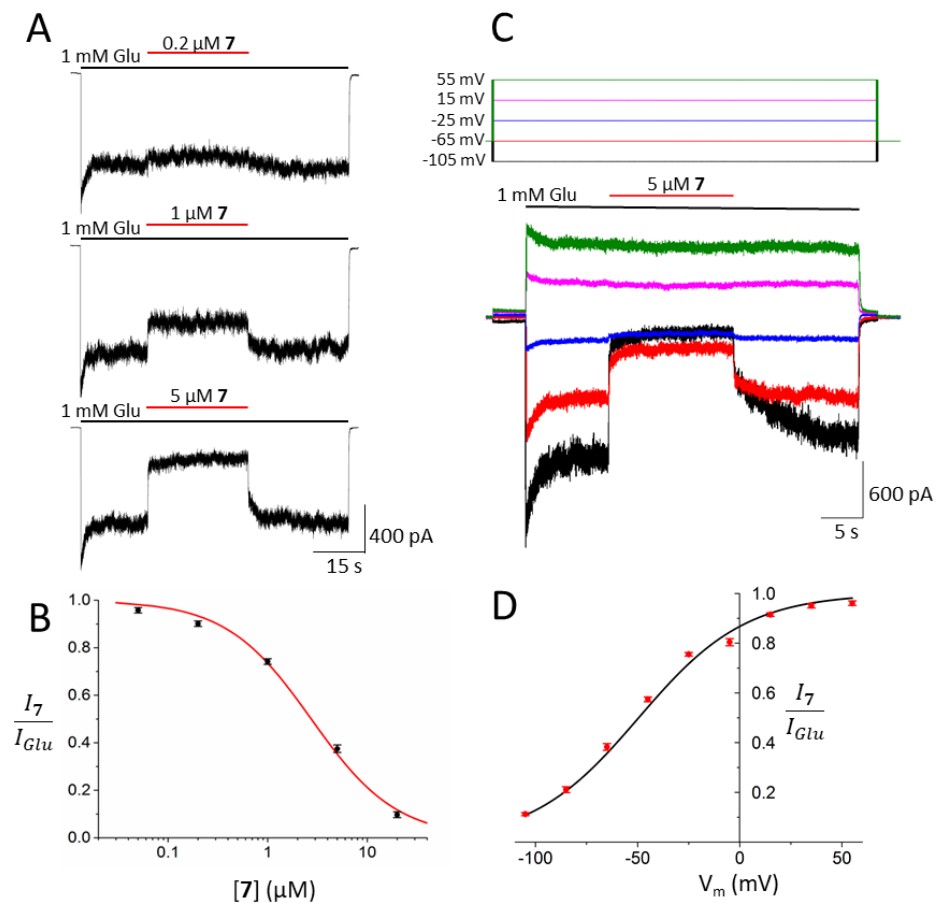
Figure 6. Concentration and voltage dependence of NMDAR inhibition by **7**. **A**, **B**. Same as Figure 5A, B, except concentration-inhibition measurements made using **7**. Line in B shows best fit of Equation 2 ($IC_{50} = 2.78 \pm 0.25$ μM, $n_H = 0.98 \pm 0.08$; n=7). **C**, **D**. Same as Figure 5C, D, except measurements of voltage-dependence made using 5 μM **7**. Line in D shows best fit of Equation 3 ($V_0 = 26.5 \pm 1.8$; n=7). Comparison of the concentration and voltage dependence of NMDAR inhibition by compounds 5, 7, 8, and 11 is shown in Figure 9.
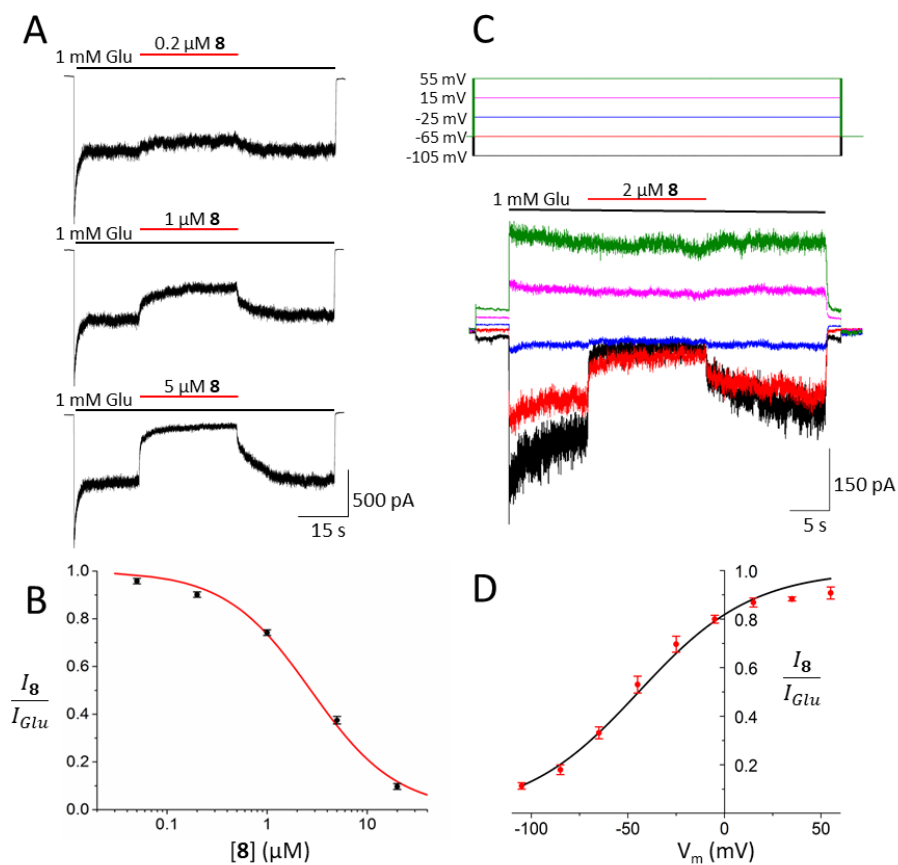
Figure 7. Concentration and voltage dependence of NMDAR inhibition by **8**. **A**, **B**. Same as Figure 5A, B, except concentration-inhibition measurements made using **8**. Line in B shows best fit of Equation 2 (IC$_{50}$ = 1.01 ± 0.13 μM, n$_H$ = 1.01 ± 0.11; n=7). **C**, **D**. Same as Figure 5C, D, except measurements of voltage-dependence made using 2 μM **8**. Line in D shows best fit of Equation 3 (V$_0$ = 29.9 ± 1.9; n=8). Comparison of the concentration and voltage dependence of NMDAR inhibition by compounds 5, 7, 8, and 11 is shown in Figure 9.
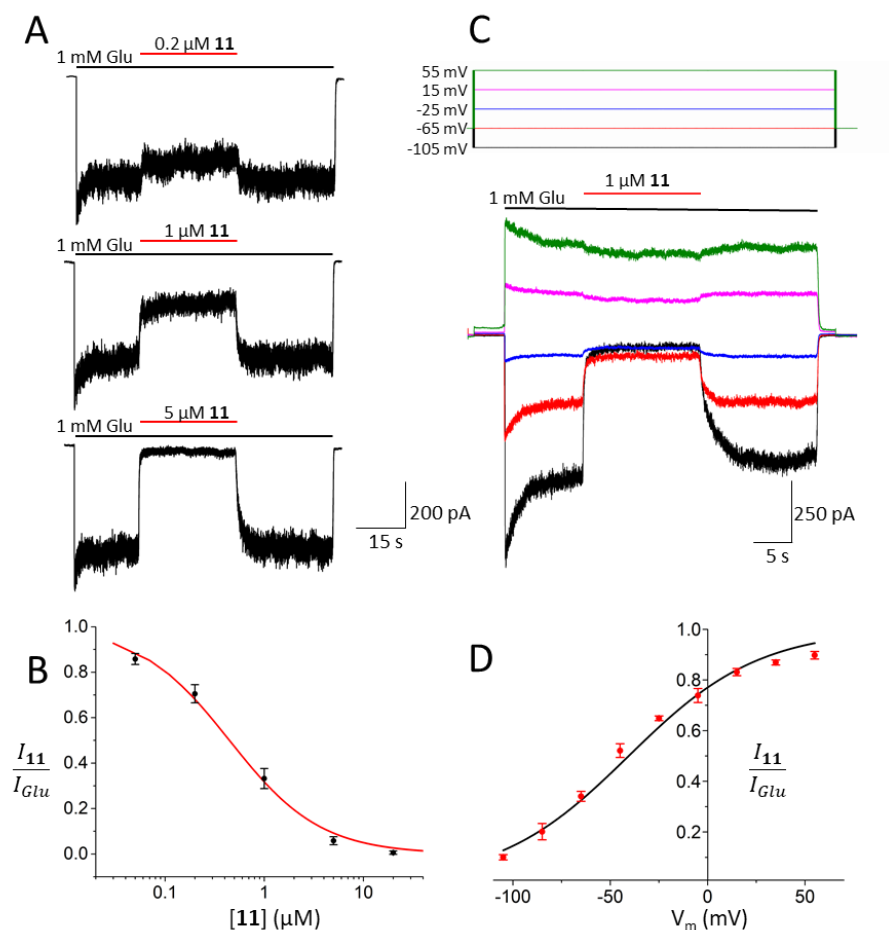
Figure 8. Concentration and voltage dependence of NMDAR inhibition by **11**. **A**, **B**. Same as Figure 5 A, B, except concentration-inhibition measurements made using **11**. Line in B shows best fit of Equation 2 (IC_{50} = 0.48 ± 0.09 μM, n_H = 1.00 ± 0.03; n=4). **C**, **D**. Same as Figures 5 C, D, except measurements of voltage-dependence made using 1 μM **11**. Line in D shows best fit of Equation 3 (V_0 = 33.6 ± 1.5; n=4). Comparison of the concentration and voltage dependence of NMDAR inhibition by compounds 5, 7, 8, and 11 is shown in Figure 9.
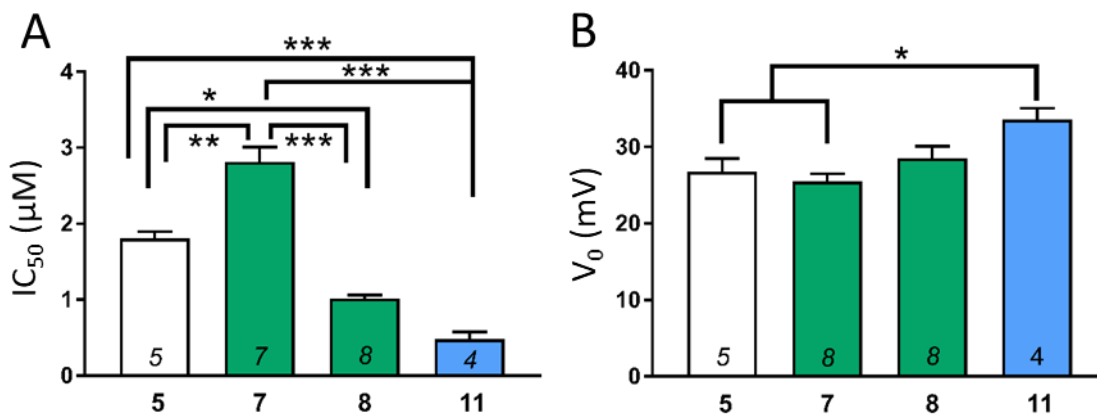
**Figure 9**. Comparison of NMDAR channel blocker properties. Sample size denoted by number inside column. **A**. Comparison of blocker IC_{50} values measured at -65 mV. **B**. Comparison of voltage dependence of inhibition by the blockers. All comparisons made by one-way ANOVA with Tukey *post hoc* analysis; *p<0.01, **p<0.001, ***p<0.0001.

CONCLUSIONS

We have described the synthesis, pharmacological evaluation and electrophysiology of a novel family of *N*-methyl-*D*-aspartic acid receptor (NMDAR) channel blockers. Despite profound structural modifications, e.g., compare diene **9** with the other compounds, or different pK_as, e.g., compare amine **10** with guanidine **11**, all the inhibitors showed similar potency as NMDAR antagonists. However, more subtle changes in the chemical structure modulated both the degree of inhibition and voltage-dependence of inhibition by the inhibitors, e.g., compare primary amine **8** with secondary amine **10** or amine **10** with guanidine **11** (Figures 3 and 4). Primary amines **7** and **8** displayed voltage-dependence and potency comparable to memantine (**5**).

METHODS

Chemistry. *(3,4,8,9-Tetramethyltetracyclo[4.4.0.0³,⁹.0⁴,⁸]dec-1-yl)amine hydrochloride* (**7**). A solution of the acid **15** (182 mg, 1.35 mmol) in DCM (5 mL) was prepared in a two-neck round-bottom flask equipped with a condenser, a gas outlet and a magnetic stirring. Concentrated H_2SO_4 (0.43 mL) was added and the reaction was heated to 50 °C. Then, NaN_3 (189 mg, 2.90 mmol) was carefully added portionwise. The reaction was kept at 50 °C for 1.5 h. The resulting mixture was cooled with an ice bath. Crushed ice (2 g) was added to the reaction and the aqueous layer was basified with 2 N NaOH to basic pH. The layers were separated, and the aqueous layer was extracted with warmed CH_2Cl_2 due to the low solubility of the product (6 x 20 mL). The combined organics were dried over anhydrous Na_2SO_4 and filtered. An excess of HCl in 1,4-dioxane was added to the residue and the suspension was concentrated under reduced pressure to give the **7·HCl** as a brown solid (182 mg, 95% yield). The analytical sample was obtained by crystallization from hot CH_2Cl_2, mp 200 °C (sublimation). IR (ATR) ν: 628, 685, 716, 1010, 1041, 1062, 1090, 1114, 1147, 1163, 1188, 1232, 1294, 1310, 1341, 1369, 1385, 1452, 1460, 1483, 1501, 1524, 1547, 1620, 1646, 2072, 2583, 2697, 2790, 2873, 2899, 2961, 3395, 3426 cm⁻¹. ¹H-NMR (400 MHz, CD₃OD) δ: 0.90 [dd, J = 11.4 Hz, J' = 2.4 Hz, 2H, 5(7)-H$_a$], 0.98-1.02 [d, J = 10.8 Hz, 2H, 2(10)-H$_a$], 1.01 [s, 6H, 3(9)-CH₃ or 4(8)-CH₃], 1.03 [s, 6H, 4(8)-CH₃ or 3(9)-CH₃], 1.94 [dd, J = 11.4 Hz, J' = 1.6 Hz, 2H, 5(7)-H$_b$], 1.99 [d, J = 10.8 Hz, 2H, 2(10)-H$_b$], 2.25 (m, 1H, 6-H). ¹³C-NMR (100.5 MHz, CD₃OD) δ: 15.4 [CH₃, C3(9)-CH₃ or C4(8)-CH₃], 15.6 [CH₃, C4(8)-CH₃ or C3(9)-CH₃], 38.9 [CH₂, C5(7)], 40.8 (CH, C6), 42.0 [CH₂, C2(10)], 45.8 [C, C3(9) or C4(8)], 46.2 [C, C3(9) or C4(8)], 58.1 (C, C1). HRMS-ESI+ m/z [M+H]⁺ calcd for [$C_{14}H_{23}N$+H]⁺: 206.1903, found: 206.1907. Anal. Calcd for $C_{14}H_{23}N \cdot HCl \cdot 0.66H_2O$: C 66.24, H 10.06, N 5.52. Found: C 66.07, H 9.59, N 5.40.

(3,4,8,9-Tetramethyltetracyclo[4.4.0.0^{3,9}.0^{4,8}]dec-1-yl)methylamine hydrochloride (**8**). A solution of **16** (96 mg, 0.41 mmol) in anhydrous toluene (10 mL) was cooled to 0 °C and Red-Al® (0.7 mL, 2.05 mmol) was added dropwise. The reaction was heated to reflux overnight. The resulting mixture was cooled with an ice bath and aqueous 10 N NaOH solution was added dropwise to basic pH. Then, the reaction was stirred for 10 min. The layers were separated and the aqueous layer extracted with DCM (3 x 20 mL). The combined organics were dried over anhydrous Na_2SO_4, filtered and HCl/Et_2O was added. After concentration under reduced pressure, **8·HCl** was obtained as a white solid (92 mg, 88% yield). The analytical sample was obtained by washing the solid with cooled Et_2O, mp 240 °C (sublimation). IR (ATR) ν: 715, 844, 933, 968, 986, 998, 1016, 1031, 1064, 1097, 1117, 1130, 1163, 1178, 1223, 1297, 1350, 1367, 1383, 1451, 1461, 1479, 1501, 1514, 1613, 2860, 2916, 2941, 3012 cm^{-1}. ^{1}H-NMR (400 MHz, CD$_3$OD) δ: 0.63 [d, J = 11.2 Hz, 2H, 2(10)-H$_a$], 0.79 [broad d, J = 11.2 Hz, 2H, 5(7)-H$_a$], 0.995 [s, 6H, 3(9)-C$\underline{H}_3$ or 4(8)-C$\underline{H}_3$], 0.999 [s, 6H, 4(8)-C$\underline{H}_3$ or 3(9)-C$\underline{H}_3$], 1.76 [d, J = 11.2 Hz, 2H, 5(7)-H$_b$], 1.82 [d, J = 11.2 Hz, 2H, 2(10)-H$_b$], 2.12 (m, 1H, 6-H), 3.01 (s, 2H, C$\underline{H}_2$NH$_2$). ^{13}C-NMR (100.5 MHz, CD$_3$OD) δ: 15.8 [CH$_3$, C3(9)-$\underline{C}$H$_3$ or C4(8)-$\underline{C}$H$_3$], 16.0 [CH$_3$, C4(8)-$\underline{C}$H$_3$ or C3(9)-$\underline{C}$H$_3$], 38.2 (CH, C6), 39.3 [CH$_2$, C5(7)], 42.1 [CH$_2$, C2(10)], 42.5 (C, C1), 45.9 [C, C3(9) or C4(8)], 47.1 [C, C3(9) or C4(8)], 48.1 (CH$_2$, $\underline{C}$H$_2$NH$_2$). HRMS-ESI+ m/z [*M*+H]$^+$ calcd for [C$_{15}$H$_{25}$N+H]$^+$: 220.2060, found: 220.2050. Anal. Calcd for C$_{15}$H$_{25}$N·HCl·0.25H$_2$O: C 69.21, H 10.26, N 5.38. Found: C 69.15, H 10.01, N 5.19.

Intracellular Ca^{2+} measurements. The functional assay of antagonist activity at NMDA receptors was performed using primary cultures of rat cerebellar granule neurons that were prepared according to established protocols.[51] Cells were grown on 10 mm poly-L-lysine coated round glass cover slips and used for the experiments after 6-9 days *in vitro*. Cells were loaded with

6 μM Fura-2 AM (Invitrogen-Molecular Probes) for 30 min. Afterwards a coverslip was mounted on a quartz cuvette containing a Mg^{2+}-free Locke-HEPES buffer using a special holder. Measurements were performed using a PerkinElmer LS-55 fluorescence spectrometer equipped with a fast-filter accessory, under mild agitation and at 37 ºC. Analysis from each sample was recorded real-time during 1600 s. After stimulation with NMDA (100 μM, in the presence of 10 μM glycine), increasing cumulative concentrations of the compound to be tested were added. The percentages of inhibition at every tested concentration were analyzed using a non-linear regression curve fitting (variable slope) using the software Prism 5.04 (GraphPad Software Inc.).

Cell culture, transfection, and recordings for electrophysiology experiments. All electrophysiological experiments were performed at room temperature using the tsA201 cell line (European Collection of Authenticated Cell Cultures) transiently cotransfected with mammalian expression plasmids containing cDNAs encoding the rat GluN1-1a and GluN2A subunits.

For Figures 3–4, cells were maintained as previously described[53] in DMEM:F12 supplemented with 10% fetal bovine serum and 1% penicillin/streptomycin (Sigma). Cells were plated at 0.1-0.2 x 10^5 cells/dish in onto 10 mm glass coverslips treated with poly D-lysine. 12–24 hours after plating, the cells were transiently transfected using PEI transfection reagent (1 mg/ml) in a 3:1 ratio (PEI:DNA). Culture medium was supplemented with the competitive NMDAR antagonist D, L-2-amino-5-phosphonopentanoate (dl-APV, Sigma, 500 μM) at the time of transfection to prevent NMDAR-mediated cell death. Whole-cell voltage-clamp recordings were performed 48 hours after transfection. Pipettes were pulled from borosilicate capillary tubing (OD = 1.5 mm, ID = 0.86 mm) using a PC-10 vertical puller (Narishige Instruments) and subsequently fire-polished to a resistance of 3–5 MΩ using an MF-830 forge (Narishige). Intracellular pipette solution contained (in mM): 140 CsCl, 10 HEPES, 5 EGTA, 4 Na_2ATP and 0.1 Na_3GTP with pH balanced

to 7.25 with CsOH. Extracellular recording solution contained (in mM): 140 NaCl, 5 KCl, 1 $CaCl_2$, 10 HEPES and 10 glucose, balanced to pH 7.2 ± 0.05 with NaOH. Drugs were diluted from concentrated stock solutions (**5** stock = 10 mM in dH_20; **7-11** stocks = 10 mM in 75% HEPES buffer and 25% ethanol) in extracellular solution each day of experiments. Whole-cell currents were recorded using an Axopatch 200B patch-clamp amplifier (Molecular Devices). Current signal was low-pass filtered at 1 kHz and sampled at 2 kHz in pClamp 10 (Molecular Devices). Series resistance was 10-15 MΩ. Solutions containing agonists (100 μM NMDA and 10 μM glycine) or agonists and 10 μM blocker were applied by piezoelectric translation (P-601.30; Physik Instrumente) of a theta-barrel application tool made from borosilicate glass (1.5 mm o.d.; Sutter Instruments).

For Figures 5–9, cells were maintained as previously described[54] in DMEM supplemented with 10% fetal bovine serum, 1% GlutaMAX (Thermo Fisher Scientific), and for some experiments 1% penicillin/streptomycin (Sigma). Cells were plated at 1 x 10^5 cells/dish in 35 mm petri dishes with three 15 mm glass coverslips treated with poly D-lysine (0.1 mg/ml) and rat-tail collagen (0.1 mg/ml, BD Biosciences). 12-24 hours after plating, the cells were transfected using FuGENE 6 Transfection Reagent (Promega) as previously described.[54] Culture medium was supplemented with 200 μM dl-APV at the time of transfection to prevent NMDAR-mediated cell death. Whole-cell voltage-clamp recordings were performed 18-30 hours after transfection. Pipettes were pulled from borosilicate capillary tubing (OD = 1.5 mm, ID = 0.86 mm) using a Flaming Brown P-97 electrode puller (Sutter Instruments) and subsequently fire-polished to a resistance of 2.5 – 4.5 MΩ using an in-house fabricated microforge. Intracellular pipette solution contained (in mM): 130 CsCl, 10 HEPES, 10 BAPTA, and 4 MgATP with pH balanced to 7.2 ± 0.05 with CsOH and an osmolality of 280 ± 10 mOsm. Extracellular recording solution contained (in mM) 140 NaCl, 2.8

KCl, 1 CaCl$_2$, 10 HEPES, 0.01 EDTA, and 0.1 glycine, and was balanced to pH 7.2 ± 0.05 with NaOH and to osmolality 290 ± 10 mOsm with sucrose. Drugs were diluted from concentrated stock solutions (**5** stock = 10 mM in dH$_2$0; **7**, **8**, and **11** stocks = 40 mM in 100% DMSO) in extracellular solution each day of experiments. Whole-cell currents were recorded using either an Axopatch 1D or Axopatch 200A patch-clamp amplifier (Molecular Devices). The current signal was low-pass filtered at 5 kHz and sampled at 20 kHz in pClamp 10 (Molecular Devices). Series resistance was compensated 80-90% in all experiments. A –6 mV liquid junction potential between the intracellular pipette solution and extracellular solution was corrected in all experiments. Glutamate and drug solutions were delivered to the cell via an in-house fabricated ten-barreled gravity-fed fast perfusion system.[40,54]

Data Analysis. The percentage of channel block, unblock and recovery shown in Figures 3 – 4 were measured with the following protocol: at a holding potential of –60 mV, NMDA (100 μM) and glycine (10 μM) were applied until current reached a clear steady-state (about 90 s). Then compounds **5**, **7**, **8**, **9**, **10** or **11** were rapidly applied by piezo control (1 ms solution exchange) for 30 seconds as described.[55] During the application of the blocker, a 5-s voltage step to +60 mV was applied in order to study the voltage dependence of block. Blockers were then removed in the presence of agonists to allow recovery of the current. During this period (around 1 min) a second voltage step (5 s duration) to +60 mV was applied. Finally, agonists were removed. Percentage of block was calculated by dividing steady state current in the presence of the blocker by steady state current in the absence of the blocker. Percentage of unblock was calculated by dividing the steady state current after blocker removal by the steady state current before blocker application. Finally, the voltage dependence (% of block at +60 mV) was calculated by using Equation 1:

$$\% \ of \ block = 100 - (\frac{I_{+60 \ (Drug)}}{I_{+60 \ (Agonist)}} * 100)$$

where $I_{+60(Drug)}$ is the steady state current at the holding voltage of +60 mV in the presence of agonists and the blocker, and $I_{+60(Agonist)}$ is the steady state current at +60 mV in the presence of agonists but absence of the blocker.

Concentration-inhibition relations were measured using the protocol shown in Figures 5–8, A and B. Glutamate (1 mM) was applied until current reached steady-state (20 s), then **5, 7, 8, or 11** at the plotted concentration was applied in the presence of glutamate until a new steady-state current level was reached (30 s). Glutamate in the absence of drug was then reapplied for 30 s to allow drug unbinding and recovery from inhibition. Cells in which recovery from inhibition did not reach 90% of steady-state current during initial glutamate application were excluded from analysis. IC$_{50}$ and n$_H$ (Hill coefficient) were estimated by fitting Equation 2 to concentration-inhibition data:

$$\frac{I_{Drug}}{I_{Glu}} = \frac{1}{1 + (\frac{[Drug]}{IC_{50}})^{n_H}}$$

where I_{Drug}/I_{Glu} was calculated as the mean current over the final 1 s of drug application (I_{Drug}) divided by the average of the mean steady state currents (final 1 s) elicited by glutamate before and after drug application (I_{Glu}). IC_{50} and n_H were free parameters during fitting.

Voltage dependence of block by **5, 7, 8**, and **11** was measured using the protocol shown in Figures 5–8, C and D. Cells were subjected to voltage jumps from -65 mV to nine voltages ranging from -105 to +55 mV. The protocol at each voltage consisted of: a 4-s wait in extracellular solution following the voltage step; application of 1 mM glutamate for 10 s; application of drug with 1 mM glutamate for 15 s; application of 1 mM glutamate for 15 s to allow drug unbinding; application of extracellular solution for 2 s. Voltage was then returned to -65 mV for 4 s before the next voltage

jump was made. ~2 times the IC_{50} of each drug was used in voltage dependence experiments.

Voltage dependence of block was calculated using Equation 3:

$$\frac{I_{Drug}}{I_{Glu}} = \frac{1}{1 + \frac{[Drug]}{IC_{50}(-65\ mV)e^{\frac{V_m+65}{V_0}}}}$$

where IC_{50} (–65 mV) is the IC_{50} at –65 mV calculated in concentration-inhibition experiments, and V_0 represents the change in voltage (in mV) that results in an e-fold change in the IC_{50} of the drug. I_{Drug}/I_{Glu} was calculated as described for concentration-inhibition data. V_0 was the only free parameter during fitting. An estimate of the fraction of the total membrane voltage field felt by the blocker at its binding site (δ)[52] was calculated using Equation 4:

$$\delta = \frac{RT}{V_0 zF}$$

Where R, T, z and F have their usual meanings. Note that, although δ is useful for comparing voltage dependence of blockers, voltage dependence of NMDAR channel block is influenced by permeant ions.[56] Therefore, δ should be used only as a rough estimate of binding site location in the voltage field.

ASSOCIATED CONTENT

Supporting Information.

The following files are available free of charge on the ACS Publications website at DOI:.

General methods for the chemical synthesis. Description of the synthesis and characterization of intermediates **13-16**. (PDF).

AUTHOR INFORMATION

Corresponding Author

*Phone: +1 4126244295. E-mail: jjohnson@pitt.edu

*Phone: +34 934024533. E-mail: svazquez@ub.edu

Author Contributions

┃These authors (R. L. and M. B. P.) contributed equally to this work. R. L. synthesized and characterized the new compounds, **7** and **8**. A. L. T. synthesized known compounds **9**, **10** and **11** and together with E. G.-B. performed electrophysiological experiments on compounds **5** and **7** – **11**. M. B. P. performed the electrophysiological experiments with compounds **5**, **7**, **8** and **11**; L. L.-G. and F. X. S. studied the antagonist activity at NMDA receptors in primary cultures of rat cerebellar granule neurons; M. B. P., D. S., F. X. S., J. W. J. and S. V. wrote the manuscript; D. S., F. X. S., J. W. J. and S. V. designed the study and supervised the project. All authors have given approval to the final version of the manuscript.

Notes

The authors declare no competing financial interest.

ABBREVIATIONS

AD, Alzheimer's disease; AMPA, (*S*)-2-amino-3-(3-hydroxy-5-methylisoxazol-4-yl)propionic

acid; iGluRs, ionotropic glutamate receptors; NMDA, *N*-methyl-*D*-aspartic acid; NMDAR,

NMDA receptor; PD, Parkinson's disease.

REFERENCES

1. Parsons, C. G., Danysz, W., Quack, G. (1998) Glutamate in CNS disorders as a target for drug development: an update. *Drug News & Perspectives 11*, 523-569.
2. Zhou, Y., Danbolt, N. C. (2014) Glutamate as a neurotransmitter in the healthy brain. *J. Neural Transm. 121*, 799-817.
3. Dingledine, R., Borges, K., Bowie, D., Traynelis, S. F. (1999) The glutamate receptor ion channels. *Pharmacol. Rev. 51*, 7-61.
4. Mayer, M. L., Armstrong, N. (2004) Structure and function of glutamate receptor ion channels. *Ann. Rev. Physiol. 66*, 161-181.
5. Traynelis, S. F., Wollmuth, L. P., McBain, C. J., Menniti, F. S., Vance, K. M., Ogden, K. K., Hansen, K. B., Yuan, H., Myers, S. J., Dingledine, R. (2010) Glutamate receptor ion channels: structure, regulation, and function. *Pharmacol. Rev. 62*, 405-496.
6. McBain, C. J., Mayer, M. L. (1994) *N*-methyl-*D*-aspartic acid receptor structure and function. *Physiol. Rev. 74*, 723-760.
7. Danysz, W., Parsons, C. G. (1998) Glycine and *N*-methyl-*D*-aspartate receptors: physiological significance and possible therapeutic applications. *Pharmacol. Rev. 50*, 597-664.
8. Iacobucci, G. J., Popescu, G. K. (2017) NMDA receptors: linking physiological output to biophysical operation. *Nat. Rev. Neurosci. 18*, 236-249.
9. Karakas, E., Furukawa, H. (2014) Crystal structure of a heterotetrameric NMDA receptor ion channel. *Science 344*, 992-997.
10. Lee, C.-H., Lü, W., Michel, J. C., Goehring, A., Du, J., Song, X., Gouaux, E. (2014) NMDA receptor structures reveal subunit arrangement and pore architecture. *Nature 511*, 191-197.
11. Zhu, S., Stein, R. A., Yoshioka, C., Lee, C.-H., Goehring, A., Mchaourab, H. S., Gouaux, E. (2016) Mechanism of NMDA receptor inhibition and activation. *Cell 165*, 704-714.
12. Zhou, Q., Sheng, M. (2013) NMDA receptors in nervous system diseases. *Neuropharmacology 74*, 69-75.
13. Tajima, N., Karakas, E., Grant, T., Simorowski, N., Díaz-Avalos, R., Grigorieff, N., Furukawa, H. (2016) Activation of NMDA receptors and the mechanism of inhibition by ifenprodil. *Nature 534*, 63-68.
14. Lü, W., Du, J., Goehring, A., Gouaux, E. (2017) Cryo-EM structures of the triheteromeric NMDA receptor and its allosteric modulation. *Science 355*, eaal3729.
15. Cull-Candy, S., Brickley, S., Farrant, M. (2001) NMDA receptor subunits: diversity, development and disease. *Curr. Opin. Neurobiol. 11*, 327-335.
16. Paoletti, P., Bellone, C., Zhou, Q. (2013) NMDA receptor subunit diversity: impact on receptor properties, synaptic plasticity and disease. *Nat. Rev. Neurosci. 14*, 383-400.

17. Glasgow, N. G., Siegler Retchless, B., Johnson, J. W. (2015) Molecular bases of NMDA receptor subtype-dependent properties. *J. Physiol. 593*, 83-95.
18. Morris, R. G. (2013) NMDA receptors and memoring encoding. *Neuropharmacology 74*, 32-40.
19. Kalia, L. V., Kalia, S. K., Salter, M. W. (2008) NMDA receptors in clinical neurology: excitatory times ahead. *Lancet Neurol. 7*, 742-755.
20. Mota, S. I., Ferreira, I. L., Rego, C. (2014) Dysfunctional synapse in Alzhimer's disease – A focus on NMDA receptors. *Neuropharmacology 76*, 16-26.
21. Ikonomidou, C., Turski, L. (2002) Why did NMDA receptor antagonists fail clinical trials for stroke and traumatic brain injury? *Lancet Neurol. 1*, 383-386.
22. Lipton, S. A. (2004) Failures and successes of NMDA receptor antagonists: molecular basis for the use of open-channel blockers like memantine in the treatment of acute and chronic neurologic insults. *NeuroRx 1*, 101-110.
23. Muir, K. W. (2006) Glutamate-based therapeutic approaches: clinical trials with NMDA antagonists. *Curr. Opin. Pharmacol. 6*, 53-60.
24. Blanpied, T. A., Clarke, R. J., Johnson, J. W. (2005) Amantadine inhibits NMDA receptors by accelerating channel closure during channel block. *J. Neurosci. 25*, 3312-3322.
25. Johnson, J. W., Kotermanski, S. E. (2006) Mechanism of action of memantine. *Curr. Opin. Pharmacol. 6*, 61-67.
26. Johnson, J. W., Glasgow, N. G., Povysheva, N. V. (2015) Recent insights into the mode of action of memantine and ketamine. *Curr. Opin. Pharmacol. 20*, 54-63.
27. Olney, J.W., Labruyere, J., Price, M.T. (1989). Pathological Changes Induced in Cerebrocortical Neurons by Phencyclidine and Related Drugs. Science 244: 1360-1362.
28. Danysz, W., Parsons, C. G., Kornhuber, J., Schmidt, W. J., Quack, G. (1997) Aminoadamantanes as NMDA receptor antagonists and antiparkinsonian agents—preclinical studies. *Neurosci. Biobehav. Rev. 21*, 455-468.
29. Lipton, S. A. (2006) Paradigm shift in neuroprotection by NMDA receptor blockade: memantine and beyond. *Nat. Rev. Drug Discovery 5*, 160-170.
30. Hubsher, G., Haider, M., Okun, M. S. (2012) Amantadine: the journey from fighting flu to treating Parkinson disease. *Neurology 78*, 1096-1099.
31. Danysz, W., Parsons, C. G. (2012) Alzheimer's disease, β-amyloid, glutamate, NMDA receptors and memantine – searching for the connections. *British J. Pharmacol. 167*, 324-352.
32. Alam, S., Lingenfelter K. S., Bender, A. M., Lindsley, C. W. (2017) Classics in chemical neuroscience: memantine. *ACS Chem. Neurosci. 8*, 1823-1829.
33. Chen, H.-S. V., Lipton, S. A. (2006) The chemical biology of clinically tolerated NMDA receptor antagonists. *J. Neurochem. 97*, 1611-1626.
34. Lipton, S. A. (2007) Pathologically activated therapeutics for neuroprotection. *Nat. Rev. Neurosci. 8*, 803-808.
35. Hardingham, G. E., Bading, H. (2010) Synaptic versus extrasynaptic NMDA receptor signaling: implications for neurodegenerative disorders. *Nat. Rev. Neurosci. 11*, 682-696.
36. Gladding, C. M., Raymond, L. A. (2011) Mechanisms underlying NMDA receptor synaptic/extrasynaptic distribution and function. *Mol. Cell Neurosci. 48*, 308-320.
37. Parsons, M. P., Raymond, L. A. (2014) Extrasynaptic NMDA receptor involvement in central nervous system disorders. *Neuron 82*, 279-293.

38. Wroge, C.M., J. Hogins, L. Eisenman, S. Mennerick (2012) Synaptic NMDA receptors mediate hypoxic excitotoxic death. J. Neurosci. 32(19): 6732-6742.

39. Zhou, X., D. Hollern, J. Liao, E. Andrechek, H. Wang (2013) NMDA receptor-mediated excitotoxicity depends on the coactivation of synaptic and extrasynaptic receptors. Cell Death Dis. 4: e560.

40. Glasgow, N. G., Povysheva, N. V., Azofeifa, A. M., Johnson, J. W. (2017) Memantine and ketamine differentially alter NMDA receptor desensitization. *J. Neurosci. 37*, 9686-9704.

41. Matsunaga, S., Kishi, T., Iwata, N. (2015) Memantine monotherapy for Alzheimer's Disease: a systematic review and meta-analysis. *PLoS One 10*, e0123289.

42. Glling, K., Jatzke, C., Wollenburg, C., Vanejevs, M., Kauss, V., Jirgensons, A., Parsons, C. G. (2007) A novel class of amino-alkylcyclohexanes as uncompetitive, fast, voltage-dependent, *N*-methyl-*D*-aspartate (NMDA) receptor antagonists – in vitro characterization. *J. Neural Transm. 114*, 1529-1537.

43. Rammes, G. (2009) Neramexane: a moderate-affinity NMDA receptor channel blocker: new prospects and indications. *Expert Rev. Clin. Pharmacol. 2*, 231-238.

44. Camps, P., Duque, M. D., Vázquez, S., Naesens, L., DeClercq, E., Sureda, F. X., López-Querol, M., Camins, A., Pallàs, M., Prathalingam, S. R., Kelly, J. M., Romero, V., Ivorra, D., Cortés, D. (2008) Synthesis and pharmacological evaluation of several ring-contracted amantadine analogs. *Bioorg. Med. Chem. 16*, 9925-9936.

45. Valverde, E., Sureda, F. X., Vázquez, S. (2014) Novel benzopolycyclic amines with NMDA receptor antagonist activity. *Bioorg. Med. Chem. 22*, 2678-2683.

46. Blanpied, T.A., Boeckman, F.A., Aizenman, E., Johnson, J.W. (1997) Trapping channel block of NMDA-activated responses by amantadine and memantine. J. Neurophysiol. 77, 309-323.

47. Limapichat, W., Yu, W. Y., Branigan, E., Lester, H. A., Dougherty, D. A. (2013) Key biding interactions for memantine in the NMDA receptor. *ACS Chem. Neurosci. 4*, 255-260.

48. Torres, E., Leiva, R., Gazzarrini, S., Rey-Carrizo, M., Frigolé-Vivas, M., Moroni, A., Naesens, L., Vázquez, S. (2014) Azapropellanes with anti-influenza A virus activity. *ACS Med. Chem. Lett. 5*, 831-836.

49. Rey-Carrizo, M., Barniol-Xicota, M., Ma, C., Frigolé-Vivas, M., Torres, E., Naesens, L., Llabrés, S., Juárez-Jiménez, J., Luque, F. J., DeGrado, W. F., Lamb, R. A., Pinto, L. H., Vázquez, S. (2014) Easily accessible polycyclic amines that inhibit the wild-type and amantadine-resistant mutants of the M2 channel of influenza A virus. *J. Med. Chem. 57*, 5738–5747.

50. Avila, W. B., Silva, R. A. (1970) 3,4,8,9-Tetramethyltetracyclo[4.4.0.0^{3,9}.0^{4,8}]decane-1,6-dioic anhydride. *J. Chem. Soc. D,* 94-95.

51. Canudas, A. M., Pubill, D., Sureda, F. X., Verdaguer, E., Camps, P., Muñoz-Torrero, D., Jiménez, A., Camins, A., Pallàs, M. (2003) Neuroprotective effects of (+/−)-huprine Y on in vitro and in vivo models of excitotoxicity damage. *Exp. Neurol. 180*, 123–130.

52. Woodhull, A. M. (1973) Ionic Blockage of Sodium Channels in Nerve. *J. Gen. Physiol. 61*, 687-708.

53. Gratacos-Batlle, E., Yefimenko, N., Cascos-García, H., Soto, D. (2014) AMPAR interacting protein CPT1C enhances surface expression of GluA1-containing receptors. *Front. Cell. Neurosci. 8*, 469.

54. Glasgow, N. G., Johnson, J. W. *Whole-Cell Patch-Clamp Analysis of Recombinant NMDA Receptor Pharmacology Using Brief Glutamate Applications*, in *Patch-Clamp Methods and Protocols*, M. Martina and S. Taverna, Editors. 2014, Springer New York: New York, NY. p. 23-41.

55. Soto, D., Olivella, M., Grau, C., Armstrong, J., Alcon, C., Gasull, X., Gómez de Salazar, M., Gratacòs-Batlle, E., Ramos-Vicente, D., Fernández-Dueñas, V., Ciruela, F., Bayés, À., Sindreu, C., López-Sala, A., García-Cazorla, À., Altafaj, X. (2018) Rett-like severe encephalopathy caused by a de novo GRIN2B mutation is attenuated by D-serine dietary supplement. *Biol Psychiatry 83*, 160-172.

56. Antonov, S. M., Gmiro, V.E., Johnson, J. W. (1998) Binding sites for permeant ions in the channel of NMDA receptors and their effects on channel block. *Nature Neurosci. 1*, 451-461.

GRAPHICAL TABLE OF CONTENTS
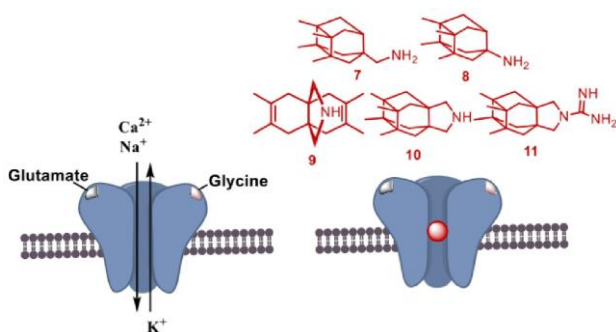
REFERENCES

Abdallah, C.G., Averill, L.A., & Krystal, J.H. (2015) Ketamine as a promising prototype for a new generation of rapid-acting antidepressants. *Ann. N. Y. Acad. Sci.*, **1344**, 66–77.

Adams, P.R. (1975) A model for the procaine end-plate current. *J. Physiol. (Lond.)*, **246**, 61P–63P.

Adams, P.R. (1976) Drug blockade of open end-plate channels. *J. Physiol. (Lond.)*, **260**, 531–552.

Ady, V., Perroy, J., Tricoire, L., Piochon, C., Dadak, S., Chen, X., Dusart, I., Fagni, L., Lambolez, B., & Levenes, C. (2014) Type 1 metabotropic glutamate receptors (mGlu1) trigger the gating of GluD2 delta glutamate receptors. *EMBO Rep.*, **15**, 103–109.

Akazawa, C., Shigemoto, R., Bessho, Y., Nakanishi, S., & Mizuno, N. (1994) Differential expression of five N-methyl-D-aspartate receptor subunit mRNAs in the cerebellum of developing and adult rats. *J. Comp. Neurol.*, **347**, 150–160.

Akgül, G. & McBain, C.J. (2016) Diverse roles for ionotropic glutamate receptors on inhibitory interneurons in developing and adult brain. *J. Physiol. (Lond.)*, **594**, 5471–5490.

Alam, S., Lingenfelter, K.S., Bender, A.M., & Lindsley, C.W. (2017) Classics in chemical neuroscience: memantine. *ACS Chem. Neurosci.*, **8**, 1823–1829.

Amidfar, M., Réus, G.Z., Quevedo, J., & Kim, Y.-K. (2018) The role of memantine in the treatment of major depressive disorder: Clinical efficacy and mechanisms of action. *Eur. J. Pharmacol.*, **827**, 103–111.

Antonov, S.M., Gmiro, V.E., & Johnson, J.W. (1998) Binding sites for permeant ions in the channel of NMDA receptors and their effects on channel block. *Nat. Neurosci.*, **1**, 451–461.

Antonov, S.M. & Johnson, J.W. (1996) Voltage-dependent interaction of open-channel blocking molecules with gating of NMDA receptors in rat cortical neurons. *J. Physiol. (Lond.)*, **493 (Pt 2)**, 425–445.

Antonov, S.M., Johnson, J.W., Lukomskaya, N.Y., Potapyeva, N.N., Gmiro, V.E., & Magazanik, L.G. (1995) Novel adamantane derivatives act as blockers of open ligand-gated channels and as anticonvulsants. *Mol. Pharmacol.*, **47**, 558–567.

Araki, K., Meguro, H., Kushiya, E., Takayama, C., Inoue, Y., & Mishina, M. (1993) Selective expression of the glutamate receptor channel delta 2 subunit in cerebellar Purkinje cells. *Biochem. Biophys. Res. Commun.*, **197**, 1267–1276.

Armstrong, C.M. (1971) Interaction of tetraethylammonium ion derivatives with the potassium channels of giant axons. *J. Gen. Physiol.*, **58**, 413–437.

Ascher, P. & Nowak, L. (1988) The role of divalent cations in the N-methyl-D-aspartate responses of mouse central neurones in culture. *J. Physiol. (Lond.)*, **399**, 247–266.

Atilgan, A.R., Durell, S.R., Jernigan, R.L., Demirel, M.C., Keskin, O., & Bahar, I. (2001) Anisotropy of fluctuation dynamics of proteins with an elastic network model. *Biophys. J.*, **80**, 505–515.

Babiec, W.E., Guglietta, R., Jami, S.A., Morishita, W., Malenka, R.C., & O'Dell, T.J. (2014) Ionotropic NMDA receptor signaling is required for the induction of long-term depression in the mouse hippocampal CA1 region. *J. Neurosci.*, **34**, 5285–5290.

Bahar, I., Lezon, T.R., Bakan, A., & Shrivastava, I.H. (2010) Normal mode analysis of biomolecular structures: functional mechanisms of membrane proteins. *Chem. Rev.*, **110**, 1463–1497.

Benamer, N., Marti, F., Lujan, R., Hepp, R., Aubier, T.G., Dupin, A.A.M., Frébourg, G., Pons, S., Maskos, U., Faure, P., Hay, Y.A., Lambolez, B., & Tricoire, L. (2018) GluD1, linked to schizophrenia, controls the burst firing of dopamine neurons. *Mol. Psychiatry*, **23**, 691–700.

Benveniste, M., Clements, J., Vyklický, L., & Mayer, M.L. (1990) A kinetic analysis of the modulation of N-methyl-D-aspartic acid receptors by glycine in mouse cultured hippocampal neurones. *J. Physiol. (Lond.)*, **428**, 333–357.

Benveniste, M. & Mayer, M.L. (1991) Kinetic analysis of antagonist action at N-methyl-D-aspartic acid receptors. Two binding sites each for glutamate and glycine. *Biophys. J.*, **59**, 560–573.

Benveniste, M. & Mayer, M.L. (1995) Trapping of glutamate and glycine during open channel block of rat hippocampal neuron NMDA receptors by 9-aminoacridine. *J. Physiol. (Lond.)*, **483 (Pt 2)**, 367–384.

Bers, D.M., Patton, C.W., & Nuccitelli, R. (2010) A practical guide to the preparation of Ca(2+) buffers. *Methods Cell Biol.*, **99**, 1–26.

Berthier, M.L., Green, C., Lara, J.P., Higueras, C., Barbancho, M.A., Dávila, G., & Pulvermüller, F. (2009) Memantine and constraint-induced aphasia therapy in chronic poststroke aphasia. *Ann. Neurol.*, **65**, 577–585.

Bhattacharya, S., Khatri, A., Swanger, S.A., DiRaddo, J.O., Yi, F., Hansen, K.B., Yuan, H., & Traynelis, S.F. (2018) Triheteromeric GluN1/GluN2A/GluN2C NMDARs with Unique Single-Channel Properties Are the Dominant Receptor Population in Cerebellar Granule Cells. *Neuron*, **99**, 315–328.e5.

Blanpied, T.A., Boeckman, F.A., Aizenman, E., & Johnson, J.W. (1997) Trapping channel block of NMDA-activated responses by amantadine and memantine. *J. Neurophysiol.*, **77**, 309–323.

Blanpied, T.A., Clarke, R.J., & Johnson, J.W. (2005) Amantadine inhibits NMDA receptors by accelerating channel closure during channel block. *J. Neurosci.*, **25**, 3312–3322.

Bolshakov, K.V., Gmiro, V.E., Tikhonov, D.B., & Magazanik, L.G. (2003) Determinants of trapping block of N-methyl-d-aspartate receptor channels. *J. Neurochem.*, **87**, 56–65.

Bondi, C., Matthews, M., & Moghaddam, B. (2012) Glutamatergic animal models of schizophrenia. *Curr. Pharm. Des.*, **18**, 1593–1604.

Bowie, D. (2008) Ionotropic glutamate receptors & CNS disorders. *CNS Neurol Disord Drug Targets*, **7**, 129–143.

Bresink, I., Benke, T.A., Collett, V.J., Seal, A.J., Parsons, C.G., Henley, J.M., & Collingridge, G.L. (1996) Effects of memantine on recombinant rat NMDA receptors expressed in HEK 293 cells. *Br. J. Pharmacol.*, **119**, 195–204.

Brickley, S.G., Misra, C., Mok, M.H.S., Mishina, M., & Cull-Candy, S.G. (2003) NR2B and NR2D subunits coassemble in cerebellar Golgi cells to form a distinct NMDA receptor subtype restricted to extrasynaptic sites. *J. Neurosci.*, **23**, 4958–4966.

Brothwell, S.L.C., Barber, J.L., Monaghan, D.T., Jane, D.E., Gibb, A.J., & Jones, S. (2008) NR2B-and NR2D-containing synaptic NMDA receptors in developing rat substantia nigra pars compacta dopaminergic neurones. *J. Physiol. (Lond.)*, **586**, 739–750.

Brunet, A., Bonni, A., Zigmond, M.J., Lin, M.Z., Juo, P., Hu, L.S., Anderson, M.J., Arden, K.C., Blenis, J., & Greenberg, M.E. (1999) Akt promotes cell survival by phosphorylating and inhibiting a Forkhead transcription factor. *Cell*, **96**, 857–868.

Budavari, S. (1989) *The Merck Index: AnEncyclopedia of Chemicals, Drugs, and Biologicals*, 11th edn. Merck, Rahway, NJ, USA.

Burnashev, N., Monyer, H., Seeburg, P.H., & Sakmann, B. (1992) Divalent ion permeability of AMPA receptor channels is dominated by the edited form of a single subunit. *Neuron*, **8**, 189–198.

Burnashev, N., Schoepfer, R., Monyer, H., Ruppersberg, J.P., Günther, W., Seeburg, P.H., & Sakmann, B. (1992) Control by asparagine residues of calcium permeability and magnesium blockade in the NMDA receptor. *Science*, **257**, 1415–1419.

Burnashev, N. & Szepetowski, P. (2015) NMDA receptor subunit mutations in neurodevelopmental disorders. *Curr. Opin. Pharmacol.*, **20**, 73–82.

Burnashev, N., Zhou, Z., Neher, E., & Sakmann, B. (1995) Fractional calcium currents through recombinant GluR channels of the NMDA, AMPA and kainate receptor subtypes. *J. Physiol. (Lond.)*, **485 (Pt 2)**, 403–418.

Carter, B.C. & Jahr, C.E. (2016) Postsynaptic, not presynaptic NMDA receptors are required for spike-timing-dependent LTD induction. *Nat. Neurosci.*, **19**, 1218–1224.

Case, D.A., Cerutti, D.S., Cheatham, T.E.I., Darden, T.A., Duke, R.E., Giese, T.J., Gohlke, H., Goetz, A.W., Greene, D., Homeyer, N., Izadi, S., Kovalenko, A., Lee, T.S., LeGrand, S., Li, P.L.C., Liu, J., Luchko, T., Luo, R., Mermelstein, D., Merz, K.M., Monard, G., Nguyen, H., Omelyan, I., Onufriev, A., Pan, F., Qi, R., Roe, D.R., Roitberg, A., Sagui, C., Simmerling, C.L., Botello-Smith, W.M., Swails, J., Walker, R.C., Wang, J., Wolf, R.M., Wu, X., Xiao, L., York, D.M., & Kollman, P.A. (2017) *Amber18* . University of San Francisco.

Chang, H.-R. & Kuo, C.-C. (2008) The activation gate and gating mechanism of the NMDA receptor. *J. Neurosci.*, **28**, 1546–1556.

Chazot, P.L., Cik, M., & Stephenson, F.A. (1995) An investigation into the role of N-glycosylation in the functional expression of a recombinant heteromeric NMDA receptor. *Mol Membr Biol*, **12**, 331–337.

Chazot, P.L., Coleman, S.K., Cik, M., & Stephenson, F.A. (1994) Molecular characterization of N-methyl-D-aspartate receptors expressed in mammalian cells yields evidence for the coexistence of three subunit types within a discrete receptor molecule. *J. Biol. Chem.*, **269**, 24403–24409.

Chazot, P.L. & Stephenson, F.A. (1997) Molecular dissection of native mammalian forebrain NMDA receptors containing the NR1 C2 exon: direct demonstration of NMDA receptors comprising NR1, NR2A, and NR2B subunits within the same complex. *J. Neurochem.*, **69**, 2138–2144.

Chen, H.S. & Lipton, S.A. (1997) Mechanism of memantine block of NMDA-activated channels in rat retinal ganglion cells: uncompetitive antagonism. *J. Physiol. (Lond.)*, **499 (Pt 1)**, 27–46.

Chen, H.-S.V. & Lipton, S.A. (2005) Pharmacological implications of two distinct mechanisms of interaction of memantine with N-methyl-D-aspartate-gated channels. *J. Pharmacol. Exp. Ther.*, **314**, 961–971.

Chen, H.-S.V. & Lipton, S.A. (2006) The chemical biology of clinically tolerated NMDA receptor antagonists. *J. Neurochem.*, **97**, 1611–1626.

Chen, P.E., Errington, M.L., Kneussel, M., Chen, G., Annala, A.J., Rudhard, Y.H., Rast, G.F., Specht, C.G., Tigaret, C.M., Nassar, M.A., Morris, R.G.M., Bliss, T.V.P., & Schoepfer, R. (2009) Behavioral deficits and subregion-specific suppression of LTP in mice expressing a population of mutant NMDA receptors throughout the hippocampus. *Learn. Mem.*, **16**, 635–644.

Chen, X., Shu, S., & Bayliss, D.A. (2009) HCN1 channel subunits are a molecular substrate for hypnotic actions of ketamine. *J. Neurosci.*, **29**, 600–609.

Choi, D.W. (1987) Ionic dependence of glutamate neurotoxicity. *J. Neurosci.*, **7**, 369–379.

Choi, D.W. (1992) Excitotoxic cell death. *J. Neurobiol.*, **23**, 1261–1276.

Chou, T.-H., Tajima, N., Romero-Hernandez, A., & Furukawa, H. (2020) Structural basis of functional transitions in mammalian NMDA receptors. *Cell*, **182**, 357–371.e13.

Clarke, R.J., Glasgow, N.G., & Johnson, J.W. (2013) Mechanistic and structural determinants of NMDA receptor voltage-dependent gating and slow Mg2+ unblock. *J. Neurosci.*, **33**, 4140–4150.

Clarke, R.J. & Johnson, J.W. (2006) NMDA receptor NR2 subunit dependence of the slow component of magnesium unblock. *J. Neurosci.*, **26**, 5825–5834.

Clarke, R.J. & Johnson, J.W. (2008) Voltage-dependent gating of NR1/2B NMDA receptors. *J. Physiol. (Lond.)*, **586**, 5727–5741.

Clements, J.D. & Westbrook, G.L. (1991) Activation kinetics reveal the number of glutamate and glycine binding sites on the N-methyl-D-aspartate receptor. *Neuron*, **7**, 605–613.

Corazza, O., Assi, S., & Schifano, F. (2013) From "Special K" to "Special M": the evolution of the recreational use of ketamine and methoxetamine. *CNS Neurosci Ther*, **19**, 454–460.

Costa, A.C. & Albuquerque, E.X. (1994) Dynamics of the actions of tetrahydro-9-aminoacridine and 9-aminoacridine on glutamatergic currents: concentration-jump studies in cultured rat hippocampal neurons. *J. Pharmacol. Exp. Ther.*, **268**, 503–514.

Courtney, K.R. (1975) Mechanism of frequency-dependent inhibition of sodium currents in frog myelinated nerve by the lidocaine derivative GEA. *J. Pharmacol. Exp. Ther.*, **195**, 225–236.

Danysz, W. & Parsons, C.G. (2012) Alzheimer's disease, β-amyloid, glutamate, NMDA receptors and memantine--searching for the connections. *Br. J. Pharmacol.*, **167**, 324–352.

Danysz, W., Parsons, C.G., Kornhuber, J., Schmidt, W.J., & Quack, G. (1997) Aminoadamantanes as NMDA receptor antagonists and antiparkinsonian agents--preclinical studies. *Neurosci. Biobehav. Rev.*, **21**, 455–468.

Di Iorio, G., Baroni, G., Lorusso, M., Montemitro, C., Spano, M.C., & di Giannantonio, M. (2017) Efficacy of memantine in schizophrenic patients: A systematic review. *J. Amino Acids*, **2017**, 7021071.

Dick, O. & Bading, H. (2010) Synaptic activity and nuclear calcium signaling protect hippocampal neurons from death signal-associated nuclear translocation of FoxO3a induced by extrasynaptic N-methyl-D-aspartate receptors. *J. Biol. Chem.*, **285**, 19354–19361.

Dilmore, J.G. & Johnson, J.W. (1998) Open channel block and alteration of N-methyl-D-aspartic acid receptor gating by an analog of phencyclidine. *Biophys. J.*, **75**, 1801–1816.

Dong, X., Wang, Y., & Qin, Z. (2009) Molecular mechanisms of excitotoxicity and their relevance to pathogenesis of neurodegenerative diseases. *Acta Pharmacol Sin*, **30**, 379–387.

Dougherty, D.A. (2007) Cation-pi interactions involving aromatic amino acids. *J. Nutr.*, **137**, 1504S–1508S; discussion 1516S.

Dravid, S.M., Erreger, K., Yuan, H., Nicholson, K., Le, P., Lyuboslavsky, P., Almonte, A., Murray, E., Mosely, C., Barber, J., French, A., Balster, R., Murray, T.F., & Traynelis, S.F. (2007) Subunit-specific mechanisms and proton sensitivity of NMDA receptor channel block. *J. Physiol. (Lond.)*, **581**, 107–128.

Dunah, A.W., Luo, J., Wang, Y.H., Yasuda, R.P., & Wolfe, B.B. (1998) Subunit composition of N-methyl-D-aspartate receptors in the central nervous system that contain the NR2D subunit. *Mol. Pharmacol.*, **53**, 429–437.

Dunah, A.W. & Standaert, D.G. (2003) Subcellular segregation of distinct heteromeric NMDA glutamate receptors in the striatum. *J. Neurochem.*, **85**, 935–943.

Dutta, A., Krieger, J., Lee, J.Y., Garcia-Nafria, J., Greger, I.H., & Bahar, I. (2015) Cooperative Dynamics of Intact AMPA and NMDA Glutamate Receptors: Similarities and Subfamily-Specific Differences. *Structure*, **23**, 1692–1704.

Ehlers, M.D., Zhang, S., Bernhadt, J.P., & Huganir, R.L. (1996) Inactivation of NMDA receptors by direct interaction of calmodulin with the NR1 subunit. *Cell*, **84**, 745–755.

Emnett, C.M., Eisenman, L.N., Taylor, A.M., Izumi, Y., Zorumski, C.F., & Mennerick, S. (2013) Indistinguishable synaptic pharmacodynamics of the N-methyl-D-aspartate receptor channel blockers memantine and ketamine. *Mol. Pharmacol.*, **84**, 935–947.

Esmenjaud, J.-B., Stroebel, D., Chan, K., Grand, T., David, M., Wollmuth, L.P., Taly, A., & Paoletti, P. (2019) An inter-dimer allosteric switch controls NMDA receptor activity. *EMBO J.*, **38**.

Fedele, L., Newcombe, J., Topf, M., Gibb, A., Harvey, R.J., & Smart, T.G. (2018) Disease-associated missense mutations in GluN2B subunit alter NMDA receptor ligand binding and ion channel properties. *Nat. Commun.*, **9**, 957.

Ferrer-Montiel, A.V., Merino, J.M., Planells-Cases, R., Sun, W., & Montal, M. (1998) Structural determinants of the blocker binding site in glutamate and NMDA receptor channels. *Neuropharmacology*, **37**, 139–147.

Freudenthaler, S., Meineke, I., Schreeb, K.H., Boakye, E., Gundert-Remy, U., & Gleiter, C.H. (1998) Influence of urine pH and urinary flow on the renal excretion of memantine. *Br. J. Clin. Pharmacol.*, **46**, 541–546.

Gaillard, T. (2018) Evaluation of AutoDock and AutoDock Vina on the CASF-2013 Benchmark. *J. Chem. Inf. Model.*, **58**, 1697–1706.

Gantz, S.C., Moussawi, K., & Hake, H.S. (2020) Delta glutamate receptor conductance drives excitation of mouse dorsal raphe neurons. *Elife*, **9**.

Gardoni, F. & Di Luca, M. (2015) Targeting glutamatergic synapses in Parkinson's disease. *Curr. Opin. Pharmacol.*, **20**, 24–28.

Gideons, E.S., Kavalali, E.T., & Monteggia, L.M. (2014) Mechanisms underlying differential effectiveness of memantine and ketamine in rapid antidepressant responses. *Proc. Natl. Acad. Sci. USA*, **111**, 8649–8654.

Gielen, M., Le Goff, A., Stroebel, D., Johnson, J.W., Neyton, J., & Paoletti, P. (2008) Structural rearrangements of NR1/NR2A NMDA receptors during allosteric inhibition. *Neuron*, **57**, 80–93.

Gielen, M., Siegler Retchless, B., Mony, L., Johnson, J.W., & Paoletti, P. (2009) Mechanism of differential control of NMDA receptor activity by NR2 subunits. *Nature*, **459**, 703–707.

Gilling, K., Jatzke, C., Wollenburg, C., Vanejevs, M., Kauss, V., Jirgensons, A., & Parsons, C.G. (2007) A novel class of amino-alkylcyclohexanes as uncompetitive, fast, voltage-dependent, N-methyl-D-aspartate (NMDA) receptor antagonists--in vitro characterization. *J. Neural Transm.*, **114**, 1529–1537.

Gilling, K.E., Jatzke, C., Hechenberger, M., & Parsons, C.G. (2009) Potency, voltage-dependency, agonist concentration-dependency, blocking kinetics and partial untrapping of the uncompetitive N-methyl-D-aspartate (NMDA) channel blocker memantine at human NMDA (GluN1/GluN2A) receptors. *Neuropharmacology*, **56**, 866–875.

Gladding, C.M. & Raymond, L.A. (2011) Mechanisms underlying NMDA receptor synaptic/extrasynaptic distribution and function. *Mol. Cell. Neurosci.*, **48**, 308–320.

Glasgow, N.G. & Johnson, J.W. (2014) Whole-cell patch-clamp analysis of recombinant NMDA receptor pharmacology using brief glutamate applications. *Methods Mol. Biol.*, **1183**, 23–41.

Glasgow, N.G., Povysheva, N.V., Azofeifa, A.M., & Johnson, J.W. (2017) Memantine and ketamine differentially alter NMDA receptor desensitization. *J. Neurosci.*, **37**, 9686–9704.

Glasgow, N.G., Siegler Retchless, B., & Johnson, J.W. (2015) Molecular bases of NMDA receptor subtype-dependent properties. *J. Physiol. (Lond.)*, **593**, 83–95.

Glasgow, N.G., Wilcox, M.R., & Johnson, J.W. (2018) Effects of Mg2+ on recovery of NMDA receptors from inhibition by memantine and ketamine reveal properties of a second site. *Neuropharmacology*, **137**, 344–358.

Grand, T., Abi Gerges, S., David, M., Diana, M.A., & Paoletti, P. (2018) Unmasking GluN1/GluN3A excitatory glycine NMDA receptors. *Nat. Commun.*, **9**, 4769.

Gray, J.A., Shi, Y., Usui, H., During, M.J., Sakimura, K., & Nicoll, R.A. (2011) Distinct modes of AMPA receptor suppression at developing synapses by GluN2A and GluN2B: single-cell NMDA receptor subunit deletion in vivo. *Neuron*, **71**, 1085–1101.

Hansen, K.B., Ogden, K.K., Yuan, H., & Traynelis, S.F. (2014) Distinct functional and pharmacological properties of Triheteromeric GluN1/GluN2A/GluN2B NMDA receptors. *Neuron*, **81**, 1084–1096.

Hardingham, G.E. (2006) Pro-survival signalling from the NMDA receptor. *Biochem. Soc. Trans.*, **34**, 936–938.

Hardingham, G.E. & Bading, H. (2010) Synaptic versus extrasynaptic NMDA receptor signalling: implications for neurodegenerative disorders. *Nat. Rev. Neurosci.*, **11**, 682–696.

Hardingham, G.E., Fukunaga, Y., & Bading, H. (2002) Extrasynaptic NMDARs oppose synaptic NMDARs by triggering CREB shut-off and cell death pathways. *Nat. Neurosci.*, **5**, 405–414.

Hasbani, M.J., Hyrc, K.L., Faddis, B.T., Romano, C., & Goldberg, M.P. (1998) Distinct roles for sodium, chloride, and calcium in excitotoxic dendritic injury and recovery. *Exp. Neurol.*, **154**, 241–258.

Hatton, C.J. & Paoletti, P. (2005) Modulation of triheteromeric NMDA receptors by N-terminal domain ligands. *Neuron*, **46**, 261–274.

Heidmann, T. & Changeux, J.P. (1986) Characterization of the transient agonist-triggered state of the acetylcholine receptor rapidly labeled by the noncompetitive blocker [3H]chlorpromazine: additional evidence for the open channel conformation. *Biochemistry*, **25**, 6109–6113.

Higley, M.J. & Sabatini, B.L. (2012) Calcium signaling in dendritic spines. *Cold Spring Harb. Perspect. Biol.*, **4**, a005686.

Hille, B. (2001) *Ion Channels Of Excitable Membranes*, 3rd edn. Sinauer Associates Is An Imprint Of Oxford University Press, Sunderland, Mass.

Hof, P.R., Cox, K., Young, W.G., Celio, M.R., Rogers, J., & Morrison, J.H. (1991) Parvalbumin-Immunoreactive Neurons in the Neocortex are Resistant to Degeneration in Alzheimer?s Disease. *J. Neuropathol. Exp. Neurol.*, **50**, 451–462.

Hof, P.R. & Morrison, J.H. (2004) The aging brain: morphomolecular senescence of cortical circuits. *Trends Neurosci.*, **27**, 607–613.

Homayoun, H. & Moghaddam, B. (2007) NMDA receptor hypofunction produces opposite effects on prefrontal cortex interneurons and pyramidal neurons. *J. Neurosci.*, **27**, 11496–11500.

Huang, Z. & Gibb, A.J. (2014) Mg2+ block properties of triheteromeric GluN1-GluN2B-GluN2D NMDA receptors on neonatal rat substantia nigra pars compacta dopaminergic neurones. *J. Physiol. (Lond.)*, **592**, 2059–2078.

Hubsher, G., Haider, M., & Okun, M.S. (2012) Amantadine: the journey from fighting flu to treating Parkinson disease. *Neurology*, **78**, 1096–1099.

Hume, R.I., Dingledine, R., & Heinemann, S.F. (1991) Identification of a site in glutamate receptor subunits that controls calcium permeability. *Science*, **253**, 1028–1031.

Humphrey, W., Dalke, A., & Schulten, K. (1996) VMD: visual molecular dynamics. *J Mol Graph*, **14**, , 27.

Hynd, M.R., Scott, H.L., & Dodd, P.R. (2004) Glutamate-mediated excitotoxicity and neurodegeneration in Alzheimer's disease. *Neurochem. Int.*, **45**, 583–595.

Iacobucci, G.J. & Popescu, G.K. (2017) Resident Calmodulin Primes NMDA Receptors for Ca2+-Dependent Inactivation. *Biophys. J.*, **113**, 2236–2248.

Iacobucci, G.J. & Popescu, G.K. (2020) Ca2+-Dependent Inactivation of GluN2A and GluN2B NMDA Receptors Occurs by a Common Kinetic Mechanism. *Biophys. J.*, **118**, 798–812.

Ibrahim, L., Diaz Granados, N., Jolkovsky, L., Brutsche, N., Luckenbaugh, D.A., Herring, W.J., Potter, W.Z., & Zarate, C.A. (2012) A Randomized, placebo-controlled, crossover pilot trial of the oral selective NR2B antagonist MK-0657 in patients with treatment-resistant major depressive disorder. *J Clin Psychopharmacol*, **32**, 551–557.

Ikonomidou, C. & Turski, L. (2002) Why did NMDA receptor antagonists fail clinical trials for stroke and traumatic brain injury? *Lancet Neurol.*, **1**, 383–386.

Ishii, T., Moriyoshi, K., Sugihara, H., Sakurada, K., Kadotani, H., Yokoi, M., Akazawa, C., Shigemoto, R., Mizuno, N., & Masu, M. (1993) Molecular characterization of the family of the N-methyl-D-aspartate receptor subunits. *J. Biol. Chem.*, **268**, 2836–2843.

Jackson, M.E., Homayoun, H., & Moghaddam, B. (2004) NMDA receptor hypofunction produces concomitant firing rate potentiation and burst activity reduction in the prefrontal cortex. *Proc. Natl. Acad. Sci. USA*, **101**, 8467–8472.

Jalali-Yazdi, F., Chowdhury, S., Yoshioka, C., & Gouaux, E. (2018) Mechanisms for zinc and proton inhibition of the glun1/glun2a NMDA receptor. *Cell*, **175**, 1520–1532.e15.

Javitt, D.C. (2004) Glutamate as a therapeutic target in psychiatric disorders. *Mol. Psychiatry*, **9**, , 979.

Johnson, J.W. & Ascher, P. (1987) Glycine potentiates the NMDA response in cultured mouse brain neurons. *Nature*, **325**, 529–531.

Johnson, J.W., Glasgow, N.G., & Povysheva, N.V. (2015) Recent insights into the mode of action of memantine and ketamine. *Curr. Opin. Pharmacol.*, **20**, 54–63.

Johnson, J.W. & Kotermanski, S.E. (2006) Mechanism of action of memantine. *Curr. Opin. Pharmacol.*, **6**, 61–67.

Johnson, J.W. & Qian, A. (2002) Interaction between channel blockers and channel gating of NMDA receptors. *Biologicheskie Membrany*, **19(1)**, 110–115.

Jones, M.V. & Westbrook, G.L. (1996) The impact of receptor desensitization on fast synaptic transmission. *Trends Neurosci.*, **19**, 96–101.

Kafi, H., Salamzadeh, J., Beladimoghadam, N., Sistanizad, M., & Kouchek, M. (2014) Study of the neuroprotective effects of memantine in patients with mild to moderate ischemic stroke. *Iran J Pharm Res*, **13**, 591–598.

Kampa, B.M., Clements, J., Jonas, P., & Stuart, G.J. (2004) Kinetics of Mg2+ unblock of NMDA receptors: implications for spike-timing dependent synaptic plasticity. *J. Physiol. (Lond.)*, **556**, 337–345.

Karakas, E. & Furukawa, H. (2014) Crystal structure of a heterotetrameric NMDA receptor ion channel. *Science*, **344**, 992–997.

Kashiwagi, K., Masuko, T., Nguyen, C.D., Kuno, T., Tanaka, I., Igarashi, K., & Williams, K. (2002) Channel blockers acting at N-methyl-D-aspartate receptors: differential effects of mutations in the vestibule and ion channel pore. *Mol. Pharmacol.*, **61**, 533–545.

Katz, B. & Thesleff, S. (1957) A study of the desensitization produced by acetylcholine at the motor end-plate. *J. Physiol. (Lond.)*, **138**, 63–80.

Kaufman, A.M., Milnerwood, A.J., Sepers, M.D., Coquinco, A., She, K., Wang, L., Lee, H., Craig, A.M., Cynader, M., & Raymond, L.A. (2012) Opposing roles of synaptic and extrasynaptic NMDA receptor signaling in cocultured striatal and cortical neurons. *J. Neurosci.*, **32**, 3992–4003.

Kavalali, E.T. & Monteggia, L.M. (2015) How does ketamine elicit a rapid antidepressant response? *Curr. Opin. Pharmacol.*, **20**, 35–39.

Kellermayer, B., Ferreira, J.S., Dupuis, J., Levet, F., Grillo-Bosch, D., Bard, L., Linarès-Loyez, J., Bouchet, D., Choquet, D., Rusakov, D.A., Bon, P., Sibarita, J.-B., Cognet, L., Sainlos, M., Carvalho, A.L., & Groc, L. (2018) Differential Nanoscale Topography and Functional Role of GluN2-NMDA Receptor Subtypes at Glutamatergic Synapses. *Neuron*, **100**, 106–119.e7.

Kinney, J.W., Davis, C.N., Tabarean, I., Conti, B., Bartfai, T., & Behrens, M.M. (2006) A specific role for NR2A-containing NMDA receptors in the maintenance of parvalbumin and GAD67 immunoreactivity in cultured interneurons. *J. Neurosci.*, **26**, 1604–1615.

Kloda, A., Lua, L., Hall, R., Adams, D.J., & Martinac, B. (2007) Liposome reconstitution and modulation of recombinant N-methyl-D-aspartate receptor channels by membrane stretch. *Proc. Natl. Acad. Sci. USA*, **104**, 1540–1545.

Kong, M., Ba, M., Ren, C., Yu, L., Dong, S., Yu, G., & Liang, H. (2017) An updated meta-analysis of amantadine for treating dyskinesia in Parkinson's disease. *Oncotarget*, **8**, 57316–57326.

Kornau, H.C., Schenker, L.T., Kennedy, M.B., & Seeburg, P.H. (1995) Domain interaction between NMDA receptor subunits and the postsynaptic density protein PSD-95. *Science*, **269**, 1737–1740.

Koshelev, S.G. & Khodorov, B.I. (1995) Blockade of open NMDA channel by tetrabutylammonium, 9-aminoacridine and tacrine prevents channels closing and desensitization. *MEMBRANE AND CELL BIOLOGY C/C OF BIOLOGICHESKIE MEMBRANY*, **9**, 93–110.

Kotermanski, S.E. & Johnson, J.W. (2009) Mg2+ imparts NMDA receptor subtype selectivity to the Alzheimer's drug memantine. *J. Neurosci.*, **29**, 2774–2779.

Kotermanski, S.E., Johnson, J.W., & Thiels, E. (2013) Comparison of behavioral effects of the NMDA receptor channel blockers memantine and ketamine in rats. *Pharmacol. Biochem. Behav.*, **109**, 67–76.

Kotermanski, S.E., Wood, J.T., & Johnson, J.W. (2009) Memantine binding to a superficial site on NMDA receptors contributes to partial trapping. *J. Physiol. (Lond.)*, **587**, 4589–4604.

Koutsilieri, E. & Riederer, P. (2007) Excitotoxicity and new antiglutamatergic strategies in Parkinson's disease and Alzheimer's disease. *Parkinsonism Relat. Disord.*, **13 Suppl 3**, S329–31.

Krieger, J., Bahar, I., & Greger, I.H. (2015) Structure, Dynamics, and Allosteric Potential of Ionotropic Glutamate Receptor N-Terminal Domains. *Biophys. J.*, **109**, 1136–1148.

Krieger, J., Lee, J.Y., Greger, I.H., & Bahar, I. (2019) Activation and desensitization of ionotropic glutamate receptors by selectively triggering pre-existing motions. *Neurosci. Lett.*, **700**, 22–29.

Krupp, J.J., Vissel, B., Heinemann, S.F., & Westbrook, G.L. (1996) Calcium-dependent inactivation of recombinant N-methyl-D-aspartate receptors is NR2 subunit specific. *Mol. Pharmacol.*, **50**, 1680–1688.

Krupp, J.J., Vissel, B., Heinemann, S.F., & Westbrook, G.L. (1998) N-terminal domains in the NR2 subunit control desensitization of NMDA receptors. *Neuron*, **20**, 317–327.

Krupp, J.J., Vissel, B., Thomas, C.G., Heinemann, S.F., & Westbrook, G.L. (1999) Interactions of calmodulin and alpha-actinin with the NR1 subunit modulate Ca2+-dependent inactivation of NMDA receptors. *J. Neurosci.*, **19**, 1165–1178.

Krupp, J.J., Vissel, B., Thomas, C.G., Heinemann, S.F., & Westbrook, G.L. (2002) Calcineurin acts via the C-terminus of NR2A to modulate desensitization of NMDA receptors. *Neuropharmacology*, **42**, 593–602.

Krystal, J.H., D'Souza, D.C., Mathalon, D., Perry, E., Belger, A., & Hoffman, R. (2003) NMDA receptor antagonist effects, cortical glutamatergic function, and schizophrenia: toward a paradigm shift in medication development. *Psychopharmacology*, **169**, 215–233.

Krystal, J.H., Karper, L.P., Seibyl, J.P., Freeman, G.K., Delaney, R., Bremner, J.D., Heninger, G.R., Bowers, M.B., & Charney, D.S. (1994) Subanesthetic effects of the noncompetitive NMDA antagonist, ketamine, in humans. Psychotomimetic, perceptual, cognitive, and neuroendocrine responses. *Arch. Gen. Psychiatry*, **51**, 199–214.

Kuner, T. & Schoepfer, R. (1996) Multiple structural elements determine subunit specificity of Mg2+ block in NMDA receptor channels. *J. Neurosci.*, **16**, 3549–3558.

Lan, J.Y., Skeberdis, V.A., Jover, T., Grooms, S.Y., Lin, Y., Araneda, R.C., Zheng, X., Bennett, M.V., & Zukin, R.S. (2001) Protein kinase C modulates NMDA receptor trafficking and gating. *Nat. Neurosci.*, **4**, 382–390.

Lau, A. & Tymianski, M. (2010) Glutamate receptors, neurotoxicity and neurodegeneration. *Pflugers Arch.*, **460**, 525–542.

Lau, C.G. & Zukin, R.S. (2007) NMDA receptor trafficking in synaptic plasticity and neuropsychiatric disorders. *Nat. Rev. Neurosci.*, **8**, 413–426.

Lee, C.-H., Lü, W., Michel, J.C., Goehring, A., Du, J., Song, X., & Gouaux, E. (2014) NMDA receptor structures reveal subunit arrangement and pore architecture. *Nature*, **511**, 191–197.

Lee, E.-J., Choi, S.Y., & Kim, E. (2015) NMDA receptor dysfunction in autism spectrum disorders. *Curr. Opin. Pharmacol.*, **20**, 8–13.

Lee, J.Y., Krieger, J., Herguedas, B., García-Nafría, J., Dutta, A., Shaikh, S.A., Greger, I.H., & Bahar, I. (2019) Druggability Simulations and X-Ray Crystallography Reveal a Ligand-Binding Site in the GluA3 AMPA Receptor N-Terminal Domain. *Structure*, **27**, 241–252.e3.

Legendre, P., Rosenmund, C., & Westbrook, G.L. (1993) Inactivation of NMDA channels in cultured hippocampal neurons by intracellular calcium. *J. Neurosci.*, **13**, 674–684.

Leiva, R., Phillips, M.B., Turcu, A.L., Gratacòs-Batlle, E., León-García, L., Sureda, F.X., Soto, D., Johnson, J.W., & Vázquez, S. (2018) Pharmacological and electrophysiological characterization of novel NMDA receptor antagonists. *ACS Chem. Neurosci.*, **9**, 2722–2730.

Lemke, J.R., Hendrickx, R., Geider, K., Laube, B., Schwake, M., Harvey, R.J., James, V.M., Pepler, A., Steiner, I., Hörtnagel, K., Neidhardt, J., Ruf, S., Wolff, M., Bartholdi, D., Caraballo, R., Platzer, K., Suls, A., De Jonghe, P., Biskup, S., & Weckhuysen, S. (2014) GRIN2B mutations in West syndrome and intellectual disability with focal epilepsy. *Ann. Neurol.*, **75**, 147–154.

Lerma, J., Zukin, R.S., & Bennett, M.V. (1990) Glycine decreases desensitization of N-methyl-D-aspartate (NMDA) receptors expressed in Xenopus oocytes and is required for NMDA responses. *Proc. Natl. Acad. Sci. USA*, **87**, 2354–2358.

Lester, R.A., Clements, J.D., Westbrook, G.L., & Jahr, C.E. (1990) Channel kinetics determine the time course of NMDA receptor-mediated synaptic currents. *Nature*, **346**, 565–567.

Lester, R.A., Tong, G., & Jahr, C.E. (1993) Interactions between the glycine and glutamate binding sites of the NMDA receptor. *J. Neurosci.*, **13**, 1088–1096.

Léveillé, F., El Gaamouch, F., Gouix, E., Lecocq, M., Lobner, D., Nicole, O., & Buisson, A. (2008) Neuronal viability is controlled by a functional relation between synaptic and extrasynaptic NMDA receptors. *FASEB J.*, **22**, 4258–4271.

Li, J.H., Wang, Y.H., Wolfe, B.B., Krueger, K.E., Corsi, L., Stocca, G., & Vicini, S. (1998) Developmental changes in localization of NMDA receptor subunits in primary cultures of cortical neurons. *Eur. J. Neurosci.*, **10**, 1704–1715.

Li-Smerin, Y. & Johnson, J.W. (1996) Effects of intracellular Mg2+ on channel gating and steady-state responses of the NMDA receptor in cultured rat neurons. *J. Physiol. (Lond.)*, **491 (Pt 1)**, 137–150.

Lieberman, D.N. & Mody, I. (1994) Regulation of NMDA channel function by endogenous Ca(2+)-dependent phosphatase. *Nature*, **369**, 235–239.

Lipton, P. (1999) Ischemic cell death in brain neurons. *Physiol. Rev.*, **79**, 1431–1568.

Lipton, S.A. (2004) Paradigm shift in NMDA receptor antagonist drug development: molecular mechanism of uncompetitive inhibition by memantine in the treatment of Alzheimer's disease and other neurologic disorders. *J. Alzheimers Dis.*, **6**, S61–74.

Lipton, S.A. (2006) Paradigm shift in neuroprotection by NMDA receptor blockade: memantine and beyond. *Nat. Rev. Drug Discov.*, **5**, 160–170.

Lipton, S.A. (2007) Pathologically activated therapeutics for neuroprotection. *Nat. Rev. Neurosci.*, **8**, 803–808.

Lisman, J., Schulman, H., & Cline, H. (2002) The molecular basis of CaMKII function in synaptic and behavioural memory. *Nat. Rev. Neurosci.*, **3**, 175–190.

Lomeli, H., Sprengel, R., Laurie, D.J., Köhr, G., Herb, A., Seeburg, P.H., & Wisden, W. (1993) The rat delta-1 and delta-2 subunits extend the excitatory amino acid receptor family. *FEBS Lett.*, **315**, 318–322.

Lu, C., Fu, Z., Karavanov, I., Yasuda, R.P., Wolfe, B.B., Buonanno, A., & Vicini, S. (2006) NMDA receptor subtypes at autaptic synapses of cerebellar granule neurons. *J. Neurophysiol.*, **96**, 2282–2294.

Luo, J., Wang, Y., Yasuda, R.P., Dunah, A.W., & Wolfe, B.B. (1997) The majority of N-methyl-D-aspartate receptor complexes in adult rat cerebral cortex contain at least three different subunits (NR1/NR2A/NR2B). *Mol. Pharmacol.*, **51**, 79–86.

Lüscher, C. & Malenka, R.C. (2012) NMDA receptor-dependent long-term potentiation and long-term depression (LTP/LTD). *Cold Spring Harb. Perspect. Biol.*, **4**.

Luthi, D., Spichiger, U., Forster, I., & McGuigan, J.A. (1997) Calibration of Mg(2+)-selective macroelectrodes down to 1 mumol l1đ⁻³ in intracellular and Ca(2+)-containing extracellular solutions. *Exp. Physiol.*, **82**, 453–467.

M.J. Frisch, G.W.T. (2009) Gaussian 09. *Gaussian*,.

MacDonald, J.F., Bartlett, M.C., Mody, I., Pahapill, P., Reynolds, J.N., Salter, M.W., Schneiderman, J.H., & Pennefather, P.S. (1991) Actions of ketamine, phencyclidine and MK-801 on NMDA receptor currents in cultured mouse hippocampal neurones. *J. Physiol. (Lond.)*, **432**, 483–508.

MacDonald, J.F., Miljkovic, Z., & Pennefather, P. (1987) Use-dependent block of excitatory amino acid currents in cultured neurons by ketamine. *J. Neurophysiol.*, **58**, 251–266.

Maki, B.A., Aman, T.K., Amico-Ruvio, S.A., Kussius, C.L., & Popescu, G.K. (2012) C-terminal domains of N-methyl-D-aspartic acid receptor modulate unitary channel conductance and gating. *J. Biol. Chem.*, **287**, 36071–36080.

Malenka, R.C. (1994) Synaptic plasticity in the hippocampus: LTP and LTD. *Cell*, **78**, 535–538.

Malenka, R.C. & Bear, M.F. (2004) LTP and LTD: an embarrassment of riches. *Neuron,* **44**, 5–21.

Martel, M.-A., Ryan, T.J., Bell, K.F.S., Fowler, J.H., McMahon, A., Al-Mubarak, B., Komiyama, N.H., Horsburgh, K., Kind, P.C., Grant, S.G.N., Wyllie, D.J.A., & Hardingham, G.E. (2012) The subtype of GluN2 C-terminal domain determines the response to excitotoxic insults. *Neuron*, **74**, 543–556.

Matsunaga, S., Kishi, T., & Iwata, N. (2015) Memantine monotherapy for Alzheimer's disease: a systematic review and meta-analysis. *PLoS One*, **10**, e0123289.

Mayer, M.L., MacDermott, A.B., Westbrook, G.L., Smith, S.J., & Barker, J.L. (1987) Agonist- and voltage-gated calcium entry in cultured mouse spinal cord neurons under voltage clamp measured using arsenazo III. *J. Neurosci.*, **7**, 3230–3244.

Mayer, M.L., Vyklicky, L., & Clements, J. (1989) Regulation of NMDA receptor desensitization in mouse hippocampal neurons by glycine. *Nature*, **338**, 425–427.

Mayer, M.L. & Westbrook, G.L. (1985) The action of N-methyl-D-aspartic acid on mouse spinal neurones in culture. *J. Physiol. (Lond.)*, **361**, 65–90.

Mayer, M.L., Westbrook, G.L., & Guthrie, P.B. (1984) Voltage-dependent block by Mg2+ of NMDA responses in spinal cord neurones. *Nature*, **309**, 261–263.

McBain, C.J. & Mayer, M.L. (1994) N-methyl-D-aspartic acid receptor structure and function. *Physiol. Rev.*, **74**, 723–760.

McGuigan, J.A., Lüthi, D., & Buri, A. (1991) Calcium buffer solutions and how to make them: a do it yourself guide. *Can. J. Physiol. Pharmacol.*, **69**, 1733–1749.

McGuigan, J.A.S., Kay, J.W., & Elder, H.Y. (2006) Critical review of the methods used to measure the apparent dissociation constant and ligand purity in Ca2+ and Mg2+ buffer solutions. *Prog. Biophys. Mol. Biol.*, **92**, 333–370.

McGuigan, J.A.S., Kay, J.W., & Elder, H.Y. (2014) An improvement to the ligand optimisation method (LOM) for measuring the apparent dissociation constant and ligand purity in Ca2+ and Mg2+ buffer solutions. *Prog. Biophys. Mol. Biol.*, **116**, 203–211.

McGuigan, J.A.S., Kay, J.W., & Elder, H.Y. (2016) Ionised concentrations in calcium and magnesium buffers: Standards and precise measurement are mandatory. *Prog. Biophys. Mol. Biol.*, **121**, 195–211.

McGuigan, J.A.S., Kay, J.W., Elder, H.Y., & Lüthi, D. (2007) Comparison between measured and calculated ionised concentrations in Mg2+/ATP, Mg2+/EDTA and Ca2+/EGTA buffers; influence of changes in temperature, pH and pipetting errors on the ionised concentrations. *Magnes Res*, **20**, 72–81.

Mealing, G.A., Lanthorn, T.H., Murray, C.L., Small, D.L., & Morley, P. (1999) Differences in degree of trapping of low-affinity uncompetitive N-methyl-D-aspartic acid receptor antagonists with similar kinetics of block. *J. Pharmacol. Exp. Ther.*, **288**, 204–210.

Mealing, G.A., Lanthorn, T.H., Small, D.L., Murray, R.J., Mattes, K.C., Comas, T.M., & Morley, P. (2001) Structural modifications to an N-methyl-D-aspartate receptor antagonist result in large differences in trapping block. *J. Pharmacol. Exp. Ther.*, **297**, 906–914.

Mecocci, P., Bladström, A., & Stender, K. (2009) Effects of memantine on cognition in patients with moderate to severe Alzheimer's disease: post-hoc analyses of ADAS-cog and SIB total and single-item scores from six randomized, double-blind, placebo-controlled studies. *Int. J. Geriatr. Psychiatry*, **24**, 532–538.

Medina, I., Filippova, N., Bakhramov, A., & Bregestovski, P. (1996) Calcium-induced inactivation of NMDA receptor-channels evolves independently of run-down in cultured rat brain neurones. *J. Physiol. (Lond.)*, **495 (Pt 2)**, 411–427.

Medina, I., Filippova, N., Barbin, G., Ben-Ari, Y., & Bregestovski, P. (1994) Kainate-induced inactivation of NMDA currents via an elevation of intracellular Ca2+ in hippocampal neurons. *J. Neurophysiol.*, **72**, 456–465.

Medina, I., Filippova, N., Charton, G., Rougeole, S., Ben-Ari, Y., Khrestchatisky, M., & Bregestovski, P. (1995) Calcium-dependent inactivation of heteromeric NMDA receptor-channels expressed in human embryonic kidney cells. *J. Physiol. (Lond.)*, **482 (Pt 3)**, 567–573.

Merrill, M.A., Malik, Z., Akyol, Z., Bartos, J.A., Leonard, A.S., Hudmon, A., Shea, M.A., & Hell, J.W. (2007) Displacement of alpha-actinin from the NMDA receptor NR1 C0 domain By Ca2+/calmodulin promotes CaMKII binding. *Biochemistry*, **46**, 8485–8497.

Mesbahi-Vasey, S., Veras, L., Yonkunas, M., Johnson, J.W., & Kurnikova, M.G. (2017) All atom NMDA receptor transmembrane domain model development and simulations in lipid bilayers and water. *PLoS One*, **12**, e0177686.

Miller, O.H., Yang, L., Wang, C.-C., Hargroder, E.A., Zhang, Y., Delpire, E., & Hall, B.J. (2014) GluN2B-containing NMDA receptors regulate depression-like behavior and are critical for the rapid antidepressant actions of ketamine. *Elife*, **3**, e03581.

Misra, C., Brickley, S.G., Farrant, M., & Cull-Candy, S.G. (2000) Identification of subunits contributing to synaptic and extrasynaptic NMDA receptors in Golgi cells of the rat cerebellum. *J. Physiol. (Lond.)*, **524 Pt 1**, 147–162.

Moghaddam, B., Adams, B., Verma, A., & Daly, D. (1997) Activation of glutamatergic neurotransmission by ketamine: a novel step in the pathway from NMDA receptor blockade to dopaminergic and cognitive disruptions associated with the prefrontal cortex. *J. Neurosci.*, **17**, 2921–2927.

Monyer, H., Burnashev, N., Laurie, D.J., Sakmann, B., & Seeburg, P.H. (1994) Developmental and regional expression in the rat brain and functional properties of four NMDA receptors. *Neuron*, **12**, 529–540.

Monyer, H., Sprengel, R., Schoepfer, R., Herb, A., Higuchi, M., Lomeli, H., Burnashev, N., Sakmann, B., & Seeburg, P.H. (1992) Heteromeric NMDA receptors: molecular and functional distinction of subtypes. *Science*, **256**, 1217–1221.

Mori, H., Masaki, H., Yamakura, T., & Mishina, M. (1992) Identification by mutagenesis of a Mg(2+)-block site of the NMDA receptor channel. *Nature*, **358**, 673–675.

Morris, R.G.M. (2013) NMDA receptors and memory encoding. *Neuropharmacology*, **74**, 32–40.

Mota, S.I., Ferreira, I.L., & Rego, A.C. (2014) Dysfunctional synapse in Alzheimer's disease - A focus on NMDA receptors. *Neuropharmacology*, **76 Pt A**, 16–26.

Mothet, J.P., Parent, A.T., Wolosker, H., Brady, R.O., Linden, D.J., Ferris, C.D., Rogawski, M.A., & Snyder, S.H. (2000) D-serine is an endogenous ligand for the glycine site of the N-methyl-D-aspartate receptor. *Proc. Natl. Acad. Sci. USA*, **97**, 4926–4931.

Muir, K.W. (2006) Glutamate-based therapeutic approaches: clinical trials with NMDA antagonists. *Curr. Opin. Pharmacol.*, **6**, 53–60.

Murphy, J.A., Stein, I.S., Lau, C.G., Peixoto, R.T., Aman, T.K., Kaneko, N., Aromolaran, K., Saulnier, J.L., Popescu, G.K., Sabatini, B.L., Hell, J.W., & Zukin, R.S. (2014) Phosphorylation of

Ser1166 on GluN2B by PKA is critical to synaptic NMDA receptor function and Ca2+ signaling in spines. *J. Neurosci.*, **34**, 869–879.

Nabavi, S., Kessels, H.W., Alfonso, S., Aow, J., Fox, R., & Malinow, R. (2013) Metabotropic NMDA receptor function is required for NMDA receptor-dependent long-term depression. *Proc. Natl. Acad. Sci. USA*, **110**, 4027–4032.

Nair, A.S. & Sahoo, R.K. (2019) Efficacy of memantine hydrochloride in neuropathic pain. *Indian J. Palliat. Care*, **25**, 161–162.

Nakagawa, T. (2019) Structures of the AMPA receptor in complex with its auxiliary subunit cornichon. *Science*, **366**, 1259–1263.

Neher, E. & Steinbach, J.H. (1978) Local anaesthetics transiently block currents through single acetylcholine-receptor channels. *J. Physiol. (Lond.)*, **277**, 153–176.

Nevian, T. & Sakmann, B. (2004) Single spine Ca2+ signals evoked by coincident EPSPs and backpropagating action potentials in spiny stellate cells of layer 4 in the juvenile rat somatosensory barrel cortex. *J. Neurosci.*, **24**, 1689–1699.

Nevian, T. & Sakmann, B. (2006) Spine Ca2+ signaling in spike-timing-dependent plasticity. *J. Neurosci.*, **26**, 11001–11013.

Nicolsky, B.P., Shultz, M.M., Belijustin, A.A., & Lev, A.A. (1967) Recent Developments in the Ion-Exchange Theory of the Glass Electrode and Its Application in the Chemistry of Glass. In Eisenman, G. (ed), *Glass Electrodes for Hydrogen and Other Cations*. Marcel Dekker, INC, New York, pp. 174–218.

Nikolaev, M.V., Magazanik, L.G., & Tikhonov, D.B. (2012) Influence of external magnesium ions on the NMDA receptor channel block by different types of organic cations. *Neuropharmacology*, **62**, 2078–2085.

Noppers, I., Niesters, M., Aarts, L., Smith, T., Sarton, E., & Dahan, A. (2010) Ketamine for the treatment of chronic non-cancer pain. *Expert Opin. Pharmacother.*, **11**, 2417–2429.

Nowak, L., Bregestovski, P., Ascher, P., Herbet, A., & Prochiantz, A. (1984) Magnesium gates glutamate-activated channels in mouse central neurones. *Nature*, **307**, 462–465.

Okamoto, S., Pouladi, M.A., Talantova, M., Yao, D., Xia, P., Ehrnhoefer, D.E., Zaidi, R., Clemente, A., Kaul, M., Graham, R.K., Zhang, D., Vincent Chen, H.S., Tong, G., Hayden, M.R., & Lipton, S.A. (2009) Balance between synaptic versus extrasynaptic NMDA receptor activity influences inclusions and neurotoxicity of mutant huntingtin. *Nat. Med.*, **15**, 1407–1413.

Olivares, D., Deshpande, V.K., Shi, Y., Lahiri, D.K., Greig, N.H., Rogers, J.T., & Huang, X. (2012) N-methyl D-aspartate (NMDA) receptor antagonists and memantine treatment for Alzheimer's disease, vascular dementia and Parkinson's disease. *Curr Alzheimer Res*, **9**, 746–758.

Olney, J.W., Labruyere, J., & Price, M.T. (1989) Pathological changes induced in cerebrocortical neurons by phencyclidine and related drugs. *Science*, **244**, 1360–1362.

Orth, A., Tapken, D., & Hollmann, M. (2013) The delta subfamily of glutamate receptors: characterization of receptor chimeras and mutants. *Eur. J. Neurosci.*, **37**, 1620–1630.

Otsu, Y., Darcq, E., Pietrajtis, K., Mátyás, F., Schwartz, E., Bessaih, T., Abi Gerges, S., Rousseau, C.V., Grand, T., Dieudonné, S., Paoletti, P., Acsády, L., Agulhon, C., Kieffer, B.L., & Diana, M.A. (2019) Control of aversion by glycine-gated GluN1/GluN3A NMDA receptors in the adult medial habenula. *Science*, **366**, 250–254.

Otton, H.J., Lawson McLean, A., Pannozzo, M.A., Davies, C.H., & Wyllie, D.J.A. (2011) Quantification of the Mg2+-induced potency shift of amantadine and memantine voltage-dependent block in human recombinant GluN1/GluN2A NMDARs. *Neuropharmacology*, **60**, 388–396.

Paoletti, P., Ascher, P., & Neyton, J. (1997) High-affinity zinc inhibition of NMDA NR1-NR2A receptors. *J. Neurosci.*, **17**, 5711–5725.

Paoletti, P., Bellone, C., & Zhou, Q. (2013) NMDA receptor subunit diversity: impact on receptor properties, synaptic plasticity and disease. *Nat. Rev. Neurosci.*, **14**, 383–400.

Paoletti, P., Perin-Dureau, F., Fayyazuddin, A., Le Goff, A., Callebaut, I., & Neyton, J. (2000) Molecular organization of a zinc binding n-terminal modulatory domain in a NMDA receptor subunit. *Neuron*, **28**, 911–925.

Papadia, S., Soriano, F.X., Léveillé, F., Martel, M.-A., Dakin, K.A., Hansen, H.H., Kaindl, A., Sifringer, M., Fowler, J., Stefovska, V., McKenzie, G., Craigon, M., Corriveau, R., Ghazal, P., Horsburgh, K., Yankner, B.A., Wyllie, D.J.A., Ikonomidou, C., & Hardingham, G.E. (2008) Synaptic NMDA receptor activity boosts intrinsic antioxidant defenses. *Nat. Neurosci.*, **11**, 476–487.

Papouin, T., Ladépêche, L., Ruel, J., Sacchi, S., Labasque, M., Hanini, M., Groc, L., Pollegioni, L., Mothet, J.-P., & Oliet, S.H.R. (2012) Synaptic and extrasynaptic NMDA receptors are gated by different endogenous coagonists. *Cell*, **150**, 633–646.

Parsons, C.G., Danysz, W., Bartmann, A., Spielmanns, P., Frankiewicz, T., Hesselink, M., Eilbacher, B., & Quack, G. (1999) Amino-alkyl-cyclohexanes are novel uncompetitive NMDA receptor antagonists with strong voltage-dependency and fast blocking kinetics: in vitro and in vivo characterization. *Neuropharmacology*, **38**, 85–108.

Parsons, C.G., Danysz, W., & Quack, G. (1999) Memantine is a clinically well tolerated N-methyl-D-aspartate (NMDA) receptor antagonist--a review of preclinical data. *Neuropharmacology*, **38**, 735–767.

Parsons, C.G. & Gilling, K. (2007) Memantine as an example of a fast, voltage-dependent, open channel N-methyl-D-aspartate receptor blocker. *Methods Mol. Biol.*, **403**, 15–36.

Parsons, C.G., Panchenko, V.A., Pinchenko, V.O., Tsyndrenko, A.Y., & Krishtal, O.A. (1996) Comparative patch-clamp studies with freshly dissociated rat hippocampal and striatal neurons on the NMDA receptor antagonistic effects of amantadine and memantine. *Eur. J. Neurosci.*, **8**, 446–454.

Parsons, C.G., Quack, G., Bresink, I., Baran, L., Przegalinski, E., Kostowski, W., Krzascik, P., Hartmann, S., & Danysz, W. (1995) Comparison of the potency, kinetics and voltage-dependency of a series of uncompetitive NMDA receptor antagonists in vitro with anticonvulsive and motor impairment activity in vivo. *Neuropharmacology*, **34**, 1239–1258.

Parsons, C.G., Stöffler, A., & Danysz, W. (2007) Memantine: a NMDA receptor antagonist that improves memory by restoration of homeostasis in the glutamatergic system--too little activation is bad, too much is even worse. *Neuropharmacology*, **53**, 699–723.

Parsons, M.P. & Raymond, L.A. (2014) Extrasynaptic NMDA receptor involvement in central nervous system disorders. *Neuron*, **82**, 279–293.

Persson, J. (2013) Ketamine in pain management. *CNS Neurosci Ther*, **19**, 396–402.

Phillips, M.B., Nigam, A., & Johnson, J.W. (2020) Interplay between Gating and Block of Ligand-Gated Ion Channels. *Brain Sci.*, **10**.

Pierson, T.M., Yuan, H., Marsh, E.D., Fuentes-Fajardo, K., Adams, D.R., Markello, T., Golas, G., Simeonov, D.R., Holloman, C., Tankovic, A., Karamchandani, M.M., Schreiber, J.M., Mullikin, J.C., PhD for the NISC Comparative Sequencing Program, Tifft, C.J., Toro, C., Boerkoel, C.F., Traynelis, S.F., & Gahl, W.A. (2014) GRIN2A mutation and early-onset epileptic encephalopathy: personalized therapy with memantine. *Ann Clin Transl Neurol*, **1**, 190–198.

Piña-Crespo, J.C. & Gibb, A.J. (2002) Subtypes of NMDA receptors in new-born rat hippocampal granule cells. *J. Physiol. (Lond.)*, **541**, 41–64.

Povysheva, N.V. & Johnson, J.W. (2016) Effects of memantine on the excitation-inhibition balance in prefrontal cortex. *Neurobiol. Dis.*, **96**, 75–83.

Premkumar, L.S. & Auerbach, A. (1996) Identification of a high affinity divalent cation binding site near the entrance of the NMDA receptor channel. *Neuron*, **16**, 869–880.

Preskorn, S.H., Baker, B., Kolluri, S., Menniti, F.S., Krams, M., & Landen, J.W. (2008) An innovative design to establish proof of concept of the antidepressant effects of the NR2B subunit selective N-methyl-D-aspartate antagonist, CP-101,606, in patients with treatment-refractory major depressive disorder. *J Clin Psychopharmacol*, **28**, 631–637.

Purohit, Y. & Grosman, C. (2006) Block of muscle nicotinic receptors by choline suggests that the activation and desensitization gates act as distinct molecular entities. *J. Gen. Physiol.*, **127**, 703–717.

Qian, A., Antonov, S.M., & Johnson, J.W. (2002) Modulation by permeant ions of Mg^{2+} inhibition of NMDA-activated whole-cell currents in rat cortical neurons. *J. Physiol. (Lond.)*, **538**, 65–77.

Qian, A., Buller, A.L., & Johnson, J.W. (2005) NR2 subunit-dependence of NMDA receptor channel block by external Mg2+. *J. Physiol. (Lond.)*, **562**, 319–331.

Qian, A. & Johnson, J.W. (2002) Channel gating of NMDA receptors. *Physiol. Behav.*, **77**, 577–582.

Rachline, J., Perin-Dureau, F., Le Goff, A., Neyton, J., & Paoletti, P. (2005) The micromolar zinc-binding domain on the NMDA receptor subunit NR2B. *J. Neurosci.*, **25**, 308–317.

Rauner, C. & Köhr, G. (2011) Triheteromeric NR1/NR2A/NR2B receptors constitute the major N-methyl-D-aspartate receptor population in adult hippocampal synapses. *J. Biol. Chem.*, **286**, 7558–7566.

Rombouts, S.A., Barkhof, F., Veltman, D.J., Machielsen, W.C., Witter, M.P., Bierlaagh, M.A., Lazeron, R.H., Valk, J., & Scheltens, P. (2000) Functional MR imaging in Alzheimer's disease during memory encoding. *AJNR Am. J. Neuroradiol.*, **21**, 1869–1875.

Rothman, S.M. & Olney, J.W. (1995) Excitotoxicity and the NMDA receptor--still lethal after eight years. *Trends Neurosci.*, **18**, 57–58.

Rozov, A. & Burnashev, N. (2016) Fast interaction between AMPA and NMDA receptors by intracellular calcium. *Cell Calcium*, **60**, 407–414.

Rudhard, Y., Kneussel, M., Nassar, M.A., Rast, G.F., Annala, A.J., Chen, P.E., Tigaret, C.M., Dean, I., Roes, J., Gibb, A.J., Hunt, S.P., & Schoepfer, R. (2003) Absence of Whisker-related pattern formation in mice with NMDA receptors lacking coincidence detection properties and calcium signaling. *J. Neurosci.*, **23**, 2323–2332.

Ruff, R.L. (1977) A quantitative analysis of local anaesthetic alteration of miniature end-plate currents and end-plate current fluctuations. *J. Physiol. (Lond.)*, **264**, 89–124.

Rycroft, B.K. & Gibb, A.J. (2002) Direct effects of calmodulin on NMDA receptor single-channel gating in rat hippocampal granule cells. *J. Neurosci.*, **22**, 8860–8868.

Rycroft, B.K. & Gibb, A.J. (2004) Inhibitory interactions of calcineurin (phosphatase 2B) and calmodulin on rat hippocampal NMDA receptors. *Neuropharmacology*, **47**, 505–514.

Salpietro, V., Dixon, C.L., Guo, H., Bello, O.D., Vandrovcova, J., *et al.* (2019) AMPA receptor GluA2 subunit defects are a cause of neurodevelopmental disorders. *Nat. Commun.*, **10**, 3094.

Sather, W., Dieudonné, S., MacDonald, J.F., & Ascher, P. (1992) Activation and desensitization of N-methyl-D-aspartate receptors in nucleated outside-out patches from mouse neurones. *J. Physiol. (Lond.)*, **450**, 643–672.

Sather, W., Johnson, J.W., Henderson, G., & Ascher, P. (1990) Glycine-insensitive desensitization of NMDA responses in cultured mouse embryonic neurons. *Neuron*, **4**, 725–731.

Schoenmakers, T.J., Visser, G.J., Flik, G., & Theuvenet, A.P. (1992) CHELATOR: an improved method for computing metal ion concentrations in physiological solutions. *BioTechniques*, **12**, , 876.

Schorge, S., Elenes, S., & Colquhoun, D. (2005) Maximum likelihood fitting of single channel NMDA activity with a mechanism composed of independent dimers of subunits. *J. Physiol. (Lond.)*, **569**, 395–418.

Schroeter, M.L., Vogt, B., Frisch, S., Becker, G., Barthel, H., Mueller, K., Villringer, A., & Sabri, O. (2012) Executive deficits are related to the inferior frontal junction in early dementia. *Brain*, **135**, 201–215.

Schwaller, B. (2010) Cytosolic Ca2+ buffers. *Cold Spring Harb. Perspect. Biol.*, **2**, a004051.

Sharp, F.R., Tomitaka, M., Bernaudin, M., & Tomitaka, S. (2001) Psychosis: pathological activation of limbic thalamocortical circuits by psychomimetics and schizophrenia? *Trends Neurosci.*, **24**, 330–334.

Sheng, M., Cummings, J., Roldan, L.A., Jan, Y.N., & Jan, L.Y. (1994) Changing subunit composition of heteromeric NMDA receptors during development of rat cortex. *Nature*, **368**, 144–147.

Shi, N., Ye, S., Alam, A., Chen, L., & Jiang, Y. (2006) Atomic structure of a Na+- and K+-conducting channel. *Nature*, **440**, 570–574.

Siegler Retchless, B., Gao, W., & Johnson, J.W. (2012) A single GluN2 subunit residue controls NMDA receptor channel properties via intersubunit interaction. *Nat. Neurosci.*, **15**, 406–13, S1.

Single, F.N., Rozov, A., Burnashev, N., Zimmermann, F., Hanley, D.F., Forrest, D., Curran, T., Jensen, V., Hvalby, O., Sprengel, R., & Seeburg, P.H. (2000) Dysfunctions in mice by NMDA receptor point mutations NR1(N598Q) and NR1(N598R). *J. Neurosci.*, **20**, 2558–2566.

Sinor, J.D., Du, S., Venneti, S., Blitzblau, R.C., Leszkiewicz, D.N., Rosenberg, P.A., & Aizenman, E. (2000) NMDA and glutamate evoke excitotoxicity at distinct cellular locations in rat cortical neurons in vitro. *J. Neurosci.*, **20**, 8831–8837.

Skeberdis, V.A., Chevaleyre, V., Lau, C.G., Goldberg, J.H., Pettit, D.L., Suadicani, S.O., Lin, Y., Bennett, M.V.L., Yuste, R., Castillo, P.E., & Zukin, R.S. (2006) Protein kinase A regulates calcium permeability of NMDA receptors. *Nat. Neurosci.*, **9**, 501–510.

Sobolevsky, A. & Koshelev, S. (1998) Two blocking sites of amino-adamantane derivatives in open N-methyl-D-aspartate channels. *Biophys. J.*, **74**, 1305–1319.

Sobolevsky, A.I. (2000) Quantitative analysis of tetrapentylammonium-induced blockade of open N-methyl-D-aspartate channels. *Biophys. J.*, **79**, 1324–1335.

Sobolevsky, A.I., Koshelev, S.G., & Khodorov, B.I. (1998) Interaction of memantine and amantadine with agonist-unbound NMDA-receptor channels in acutely isolated rat hippocampal neurons. *J. Physiol. (Lond.)*, **512 (Pt 1)**, 47–60.

Sobolevsky, A.I., Koshelev, S.G., & Khodorov, B.I. (1999) Probing of NMDA channels with fast blockers. *J. Neurosci.*, **19**, 10611–10626.

Sobolevsky, A.I., Rosconi, M.P., & Gouaux, E. (2009) X-ray structure, symmetry and mechanism of an AMPA-subtype glutamate receptor. *Nature*, **462**, 745–756.

Sobolevsky, A.I. & Yelshansky, M.V. (2000) The trapping block of NMDA receptor channels in acutely isolated rat hippocampal neurones. *J. Physiol. (Lond.)*, **526 Pt 3**, 493–506.

Sommer, B., Köhler, M., Sprengel, R., & Seeburg, P.H. (1991) RNA editing in brain controls a determinant of ion flow in glutamate-gated channels. *Cell*, **67**, 11–19.

Song, X., Jensen, M.Ø., Jogini, V., Stein, R.A., Lee, C.-H., Mchaourab, H.S., Shaw, D.E., & Gouaux, E. (2018) Mechanism of NMDA receptor channel block by MK-801 and memantine. *Nature*, **556**, 515–519.

Sonkusare, S.K., Kaul, C.L., & Ramarao, P. (2005) Dementia of Alzheimer's disease and other neurodegenerative disorders--memantine, a new hope. *Pharmacol. Res.*, **51**, 1–17.

Sornarajah, L., Vasuta, O.C., Zhang, L., Sutton, C., Li, B., El-Husseini, A., & Raymond, L.A. (2008) NMDA receptor desensitization regulated by direct binding to PDZ1-2 domains of PSD-95. *J. Neurophysiol.*, **99**, 3052–3062.

Sousa, S.F., Fernandes, P.A., & Ramos, M.J. (2006) Protein-ligand docking: current status and future challenges. *Proteins*, **65**, 15–26.

Spruston, N., Jonas, P., & Sakmann, B. (1995) Dendritic glutamate receptor channels in rat hippocampal CA3 and CA1 pyramidal neurons. *J. Physiol. (Lond.)*, **482 (Pt 2)**, 325–352.

Standley, S. & Baudry, M. (2000) The role of glycosylation in ionotropic glutamate receptor ligand binding, function, and trafficking. *Cell Mol. Life Sci.*, **57**, 1508–1516.

Stein, I.S., Gray, J.A., & Zito, K. (2015) Non-Ionotropic NMDA Receptor Signaling Drives Activity-Induced Dendritic Spine Shrinkage. *J. Neurosci.*, **35**, 12303–12308.

Stroebel, D., Carvalho, S., Grand, T., Zhu, S., & Paoletti, P. (2014) Controlling NMDA receptor subunit composition using ectopic retention signals. *J. Neurosci.*, **34**, 16630–16636.

Stroebel, D., Casado, M., & Paoletti, P. (2018) Triheteromeric NMDA receptors: from structure to synaptic physiology. *Curr. Opin. Physiol.*, **2**, 1–12.

Sun, W., Hansen, K.B., & Jahr, C.E. (2017) Allosteric Interactions between NMDA Receptor Subunits Shape the Developmental Shift in Channel Properties. *Neuron*, **94**, 58–64.e3.

Swanger, S.A., Vance, K.M., Acker, T.M., Zimmerman, S.S., DiRaddo, J.O., Myers, S.J., Bundgaard, C., Mosley, C.A., Summer, S.L., Menaldino, D.S., Jensen, H.S., Liotta, D.C., & Traynelis, S.F. (2018) A Novel Negative Allosteric Modulator Selective for GluN2C/2D-Containing NMDA Receptors Inhibits Synaptic Transmission in Hippocampal Interneurons. *ACS Chem. Neurosci.*, **9**, 306–319.

Tajima, N., Karakas, E., Grant, T., Simorowski, N., Diaz-Avalos, R., Grigorieff, N., & Furukawa, H. (2016) Activation of NMDA receptors and the mechanism of inhibition by ifenprodil. *Nature*, **534**, 63–68.

Thomas, C.G., Krupp, J.J., Bagley, E.E., Bauzon, R., Heinemann, S.F., Vissel, B., & Westbrook, G.L. (2006) Probing N-methyl-D-aspartate receptor desensitization with the substituted-cysteine accessibility method. *Mol. Pharmacol.*, **69**, 1296–1303.

Tong, G. & Jahr, C.E. (1994) Regulation of glycine-insensitive desensitization of the NMDA receptor in outside-out patches. *J. Neurophysiol.*, **72**, 754–761.

Tong, G., Shepherd, D., & Jahr, C.E. (1995) Synaptic desensitization of NMDA receptors by calcineurin. *Science*, **267**, 1510–1512.

Tovar, K.R., McGinley, M.J., & Westbrook, G.L. (2013) Triheteromeric NMDA receptors at hippocampal synapses. *J. Neurosci.*, **33**, 9150–9160.

Tovar, K.R. & Westbrook, G.L. (1999) The incorporation of NMDA receptors with a distinct subunit composition at nascent hippocampal synapses in vitro. *J. Neurosci.*, **19**, 4180–4188.

Tran, V., Park, M.C.H., & Stricker, C. (2018) An improved measurement of the Ca2+-binding affinity of fluorescent Ca2+ indicators. *Cell Calcium*, **71**, 86–94.

Traynelis, S.F., Wollmuth, L.P., McBain, C.J., Menniti, F.S., Vance, K.M., Ogden, K.K., Hansen, K.B., Yuan, H., Myers, S.J., & Dingledine, R. (2010) Glutamate receptor ion channels: structure, regulation, and function. *Pharmacol. Rev.*, **62**, 405–496.

Trott, O. & Olson, A.J. (2010) AutoDock Vina: improving the speed and accuracy of docking with a new scoring function, efficient optimization, and multithreading. *J. Comput. Chem.*, **31**, 455–461.

Twomey, E.C. & Sobolevsky, A.I. (2018) Structural mechanisms of gating in ionotropic glutamate receptors. *Biochemistry*, **57**, 267–276.

Twomey, E.C., Yelshanskaya, M.V., Grassucci, R.A., Frank, J., & Sobolevsky, A.I. (2017) Channel opening and gating mechanism in AMPA-subtype glutamate receptors. *Nature*, **549**, 60–65.

Twomey, E.C., Yelshanskaya, M.V., Vassilevski, A.A., & Sobolevsky, A.I. (2018) Mechanisms of Channel Block in Calcium-Permeable AMPA Receptors. *Neuron*, **99**, 956–968.e4.

Tymianski, M., Charlton, M.P., Carlen, P.L., & Tator, C.H. (1993) Source specificity of early calcium neurotoxicity in cultured embryonic spinal neurons. *J. Neurosci.*, **13**, 2085–2104.

Urakubo, H., Honda, M., Froemke, R.C., & Kuroda, S. (2008) Requirement of an allosteric kinetics of NMDA receptors for spike timing-dependent plasticity. *J. Neurosci.*, **28**, 3310–3323.

Vargas-Caballero, M. & Robinson, H.P.C. (2003) A slow fraction of Mg2+ unblock of NMDA receptors limits their contribution to spike generation in cortical pyramidal neurons. *J. Neurophysiol.*, **89**, 2778–2783.

Vicini, S., Wang, J.F., Li, J.H., Zhu, W.J., Wang, Y.H., Luo, J.H., Wolfe, B.B., & Grayson, D.R. (1998) Functional and pharmacological differences between recombinant N-methyl-D-aspartate receptors. *J. Neurophysiol.*, **79**, 555–566.

Villarroel, A., Regalado, M.P., & Lerma, J. (1998) Glycine-independent NMDA receptor desensitization: localization of structural determinants. *Neuron*, **20**, 329–339.

Vissel, B., Krupp, J.J., Heinemann, S.F., & Westbrook, G.L. (2002) Intracellular domains of NR2 alter calcium-dependent inactivation of N-methyl-D-aspartate receptors. *Mol. Pharmacol.*, **61**, 595–605.

von Engelhardt, J., Coserea, I., Pawlak, V., Fuchs, E.C., Köhr, G., Seeburg, P.H., & Monyer, H. (2007) Excitotoxicity in vitro by NR2A- and NR2B-containing NMDA receptors. *Neuropharmacology*, **53**, 10–17.

Vorobjev, V.S. & Sharonova, I.N. (1994) Tetrahydroaminoacridine blocks and prolongs NMDA receptor-mediated responses in a voltage-dependent manner. *Eur. J. Pharmacol.*, **253**, 1–8.

Vyklický, L. (1993) Calcium-mediated modulation of N-methyl-D-aspartate (NMDA) responses in cultured rat hippocampal neurones. *J. Physiol. (Lond.)*, **470**, 575–600.

Vyklicky, V., Stanley, C., Habrian, C., & Isacoff, E.Y. (2021) Conformational rearrangement of the NMDA receptor amino-terminal domain during activation and allosteric modulation. *Nat. Commun.*, **12**, 2694.

Wang, R. & Reddy, P.H. (2017) Role of glutamate and NMDA receptors in alzheimer's disease. *J. Alzheimers Dis.*, **57**, 1041–1048.

Watanabe, M., Inoue, Y., Sakimura, K., & Mishina, M. (1992) Developmental changes in distribution of NMDA receptor channel subunit mRNAs. *Neuroreport*, **3**, 1138–1140.

Wenk, G.L., Parsons, C.G., & Danysz, W. (2006) Potential role of N-methyl-D-aspartate receptors as executors of neurodegeneration resulting from diverse insults: focus on memantine. *Behav. Pharmacol.*, **17**, 411–424.

Widman, A.J. & McMahon, L.L. (2018) Disinhibition of CA1 pyramidal cells by low-dose ketamine and other antagonists with rapid antidepressant efficacy. *Proc. Natl. Acad. Sci. USA*, **115**, E3007–E3016.

Witt, A., Macdonald, N., & Kirkpatrick, P. (2004) Memantine hydrochloride. *Nat Rev Drug Discov*, **3**, 109–110.

Woodhull, A.M. (1973) Ionic blockage of sodium channels in nerve. *J. Gen. Physiol.*, **61**, 687–708.

Wright, J.M. & Nowak, L.M. (1992) Effects of low doses of bicuculline on N-methyl-D-aspartate single-channel kinetics are not evident in whole-cell currents. *Mol. Pharmacol.*, **41**, 900–907.

Wroge, C.M., Hogins, J., Eisenman, L., & Mennerick, S. (2012) Synaptic NMDA receptors mediate hypoxic excitotoxic death. *J. Neurosci.*, **32**, 6732–6742.

Wyllie, D.J., Béhé, P., & Colquhoun, D. (1998) Single-channel activations and concentration jumps: comparison of recombinant NR1a/NR2A and NR1a/NR2D NMDA receptors. *J. Physiol. (Lond.)*, **510 (Pt 1)**, 1–18.

Wyllie, D.J.A., Livesey, M.R., & Hardingham, G.E. (2013) Influence of GluN2 subunit identity on NMDA receptor function. *Neuropharmacology*, **74**, 4–17.

Wyszynski, M., Lin, J., Rao, A., Nigh, E., Beggs, A.H., Craig, A.M., & Sheng, M. (1997) Competitive binding of alpha-actinin and calmodulin to the NMDA receptor. *Nature*, **385**, 439–442.

Xia, P., Chen, H.V., Zhang, D., & Lipton, S.A. (2010) Memantine preferentially blocks extrasynaptic over synaptic NMDA receptor currents in hippocampal autapses. *J. Neurosci.*, **30**, 11246–11250.

Yamazaki, M., Araki, K., Shibata, A., & Mishina, M. (1992) Molecular cloning of a cDNA encoding a novel member of the mouse glutamate receptor channel family. *Biochem. Biophys. Res. Commun.*, **183**, 886–892.

Yan, J., Bengtson, C.P., Buchthal, B., Hagenston, A.M., & Bading, H. (2020) Coupling of NMDA receptors and TRPM4 guides discovery of unconventional neuroprotectants. *Science*, **370**.

Yi, F., Traynelis, S.F., & Hansen, K.B. (2017) Selective Cell-Surface Expression of Triheteromeric NMDA Receptors. *Methods Mol. Biol.*, **1677**, 145–162.

Yi, F., Zachariassen, L.G., Dorsett, K.N., & Hansen, K.B. (2018) Properties of triheteromeric NMDA receptors containing two distinct GluN1 isoforms. *Mol. Pharmacol.*, **93**, 453–467.

Yuan, H., Low, C.-M., Moody, O.A., Jenkins, A., & Traynelis, S.F. (2015) Ionotropic GABA and glutamate receptor mutations and human neurologic diseases. *Mol. Pharmacol.*, **88**, 203–217.

Zanos, P., Moaddel, R., Morris, P.J., Georgiou, P., Fischell, J., Elmer, G.I., Alkondon, M., Yuan, P., Pribut, H.J., Singh, N.S., Dossou, K.S.S., Fang, Y., Huang, X.-P., Mayo, C.L., Wainer, I.W., Albuquerque, E.X., Thompson, S.M., Thomas, C.J., Zarate, C.A., & Gould, T.D. (2016) NMDAR inhibition-independent antidepressant actions of ketamine metabolites. *Nature*, **533**, 481–486.

Zhang, S., Ehlers, M.D., Bernhardt, J.P., Su, C.T., & Huganir, R.L. (1998) Calmodulin mediates calcium-dependent inactivation of N-methyl-D-aspartate receptors. *Neuron*, **21**, 443–453.

Zhao, X., Marszalec, W., Toth, P.T., Huang, J., Yeh, J.Z., & Narahashi, T. (2006) In vitro galantamine-memantine co-application: mechanism of beneficial action. *Neuropharmacology*, **51**, 1181–1191.

Zheng, F., Erreger, K., Low, C.M., Banke, T., Lee, C.J., Conn, P.J., & Traynelis, S.F. (2001) Allosteric interaction between the amino terminal domain and the ligand binding domain of NR2A. *Nat. Neurosci.*, **4**, 894–901.

Zheng, F., Gingrich, M.B., Traynelis, S.F., & Conn, P.J. (1998) Tyrosine kinase potentiates NMDA receptor currents by reducing tonic zinc inhibition. *Nat. Neurosci.*, **1**, 185–191.

Zheng, W., Li, X.H., Yang, X.H., Cai, D.B., Ungvari, G.S., Ng, C.H., Wang, S.B., Wang, Y.Y., Ning, Y.P., & Xiang, Y.T. (2018) Adjunctive memantine for schizophrenia: a meta-analysis of randomized, double-blind, placebo-controlled trials. *Psychol. Med.*, **48**, 72–81.

Zhong, J., Carrozza, D.P., Williams, K., Pritchett, D.B., & Molinoff, P.B. (1995) Expression of mRNAs encoding subunits of the NMDA receptor in developing rat brain. *J. Neurochem.*, **64**, 531–539.

Zhong, J., Russell, S.L., Pritchett, D.B., Molinoff, P.B., & Williams, K. (1994) Expression of mRNAs encoding subunits of the N-methyl-D-aspartate receptor in cultured cortical neurons. *Mol. Pharmacol.*, **45**, 846–853.

Zhou, H.-Y., Chen, S.-R., & Pan, H.-L. (2011) Targeting N-methyl-D-aspartate receptors for treatment of neuropathic pain. *Expert Rev Clin Pharmacol*, **4**, 379–388.

Zhou, Q. & Sheng, M. (2013) NMDA receptors in nervous system diseases. *Neuropharmacology*, **74**, 69–75.

Zhou, X., Hollern, D., Liao, J., Andrechek, E., & Wang, H. (2013) NMDA receptor-mediated excitotoxicity depends on the coactivation of synaptic and extrasynaptic receptors. *Cell Death Dis.*, **4**, e560.

Zorumski, C.F. & Olney, J.W. (1993) Excitotoxic neuronal damage and neuropsychiatric disorders. *Pharmacol. Ther.*, **59**, 145–162.